United States
Environmental Protection
Agency

Office of Research and
Development
Washington DC 20460

EPA/600/R-99/041
June 1999

Laser Fluorescence EEM Probe for Cone Penetrometer Pollution Analysis

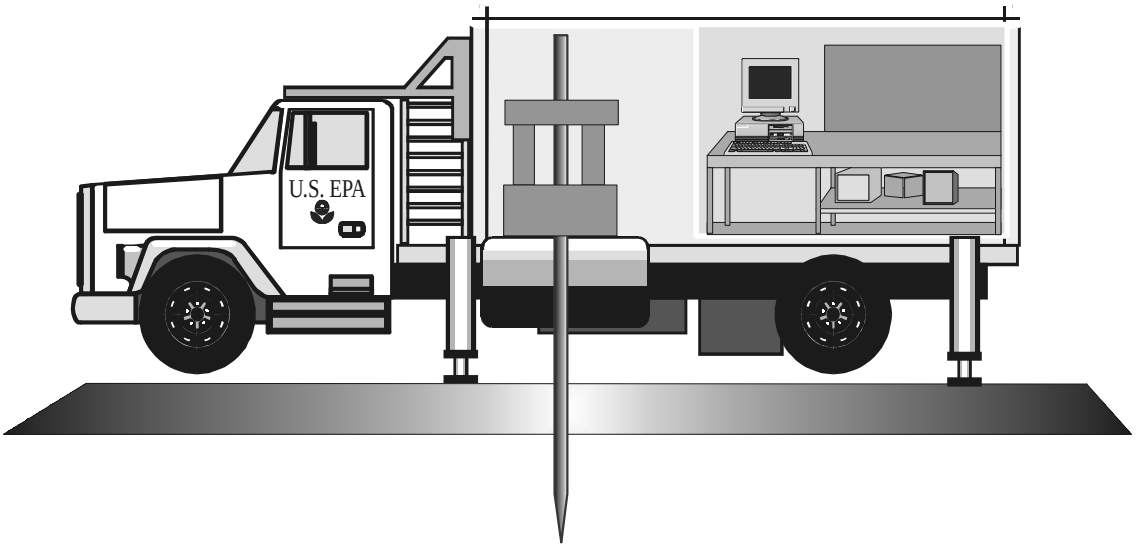

EPA/600/R-99/041
June 1999

LASER FLUORESCENCE EEM PROBE FOR CONE PENETROMETER POLLUTION ANALYSIS

by

Jonathan E. Kenny
Tufts University, Chemistry Department
Medford, MA, 02155

Cooperative Agreement CR-821856

Project Officer
Bob K. Lien
Subsurface Protection and Remediation Division
National Risk Management Research Lab
Ada, OK, 74820

National Risk Management Research Laboratory
Office of Research and Development
U.S. Environmental Protection Agency
Cincinnati, OH 45268

EPA/600/R-99/041
June 1999

LASER FLUORESCENCE EEM PROBE FOR CONE PENETROMETER POLLUTION ANALYSIS

by

Jonathan E. Kenny
Tufts University, Chemistry Department
Medford, MA, 02155

Cooperative Agreement CR-821856

Project Officer
Bob K. Lien
Subsurface Protection and Remediation Division
National Risk Management Research Lab
Ada, OK, 74820

National Risk Management Research Laboratory
Office of Research and Development
U.S. Environmental Protection Agency
Cincinnati, OH 45268

NOTICE

The U. S. Environmental Protection Agency through its Office of Research and Development partially funded and collaborated in the research described here under Cooperative Agreement No. CR-821856 to Tufts University. It has been subjected to the Agency's peer and administrative review and has been approved for publication as an EPA document. Mention of trade names or commercial products does not constitute endorsement or recommendation for use.

All research projects making conclusions or recommendations based on environmentally related measurements and funded by the Environmental protection Agency are required to participate in the Agency Quality Assurance Program. This project was conducted under an approved Quality Assurance Project Plan. The procedures specified in this plan were used without exception. Information on the plan and documentation of the quality assurance activities and results are available from the Principal Investigator.

FOREWORD

The U.S. Environmental Protection Agency is charged by Congress with protecting the Nation's land, air, and water resources. Under a mandate of national environmental laws, the Agency strives to formulate and implement actions leading to a compatible balance between human activities and the ability of natural systems to support and nurture life. To meet these mandates, EPA's research program is providing data and technical support for solving environmental problems today and building a science knowledge base necessary to manage our ecological resources wisely, understand how pollutants affect our health, and prevent or reduce environmental risks in the future.

The National Risk Management Research Laboratory (NRMRL) is the Agency's center for investigation of technological and management approaches for reducing risk from threats to human health and the environment. The focus of the Laboratory's research program is on methods for the prevention and control of pollution to air, water, and subsurface resources; protection of water quality in public water systems; remediation of contaminated sites and ground water; and prevention and control of indoor air pollution. The goal of this research effort is to catalyze development and implementation of innovative, cost-effective environmental technologies; develop scientific and engineering information needed by EPA to support regulatory and policy decisions; and provide technical support and information transfer to ensure effective implementation of environmental regulations and strategies.

This project represents a cooperative effort between the Tufts University and the Environmental Protection Agency. This report summarizes research, development, and field test of a multi-channel fiber optic LIF (laser induced fluorescence) EEM (excitation emission matrix) instrument for CPT (cone penetrometer technology) field deployment. The findings of this project are directly applicable to the site characterization and subsurface pollution analysis at hazardous waste sites.

Clinton W. Hall, Director
Subsurface Protection and Remediation Division
National Risk Management Research Laboratory

PREFACE

For the past fifteen years, our research group has been interested in developing new technology for monitoring groundwater and soil quality, using lasers and fiber optics to perform *in situ* measurements. Our original application was surface waters and monitoring wells, and, after enough laboratory studies to convince ourselves of the feasibility of the laser-induced fluorescence approach, we performed a very limited number of field tests of a first-generation instrument. This work was published in *Analytical Instrumentation* in 1987, and we returned to the laboratory to develop new, more powerful instrumentation that would develop some of the potential of laser-induced fluorescence that the first-generation instrument had left unexplored.

We had no particular plans to return to the field, but were content to develop field-adaptable instrumentation in the relative comfort of the laboratory for the next few years, especially when a commercial instrumentation company showed an interest in our work. All this changed in early 1993 when we were invited to an army-sponsored conference on cone penetrometer technology as a way to put fiber-optics-based probes into the subsurface, an idea we had acknowledged early on as having economic merit, because it would save the cost of digging wells. We also received a request for proposals from EPA about the same time, so, still unsure about our interest in returning to the field, we decided to submit a preproposal, attend the conference, and see what would happen.

I sent my postdoctoral fellow of four years, Todd Taylor, to the conference, and he came back highly enthused. We were invited to submit a full proposal, and a few months later, we were back in the business of field analytical chemistry, with the EPA Robert S. Kerr Environmental Research Laboratory (RSKERL) in Ada, Oklahoma as partners.

Unfortunately for the group, Todd Taylor found a permanent job, and left the group just as work was getting started. This made it very challenging for the two new people, graduate student Sean Hart and postdoctoral fellow Jie Lin, to finish designing and constructing an instrument that had been conceived by Taylor. Adding to the challenge was the fact that the EPA's new cone penetrometer (CPT) vehicle would not come to Tufts for an orderly installation, but, it turned out, had to be assembled in two stages, the first in Ada, and the second a few weeks later, on site at Hill Air Force Base in Utah.

After this exciting experience, the instrument returned to the lab and saw no field work the second year, because of the peculiarities of the EPA team's travel budget. We finally found an opportunity, using funding available from the Northeast Hazardous Substances Research Center through the Tufts University Center for Field Analytical Studies and Technology (CFAST), to bring the EPA CPT team and vehicle to the greater Boston area in June of the final year of the project. The system was installed and demonstrated

at Hanscom Air Force Base, in Bedford, Massachusetts through the help of our Air Force coordinator at the site, Tom Best. Tom familiarized us with the site, shared his data and ideas, and arranged for us to receive whatever other assistance we needed, including storage of the vehicle at the end of the study. Over the next three months, our field schedule provided us with all the excitement we had experienced that first summer, and lacked that long second year. After field work under EPA sponsorship at Elizabeth City, North Carolina, we returned to Hanscom for a second visit, thanks in part to funding for our EPA team's travel expenses provided by Tom Best and Hanscom. Since the field work ended in September, 1996, we have been dividing our time between data analysis, final improvements to the instrument, and preparation of reports. It has been a very productive return to the field for our research group, and we look forward to continued collaboration with our friends at RSKERL in Ada.

ABSTRACT

A fiber optic LIF (Laser induced fluorescence) EEM (Excitation emission matrix) instrument for CPT deployment has been successfully developed and field tested. The system employs a Nd:YAG laser and Raman shifter as a rugged field portable excitation source. This excitation source simultaneously produces > 20 beams of differing wavelength in the UV that can be selectively chosen for launch into fiber optics. The system uses a pair of silica-clad-silica optical fibers for each of its channels (eight of which were used in the work described), one to deliver excitation light from the multi-wavelength laser excitation source to the sample, and the other to conduct contaminant fluorescence to a grating spectrograph which utilizes a charge-coupled device detector to record fluorescence intensity as a function of both excitation and emission wavelength. The system has automatic data acquisition (depth and LIF) and some real time data analysis capability. The instrument has undergone several different calibrations including wavelength, analyte concentration, and standard compound fluorescence as a function of incident energy. Many sample types have been characterized in the laboratory including single components on sands of different particle sizes and clay, and fuel mixtures in solution and on sands.

This system has been installed in a CPT vehicle and has undergone four field tests at three different sites. The first field test was at Hill AFB in Utah; hardware failure and low contaminant levels prevented successful demonstration of the technology. The second field test was at Hanscom AFB in Massachusetts, where we achieved our goals of instrument characterization and demonstration. The third field test, at the U.S. Coast Guard Station in Elizabeth City, North Carolina, was intended as a demonstration of the system's site characterization capabilities. The fourth and final demonstration was a return visit to Hanscom AFB with the intent to perform a more detailed characterization of the site. The last three field demonstrations were successful in that the instrument was operational and depth - encoded LIF data were collected for a significant number of surface push locations.

The matrix-formatted field data are displayed as three-dimensional fingerprints of contamination at given push locations and depths; they are also reduced in dimension by summing over one or both wavelength axes and plotting summed fluorescence vs. depth to facilitate visualization of the approximate extent of the contaminant plume. The summed fluorescence data have been photon - normalized to the incident excitation energy during the push in which they were measured. Selected EEMs from each push location are examined for characteristic patterns and are qualitatively compared to standard EEMs of pure compounds and fuels.

Several hardware and software challenges remain unmet and the subject of ongoing research.

CONTENTS

FIGURES

TABLES

ACKNOWLEDGEMENTS

There are many people who deserve credit for their effort at different stages of the project. I would like to thank my Project Manager, Bob Lien, for his help and enthusiasm. This was the first project he managed, and he deserves much credit for his patience, flexibility, and general helpfulness. Bob has a wonderful attitude toward science: he loves what he's doing, believes in a hands-on approach, and is always the first one to dive in and make something happen. Anyone who has seen him driving the 30-ton Mack from one push location to another, or swing the rods in the hydraulic compartment, or make his way through the lunch buffet at the Great Wall Restaurant, knows what I'm talking about. Postdoctoral researcher Todd A. Taylor was involved in the development of earlier versions of our instrument, and helped conceive this project and write the proposal. The work was taken over by postdoctoral researcher Jie Lin and graduate student Sean J. Hart, who together successfully met the challenges of design and assembly of the instrument under the heavy pressure of a fiscal year deadline for the first field test. When Jie Lin left to pursue his own academic research and teaching career, Sean provided the continuity and leadership needed while Jie's successor was searched for, hired, and trained. Yu-min Chen arrived near the end of the project and was an active contributor in the field testing, and the development of several protocols, hardware, and software for data acquisition and processing. Jim Bodah of the Chemistry department electronics shop and Frank Mellon of the department machine shop each deserve credit for their input into our work. Throughout the field work, our project manager, Bob Lien, researcher Susan Mravik, and technician, John Hoggatt, were indispensable in the operation of the CPT vehicle and handling of the probe during pushes. Dr. John Wilson is acknowledged for coordinating and assisting our work at the U.S. Coast Guard Station in Elizabeth City, NC. At Hanscom AFB, the site manager, Tom Best, provided us with much support and direction during the work in addition to detailed site information and well samples.

I. INTRODUCTION

The possibility of performing *in situ* (or even simply on-site) chemical analysis of hazardous waste sites is growing increasingly attractive to government and private parties alike, because of the possibility of obviating all or some of the following problems: worker exposure, sample collection, labeling, waiting, unwanted chemical transformations of samples, transport, waiting, loss of volatiles, chain of custody, waiting, standard laboratory analysis, waiting, etc. A particularly attractive stage for *in situ* sampling is provided by cone penetrometer technology (CPT), which uses a hydraulic system to push a small-diameter rod directly into the ground, using the weight of the truck which houses and transports the unit as ballast. This technology has been used for decades for physical characterization of soils and site geology; recently, it has become the darling of those wishing to perform chemical characterizations as well. The technology appears to be ideal for insertion of fiber optics which connect the subsurface sample to a spectrometer located in the vehicle, at last making good on the promise of fiber optic promoters to provide cheaper access to the subsurface than the conventional method of well digging. Coupling these optical fibers to laser light sources permits sensitive *in situ* measurements to be made in many cases. One such case is detection of fluorescent analytes, such as benzene, toluene, ethylbenzene, and xylenes (BTEX) and polycyclic aromatic hydrocarbons (PAH). Several years ago, we demonstrated the feasibility of *in situ* detection of groundwater contaminants using short-wavelength ultraviolet laser light and optical fibers[1-4]. Shortly thereafter, we developed instrumentation for *in situ* detection of fluorescent analytes by LIF, using a single wavelength (266 nm) from a compact YAG laser and a simple two-fiber probe which could be lowered into a conventional PVC-lined monitoring well[5]. After brief field-testing of the instrument[5], we returned to the laboratory to develop more sophisticated instrumentation with multiple-wavelength laser excitation[6-8]. Meanwhile, two other research groups, those of Lieberman[9-15] and Gillispie[16-21], pioneered the CPT deployment of LIF optical fiber probes.

The work described in this report has grown out of our laboratory development project mentioned above. The fundamental work on the development of the laser / Raman shifter excitation source was paramount in the progress of this project.[22] The instrument described herein represents the fourth generation of fiber optic LIF-EEM systems developed by this laboratory. However, this work is the first that has attempted to field deploy the instrument in a CPT vehicle.

The field deployment of such a system in a CPT vehicle has several complications associated with it. The most important aspect is the mating of fibers and CPT probe. The fibers have to be packaged for their protection during the CPT push routine, and hardware must be developed to couple the light from the fiber to the soil through a sapphire window on the probe body. In addition, the instrument must be rugged enough to withstand the rigors of travel in the rear compartment of the CPT truck. In keeping

with that goal, the system components have been chosen with attention to their individual track records in field use in addition to their scientific performance specifications. Once the instrument has been designed, assembled, and installed, the characterization and refinement of its functions must begin.[23] This is the stage of greatest importance, when the instrument's capabilities and shortcomings are revealed in full. The complete characterization and calibration of the instrument allow a more robust analysis of field data to be accomplished. Towards that goal, several calibrations of the instrument's performance have been undertaken.

The potential of our LIF-EEM system for site characterization lies in the type and quantity of data that are generated in a single detector exposure. Fluorescence depends on a number of molecular and instrumental parameters; if its intensity dependence on a sufficient number of appropriate parameters is measured, one can hope to perform a mathematical separation on the data set that replaces the physical separation of the various components of the sample that is part of a laboratory analysis. Thus, it is a technique highly suited to the demands of "hands-off" *in situ* measurement. Of all the parameters that might be measured, we decided to measure fluorescence intensity, *M*, as a function of excitation and emission wavelengths, λ_x and λ_m, respectively. The elements, $M(\lambda_x, \lambda_m)$, of an EEM for a single fluorescing compound are given[24] by equation 1,

$$M(\lambda_x, \lambda_m) = kI(\lambda_x)\varepsilon(\lambda_x)\Phi'(\lambda_m)D(\lambda_m)c \qquad (1)$$

where k is an instrument-dependent constant, I is the excitation light intensity at the sample, ε is the molar absorptivity, Φ' is the derivative of the fluorescence spectrum with respect to λ_m, D is the detector response, and c is the concentration of the emitting species. The wavelength dependencies are indicated in parentheses. In the derivation of Equation 1, the optically dilute limit has been assumed, i.e., the absorbance is so weak that I is essentially constant across the sample. For an optically dilute sample containing multiple noninteracting species, Equation 1 would need to be modified by setting M equal to a sum of terms of the type shown on the right-hand side, one for each component in the mixture. Environmental samples of interest do not always meet the noninteracting and diluteness requirements for eq. 1 to be strictly valid. At high analyte concentrations which often prevail in many subsurface regions of a contaminated site, the quantitative analysis can be hampered by non-linear effects such as the inner filter (IF) effect and energy transfer (ET).

Our instrumentation allows us to collect an emission spectrum for each of up to ten excitation wavelengths; from these data an EEM can be constructed and mathematically analyzed. Two of the multidimensional fitting techniques that may be used are least squares and rank annihilation. Using

these, the identity and concentration of species contributing to an experimental EEM may be determined. The approach in the least squares calculation is to express the mixture EEM as a linear combination of library EEMs for individual fluorescent analytes; the coefficient of each library EEM is simply related to the concentration of that component in the mixture. The coefficients are arrived at by minimization of an error matrix equal to the difference between the measured and calculated EEMs. This method should only be used when all components of the sample are also in the library. By contrast, the rank annihilation method allows the concentration of a given component in the library to be estimated even if fluorescent species not in the library are contributing to the total signal. In this method, the component EEM is multiplied by a scalar and that product is then subtracted from the experimental EEM. If the scalar is equal to the amount of that component in the sample divided by the amount in the standard, the resultant product matrix will have a rank (i.e., number of independent rows and/or columns) one lower than the rank of the experimental EEM.

Although these data analysis methods have been successful in laboratory analyses of fluorescent mixtures, there is no guarantee of equal success in the case of field data. This is because of the assumption of optical diluteness, the limited number of laser wavelengths that can reasonably be launched into a fiber bundle, the generally unknown perturbation that the soil and other subsurface components can produce in the EEM of a given analyte, and the unknown number and type of reference EEMs that are needed. One challenge of this project (and presumably of future related work) is to determine the applicability of these analysis techniques to field data. Our expectation is that chemicals can be classified into groups, and amounts in each group determined semiquantitatively, using the current instrumentation. If this expectation is realized, it would represent a significant improvement over fluorescence techniques that produce a single number, e.g., total fluorescence intensity, versus depth of the probe, and an important milestone along the way to more complete chemical speciation.

II. CONCLUSIONS

Our goals of assembling, optimizing and demonstrating a sophisticated CPT LIF probe have been significantly advanced. In very general terms, the hardware part of the problem has been largely solved, but the data base, the strategies for data analysis and the generation of software capable of performing the analyses in a timely manner are very much works in progress. In our opinion, the success of the hardware development program and the qualitative assessment of the field data provide justification for devoting the necessary time and energy to the remaining problems. We have already begun to do so in this and other related projects. (See section 6 of this report, Summary, for further relevant discussion in support of the conclusions presented here.)

The instrument has been designed, developed, refined, characterized and finally field tested on four separate occasions at three different sites: Hill AFB, Hanscom AFB I, Elizabeth City CGS, and Hanscom AFB II. Our research has succeeded in producing an instrument capable of characterizing fuel-contaminated sites with the measurement of multidimensional data. We have increased the quantity of data collected by at least 8 fold (8 data channels compared with 1 for standard LIC-CPT systems). Having multiple excitation wavelengths, in addition to emission wavelengths, i.e. EEMs, permits one to identify similarities between the spectral signatures of the field contamination and reference contaminants, which may be cataloged as individual chemical species, mixtures, or classes of compounds. This capability has been demonstrated in a qualitative way for both laboratory and field measurements.

The instrument has been used at the same site, Hanscom AFB, at different times, 3 months apart. The site investigated was undergoing large scale remediation at the time and on our return visit we were able to delineate changes in the site, thought to be attributable to the site cleanup. This work was valuable in characterizing the site dynamics, and was accomplished with only 3 days of active CPT sampling on each occasion.

Calibration curves have been measured, testing the system's response to different analytes. A study of an aqueous solution of phenol, an important single-ring aromatic compound, using 266.0 nm excitation, indicated a reasonably low detection limit of 2.7 ppm. Measurements of single components and mixtures in various media include the following: aqueous phenol in solution and on a medium sand; naphthalene and anthracene in cyclohexane; a benzene, naphthalene and anthracene mixture in cyclohexane; JP-4 in cyclohexane; JP-5 in cyclohexane and on a medium sand; and JP-8 mixed on a silty clay. The data on these standard compounds serve as reference tools for the analysis of the field-measured EEMs.

An important step for quality assurance of fluorescence data is to normalize the intensity of fluorescence to that of the excitation source, so that changes or fluctuations in laser power might not be misinterpreted as changes in contaminant concentrations. We measured the probe's response to a standard quinine sulfate solution before and after each push; these readings were interpreted using the results of the calibration of the quinine sulfate fluorescence response to incident energy variations. This procedure allowed the summed fluorescence data to be corrected for excitation energy variation from push to push, and provided a way to monitor overall instrument performance regularly during field work.

The field data were analyzed in a standard manner for each field test, starting with an examination of the quinine sulfate calibration data. During the first field test at Hanscom AFB, only before-push calibrations were performed, and during the subsequent two, both before and after measurements were made. For all field tests, depth vs. summed fluorescence plots were prepared for each excitation wavelength at each push location. EEMs from the peak fluorescence depth region at each push location were generated and the patterns compared with those of the reference EEMs. There were several features in the EEMs measured during each field test that were comparable to some of the reference EEMs. Many of the *in situ* EEMs are directly comparable to the standard jet fuels, JP-4 and JP-5, confirming the presence of jet fuel contamination. There are several field measured EEMs that contain fluorescence patterns similar to naphthalene. In a particular EEM, measured during the first field test at Hanscom AFB, there was contamination with features indicating the presence of anthracene in addition to other species.

The success of the EEM analysis, either by visual pattern recognition or mathematical algorithms, depends on the quality and number of the reference EEMs available for comparison. A complete identification of the fluorescent chemical composition of these *in situ* measured EEMs requires a large library of reference EEMs, analogous to reference spectra in the fields of UV-VIS, IR, and NMR spectroscopies, etc. The uses of such a library include not only visual pattern recognition, but also the mathematical fitting of the library EEMs to the field data. A relatively small library of reference EEMs has limited our attempts at visual pattern recognition. This is due in part to the number of field tests performed in the last year of the project.

Even with the currently available EEM library, more quantitative pattern recognition methods are potentially applicable. These include least-squares, rank annihilation matrix methods, and neural network pattern recognition. These techniques are being investigated to determine which method will be most suitable for the analysis of field data. Some of the methods require (or at least are normally implemented under the assumption of) optical diluteness, which simplifies the mathematical relationships involved in

EEM analysis considerably. It is clear that in the field, this assumption often does not hold, and analysis schemes will have to accommodate this possibility if even semiquantitative results are to be obtained.

Our recommendation is that the project be given additional support to permit the completion and testing of the hardware and the further development of data analysis schemes. These include stabilization of the laser output at all desired wavelengths, automation of data acquisition, and reduction of optical fiber damage. In our estimation, the hardware issues should be resolvable in one year or less, while the data analysis project will require about two years, although intermediate analysis methods can be developed faster. At least one or two more field demonstrations, supported by extensive laboratory measurements, should be included in the development plan.

III. OVERVIEW

The objectives of this project have been of considerable scope and depth. While there has been one main goal, the development of the LIF-EEM instrument for CPT deployment, there have been many smaller supporting sub-projects. During the course of developing the main system, our goals were modified, as more was understood about the nature and relative importance of the tasks at hand. Some of the sub-goals were accomplished, while others were deemed unfeasible within the scope of the current project. For example, if work on a sub-task would draw too many resources away from the main goal, then it was deemed appropriate to sacrifice it for the overall good of the project.

In addition to the development and construction of the LIF-EEM instrument, many sub-tasks were outlined in the original proposal. These tasks and goals are arranged below in order of decreasing importance: a) *In situ* LIF-CPT measurements to be carried out at a well characterized site, b) Software development for data analysis, c) The development of an HPLC LIF-EEM system that is field portable, d) Lamp-based EEM system developed and tested in CPT vehicle, e) A bioremediated site revisited to determine short term changes, f) A video imaging system for the characterization of soil types, g) Incorporation of novel sensors into "spare channels" of our system.

In retrospect, the tasks and goals described above may have been overly ambitious, given our inexperience with cone penetrometers and the amount of time and funding available. Therefore, they were modified according to their overall impact upon the project's main objective. The field portable HPLC LIF-EEM instrument was considered an important and valuable addition to the LIF probe instrument. Its development was begun, but the rigorous field test schedule required all efforts to be focused upon the readying of the LIF probe instrument. The video imaging system, while a useful addition, was deemed unfeasible given current camera technology (soon afterward, Lieberman's group[26] proved otherwise). Incorporation of novel third party sensors into our system has not been attempted, but the system is sufficiently modular that this could still be done fairly easily in the future. The installation of a lamp-based EEM system was not attempted, although this possibility was briefly examined in a related project with separate funding. Software and algorithms for data analysis were developed and written in C++ and were used in the analysis of field data. Our early LIF-CPT measurements were carried out at well characterized sites. The final version of the instrument was tested at Hanscom AFB in Massachusetts. This site is currently under remediation and the extent of the contamination plume is fairly well defined. The short-term changes at a bioremediation site were to be monitored using our system. A site where bioremediation was being induced externally was not available, but Hanscom AFB is undergoing remediation including soil vapor extraction (SVE), groundwater treatment facilities, and significant natural bioremediation as evidenced by the large amounts of bacteria that are routinely found

in the treatment hardware. A return visit was made 3 months after the first characterization and significant changes were discovered.

The main purpose of this project, the development and field deployment of our LIF-EEM instrument, has been accomplished. The instrument has been developed and has successfully completed three field tests at two different sites. Two of the field test data sets (Hanscom AFB) were measured three months apart, enabling us to determine that the remediation efforts at that site have produced changes in the contaminant levels. An HPLC system was procured for use in the field and the design of the LIF-EEM HPLC detection system has been furthered. Data analysis and processing programs have been developed that enable the data reduction and presentation of field data to be accomplished in a short amount of time. In addition, the design of an automatic data acquisition and storage system has been completed. This system allows the automatic collection of depth data and synchronized LIF data collection and storage with real time display of total summed fluorescence for each excitation channel. This automated data collection feature has been constructed and tested in the CPT vehicle and laboratory, but has not been used during a field test.

IV. INSTRUMENTATION

A) Design and Construction

1) Excitation source and launch system

The excitation source in our LIF system is comprised of a Q-switched flashlamp-pumped Nd:YAG laser (Surelite I, Continuum, Santa Clara, CA) operated at a frequency of 20 Hz. The laser has frequency-doubling and quadrupling crystals installed, converting its 1064 nm fundamental beam to 532 nm and 266 nm radiation respectively. The 266 nm UV radiation serves as a pump beam for the Raman shifter. The Raman shifter is a high pressure gas cell with UV transparent windows, filled with methane and hydrogen (in a ratio of 55:45). When the 266 nm pump beam is focused into the Raman shifter, a SRS (stimulated Raman scattering) process occurs. This process generates many beams[22] (> 20) of different wavelengths that can then be separated and used. Most of the SRS beams are of longer wavelength than the pump beam and are called Stokes-shifted beams. There are, however, several beams that are of shorter wavelength than the pump, and these are called anti-Stokes shifted beams.

A diagram of the excitation source and the launch system is shown in Figure 1. Two dichroic mirrors (CVI, Livermore, CA) are used to remove the fundamental (1064 nm) and the second harmonic (532 nm) beams from the laser output. The fourth harmonic (266 nm) is reflected by a mirror, focused by a lens (f.l. = 75 cm), and reflected by another mirror through a 75 cm long Raman shifter.[23,25] The beam exiting the Raman shifter is collimated and passes through a prism system for the re-direction and dispersion of the beams on the optical breadboard (TMC, Peabody, MA). The Raman shifted beams of different wavelengths pass through a prism system where they are dispersed according to wavelength. Five prisms are employed, four of them having a refracting angle of 60^o and the other having a refracting angle of 45^o. The incident angle on the first prism and the angles between prisms are adjusted so that the aberration for the central beam is minimized. The beams are refracted approximately 180^o on the optical breadboard. The last two prisms are again 60^o but have larger apertures compared to the first three to accommodate the dispersing beams. The dispersed beams emergent from the prism system are focused by a lens (f.l. = 75 cm) and launched into optical fibers to be delivered to the sample. Each fiber is held on an X-Y positioner (Newport, Irvine, CA), mounted on a breadboard post, to allow adjustment of the fiber launch end. For each mount, the fiber is held in a fiber-optic chuck (FPJ-H, Newport, Irvine, CA) that is mounted on the X-Y positioner with provision for the fiber end position to be adjusted along the Z-axis (optical axis) as well.

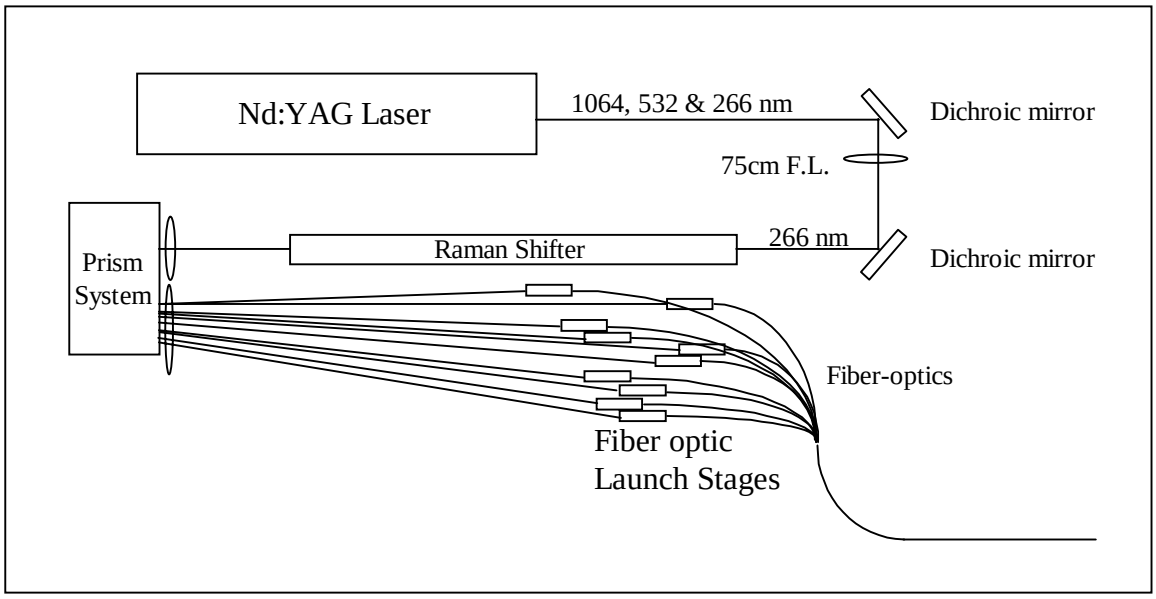

Figure 1. Diagram of the optical layout of the excitation source and fiber-optic launch stages.

Up to ten (eight used in this work) Raman shifted beams were selected based on their pulse energies and the wavelength intervals (i.e., approximately equal wavelength spacing). The wavelengths were calibrated with a mercury lamp and the pulse energies were determined with RjP 735 and 765 probes and an Rj 7000 energy meter from Laser Precision (Utica, NY). The wavelengths and pulse energies for the ten beams are listed in Table 1. The total dispersion distance for these ten beams at the focal plane is about 10 cm. The pulse energies of the beams range from 3.8 to 848 μJ. Some of the beams are too intense and therefore damage the fiber at the focal point. For our system, which was not fully optimized in this regard, we found that beams which have pulse energy higher than 100 μJ were likely to cause damage to the fiber, particularly around the focal point of the beam. Other factors which influence optical fiber launch damage include the light wavelength, fiber diameter and surface condition. The most practical solution to the fiber damage problem was to move the fibers away from the focal points. A position was found for each fiber where an appropriate power density (which did not necessarily correspond to the entire beam) could be launched into the fiber without damaging it.

The beams were launched into a 10 m fiber cable which was attached to a 20 m cable at a panel using standard ST bulkhead connectors. The energies emergent from the other end of the 30 m cable at the sample were measured for each of the beams. These excitation energies are listed in the last column of Table 1. They are dependent on the amount of light launched into the fibers, the attenuation of the beams by the fibers, and the coupling efficiencies of the connectors. As can be seen, the beams at intermediate wavelengths have the highest excitation energies available. This is because those beams have high total energies and medium attenuation by the fiber optics. The beam at 266 nm has the highest

total energy, but only a small portion of the beam is launched into the fiber (to avoid fiber damage) and the attenuation by fiber at this wavelength is very high. As a result, the excitation energy available at 266 nm is not very high.

Table 1. Raman shifter output and excitation energy available.

Wavelength (nm)	Beam origin[a] (H, M)	total energy[b] (μJ/pulse)	excitation energy[b] (μJ/pulse)
257.5	1, -1	9.6	0.01
266.0	0, 0	848	6.4
278.5	1, -2	9.8	0.04
288.4	0, -1	98	15
299.1	-1, 0	197	65
314.9	0, -2	188	40
327.7	-1, -1	92	10
341.6	-2, 0	138	25
362.1	-3, 1	7.4	0.03
378.8	-1, -2	3.8	0.02

[a] H, M are the numbers of hydrogen and methane quanta shifted, respectively.

[b] Total energy is that of the laser beam before launch; excitation energy is that available at the distal end of the fiber for fluorescence excitation.

2) Fiber cable assembly

The choice of optical fiber was based upon several competing factors. These include mechanical strength, resistance to light damage during launch, light attenuation, and cost. The mechanical strength is very dependent upon the jacket, or protective coating, used to cover the fused silica fiber core and cladding. The diameter of the fibers is also very important. The fiber diameter in part determines the minimum fiber bend radius which the fibers can withstand without damage or loss of performance. The larger the core diameter, the larger the minimum bend radius. This is an important consideration because the fibers make a tight turn between rods in the racks of the CPT vehicle. In addition, the diameter has an effect on the ability of the polished fiber launch face to withstand damage. In general it seems that the larger diameter core fibers have the greater resistance to light launch damage. This may be because damage occurs at the core-cladding interface when the beam is larger than the fiber core diameter.

The fiber was manufactured by Polymicro Technologies, Inc. (Phoenix, AZ). The diameters for the silica core (doped with fluoride), silica cladding, and polyimide coating are 400, 440, and 470 mm,

respectively. The fiber cables were assembled in-house. The cable tubing is composed of a polypropylene inner tube (i.d.= 1.2 mm), a PVC outer tube (o.d.= 3.8 mm), and a layer of Kevlar yarn in between. Up to four fibers can be pulled through the cable by using a UV-curing epoxy to glue the fibers onto a nylon thread inside the inner tube.

Before the fibers were polished or installed into the connectors, one half to one centimeter of polyimide coating was removed by burning, and the exposed portion of the fiber was cleaned with ethanol. The fiber ends were polished with 12, 3, 1, and 0.3 μm lapping papers and the finished ends were examined under a microscope for surface smoothness and absence of fiber edge chips or lips.

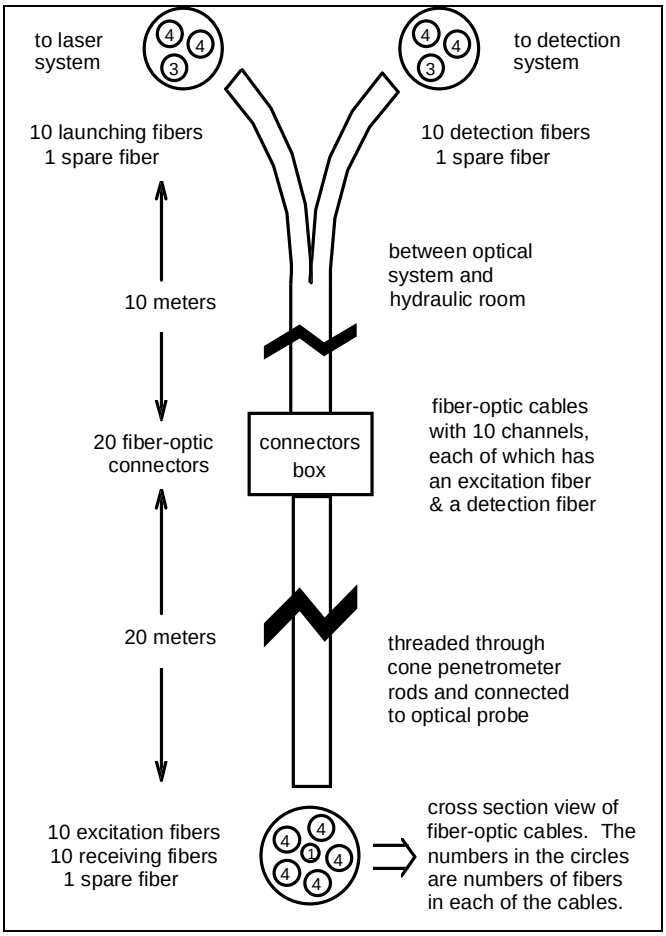

Figure 2. Fiber-optic cables for Cone penetrometer system.

The configuration of the fiber-optic cables is shown in Figure 2. A short cable (length = 10 m) runs between the optical system and the hydraulic room in the cone penetrometer vehicle. This cable splits into two branches, each containing ten fibers, at the optical bench: one is connected to the launching stages and the other is interfaced to the detection system. A long cable (length = 20 m) containing all 20 fibers

goes through the cone penetrometer rods and is connected to the optical probe. The two cables are connected in the hydraulic room by 20 fiber-optic connectors (ST type, Augat, Kent, WA). Basically, there are 10 channels available, each of which has a pair of fibers, one for delivering the light to the sample and other for collecting the fluorescence. The lengths of fiber used in this work are short relative to those used by other more established systems which are capable of pushing to 100 ft to 150 ft.[15,21] We chose to use shorter fibers to enhance the possibility of BTEX detection using the shorter uv wavelengths available from our system. Attenuation of laser power becomes significant at wavelengths less than about 290 nm.

3) Probe design

The diagram for the entire probe is shown in Figure 3. The outer probe body is a heat-treated, hardened steel tube that is threaded on both ends to permit attachment to the CPT push rods.

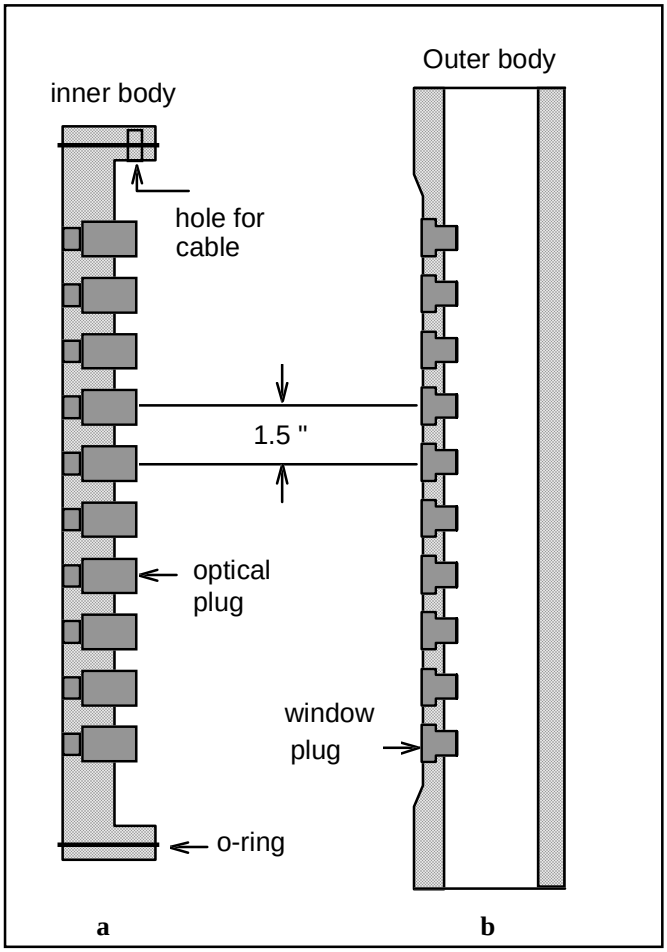

Figure 3. Probe inner (a) and outer (b) bodies, window and optical plugs.

The CPT rod screws into the top of the probe outer body, while the cone tip is screwed onto the bottom of the probe body. The probe outer body has ten holes bored through it in a column that are countersunk to

accommodate the sapphire window holders. The probe inner body fits into the probe outer body and is sealed by o-rings at the top and bottom. The inner body is a half cylinder with 10 holes bored along its length with counter-sunk holes to accommodate the optical mating between the sapphire window and the fibers. The inner probe body is held in place by the sapphire window holders that screw through the probe outer body. The fiber-optic cable is pushed through the hole on the top of the probe body and sealed with RTV silicone sealant. The fibers are installed into the optical plugs that are held onto the probe body by set-screws. The inner probe body is inserted into the outer housing and they are aligned. The o-rings on the top and bottom of the probe body provide sealing so that the groundwater does not leak into the probe. Then the window plugs are screwed into the probe body, holding the probe body and outer housing together. The space between the probe outer body and the sapphire window are sealed using both copper washers and RTV silicone sealant.

The hardware for the first optical probe, used during the first field test at Hill Air Force Base, was machined by Applied Research Associates, Inc. (South Royalton, VT) as per our design. The optical design involved a mirror and a short focal length lens mounted in a cylinder with a hole and set screw for the optical fibers to be mounted and interfaced with the mirror / lens system.[25] The light from the excitation fiber is reflected by the first surface reflecting mirror, then focused by the lens onto the outer surface of the sapphire window, where the window contacts with the soils. Similarly, the fluorescence of pollutants is collected by the detection fiber. The two fibers (excitation and detection) are held inside a stainless steel tubing. A semi-circle filter is placed in front of the detection fiber to cut down reflected and scattered excitation light. For different excitation beams, different filters were used.

In practice several factors contribute to inefficiency in this optical system. Firstly the lens and mirror were not anti-reflection coated (due to cost and time constraints); this led to light reflection losses that approach the unacceptable limit. When assembling the lens and mirror, the tiny size of the optics made the insertion and cementing of them in the cylinder difficult, with smearing of the cement and some misalignment of both lens and mirror. For these reasons, an alternative that would address these issues was sought after the first field test.

The next optical probe design involved a much simpler approach: have the optical fibers bend 90° and make optical contact with the sapphire window. This method of light delivery (parallel fibers against a sapphire window) has been used by others[17]. We incorporated a fiber end geometry that maximized the overlap of the fiber optic distal cones at the outer surface of the sapphire window. Two geometries were compared with the standard parallel fiber model and one was chosen for its simplicity, ruggedness and good performance. Figure 4 is a design and fluorescence spectrum comparison of the three geometries fabricated, tested and compared: parallel, beveled ends, and angled flat ends. It can be seen that the

fluorescence for either of the new probe designs, A and B in Figure 4, is larger than that for the simple two parallel fiber design. Using the modified two fiber probe designs, a detailed study of probe improvement factors (ratio of new probe to old design: B/A and C/A) was undertaken. Improvement factors up to 14 were seen for the new probes in different solid-containing media.[27] Refer to appendix E for the details of the two fiber probe experiments.

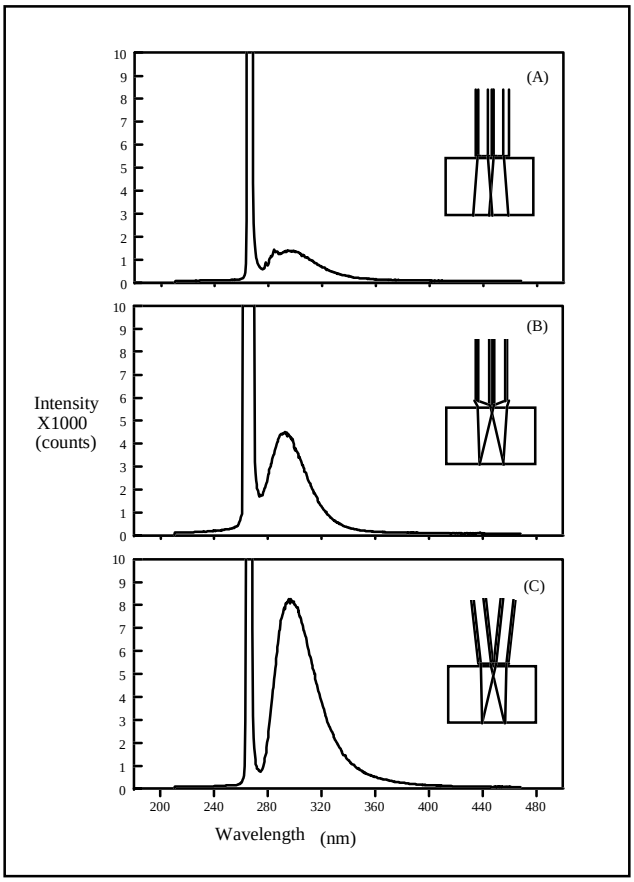

Figure 4. Two fiber probe designs and the fluorescence of 0.1 M phenol solution. A) parallel fibers, B) beveled ends, and C) angled fibers with flat tips.

The use of the new probe design required a system to push the fibers against the sapphire window. The major problem in implementing this with the probe inner and outer bodies was that when the fibers are extended the inner probe body cannot be put inside the outer probe housing. The solution to this problem involves holding the fibers in the probe inner body with a set-screw in the sapphire window threaded opening until the assembly is completed. With the fibers held back, the probe inner body can be inserted into the probe outer body. Then the set-screw is removed and the fibers in their holder are released and the sapphire window can be screwed into place with the fibers pressing against it. The final

design of the probe plug and the fiber holder is shown in Figure 5. The probe plug is a cylinder with a center hole and another underneath. The center hole is for the fiber holder and the one underneath is for a key attached to the holder. The key keeps the fiber holder in position and prevents rotation. A spring in the lower hole is used to push the fiber holder forward. The fiber holder slides forward and

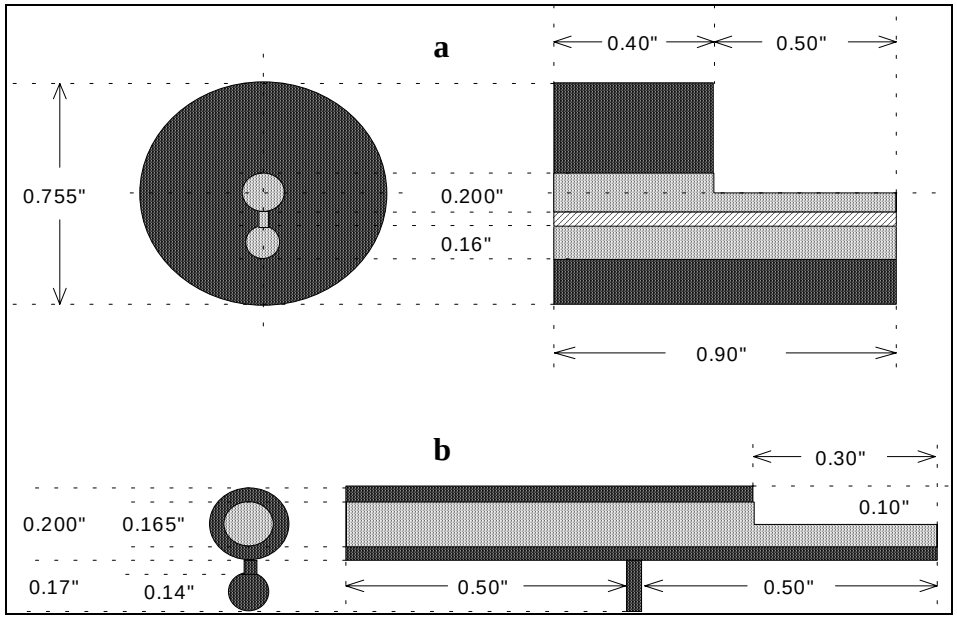

Figure 5. Fiber holder (b) and probe inner body mounting hardware (a).

backward in the probe plug. The preparation of the fibers involves the epoxying of the fibers at the set angle 16.4°. The fibers, exposed from the main fiber cable, are covered with PVC tubing and slipped into the fiber holder tube. Then epoxy is inserted into the assembly to set the fibers against the holder walls. A small bead is allowed to form on the tip so that the epoxy can be polished away exposing the fiber tips.

4) Scattered light rejection

In a fluorescence experiment, some of the excitation light is coupled towards the detector through either Rayleigh scattering or reflection off optical elements and soils used in the measurement. If the detector is sensitive to this exciting light, it may become saturated with this residual scattered light. Often it is necessary to remove this light due to its spectral interference with the desired fluorescence response. The most common way to accomplish this light filtering is to place a long-pass absorption filter in front of the detector. Ideally, using this technique, the scattered light is reduced or removed and the fluorescence is not affected in any way. There are only certain cut-off wavelength filters commercially available, and

these are not always of the ideal cut-off wavelength for the Raman shifted beams used. In some cases, some fluorescence must be sacrificed for the sake of scattered light removal.

For different excitation beams, filters with different cut-off wavelengths were selected, based on the transmission of filter and fiber (30 m long). It was intended not to completely remove the reflected and scattered light, so that small residual Rayleigh scattering and water Raman signals could be used for diagnostic purposes (potentially, to obtain information about the sizes of soil particles or water content, or as calibration wavelengths in the detection system). The wavelength of water Raman shifted light is calculated from the excitation wavelength and a water Raman shift frequency of 3400 cm^{-1}. The transmission of the filter and fiber at each of the wavelengths is determined from their spectra. Total transmission, calculated as the product of transmission by filter and fiber, is listed in Table 2. As seen, more than 90 % of the reflected and Rayleigh scattered light will be removed by the filters (except the longest wavelength for which an appropriate filter is not available).

Table 2. Transmission of filters and fiber at each excitation wavelength.[a]

Wavelength (nm)	Schott Filter Number (Hill AFB)	Schott Filter Number (All other work)	Total transmission (%) $WL_{Rayleigh}$	WL_{Raman}
257.5	WG 280	None	0.4	18
266.0	WG 280	WG 280	4.3	31
278.5	WG 295	WG 295	2.9	36
288.4	WG 305	WG 320	9.0	45
299.1	WG 320	WG 345	5.4	53
314.9	WG 335	WG 345	2.3	58
327.7	WG 345	WG 360	3.0	63
341.6	WG 360	WG 360	3.6	69
362.1	GG 395	GG 395	7.9	68
378.8	GG 395	GG 395	36	76

[a] $WL_{Rayleigh}$ is the wavelength for Rayleigh scattering and reflected light, and WL_{Raman} is the wavelength for water Raman shifted light.

Normally, the filter is placed directly before the detector's sensing surface, where the light is being delivered to the detector. In a system such as ours where there are multiple channels containing different information (i.e. different exciting wavelengths), there is generally a different filter for each channel.

Since each channel is defined by the emission fiber carrying fluorescence to the detector, there must be a filter not much larger than the fiber diameter, 400 μm. With the fibers arranged in a column at the entrance slit of our spectrograph (see below) with at most a 200 μm spacer in between them, the filters would need to be cut into ½ mm strips and aligned with respect to the appropriate fiber. It is a challenge, first, to cut the filters cleanly, and, secondly, to align them accurately. Furthermore, if the channels needed to be changed, (as occasionally happens during field work, due to fiber damage) the filter attached to one fiber on the detection end would be inappropriate for the new channel.

The solution adopted involves the use of the standard fiber optic connectors used in our system to join the excitation source and detector to the optical probe in the hydraulic room. The approach involves the placement of filters in the fiber optic connectors. The filter material is cut and filed into circles that closely fit in the fiber optic adapter that mates the two connector ends. The connector ends then are inserted and locked into place in the adapter, but are separated by the thickness of the filter. Naturally, there is a loss associated with the separation of the fiber ends but it is comparable to the loss incurred for a standard fiber connection.

The loss depends upon the material separating the fiber connectors and the distance of separation. The larger the separation, the larger the fraction of light that is not coupled into the receiving fiber. In addition, the refractive index of the material between the fiber ends affects the light refraction and therefore the loss. Figure 6 is a ray tracing illustration of 266 nm light in a fiber optic connector for two

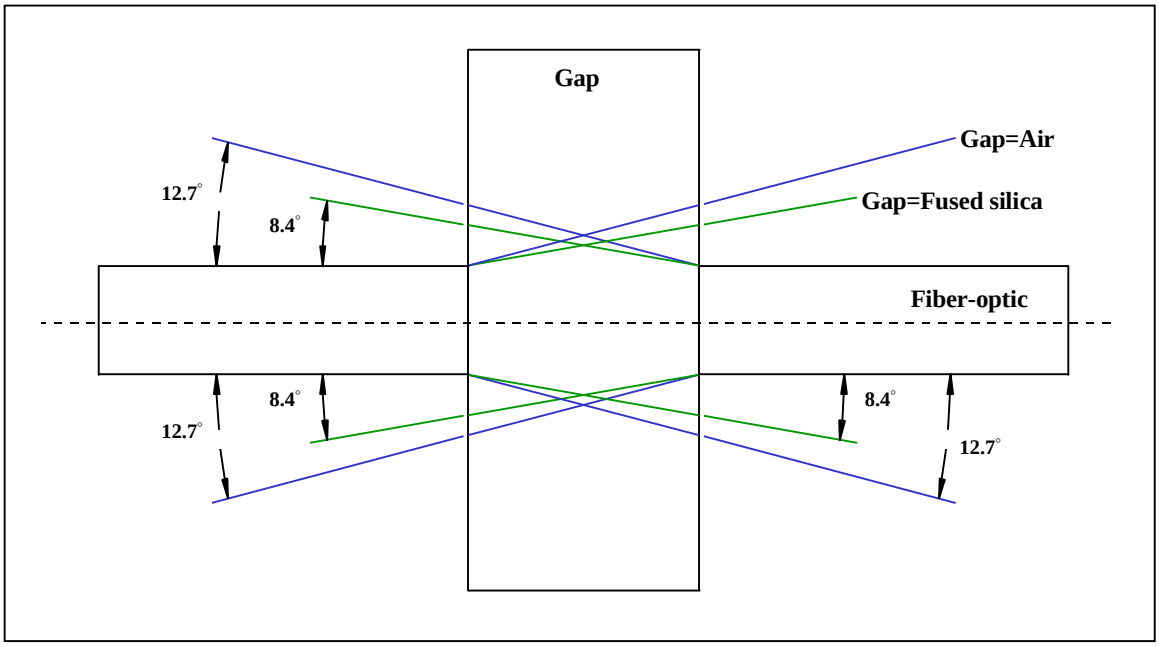

Figure 6. Ray tracing of 266 nm light in a fiber optic connector with the ends separated by a 1 mm gap. Two gap mediums are illustrated: fused silica and air.

different cases: a fused silica flat and an air gap. The filter ray trace is not shown because its refractive index at 266 nm (n = 1.52) is very close to that of fused silica (n = 1.54). The ray tracing was done for the limiting ray emerging from or entering the fiber, as calculated from the fiber's numerical aperture: N.A. = 0.22 = n sin θ, where n is the refractive index and θ is the angle of the light ray with respect to the fiber axis. It can be seen from the ray traces that the air gap should have a larger loss associated with it due to the larger angle exiting the fiber and thus a larger fraction of the beam's cross section not being coupled into the receiving fiber.

The advantages of filters include their being easily manufactured, implemented, and replaced if needed, with an acceptable light loss. The inclusion of filters in fiber optic connectors is consistent with the desire to keep the system as modular as possible: If a channel must be changed, then its filter can easily be exchanged with a different one for the new channel.

5) Detection system

The detection system is composed of an imaging spectrograph (SpectraPro 150, Acton Research Corporation, Acton, MA) and a CCD detector (TE/CCD-576EMUV from Princeton Instruments, Trenton, NJ).

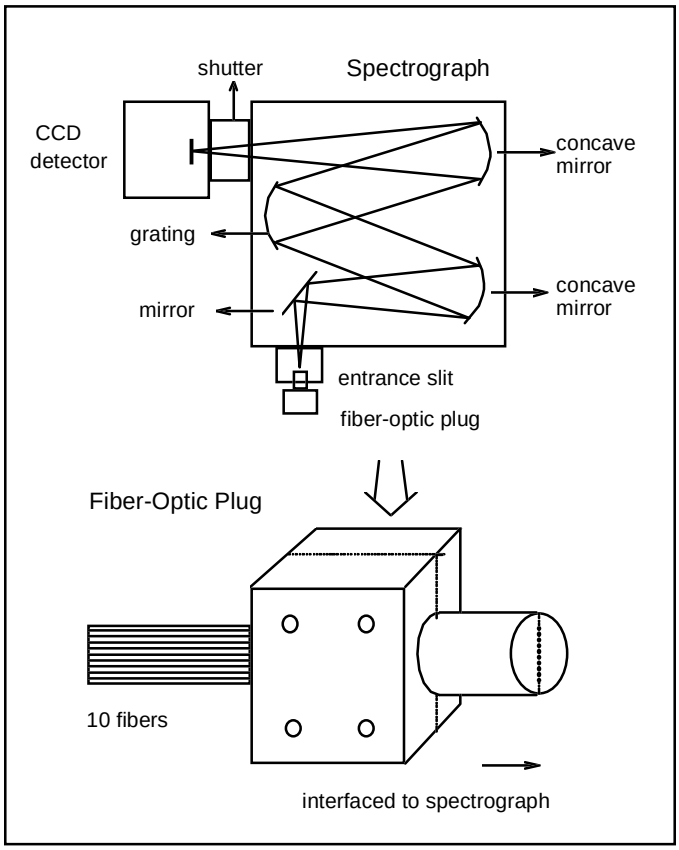

Figure 7. Detection system: fiber optic plug, spectrograph and CCD camera.

Ten detection fibers are held in a column by an aluminum plug, which is interfaced to the spectrograph. The grating is set so that wavelengths in the region of 250 to 500 nm are detected in first order by the CCD detector. The fiber optic interface plug, the spectrograph and CCD are shown in Figure 7. The light path through the spectrograph is shown starting with the light from the fibers entering the spectrograph's entrance slits. The image of the fibers is focused onto the CCD chip held at the exit plane of the spectrograph. A shutter between the CCD and spectrograph controls the CCD chip exposure time.

The CCD detector has a UV coated EEV chip with 576 by 368 pixels, which is cooled to -30 ^{o}C thermoelectrically. The long axis of the CCD chip is set horizontally and used as the wavelength axis. For this work, the CCD was binned into eight channels to detect the fluorescence from the eight detection fibers. Each channel is composed of 18 - 20 rows of pixels with five to ten unused rows in between to reduce the cross-talk between the channels due to charge blooming and spectrograph aberrations. Along the long x axis there are 576 pixels defining the maximum emission resolution. Our actual resolution was 2.0 nm – 4.0 nm depending upon the spectrometer slit width. We could have binned pixels in this direction to correspond to the actual resolution, but this was not done during data collection. The software used to collect spectroscopic data was CSMA for DOS (Princeton Instruments, Trenton, NJ) for work

through the first field test and Winspec for Windows 3.1 (Princeton Instruments, Trenton, NJ) for all work thereafter.

6) Automatic data acquisition

In the field it is desirable to have the ability to collect both LIF and push depth data simultaneously with little operator intervention. The system, during the first 4 field tests, had no automation hardware or software; therefore the probe was stopped at a given depth and operators manually initiated data collection and recorded the tip depth. After these initial experiences, a system to enable automatic data acquisition was developed.

The automatic data acquisition system depends upon the use of two computers: one for LIF data acquisition and storage (high speed Pentium PC), and the other (486 PC) as a slave for the collection of depth data and triggering of the first computer. The scheme for automatic data acquisition is shown in Figure 8.

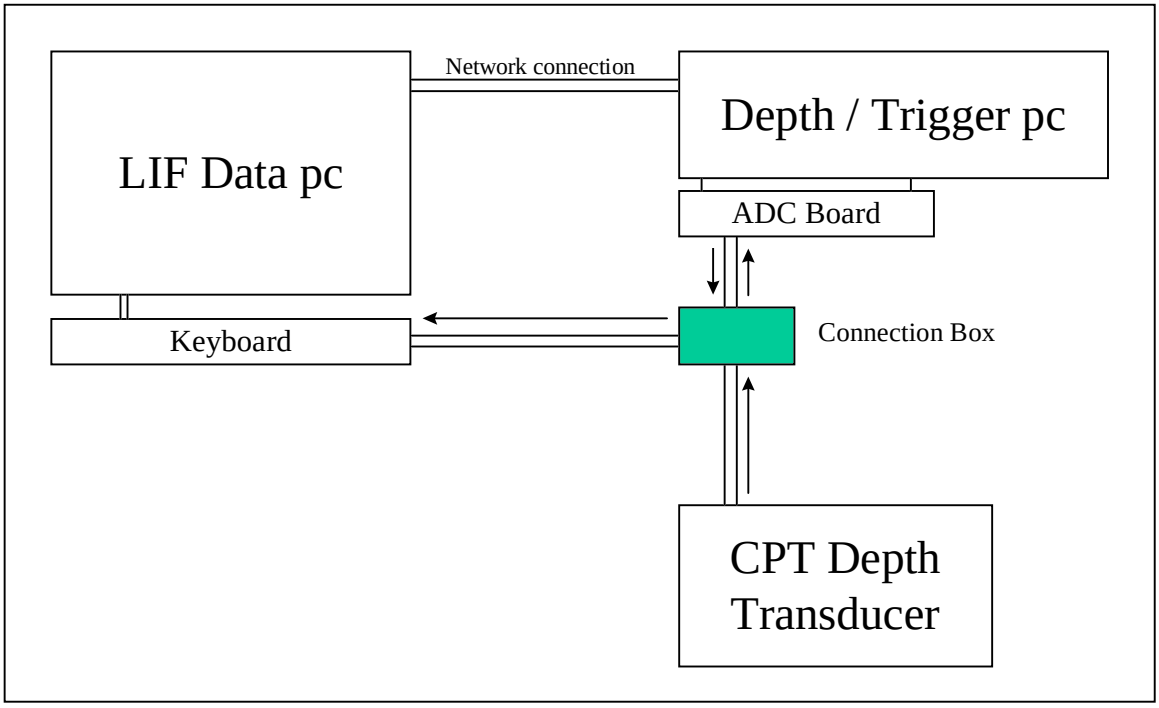

Figure 8. System for automatic acquisition of LIF and depth data.

The depth transducer in the hydraulic room of the CPT vehicle feeds a signal to a connection box, which serves to route the signal to the appropriate places. The voltage from the depth transducer is

captured by an 8 bit ADC board, and custom software written in visual basic (VB) converts the voltage signal to a depth reading. At depth intervals (0.125 to 1 foot) set in the VB software, two trigger signals are sent to the LIF data PC's keyboard by the depth / trigger PC to simulate commands. The first trigger starts data collection, saves the binary data file, and creates the new file for the next trigger. The second trigger initiates the conversion of the binary files to ASCII and the summation of the LIF data in each strip. The summed data can be transferred to the depth / trigger PC for graphical display or can be plotted on the data PC directly. The software developed for data acquisition and post processing also has the ability to display in real time the progress of the push: depth vs. total summed fluorescence for each channel. This system was not developed in time to be used during any of the field work described.

7) CPT vehicle installation of instrument

The fiber optic LIF-EEM instrument must be installed in the rear room of the CPT vehicle. All of the equipment must be secured and protected for the journeys between sites and for maneuvers on site. Towards that end, our system was ruggedized: the optical breadboard was mounted on a table built from Unistrut metal bars that were mounted on spring shock absorbing mounts (VMC, Bloomingdale, NJ). The electronic components were placed in standard 19" rack mount cases and secured in a rack that was bolted to the vehicle floor.

The laser system and the data acquisition equipment are kept in the rear room while the probe and fiber connectors are kept in the front hydraulic room. A short cable (length = 10 or 5 m) runs between the optical system and the hydraulic room in the cone penetrometer vehicle. Further details of the fiber optic cabling have been described in section 2) above.

8) LIF-EEM HPLC

The development and incorporation of HPLC into the field work was planned in two stages: 1) Incorporation of standard HPLC in the field using rapid extraction techniques for quick screening methods and, 2) The development of the LIF-EEM HPLC system for the analysis of core samples for comparison with *in situ* measurements. The standard HPLC system has been purchased, assembled, and tested. The methodology for rapid extraction and sample pre-treatment before HPLC sample injection has been chosen but not tested. The LIF-EEM detection system was designed to be added to the standard HPLC system so that the standard and LIF-EEM detectors operate in series. It involves the use of fused silica capillaries (Polymicro Technologies, Phoenix, AZ) to carry the post column eluent. The fused silica capillary has its jacket removed enabling the light from the excitation fibers to be focused into it and the fluorescence to be collected by detection fibers oriented 90° from the excitation fibers. Due to a rigorous

field testing schedule for the *in-situ* LIF-EEM probe (three field tests in four months), the development of the HPLC capability was not completed during the project.

B. Instrument Characterization

1) Wavelength calibration

One of the first and most important calibrations needed for the collection of useful spectral information is that of wavelength. The CCD camera can rotate within the spectrograph's exit opening before tightening a set-screw to fix its position. The rotational alignment must be carefully checked by observing the fiber images on the monitor to ensure that the wavelength axis of the spectrograph is parallel to the long axis of the CCD. Once this is accomplished, the CCD is then carefully focused to bring the CCD chip surface into the focal plane of the spectrograph. Once both alignments have been accomplished, the position is set and calibration can begin. The usual output of the CCD data acquisition is pixel numbers (the light intensity at each pixel across the horizontal axis). To calibrate to wavelength a standard mercury vapor lamp is used.

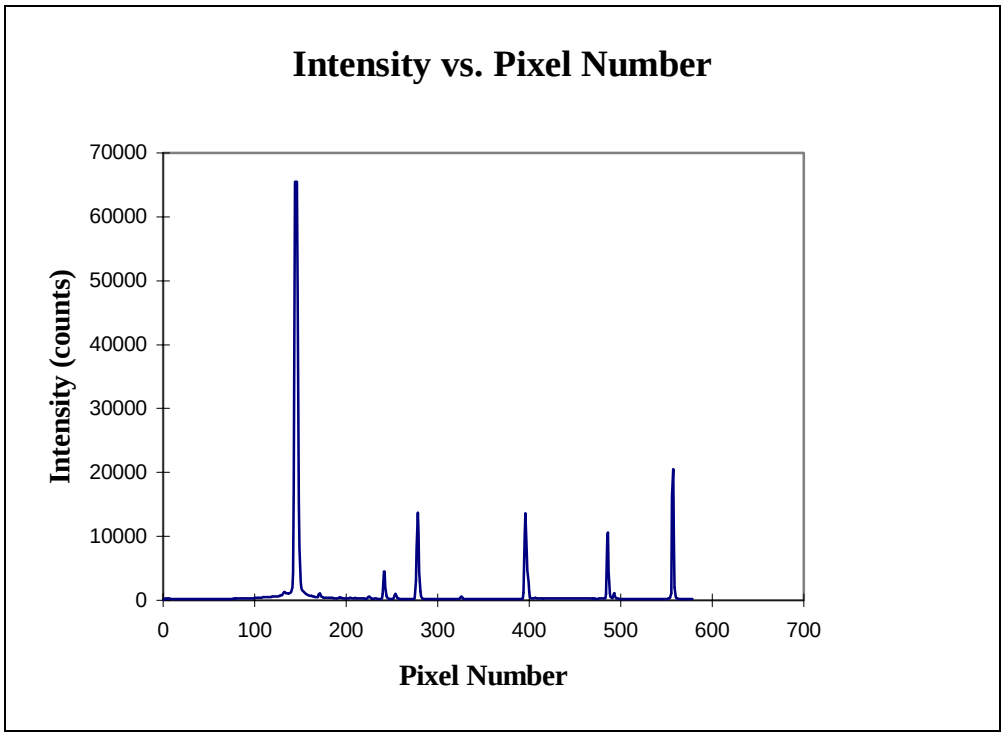

Figure 9. Standard mercury lamp spectrum used for calibration of the spectrograph and CCD detection system. The 6 peaks are assigned, in order from left to right: 253.65 nm, 296.73, 312.57, 365.02, 404.66, 435.83.

This is positioned a ¼ m away from a fiber bundle (a 5 m section of fiber cable with a spectrograph plug on one end and fiber connectors on the other). This is connected to the short cable in the CPT vehicle and the connectors attached to the emission fiber channels. The result is that mercury light is delivered to the spectrograph in exactly the same way (through the same fiber in the same positions) that calibrant and contaminant fluorescence will be delivered. Figure 9 is a typical mercury lamp spectrum showing the five largest lines in the wavelength region 250 nm - 450 nm. Using the known wavelengths of the major lines in the mercury spectrum, the data can be easily converted from pixel numbers to wavelengths using a linear or cubic polynomial fit.

2) Calibration curves

The overall response of the system to fluorescent compounds depends upon many factors beginning with the excitation source. The more excitation light that can be delivered to the sample (up to the compound's saturation or decomposition point), the more fluorescence will be seen. The amount of 266 nm light available from the laser to pump the Raman shifter will directly affect the amount of Raman shifted light available to be launched into the fiber optics. The position and condition of the fiber at the launch point has a dramatic effect on the amount of light delivered. The fiber optics have significant attenuation in the deep UV; therefore, when delivering short wavelength excitation beams they will deliver less light to the sample. Other factors affecting the overall sensitivity of the instrument include the overlap of the fiber optic distal cones on the sample surface, the efficiency of the fiber optic connectors, the coupling efficiency of the fiber optic / spectrograph plug, the throughput of the spectrograph, and the sensitivity of the CCD chip pixels. Overall performance has been quantified by generating calibration curves for a specific compound, and for a fuel in solvent on sand.

a) Aqueous phenol

In Figure 10, a plot of peak fluorescence response vs. aqueous phenol concentration is shown. The linear fit of the data is enhanced considerably when the highest concentration is eliminated, suggesting that the upper limit of phenol's signal response linearity is about 100 ppm. By extrapolation with the minimum detection signal set to baseline counts plus 3 times the baseline standard deviation, the LOD (limit of detection) for phenol in water was determined to be 2.7 ppm.

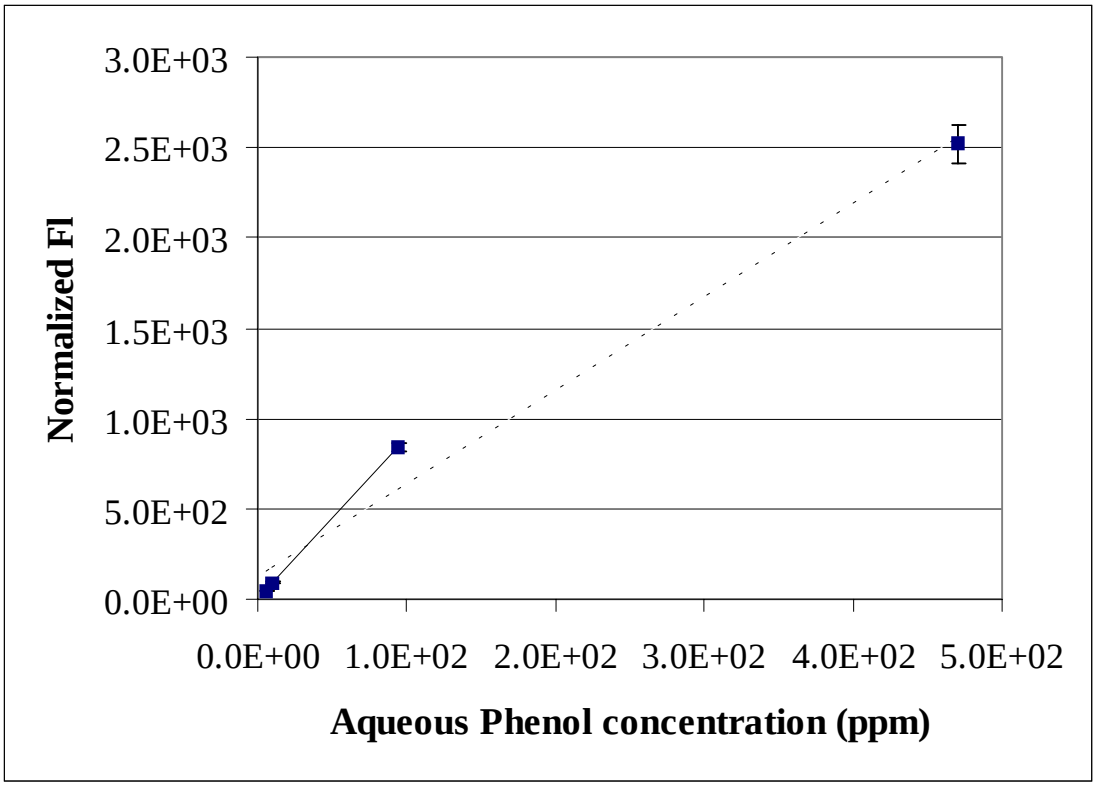

Figure 10. Calibration curve for aqueous phenol measured with fiber optic LIF-EEM probe with excitation at 266 nm. The equation of the line for the entire data (dashed line) set is y = 5.18x + 125.44, with r^2 = 0.9820, while the equation of the line for the data set less the highest concentration (solid line) y = 8.89x + 6.03, with r^2 = 1.0000.

b) JP5 in cyclohexane

The calibration of a LIF-CPT instrument using a complex mixture, known to be similar to the type of contamination found *in situ,* is a common method of converting LIF signal into a quantity well understood by the site characterization community[12]. A common contamination source at military petroleum-contaminated waste sites is jet fuel of the JP-X series, whereas at industrial sites diesel, gasoline and fuel oils are a more common source of contamination. Commonly, sites with older spills have either aviation-gas (av-gas) or JP-4 contamination. Currently, fuels such as JP-5 and JP-8 are being used and the former fuels are difficult to obtain. The compositions of these fuels are known to be similar, but with differing concentrations of fluorescent species[28]. The response of the instrument when the probe is exposed to a fuel is due to fluorescence from the many different fluorescent components present in jet fuels, potentially including interactions among the component species.

The use of a generic standard to quantify the *in situ* contamination, while useful, has many difficulties. Ideally, the *in situ* contamination should very closely approximate the fuel standard to allow a

positive identification to be made. This may sometimes be the case, but even if the original contaminant material were identical to the standard, weathering of the contaminant (e.g., loss of volatiles, bioremediation) generally occurs at different rates for the different components, resulting in an imperfect match between the weathered contaminant and the standard. However, the calibration of the instrument using a standard fuel is important for the characterization of the instrument even if the resulting calibration data are not applied to the actual field data.

In Figure 11, the response of the instrument to JP-5 in cyclohexane mixed with a medium grade sand is shown, measured on-site. Excess JP-5 solution was mixed with the sand and the mixture was allowed to stand. The excess solution was removed prior to measurement in a trough style sample holder onto which the probe is placed with the sapphire windows against the sample. The concentrations of JP-5 in cyclohexane were chosen to allow us to determine the response of the system to both low and high concentrations of jet fuel. The concentrations were in the 0.6 % (w/w) to 72.2 % (w/w) range. The lower concentration is similar to a smear zone or lightly contaminated zone, whereas the upper concentration is more similar to a pure product region, or saturated zone; both concentration regimes are expected to be present at jet fuel contaminated sites.

The responses of the instrument to the jet fuel on sand were linear with correlation coefficient squared values, r^2, generally above 0.9, with an average value of 0.951. There may be inner filter effects hampering the measurement of the upper concentration, 563 g/L. When the fits are repeated with this point deleted, regression coefficients (average 0.965) and intercept values generally improve. The regression coefficients for each excitation wavelength are listed in Table 3. These data were produced from detector dark current subtracted fluorescence sums and normalized with excitation energies derived from quinine sulfate

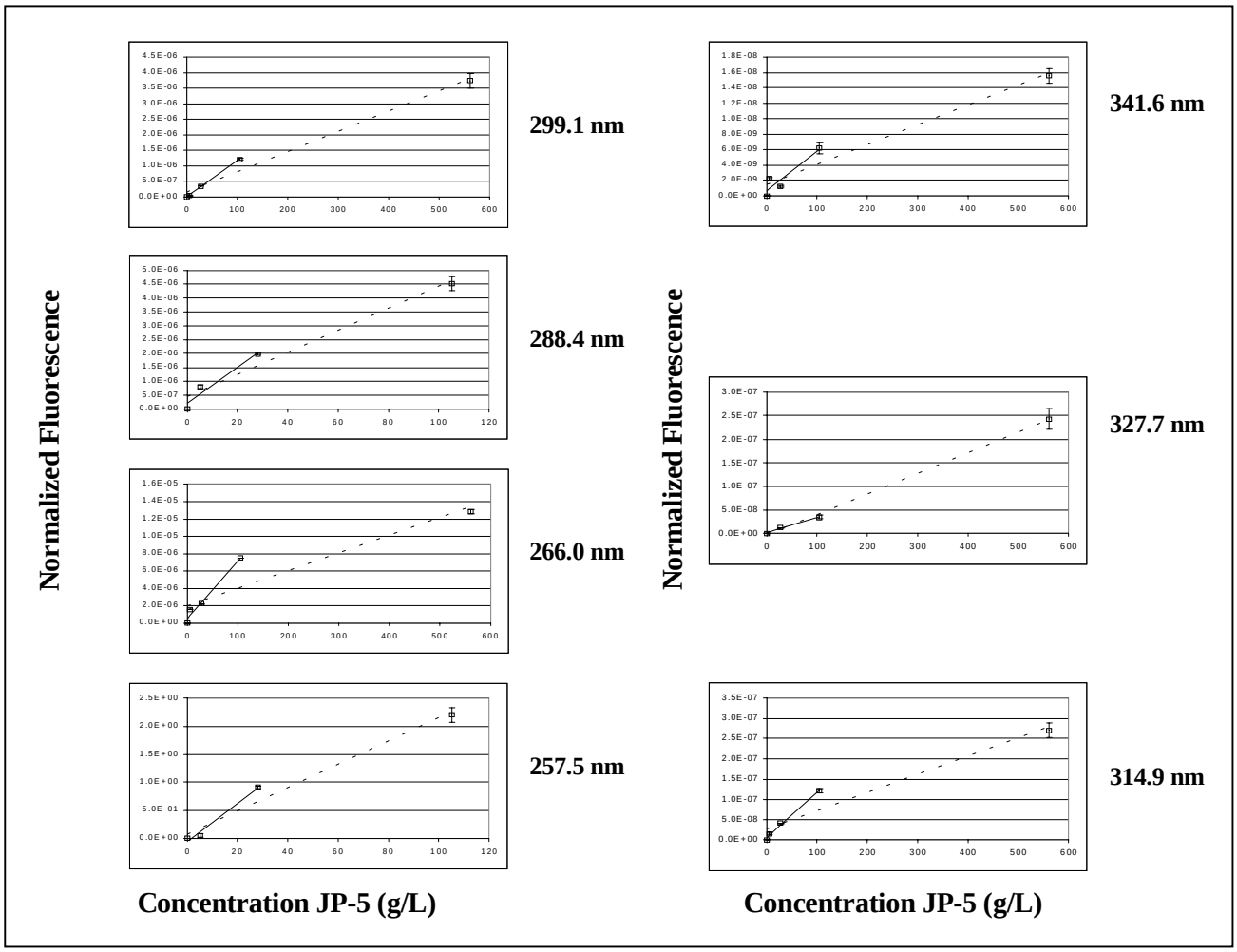

Figure 11. Calibration curves at each excitation wavelength for JP-5 in cyclohexane mixed with sand from USCG station, EC, NC measured with fiber optic LIF-EEM probe.

calibrations before and after each measurement. This is the same procedure used to analyze the field data (refer to section B.4). This was done to allow the direct comparison of the *in situ* summed fluorescence quantities to be correlated with a known amount of jet fuel, thought to be similar to some of the contamination seen at all of the sites involved. A comparison of field data EEMs (Figures 26, 27, 33, 36) with the JP-5 EEM (Figure 14 b) indicates that there are some *in situ* EEMs that are directly comparable to the reference jet fuel EEM, while others are unrelated indicating an entirely different type of contamination. For the related EEMs, the signal may be attributable to similar jet fuel contamination levels.

Table 3. JP-5 calibration curve regression summary. All data have been normalized using excitation energy data except the 257.53 nm channel where a quinine sulfate fluorescence sum was used without conversion.

		Full data set			Less highest concentration		
Beam	Excitation λ (nm)	Slope	y-int	r^2	Slope	y-int	r^2
-1	257.5	0.0209	0.0714	0.9726	0.0339	-0.0509	0.9874
0	266.0	2.044E-08	1.967E-06	0.8551	6.643E-08	5.341E-07	0.9745
1	278.5	-	-	-	-	-	-
2	288.4	3.988E-08	4.554E-07	0.9637	6.515E-08	2.174E-07	0.9406
3	299.1	6.478E-09	1.646E-07	0.9804	1.161E-08	4.805E-09	0.9990
4	314.9	4.514E-10	2.622E-08	0.9366	1.104E-09	5.894E-09	0.9928
5	327.7	4.343E-10	-3.211E-09	0.9979	3.226E-10	1.317E-09	0.9916
6	341.6	2.577E-11	1.439E-09	0.9515	5.181E-11	6.277E-10	0.8706

In calculating the LOD (limit of detection), a baseline sum y-intercept plus 3 times the error in the baseline was used. This corresponds to the summed fluorescence base line in the absence of JP-5 fluorescence. The calculated LOD for JP-5 in cyclohexane on a medium sand in 0.29 g/L. This LOD is for the channel most sensitive (containing the greatest fluorescence) to JP-5: the 288.40 nm excitation channel. All other channels should have higher LODs due to the lower light levels that are closer to the signal baseline.

3) Quinine sulfate fluorescence - system diagnostic tool and calibrant

A system calibration was performed before each push to accomplish two goals: 1) confirm system operation and channel integrity and 2) provide a measurement of beam intensity for photon normalization. The calibration compound used was quinine sulfate, well known as a fluorescence standard and to a lesser extent as a quantum counter. This calibrant was dissolved in ethanol and not the usual dilute H_2SO_4 due to damaging reaction of the latter with the steel probe body.

All of the probe channels report fluorescence, although not uniformly. This is due to several factors including the fiber optic attenuation of the strongest UV beams, and the low energy of the high order Stokes and first anti-Stokes beam. The net result is that the central channels (288.5 nm - 314.5 nm) have the largest signal. The emission spectra at the excitation wavelengths measured for standard quinine sulfate solution in ethanol (0.2 g/L) are shown in Figure 12.

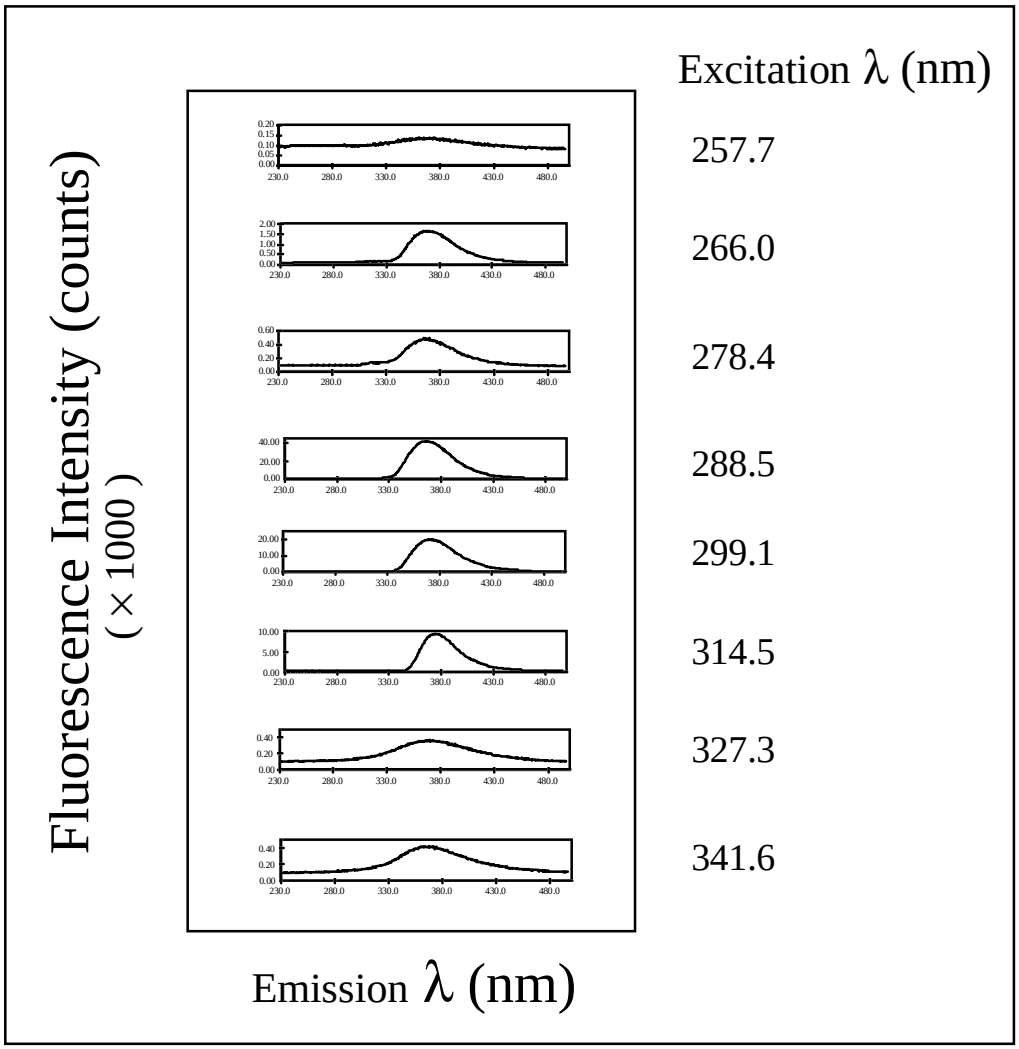

Figure 12. Fluorescence spectra of standard calibrant, 0.2 g/L quinine sulfate in ethanol, at the excitation wavelengths normally used.

For most fluorescent molecules in condensed phases, the distribution of fluorescence emission as a function of emission wavelength is independent of excitation wavelength; therefore the wavelength of fluorescence peaks of quinine sulfate at the different excitation wavelengths should be identical. This is not the case for the spectra shown in Figure 12 where there are apparent shifts in the emission maxima. The spectral shifts are due to the different cutoff filters used in each channel to reject scattered light.

4) Incident intensity vs. quinine sulfate fluorescence calibration

The correction of the probe-measured data for instrumental artifacts must be accomplished if the field data are to be compared to standard reference EEMs. If the reference EEMs are not standard, but are

produced on the same instrument, then full correction of the field data is not required, but reference EEMs for all analytes of interest must be collected whenever the instrument configuration changes, e.g., increasing fiber length to access deeper plumes. However, even when reference EEMs have been obtained on the instrument as configured for the field, variations in excitation energy in each channel can be appreciable and must be accounted for.

An expansion of Equation 1 to include the quantitative details of the fluorescence dependence is shown in Equation 2:

$$M(\lambda_x, \lambda_m) = k' G I_{pl}(\lambda_x) L(\lambda_x) T_x(\lambda_x) \varepsilon(\lambda_x) \Phi'(\lambda_m) T_m(\lambda_m) F(\lambda_m) S(\lambda_m) CCD(\lambda_m) c. \quad (2)$$

Comparison with Equation (1) shows that we have expanded $I(\lambda_x)$ into separate factors: $I_{pl}(\lambda_x)$, the pre-launch intensity of the excitation laser beam, $L(\lambda_x)$, the launch efficiency of the beam, and $T_x(\lambda_x)$, the transmission of the excitation fiber. Similarly, the detection sensitivity $D(\lambda_m)$ has been expanded to include $T_m(\lambda_m)$, the transmission of the emission fiber, $F(\lambda_m)$, the transmission of the selected cutoff filter, $S(\lambda_m)$, the spectrograph efficiency, and $CCD(\lambda_m)$, the sensitivity of the detector itself. Lastly, the instrument constant k of Eq. 1 has been replaced by $k'G$, where G is a geometrical factor accounting for the collection efficiency of the probe. G and S should have little or no intrinsic dependence on λ_x, but the fact that each excitation channel uses a different pair of fibers and a different path through the spectrograph can result in different numerical values of these two quantities for each excitation channel. For example, $S(\lambda_m)$ can vary for emission fibers positioned at different heights along the entrance slit of the spectrograph because of vignetting (smaller effective aperture of spectrograph for off-axis points) or other imaging aberrations.

For a given instrument configuration, we can reasonably expect the last four instrument factors in Eq. 2 to remain constant. Each of the component factors of $I(\lambda_x)$ can change: $I_{pl}(\lambda_x)$ varies in the short term because of shot-to-shot variations in the pump laser power, which are amplified by the nonlinear processes used to generate new frequencies, and it steadily degrades over the long term as the flashlamp ages and as optical elements degrade (especially, uv mirrors losing their high reflectivity). $L(\lambda_x)$ may vary from shot to shot as well; if the beam profile at the launch end of the excitation fiber has a spatial extent about the same as or larger than the fiber aperture, then any small variations in this profile can change the fraction of the beam that is successfully launched into the excitation fiber. In addition, any mechanical instabilities that result in movement of either the laser beam or the fiber end will reduce $L(\lambda_x)$ from its optimal value. Jarring shocks such as may be experienced when the cone penetrometer hits a cobble might induce such changes instantaneously during a push. Finally, $T_x(\lambda_x)$ can change due to

solarization, the loss of transmissivity experienced by a fiber that is strongly illuminated by ultraviolet light. This effect occurs relatively slowly over time, over hundreds of thousands or millions of laser shots, but at high laser repetition rates, its effects might be significant over the duration of a single site investigation. Of course, instantaneous fiber damage may occur if allowable peak power levels are exceeded, but we have already discusses strategies to avoid this more acute case of laser-induced decreases in $T_x(\lambda_x)$. By contrast, the emission fiber is not exposed to focused laser light at all; although the intensity of scattered laser light incident on the emission fiber is much higher than that of fluorescence, the laser light has been significantly attenuated by the excitation fiber and scattering by the sample, so solarization of the emission fiber is unlikely, as implied above. G should remain constant for a given probe channel unless physical damage occurs; this would be detectable by means of the visual inspection that is done routinely before and after every push.

In this work, we compared field EEMs only to reference EEMs generated with the same instrument; this allowed us to ignore both corrections for $D(\lambda_m)$ and the channel dependence of G. In the absence of visual detection of damage, G is considered constant for each channel. We utilized the average of fluorescence measurements of a standard solution of quinine sulfate in ethanol (into which the probe is dipped) immediately before and after each push to provide an estimate of $I(\lambda_x)$ during that push. In order to facilitate cleaning of the probe after this measurement, as well as for economic reasons, the quinine sulfate was not used at high quantum-counter type concentrations which would render its fluorescence response independent of its own wavelength-dependent absorptivity. Therefore the fluorescence response in each channel is not simply proportional to $I(\lambda_x)$ but contains a dependence on the concentration of quinine sulfate and its wavelength-dependent absorptivity. (This dependence could be removed, mathematically, in theory, but in practice the correction is hampered by our non-standard probe geometry, for which published analyses of signal level are nonexistent, and the fact that our quinine sulfate is neither quantum-counter thick nor optically thin.)

This complication, simply another channel-dependent correction factor, need not concern us as long as we are comparing EEMs from the same instrument. One simply normalizes the fluorescence intensity in each channel by dividing it by the average of before and after triplicate measurements of quinine sulfate fluorescence signal for that push; the resulting intensities are counts/quinine sulfate counts, or effectively dimensionless. We initially performed all our fluorescence normalizations this way. However, to better characterize our system and to pave the way for more complete data reduction schemes in the future, we also calibrated the quinine sulfate response in each channel by comparing it to the laser intensity at the sample as measured by laser energy probes. A post calibration (after field work was complete) was performed on the instrument using the same fiber optics, probe assembly, and operating parameters. The incident excitation energy was varied by adjusting the laser output power, and the fluorescence response of

quinine sulfate was measured as a function of laser pulse energy for each channel. The laser pulse energies, measured before and after the quinine sulfate response and averaged, were converted to photon numbers and plotted against quinine sulfate fluorescence counts as shown in Figure 13. The data are plotted with x and y error bars, and the regression line reflects a weighted fit using the summed fluorescence error bars. A summary of the regression coefficients is given in Table 4, r^2 values of 0.9 or higher. The quinine sulfate measurements made during the field test were then converted to the number of photons per pulse incident on the sample. This number, obtained from the calibration curve, was then used for the photon normalization of the data from each push. The resulting photon normalized number has units of fluorescence counts per photons of excitation light delivered. Post calibration data were taken for all excitation channels except 257 nm and 278 nm. For these channels, the summed fluorescence could not be converted to photons per pulse, so the raw number of summed fluorescence counts was used as the normalizing factor.

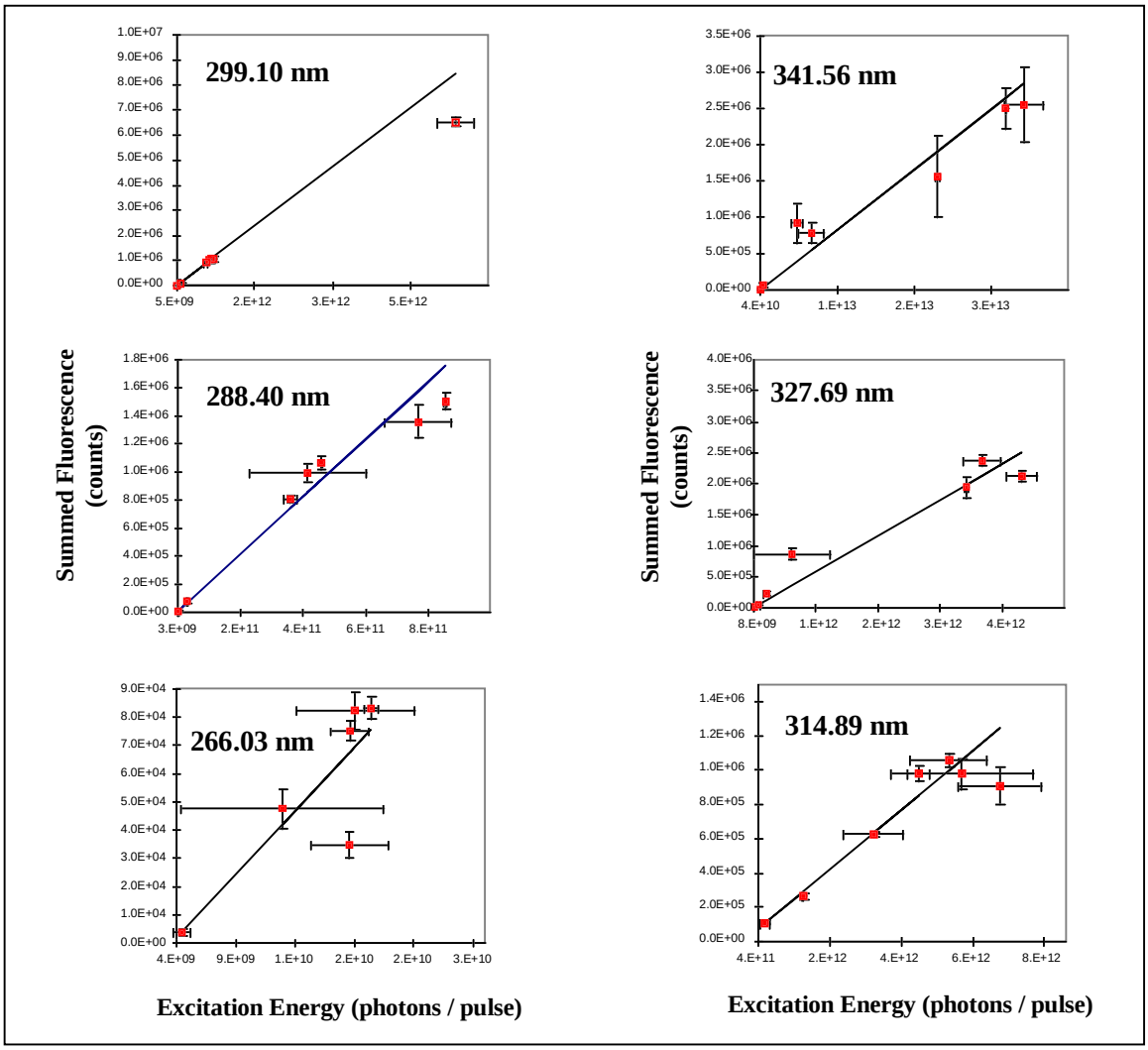

Figure 13. Calibration curves of incident excitation energy vs. quinine sulfate fluorescence.

Table 4. Quinine sulfate fluorescence vs. Incident excitation energy calibration curve regression summary.

Excitation λ (nm)	Slope	y-int	r^2
266.03	4.49E-06	-16233.30	0.8708
288.40	2.04E-06	3986.95	0.9830
299.10	1.57E-06	-678.89	0.9928
314.89	1.73E-07	6523.23	0.9929
327.69	5.76E-07	3641.85	0.9473
341.56	8.26E-08	3632.82	0.9081

5) Complex mixture measurements

Jet fuels

Lab measurements of jet fuels were made in various media. JP-4 was measured in cyclohexane (11 ppm), JP-5 measured in cyclohexane mixed with a medium sand (105 g/L), and JP-8 was measured neat on a soil sample (silty clay) from Hanscom AFB. The EEMs of these mixtures are shown in Figure 14, a,b,c. In Figure 14 a, the fluorescence intensity is low due to the low concentration of fuel relative to the others. In both Figures 14 b and c, the fluorescent intensities are much higher, as expected, due to the higher fuel concentrations.

The JP-4 EEM has significant signal arising from both the 288.4 nm and 299.1 nm excitation channels, with a peak EEM fluorescence at (λ_x, λ_m) of 299.1 nm, 340 nm. Similarly, the JP-5 EEM has signal arising from both the 288.4 nm and 299.1 nm excitation channels, but with a peak EEM fluorescence at (λ_x, λ_m) of

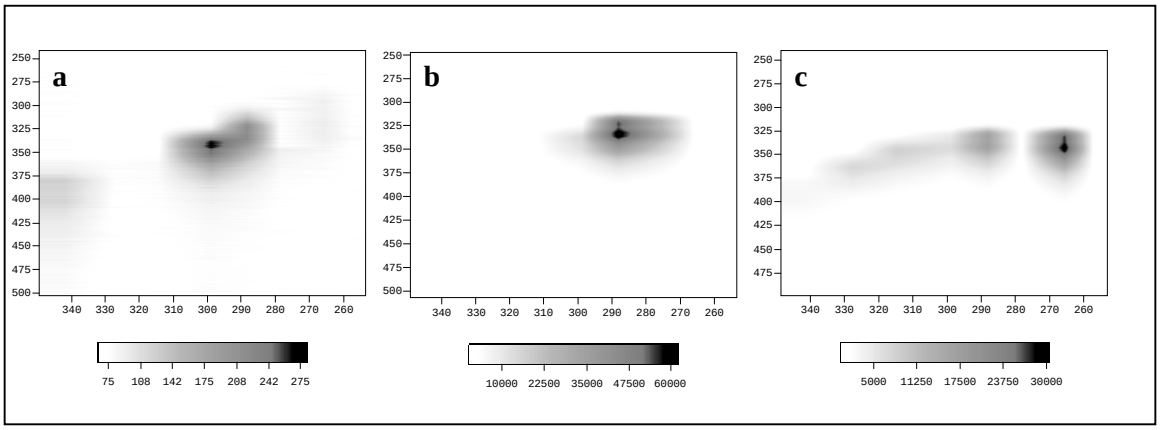

Figure 14. EEMs of a) 11 ppm JP-4 in cyclohexane, b) 105 g/L JP-5 in cyclohexane mixed with sand from USCG, EC, NC and, c) neat JP-8 mixed with silty clay from Hanscom AFB . In each case, the vertical axis represents excitation wavelength (nm) and the horizontal axis represents emission wavelength (nm).

288.4 nm, 330 nm. The JP-4 EEM has other features, notably the long wavelength fluorescence extending from 375 nm to 450 nm in the 341.1 nm excitation channel. The JP-8 sample has a different EEM pattern characterized by a peak EEM fluorescence at (λ_x, λ_m) of 266.0 nm, 340 nm. There is additional

fluorescence at excitation wavelengths 288.4 nm – 327.7 nm.

6) Single component EEMs

The collection of single component EEMs with the LIF probe is important for EEM analyses. Having a library of carefully measured EEMs of suspected contaminants is essential for a complete comparison of unknown field data EEMs with the standards. In some cases the fitting of standard mixtures such as jet fuels (JP - 4, 5, 8) is acceptable, but in other situations a more specific answer is sought. Towards that end EEMs of single compounds were measured in differing solvents.

Figure 15 shows EEMs of a) 10 mM phenol in distilled water, b) 0.126 g/L naphthalene in cyclohexane, and c) 50 mM anthracene in cyclohexane. As seen, EEMs provide very fine fingerprints of the compounds which can be used for identification and quantitation of fluorescent contaminants. These three EEMs illustrate distinct

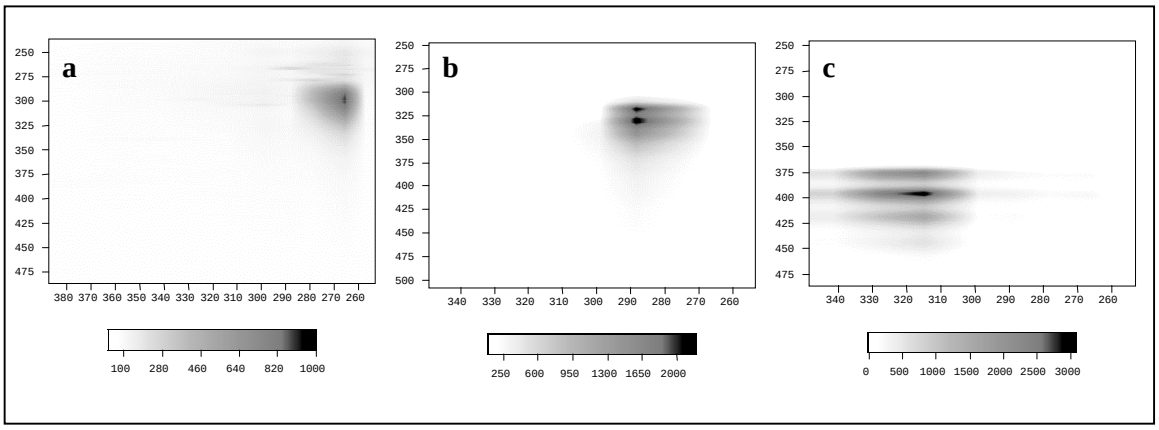

Figure 15. EEMs of a) 10 mM phenol in water, b) 0.126 g/L naphthalene in cyclohexane and, c) 50 mM anthracene in cyclohexane. In each case, the vertical axis represents excitation wavelength (nm) and the horizontal axis represents emission wavelength (nm).

regions of compound fluorescence excitation and emission that our system is capable of measuring. In addition, these compounds represent three major classes of aromatic contaminants: single, double and triple ring species. The EEM of the phenol sample has its peak EEM fluorescence at (λ_x, λ_m) at short wavelengths: (266 nm, 300 nm), while the naphthalene EEM is shifted towards the center of the EEM with maxima at (289 nm, 325 nm). Furthermore, as the aromatic conjugation is increased with increasing ring number, the excitation and emission are further shifted to longer wavelengths such as with anthracene, Figure 15, c, whose EEM maximum occurs at (315 nm, 400 nm).

The naphthalene EEM, Figure 15b, and JP-4 and JP-5 EEMs, Figures 14 a and b, are directly comparable. One would expect the reference samples (naphthalene, JP-4 and JP-5) to resemble each other because of the presence of naphthalene fluorescence in the jet fuel EEMs. This is consistent with our knowledge that the characteristic fluorescence signatures of these jet fuels are dominated by naphthalene and its derivatives, which have higher absorbances and fluorescence quantum yields than the BTEX components.

7) Multicomponent EEMs

Benzene, naphthalene, anthracene

An important measurement made was a 3 component mixture of representative 1, 2, and 3 ring compounds. This measurement allows us to clearly examine the instrumental response from three important classes of compounds. The standard mixture measured contained: 3 % (v/v) benzene, 86 ppm (w/w)

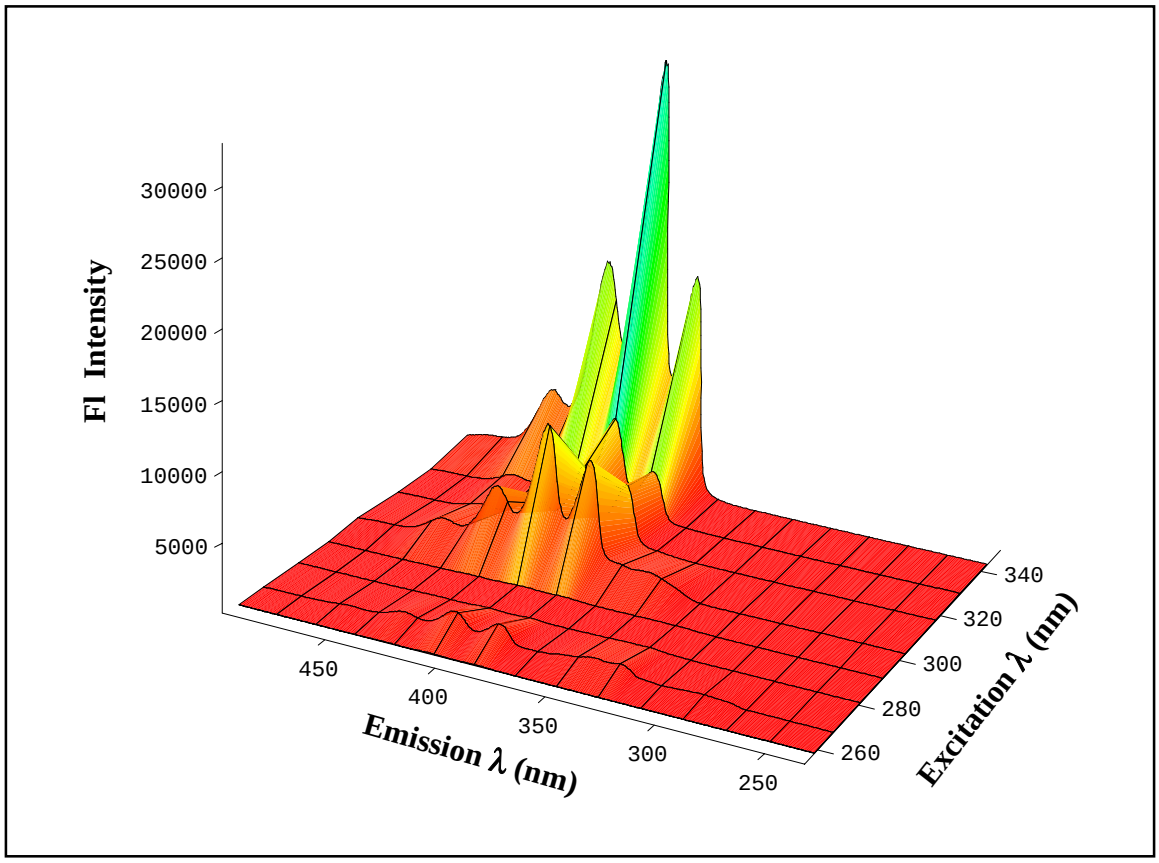

Figure 16. EEM of 3% Benzene, 86 ppm naphthalene, 86 ppm anthracene mixture in cyclohexane. FL intensity is given in counts.

naphthalene and 86 ppm (w/w) anthracene in cyclohexane. The EEM of the 3-component mixture is shown in Figure 16. The characteristic quadruplet of anthracene dominates, and to shorter excitation and emission wavelengths the naphthalene doublet (330 nm peak) and finally the emission of benzene (280 nm peak) can be seen in the 266.0 nm excitation channel. The single spectrum for the 266.0 nm excitation channel for the standard mixture is shown in Figure 17. While the anthracene fluorescence in the long wavelength excitation channels of the EEM in Figure 17 is still the most intense, the smaller naphthalene and benzene signals can clearly be seen. There are three distinct regions of fluorescence emission in this EEM, and the excitation channels contain little overlap. The 266 nm channel has emission from all three compounds, and the 299 nm channel has both naphthalene and anthracene, but the rest remain separated. This separation shows the ability to discriminate between these classes of compounds in the emission dimension. The excitation dimension is omitted only to more clearly show the emission spectrum detail.

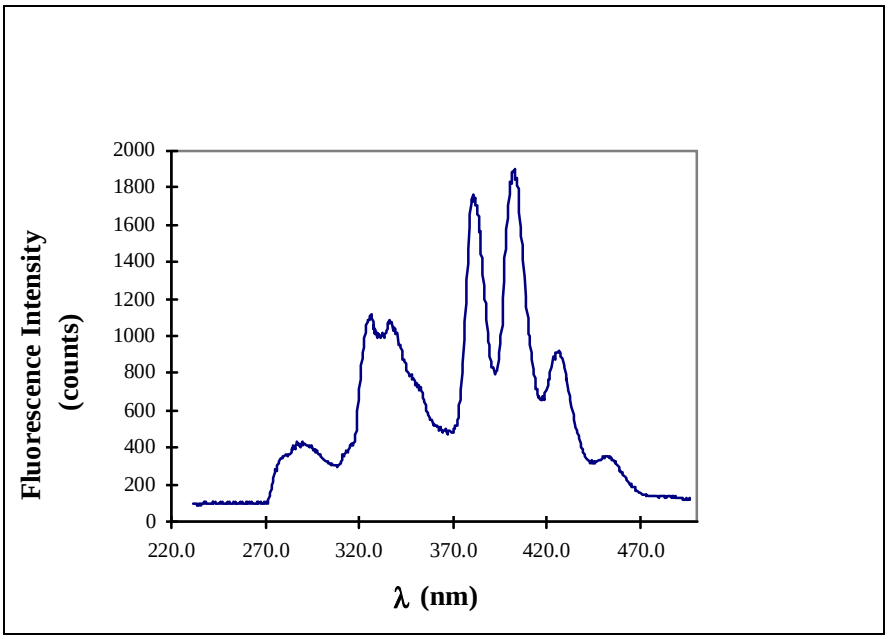

Figure 17. Fluorescence spectrum (266.0 nm excitation) from 3 % benzene, 86 ppm naphthalene, 86 ppm anthracene mixture EEM.

8) Solid-containing samples

Aqueous phenol solution was measured in Ottawa Sand (EM Science, Gibbstown, NJ). The EEM of phenol in solution alone is shown in Figure 18a for comparison, and the EEM of phenol in Ottawa sand is shown in Figure 18b. The absolute peak signal in solution was 860 counts vs. 554 counts when the phenol solution was mixed with sand. This 36 % loss of signal is at least partly due to the excitation light penetration depth being reduced in Ottawa sand (particle size 420-595 mm) vs. that in solution.[27]

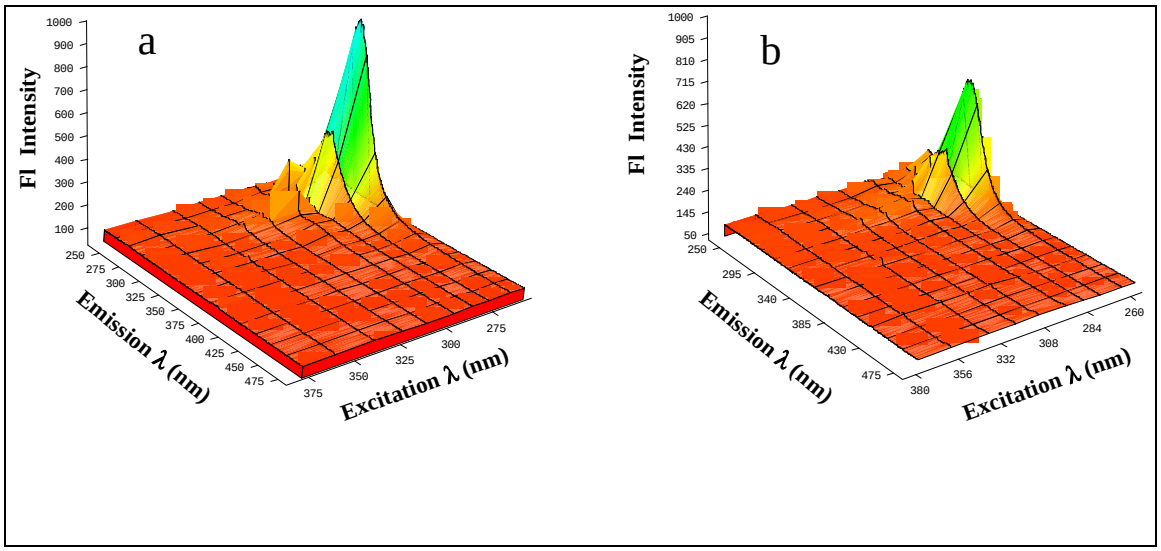

Figure 18. a) Aqueous phenol (940 ppm), b) Aqueous phenol (940 ppm) mixed with Ottawa sand.

V. FIELD WORK

A. Methods

1) Operations

a) Installation and optimization

The first task when arriving at a site for field testing is the physical installation of the system in the rear room of the CPT vehicle. This involves the mounting of the optical breadboard on the spring mounted table, and all electronics in the rack mount cabinet. All other instruments must be secured before movement of the CPT. The fiber cable ends are threaded through the hole in the wall separating the instrument and hydraulic rooms. The two cables are connected at the fiber connector box and the cable ends are attached to the appropriate instruments. The probe end with the ten fiber holders is threaded through the push rods and then the assembly of the probe can commence.

After the physical installation has been completed, the calibration and optimization of the system can begin. Wavelength calibration is done first, as described above, before the filters are placed in the fiber optic connectors. The filters are then installed and the operation of the system is evaluated beginning with the 4^{th} harmonic output power of the laser and the appearance of the Raman shifted beams. The beams are launched into the fibers and the identities of the beams at the probe end are confirmed. The probe can then be placed in the quinine sulfate standardization solution for optimization. The x, y, and z positions of each fiber launch stage are adjusted until a maximum signal is seen due to the increased amount of excitation light being launched. After obtaining acceptable signal levels in all channels, the system is ready for performing field measurements.

b) CPT-LIF measurements

Each push begins with a measurement of the standardization solution: quinine sulfate in ethanol. This measurement performs two functions: 1) It alerts the operator of any changes in the performance of the system and, 2) It records the specific performance data for the given push that is used in the data analysis routines to power normalize the resulting push data. The push begins at low resolution (1/2 to 1 foot) until contaminant signal is seen, when the push is slowed and the resolution increased (1/4-1/8 foot). Another mode of operation is possible where the CPT operator advances the probe at a standard rate (ASTM, 2cm/s for example) and the LIF instrument operator collects data continuously. If any push locations appear to have more regions of interest missed during the descent, they can be probed on the

way up, although this type of analysis may be plagued by soil and contamination smearing against the sapphire window. At the end of the push, the probe is cleaned and the same quinine sulfate solution is re-measured to document any changes in the instrument performance.

2) Data analysis

a) Accomplishments to date

A system such as our LIF EEM probe generates a large quantity of data. Several data analyses can be performed at different levels of complexity for various purposes. The simplest analysis scheme we have used involves total fluorescence in each channel, i.e., the summation of detector pixel intensities at all wavelengths greater than the excitation wavelength of the channel in question. This amounts to data reduction where the emission wavelength information is suppressed in order to allow rapid visualization of total signal as a function of depth. This type of data analysis has been utilized to produce the plots of total signal vs. depth similar to total or peak fluorescence intensity vs. depth provided by other LIF-CPT tools (in addition to their other display modes). The main difference is that our system has 7 - 10 signal vs. depth plots (7 - 10 excitation λ) for each push location compared with one for other LIF-CPT systems. This simple analysis has been incorporated into our automatic data acquisition and processing software. It provides a crude estimate of contamination level versus push depth. The differences among the signal vs. depth plots for each excitation wavelength provide evidence of changes in contaminant composition (and/or soil type, moisture content, etc.).

An algorithm and program have been developed for a more robust version of the above data analysis. The simple data analysis described above does not correct for any instrument functions and is therefore only a crude indicator of the contamination levels encountered by the probe. The robust version includes a background (in this context, detector background, due to dark counts and read noise) subtraction, summation after excitation peaks, normalization, and full error propagation of the resulting intensities. The normalization amounts to the division of the summed intensities by a number specific to each channel. This number is the average of the background-subtracted summed fluorescence of the quinine sulfate measured before and after each push. This procedure accounts for variations in the system performance from push to push.

A further variation on this theme is the use of a calibration curve, fluorescence of quinine sulfate as a function of incident excitation energy, for photon normalization as discussed in detail above (II.B.4). With this working curve, and the relation $E_{photon} = hc/\lambda_x$, the quinine sulfate sums can be converted to the number of photons per pulse for each push. The data are treated in exactly the same way, but with the

normalization data in photons per pulse being calculated from the working curve. It must be noted that while the normalization procedure accounts for push to push variations, short-term variations (point to point within a push) cannot be corrected.

An extension of the summed fluorescence analysis to obtain a concentration plot for each push location has been done. This involves the use of a system calibration curve with a known standard fuel mixture. The standard fuel fluorescence is treated in exactly the same way as the field data. Using this calibration curve, the field data can be converted to equivalents of the standard calibration fuel and the concentration can be plotted as a function of depth. The standard fuel chosen must have significant spectral similarities with the EEMs seen at the site for this to be valid.

Further compression of the multidimensional data to give a single "grand" fluorescence sum as a function of depth might be desirable to provide operators with a real-time display, or for general use as a simple indicator of contaminant distribution. Because variations in laser output, both absolute and relative, in the various excitation channels, such a summation should use background-subtracted, photon-normalized summed fluorescence from each channel as input into the "grand sum." Because the different excitation wavelengths of our current probe sample the soil at different depths, some interpolation or other approximation must be made to obtain the "grand sum" at a specified depth. Work is in progress to provide such plots for each push at Hanscom I and II and EC.

B. Field Sites

1) Hill Air Force Base

The site chosen for the first deployment of our LIF fiber-optic probe sensor was Hill Air Force Base, near Salt Lake City, Utah. It was selected by EPA personnel at RSKERL (Robert S. Kerr Environmental Research Laboratory) in Ada, Oklahoma due to their previous experience at that site. A map of the AFB is shown in Figure 19 with the area of investigation circled. The area of CPT investigation was an abandoned fire fighting pit and fuel storage facility.

a) Site Operations

The field work performed at Hill Air Force Base (AFB) in Salt Lake City, Utah on September 12-20, 1994, represents the first CPT vehicle deployment of our system[25,29]. The system deployed was the first version that had just been assembled prior to departure for the field exercise. The field test was preceded by an installation in late August, 1994 of the system in the CPT vehicle stationed at the RSKERL in Ada,

Oklahoma. The CPT truck with the installed system was driven from Ada, OK to the AFB in Utah where work began September 12, 1994. This first field exercise was hampered by the arrival of the designed probe components only days before departing for the field test. In fact several of the needed items were shipped from the probe manufacturer (ARA, South Royalton, VT) directly to the field location. The installation of the probe took three days and on September 15, 1994, the first push was made.

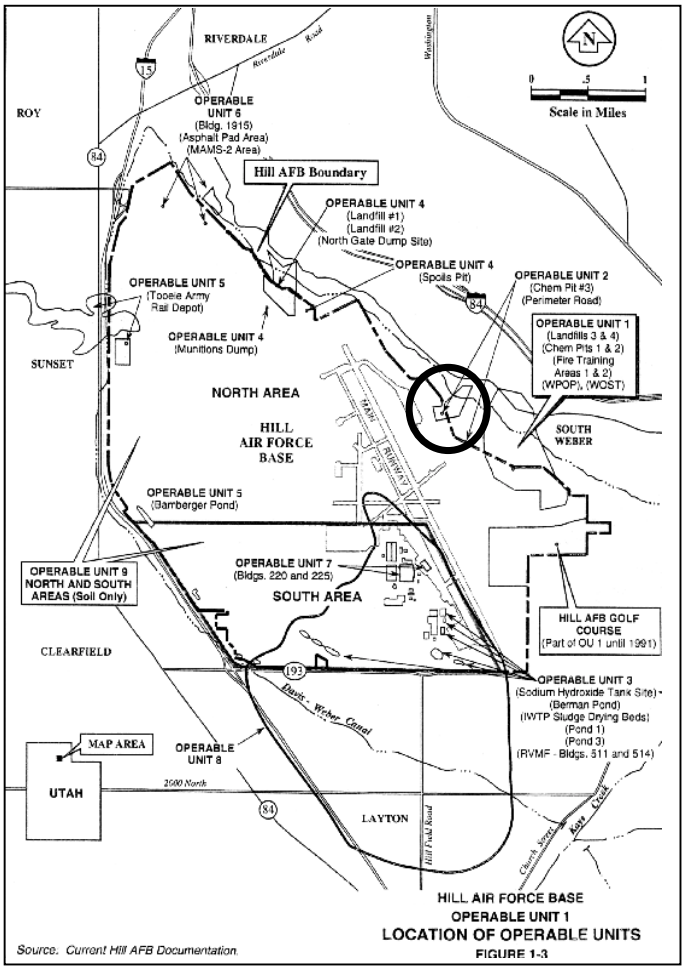

Figure 19. Jet fuel contaminated site at Hill Air Force Base situated near SLC, Utah. The circle indicates the location on the base of the LIF-CPT testing.

Two of ten sapphire windows were broken during the first push, presumably because some of the window plugs could not be screwed into the probe body completely and, thus, the sapphire windows were not flush with the probe surface. They were replaced and other window plugs were readjusted. No window breakage occurred during the following two pushes. About fifty exposures of the CCD camera detector were taken at different depths during each of the pushes (to a depth of about 20 feet). Each exposure acquired nine fluorescence spectra each of which was excited by a different laser wavelength.

(Two of twenty-one fibers in the long cable were broken and, thus, only nine channels were available with the remaining nineteen fibers).

Three pushes were completed in total during the field test that was cut short by damage to our laser power supply, probably caused by inadequate generator capacity. The CPT vehicle generator was not capable of supporting both our laser and the rod steam cleaning system simultaneously. Nor could the instrument remain powered up when the vehicle was in motion, maneuvering between push locations at the site. This necessitated turning the laser system on and off many times during the day, a very unfavorable situation. On one particular occasion, the electrical system was shut down and then restarted without warning. The generator surge pulse damaged a PC logic board in the laser resulting in unrecoverable failure. The three pushes accomplished were later found to be in a region that had < 200 ppb contamination (equivalents of fuel), i.e., below detection limits as measured by another more established LIF system. In the absence of fluorescence data, the scattered light was analyzed as a function of depth.

b) Field Results

As discussed above, the scattered light (reflection from surfaces, scattering by soil particles, and Rayleigh scattering) is reduced by long-pass cut-off filters. More than 90% of the back-scattered light is removed by the filters and by attenuation over the optical fibers. It is intended not to completely remove the scattered light because (1) complete removal results in significant reduction of the fluorescence emission and (2) the small residual scattered light can be used for diagnostic purposes.

Figure 20 shows profiles of scattered light vs. depth profiles for different excitation wavelengths obtained at Hole T-13 during the field test. The variations in the scattered light appear to be caused by the changes in soil samples because (1) the variations in the scattered light are larger than the variations in intensities of the laser beams and (2) the patterns of the variations are fairly consistent among the different wavelengths. The profiles seem to indicate that there were some noticeable changes at depths of 2, 13, and 17 feet.

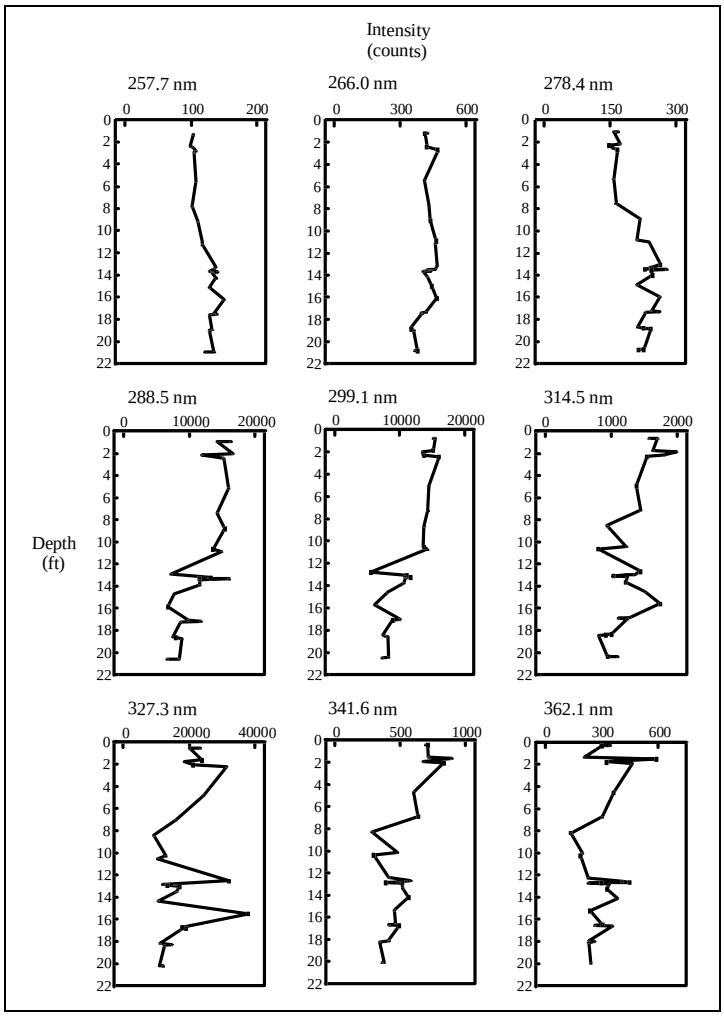

Figure 20. Scattered light vs. depth for different excitation channels for push T-13 at Hill AFB.

2) Hanscom Air Force Base I

Hanscom AFB is located in the central part of Middlesex County, Massachusetts, approximately 14 miles northwest of downtown Boston and 11.5 miles south of downtown Lowell, Massachusetts. The Base comprises approximately 826 acres and occupies land in the towns of Bedford, Concord, Lexington, and Lincoln as shown in Figure 21. Prior to 1973, the primary mission of Hanscom AFB was the operational maintenance of fighter aircraft and research and development (R&D) support. In August 1974, the original

lease permitting the operation and maintenance of the runway and flightline activities was canceled following the termination of Air Force flying activities in 1973. The airfield reverted to state control and was renamed L.G. Hanscom Field, currently operated by the Massachusetts Port Authority (Massport) as a

civilian airport. The remainder of the property was retained by the Air Force to support the current mission which is Research and Development and Command, Control, Communications, and Intelligence.

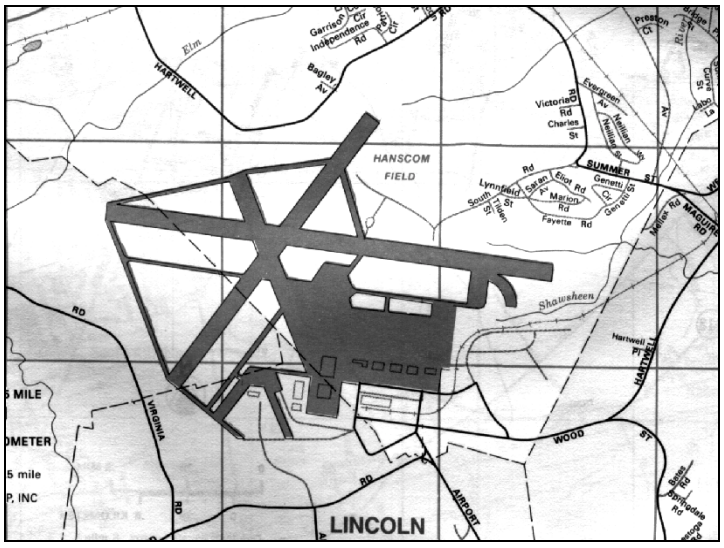

Figure 21. Map of Hanscom AFB, MA and Surrounding Area.

The site under investigation is the former fuels area which included off-loading, storage and dispensing facilities for jet fuel, aviation gasoline, and more recently, No. 2 fuel oil. The site is approximately 7.5 acres in size and is located in the northeast corner of Hanscom AFB, south of Massport Runway 29 and the Shawsheen River. The storage facilities included two 500,000 gallon above ground jet fuel tanks, five above ground 50,000 gallon aviation gasoline tanks (ASTs) and six underground 12,000 gallon jet fuel/aviation gasoline tanks (USTs). Also included at the site were fuel loading/off-loading stands, a rail siding, and pump houses. The aviation gas system was taken out of service in 1973 and the 50,000 gallon ASTs were removed in 1986. The 500,000 gallon jet fuel storage tanks were abandoned in 1973; however, they were not removed until 1990 when both tanks were pumped free of oil, cleaned and dismantled. During the oil shortage period in the 70's the westernmost 500,000 gallon tank was used for the storage of No. 2 fuel oil.

In 1990 Hanscom AFB discovered evidence of historic releases of jet fuel and/or No. 2 fuel oil. Investigations to date confirm that there are two separate plumes of light non-aqueous phase liquid (LNAPL) and that there are multiple locations of petroleum contaminated soils and BTEX contaminated groundwater. The sources of this contamination are believed to be the underground piping associated with former rail siding unloading systems and one or both of the former 500,000 gallon above ground jet fuel storage tanks. A map of the site is shown in Figure 22.

The availability of information regarding location and quantity of contamination and type (pure product vs. smear zones) was important in choosing this site. The history of the site provides us with additional clues about where the product is traveling to or where it might be pooling and collecting. In Figure 21, the

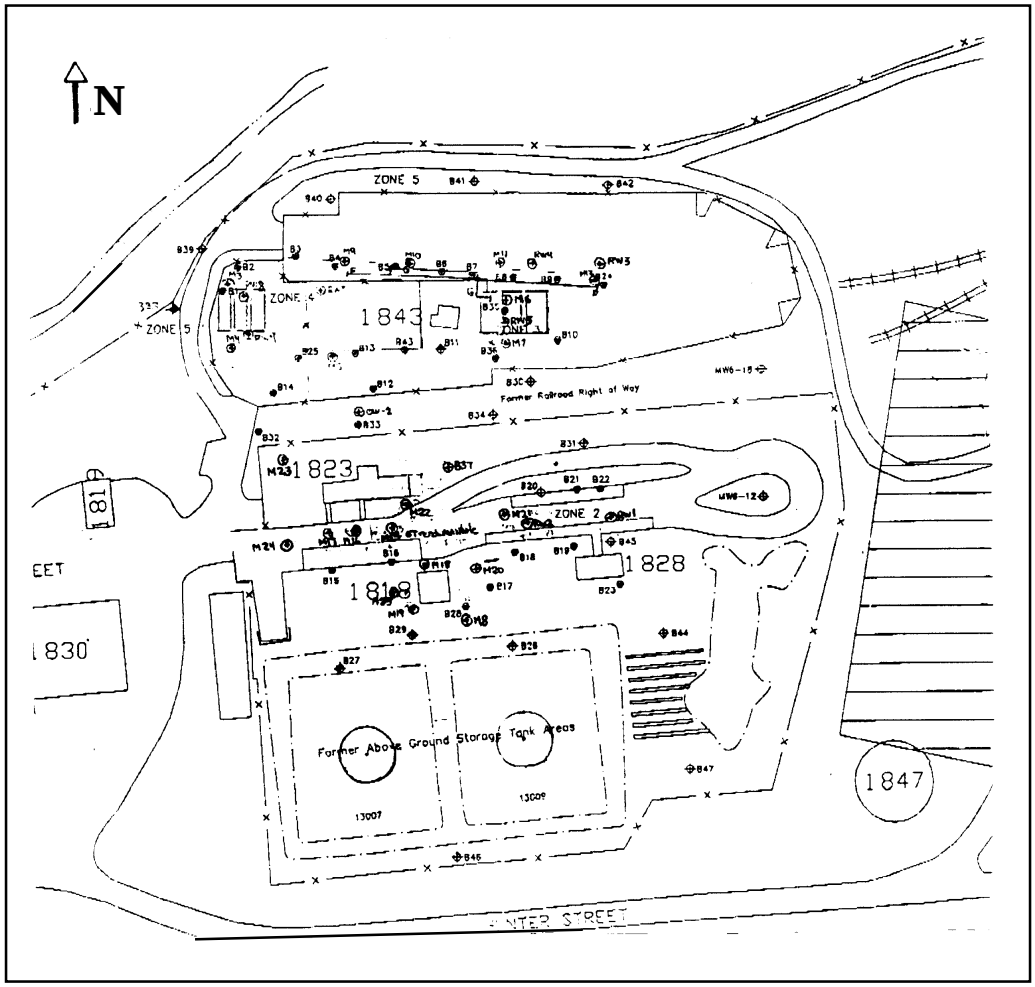

Figure 22. Map of Hanscom AFB Former Fuels Area.

Shawsheen River can be seen immediately northwest of the site. The Shawsheen River recharges the Town of Bedford wellfield 1.5 miles downstream and the Town of Burlington has a water supply inlet 4 miles downstream. With the river so nearby, it is imperative to know the boundaries of the pure fuel product plumes and the extent of BTEX contaminated groundwater.

Hanscom AFB is conducting a CERCLA Remedial Investigation of the site to determine the complete nature and extent of contamination and has conducted interim removal actions since the original

discovery of the petroleum contamination. Hanscom AFB is currently conducting a CERCLA Removal Action which includes groundwater treatment and soil vapor extraction (SVE) systems. The current system involves nine (9) dual phase recovery wells and three (3) dual phase recovery trenches. The soil vapor extraction system is designed to remove volatile compounds from the soil gas whereas the groundwater treatment system removes floating product and BTEX. Over 2,000 gallons of product has been recovered since this dual phase system commenced operation in October 1995.

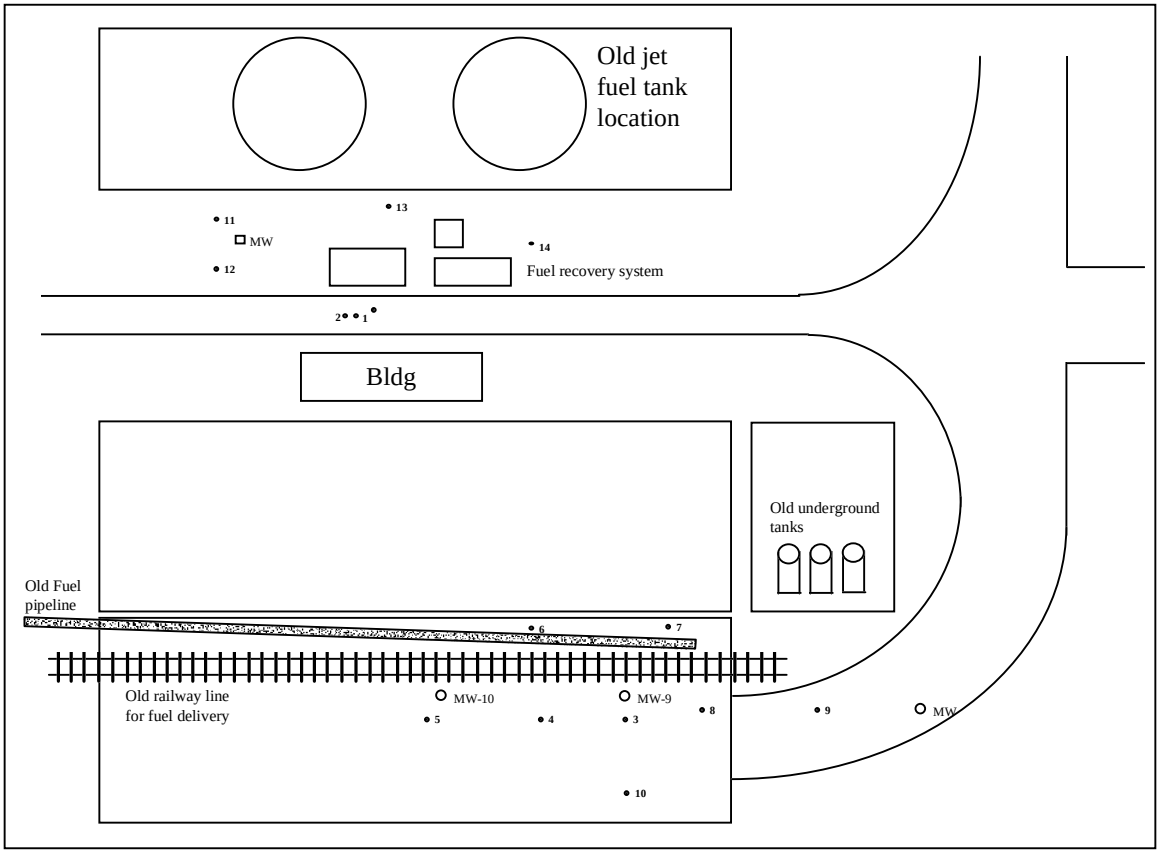

Figure 23. Map of CPT-LIF push sites at Hanscom AFB.

a) Site Operations

The CPT vehicle arrived at Hanscom AFB on June 20, 1996, in order for the installation to be completed before EPA personnel arrived for the start of data collection. Preparation of the vehicle for the arrival of the instrument was needed before any items were brought to the site. The moving and installation of the instrument began immediately thereafter. The adaptation of the laser electrical supply cables to the output connectors of the portable generator that had been rented was needed. The extra long

insulated cable (30 feet) was constructed and the entire electrical system was tested before the actual test began. As soon as all items were in place and in order, the installation of the probe began. During the probe installation, the first difficulties were encountered: the inner probe body was scratched and it would not fit into the outer body housing. The tolerances of the two probe pieces are quite small and any bends and/or scratches make the fit difficult. This was overcome by a trip to a machine shop where the tolerances on the pieces were opened up slightly. After the reworking of the probe inner and outer housings, the installation went smoothly, but we had been put behind schedule by two days. The installation was completed on June 25, when the EPA personnel arrived. One more day was necessary for instrument setup and calibration and by the morning of June 27, we were ready to begin operation. During the following field measurements, 14 locations were pushed in 2.5 days of sampling. The push locations for Hanscom AFB I are shown in Figure 23. In brief, *in situ* fluorescence was detected at push sites 1-13 and none was seen at push 14.

b) Field Results[23,30]

Our primary objective during this work was the demonstration of our instrumentation, not site characterization. The outcome of our field test at Hanscom AFB will be evaluated on that basis. While the instrument and the analysis of the data are still the subject of much research and development, we note the successful collection of a significant number of calibration and measurement data sets. Approximately 30 files were recorded during a push including calibration data. The total amount of raw data per push stored on the computer's hard disk is approximately 2 MB; with files generated during analysis that number is easily tripled. Even in the crudest mode of operation (detect or non-detect at > 20 depths / push location) the data show the capability of the system to rapidly characterize a site and the extent of contamination. The data shown and discussed are by no means a complete and representative sampling of the type and scope of data analysis that is possible with the data collected. In fact the current data analysis consists of one of the simplest analysis schemes involving raw data reduction. Future work involves a more complete mathematical analysis of the data using matrix least squares fitting algorithms with library EEMs for speciation.

In the assessment of our instrument's operation during field work, the first step is the analysis of the calibration data. The next step is the production of plots of summed fluorescence vs. depth for each push, which allow easy examination of the peak contaminant signals versus depth. The current analysis does not involve EEM analysis but qualitative discussion of representative EEMs is presented and demonstrate the "fingerprint" quality of the EEM data obtained.

1. Calibration data

The quinine sulfate solution was measured in triplicate before each push. The results are shown graphically in Figure 24. The changes in the fluorescence response of the calibrant, quinine sulfate, throughout the entire field test are given for each of the excitation wavelengths. In addition, error bars (standard deviations at the 95 % confidence level) for each quinine sulfate summed fluorescence average are given. The percent standard deviation ranged from 0.2 to 28. The data were used to normalize the fluorescence data from each push relative to the incident excitation intensity available during that particular push. The variations were large and could have adversely affected any attempts at contamination quantification.

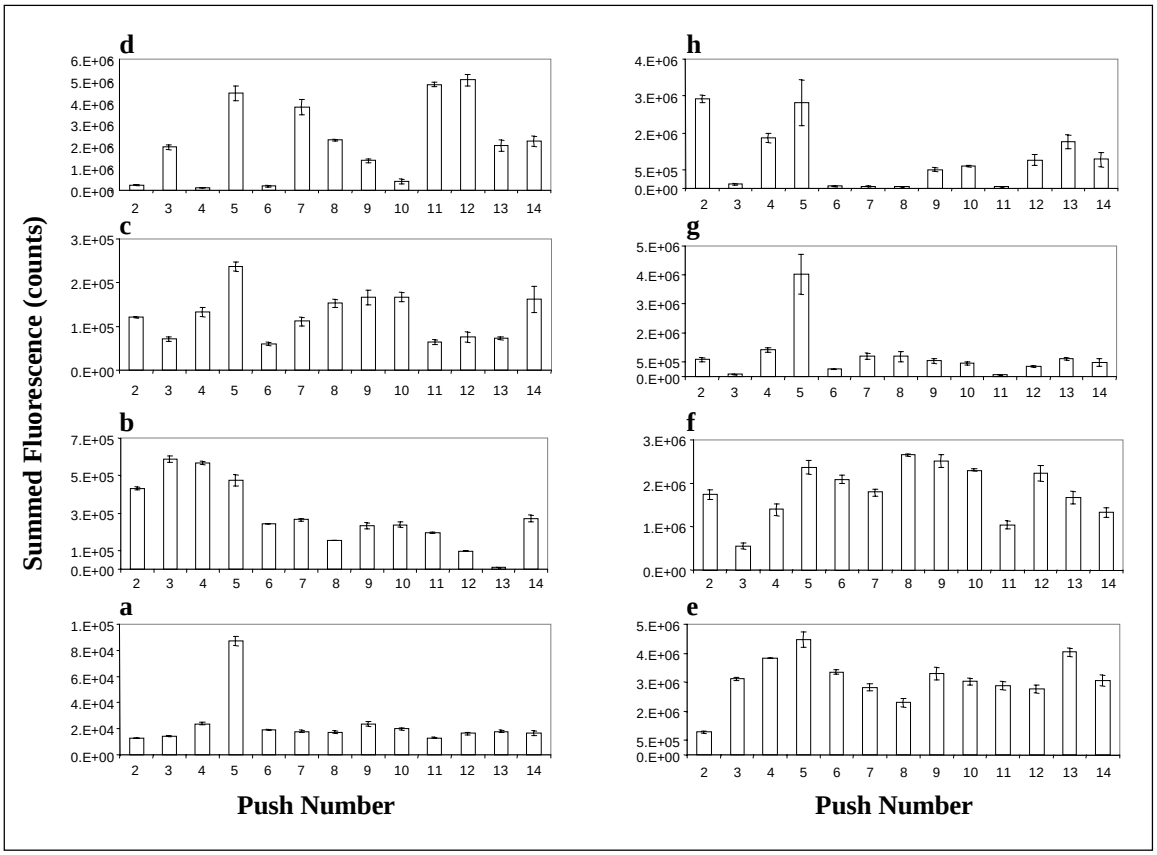

Figure 24. Average quinine sulfate standard solution summed fluorescence (detector counts) calibration summary for each of the excitation wavelengths at each push location made at Hanscom AFB. Insets a – e represent summed fluorescence averages at excitation wavlengths (nm), 257.7, 266, 278.5, 288.4, 299.1, 314.9, 327.7, and 341.6 respectively.

Depth vs. summed fluorescence data

During each push, a single measurement (2 seconds exposure, fluorescence from 40 excitation laser pulses summed) was made at each depth. Each measurement contained 8 channels of data, one for each

of the excitation wavelengths used. The summed fluorescence vs. depth data are shown for pushes 2 - 14 (push 1 was a practice run and no data were collected) in Figures 1 - 12 in Appendix B. The fluorescence data are plotted as a function of the actual depth (offset from the tip depth) of the window utilized by each channel. An examination of the data shows that almost all push sites (except push # 14) contained some degree of contaminant fluorescence. This was by design; to achieve our goal of demonstrating the instrument's capability, we wanted to see as much contamination as possible. A characterization of a site depends as much on contamination non-detects as it does upon detects, for they define the boundaries of the pollution plume. In performing this field test of our instrument, we were interested in its response to contamination and not accomplishing a site characterization. The push sites were chosen based upon the amount of contamination that was expected at a particular location, based on monitoring well data collected by Tom Best of the Air Force, our site coordinator.

In a general sense the molar absorptivities of classes of compounds can be summarized for the excitation wavelengths used in our system as follows: excitation wavelengths 257 nm, 266 nm, and 278 nm are known to excite BTEX compounds, so any fluorescence in those channels might be attributable to that type of species. The channels with excitation wavelengths 289 nm, 299 nm, 315 nm are known to efficiently excite fluorescence in naphthalene type compounds. Larger ring species will be most efficiently excited by the excitation wavelengths 327 nm and 342 nm. These broad simplified categories are not exclusive. For instance, some three ring species such as anthracene absorb 266 nm light, but to a lesser extent than they do at longer wavelengths. These generalized categories provide some insight into the trends seen from push to push. A summary of the excitation wavelengths that correspond to the maximum intensity channel in the most intense EEM of each push is given in Table 5. The peak intensity and associated depth for each of the

Table 5. Summary of normalized summed peak fluorescence and depths.

Push #	Maximum Summed Peak Height (relative units)	Peak Depth (ft)	Excitation λ (nm)
2	2.2E-08	18.1	289
3	2.4E-07	13.4	327
4	2.3E-07	12.0	266
5	4.1E-07	7.1	289
6	9.1E-07	12.1	299
7	1.6E-06	16.0	266
8	1.8E-07	13.0	266
9	6.6E-07	13.0	266
10	1.0E-07	13.0	266
11	3.5E-06	9.6	289
12	1.8E-07	9.6	299
13	2.3E-06	12.6	299
14	No peak	No peak	No peak

pushes is given with the excitation channel responsible. The push with the maximum peak signal was # 11 and the lowest peak signal seen was in push 2. The peaks arise largely from excitation wavelengths that best excite naphthalene and BTEX type compounds. Of the 12 pushes that had contaminant signal, 5 out of 12 had their maximum peak due to 266 nm excitation, 6 out of 12 had their peak due to 289 nm or 299 nm excitation. Only one channel had a maximum signal in the 327 nm channel, perhaps indicating a greater quantity of higher order PAHs at that depth. The dominance of naphthalene and BTEX type compounds is consistent with our knowledge of the fluorescent compound composition of jet fuels such JP4, the fuel spilled at this site. In general, the peaks in the depth vs. fluorescence plots for the different excitation channels correlate well with one another. The exact location of a peak along the depth axis may vary due to the specific composition distribution within the plume.

Of interest to us in terms of detection limits and environmental concern is the detection of fluorescence due to compounds dissolved in the groundwater. In terms of detection limits, the water solubility of BTEX compounds and PAHs is very low. Any signal arising from depths known to be below the water table indicates signal arising from small quantities of compounds in the zone. In Figure 4, Appendix B, the results for push 5 are shown for all of the excitation channels. This push site was located near monitoring well 10 (MW-10 in Figure 2). The depths of the fuel product and the top of the water table from the ground surface were determined to be 15 and 16.5 feet respectively. In Figure 4, Appendix B, there is signal in several channels at 17 and even 18 feet. While these signals are small, they are significant due to the region in which they have arisen. The water table depth is known to vary significantly over the course of a year and so there may very well be product that has been left behind on the soil in the water table. The signal seen is likely to be due to a smear zone below the water level. The depths of the fuel product and the water layer are not known for all of the push sites, but are known to vary significantly from one push site to another.

3. Representative EEMs

A desirable goal of data analysis for this instrument is the complete automated EEM analysis of the field data. The rapid fitting of library (laboratory measured) EEMs to the *in situ* EEMs taken during field work (after correcting the latter for soil effects) would be the ideal analysis scenario. Even such a sophisticated analysis must be preceded by the type of analysis described in this section. The summed fluorescence vs. depth plots described in this section are not normalized, but the qualitative shapes and peak positions are sufficient for comparison and discussion.[23] In push site 6, seen in Figure 25, two depth regions of maximum fluorescence were seen with peaks at 8.2 feet and 13.5 feet. There are significant differences in the EEMs at the two depths. At 8.2 feet, the fluorescence emission is at much longer

wavelengths extending beyond the longest wavelengths measured by the detector. This is in contrast to the EEM taken at 13.5 feet where the fluorescence emission in the middle four channels begins at shorter wavelengths and does not extend as far to the long wavelengths as that in the previous EEM. This provides evidence that the contaminants at 8.2 feet have a different chemical composition than those at 13.5 feet. At this site, the old fuel pipeline was thought to be buried just below our push site at approximately 6-8 feet. Our fluorescence data confirms this with signal beginning at 8 feet and extending down to 10 feet. In addition, during the

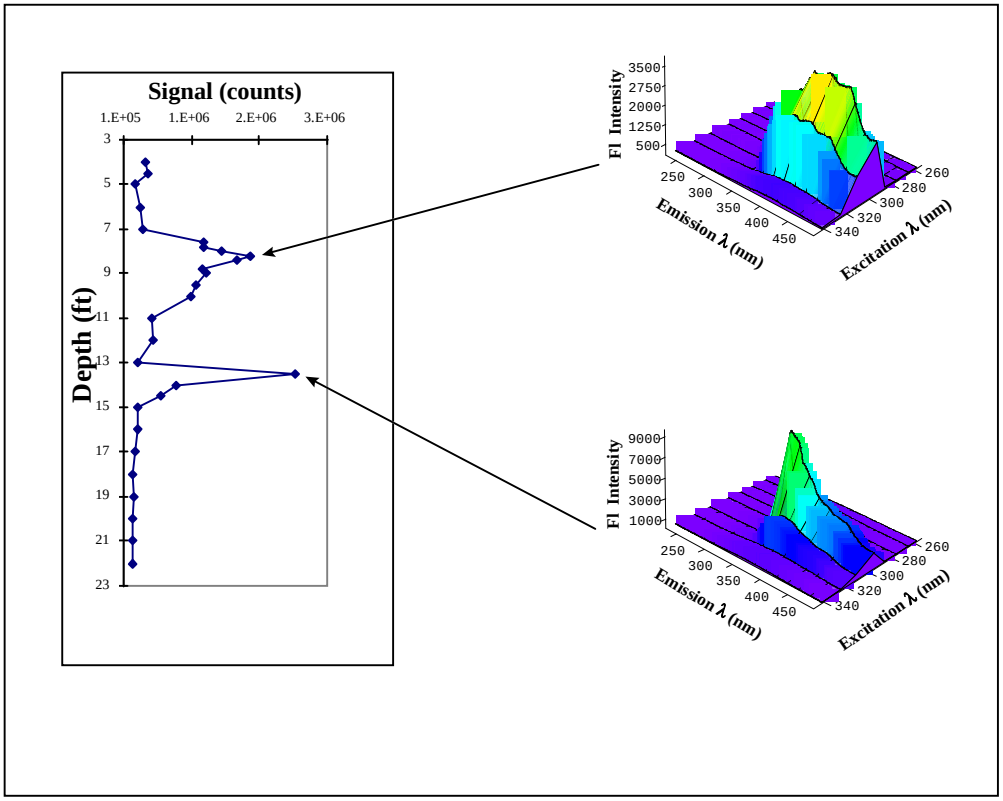

Figure 25. Summed fluorescence vs. depth for push site 6 with peak EEMs.

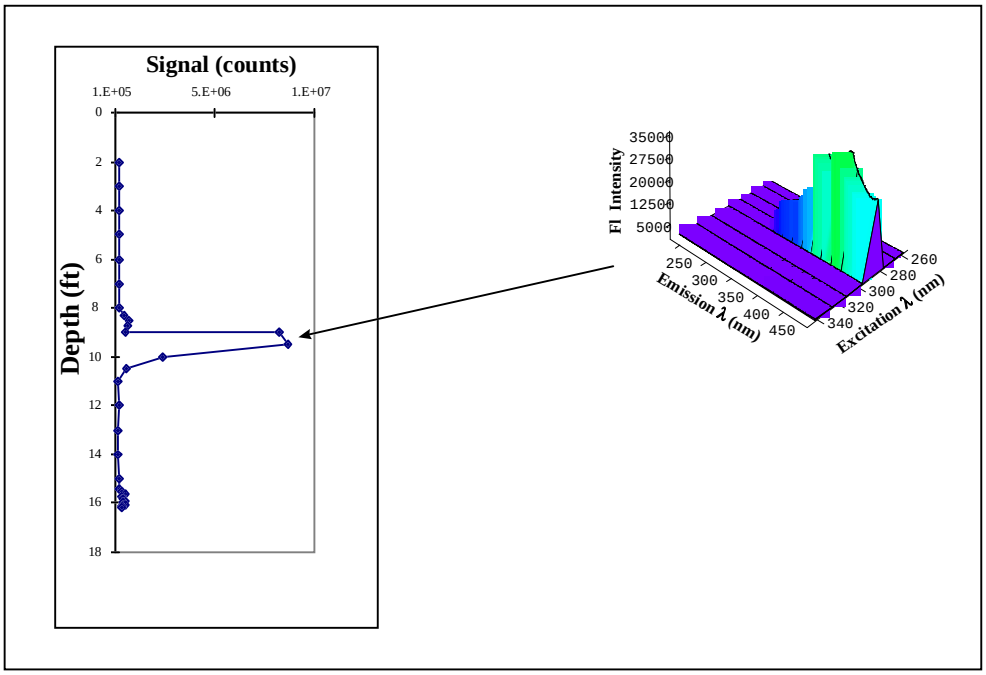

Figure 26. Summed fluorescence vs. depth for push site 11 with peak EEM.

push significant resistance was experienced and the cone tip pressure was elevated at around 8 feet. This indicates that we may have been pushing through the old pipeline with residual fuel product in the vicinity.

On the other side of the site, near the large above ground tank locations, we encountered the largest signal at push site 11 seen in Figure 26. For this peak contamination region beginning at 9 feet, the contaminant is fluorescing most strongly with 288.5 nm excitation, with a maximum intensity of approximately 30,000 counts. The high summed fluorescence indicates a large plume between 9 and 10 feet. Signal was seen at all depths below this plume, but at much lower light levels (500-1500 counts).
It is plausible that a foot of fuel product was resting on top of the groundwater and the signal seen below that was due to groundwater contamination and/or residual fuel product that has adsorbed on the soil as the groundwater level varied over time.

4. Peak fluorescence EEMs

An EEM from the depth of maximum fluorescence at each push location at the site was generated and they are shown in Figure 27. These EEMs illustrate the changes in the contamination at each push location across the site at the specified depth of peak summed fluorescence. One EEM was generated at the region of maximum fluorescence seen at each push location. The EEMs vary significantly throughout

the push locations at the site, indicating a wide variety of chemical species present. The peak EEMs from each location can be grouped according to their respective EEM patterns. Push locations #3 - #9 all have at least some contribution from a compound(s) with (λ_x, λ_m) maxima in the middle region, (290 nm - 300 nm, 350 nm). This correlates reasonably well with the EEMs of naphthalene and both jet fuels, indicating the most likely contamination at these locations to be due to jet fuels. At push locations #2, #5, and #11 - #13, the EEM patterns are comparable indicating similar fluorescent compound composition. An overall summary of the site based upon EEM patterns allows the grouping of regions based upon contaminant fluorescence, and hence type. Variations in soil composition and fuel distribution will hamper the interpretation of our EEM data due to the 1.5" offset of the windows. Even with EEMs that have been reconstructed from data measured in successive exposures, small differences may exist between the soil regions probed by each window.

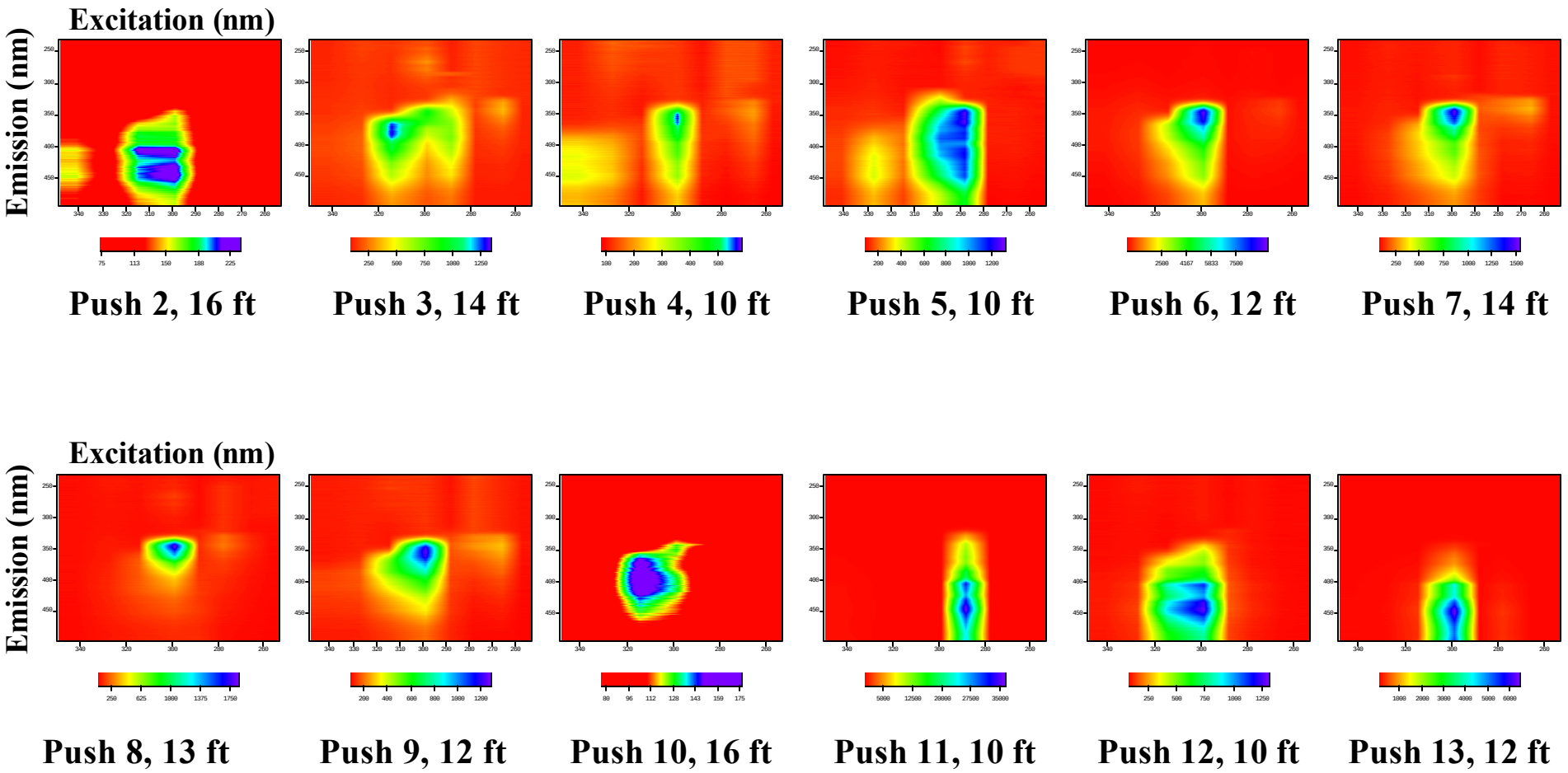

Figure 27. EEMs measured *in situ* at Hanscom AFB, Bedford, MA. The labels are the push #, EEM depth, and the plot axes are vertical: emission (nm), and horizontal: excitation (nm).

5. Depth corrected EEMs

The qualitative examination of *in situ* measured EEMs can yield information on the type of contamination encountered. The comparison of reference EEMs with field measured EEMs can indicate regions of specific contamination such as JP-4, JP-5, and fuel oils. Alternatively, regions can be grouped according to contamination type, single rings (BTEX), double rings (naphthalenes), and larger species.

The analysis of the peak EEMs, with maximum fluorescence signal, from each push location allows the identification of the types and sources of contamination present. The EEMs in the following discussion are all depth corrected, which involves constructing an EEM from channels at the same depth. The peak fluorescence EEMs from push locations #6, #7, and #11 are shown in Figure 28, a and b, c and d, e and f, respectively.

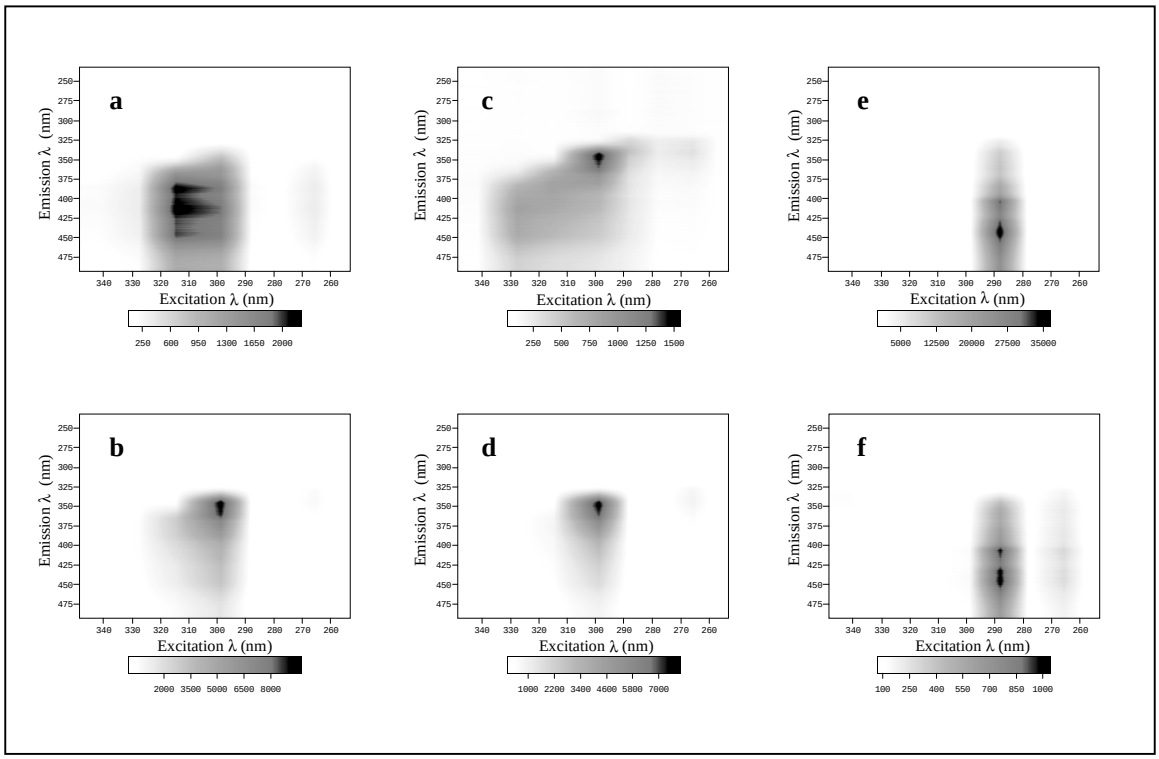

Figure 28. EEMs from the peak fluorescence depth regions of push locations a) #6: 6.5 ft ± 0.2 ft, b) #6: 12.1 ft ± 0.1 ft, c) #7: 14.1 ft ± 0.3 ft, d) #7: 16.1 ft ± 0.1 ft, e) #11: 9.7 ft ± 0.1 ft, f) #11: 16.0 ft ± 0.1 ft.

The depths of the EEMs generated for the peak fluorescence regions at push location # 6 were 6.5 ft ± 0.2 ft and 12.1 ft ± 0.1 ft. There is considerable difference between the contamination seen at each depth as evidence by the EEMs, Figure 27, a and b. The contamination at 6.5 ft had an EEM with a

maximum at (315 nm, 415 nm), while the contamination at 12.1 ft had an EEM maximum at (300 nm, 350 nm). The contamination at 12.1 ft has an EEM that is fairly similar to either of the jet fuels seen in Figures 15, a and b, with EEM maxima at (289 - 299 nm, 340 nm). At 6.5 ft, there may be some fluorescence from species, such as naphthalene, found in jet fuels, but the majority of the signal is at longer excitation and emission wavelengths indicating the presence of species which have higher conjugation. Consider the EEM of anthracene in Figure 14 c, with long wavelength excitation (299 nm - 342 nm) and an EEM maximum at (315 nm, 395 nm). This EEM pattern is similar to the long wavelength excitation and emission found in the EEM measured at 6.5 ft. Furthermore, the characteristic anthracene peaks can clearly be seen in the emission of the EEM from 6.5 ft at push location #6. The smaller amount of short wavelength excitation (266 nm) similar to that in the EEM of anthracene can also be seen in this EEM. In addition to anthracene, the *in situ* EEM indicates that there are other species present. This is seen by considering that there is significant fluorescence intensity in the EEM from 450 nm - 500 nm which is not present in the reference anthracene EEM. This fluorescence EEM pattern could be due to a compound such as pyrene (four fused rings), known to be excited most efficiently by our 315 nm channel and emit fluorescence from 370 nm - 530 nm.[31] However, pyrene is only one possible identity, as many compounds emit fluorescence in this region.

The depths of the EEMs generated for the peak fluorescence regions at push location # 7 were 14.1 ft ± 0.3 ft and 16.1 ft ± 0.1 ft. There is a similar difference between these EEMs, Figure 7, c and d, as there was with those seen at push location #6. The EEMs at shallow depths have a greater amount of long wavelength excitation and emission wavelength fluorescence than do the deeper layers. This is not unexpected due to the proximity of the push locations, seen in Figure 1. While the contamination depth layers are different, the characteristic patterns are comparable. However, there is a dominance of jet fuel type fluorescence in the shallow layer at push location #7 and a smaller amount of long wavelength excitation and emission wavelength fluorescence.

The depths of the EEMs generated for the peak fluorescence regions at push location # 11, on the other side of the site, were 9.7 ft ± 0.1 ft and 16.0 ft ± 0.1 ft, shown in Figure 24, e and f. The EEMs seen at this push location are completely different from those seen at either push location #6 or #7, indicating a different type and source of contamination. The EEMs at push location #11 are characterized by strong excitation by the 289 nm channel and long wavelength fluorescence (325 nm - 500 nm). In addition, both EEMs have some 266 nm excitation, but it is not seen in the first shallow layer due to the overwhelming signal in the 289 nm channel. While there are different concentrations, indicated by the fluorescence light levels, the contamination appears to be the same at each depth. This may indicate a single source of contamination in this site region and that the contamination has partitioned itself at two depths as the water table has varied from 9 ft to 18 ft below ground surface between 9/95 and 2/97. The variation was

determined via periodic measurements made during this period with an oil / water interface probe deployed in a well.

3) Coast Guard Station, Elizabeth City, NC

The site chosen by the EPA project leaders at RSKERL in Ada, OK for the second official test of our instrument was the Elizabeth City Coast Guard Station in Elizabeth City, North Carolina, seen in Figure 29. A detailed map of the support center is shown in Figure 30. The site was in the process of being studied by conventional drilling and a combination of simple on-site analysis and standard analytical lab analyses. This conventional analysis was being performed by another team from RSKERL.

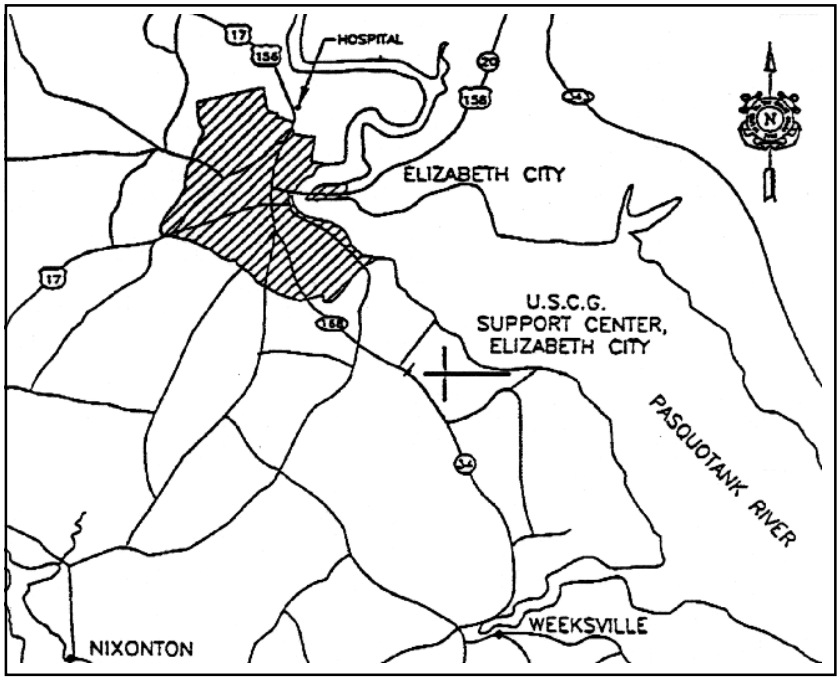

Figure 29. Map showing the location of the U.S.C.G. support center in Elizabeth City, North Carolina, and surrounding areas.

a) Site Operations

Upon arrival at the site on August 28, 1996, the field research team began working on the final installation and testing of the system in the CPT vehicle and the assembly and testing of the generator purchased to power our instruments in the field. After one and a half days, the system was operational and the field measurements began. There was some re-optimization of the system with fiber channel reassignments during the latter portion of the first operation day.

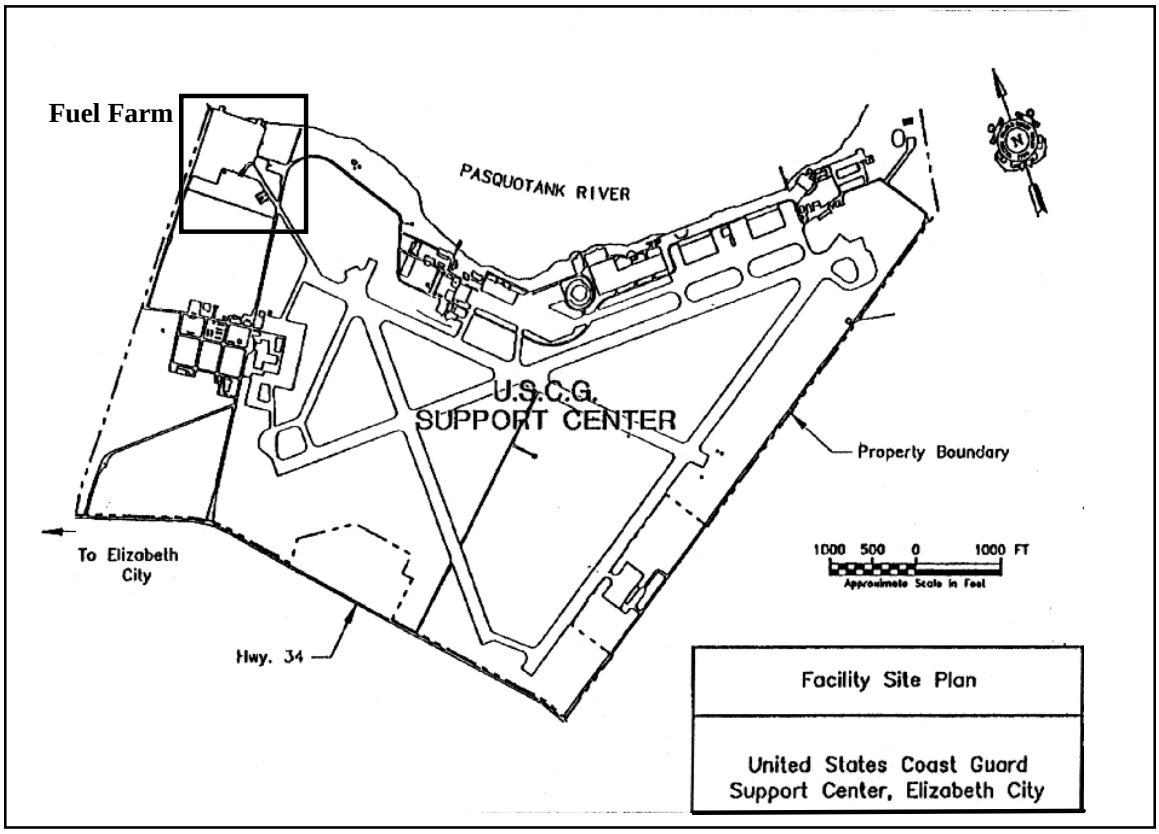

Figure 30. Detailed map of entire U.S.C.G. support center in Elizabeth City, NC, with the area of CPT investigation, the fuel farm shown in the upper left-hand corner.

The system had been set up for increased depth capability, by increasing the launch / detection cable by 5 meters. This allowed the fiber optic connector junction box to be closer to the rod racks, enabling more of the 20 meter cable to be threaded through the push rods. The efforts to increase push depth were successful and the maximum push depth attained in NC was 37 feet during the first push. This represents a significant improvement over previous operation with 25 feet total push depth capability. While the ability to push to such a depth using our LIF probe system is important, the apparent lack of contamination at those depths indicates that the shorter fiber optic cable might have been more appropriate. With shorter fibers, the light losses due to fiber optic attenuation are less and therefore the system's detection limits would be lower. The lengths of fiber used in this work were shorter than those that can be used with either ROST or SCAPS LIF-CPT systems. However, using the longer wavelengths such as those used by the systems mentioned above would enable our system to probe the same depths if desired.

Several days into the field work, the laser head temperature sensor failed. This was not a fatal failure and turned out to be only a relatively minor setback (½ day), solved by replacing the temperature sensor with one shipped to us by the laser manufacturer. The field work then continued successfully: Large contaminant signals were seen and the amount of signal observed was in agreement with available information on where the contamination plume should extend.

During the second week of the field test, we had a laser cooling water line rupture. This failure, too, was easily remedied by purchasing and installing tubing obtained locally. This setback amounted to another ½ day of instrument down time. Field data collection continued normally for the remainder of the week until the system and truck were packed and prepared for the journey back to Massachusetts for our third field exercise of the summer, again at Hanscom AFB.

b) Field Results

The objective of our work at the U.S.C.G. Support Center in Elizabeth City, North Carolina, was to demonstrate the instrument and characterize the extent and type of contamination at the fuel farm. Towards those goals, much was accomplished with 27 pushes in less than two weeks. Of the 27 push locations, many were detects, but several were non-detects indicating the boundaries of the plume. The LIF push locations, core sampled locations, and site features are shown in Figure 31.

The stability of the system during the field measurements was fairly good, but with room for improvement. The average deviation of the before and after each push calibrant measurements was usually better than 35 %. However, there were several cases where one channel underwent an order of magnitude change. These drastic changes are most likely due to severe fiber damage or misalignment and were corrected before the next measurement by re-polishing or re-aligning the fiber end.

Normalized summed fluorescence versus depth plots were generated using the excitation intensity average for each push location. These plots were compared with plots of contaminant concentration obtained from conventional laboratory analyses performed on core samples taken near some of our LIF push sites. The summed fluorescence data was used to generate a 3-dimensional site map for plume visualization.

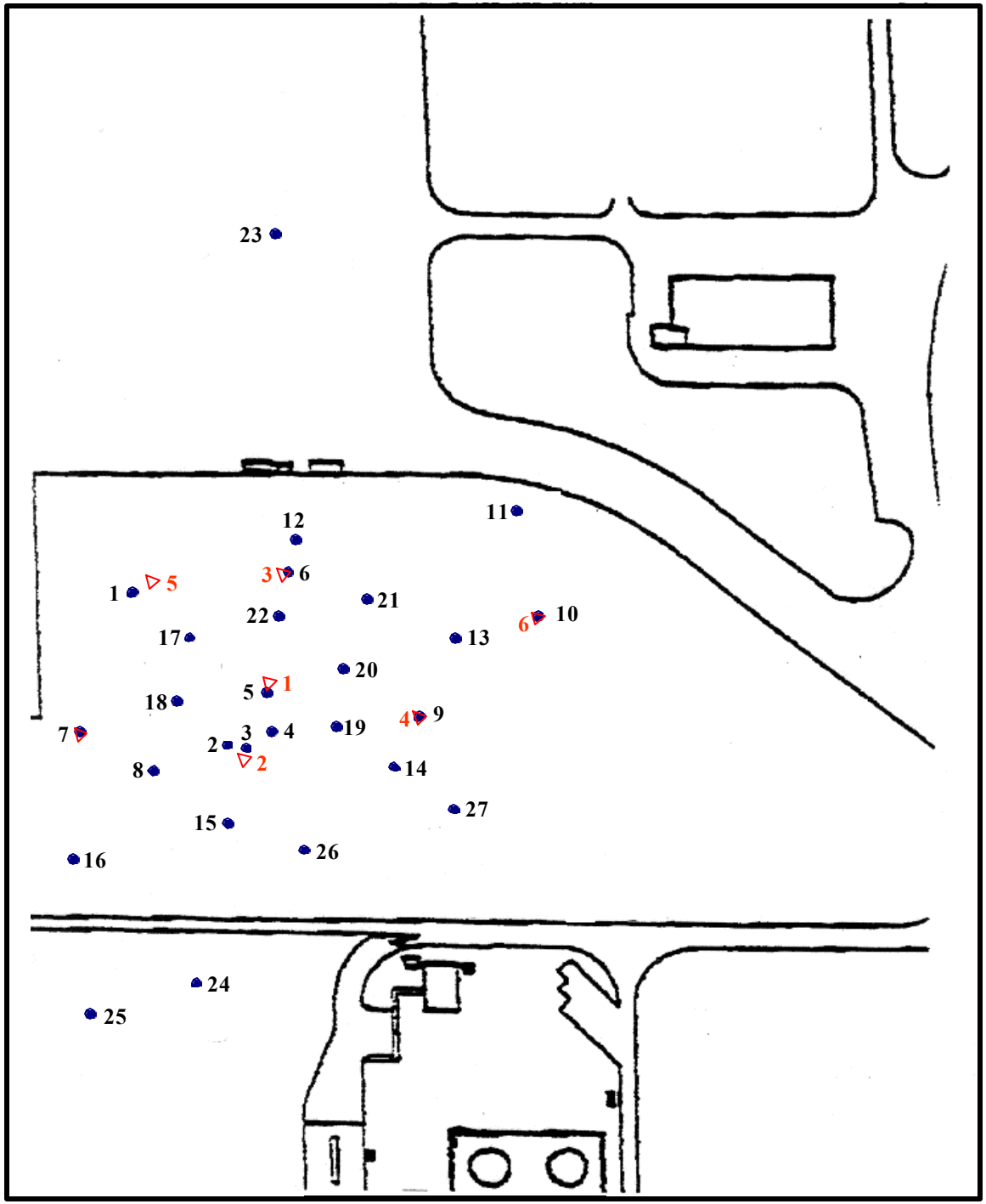
23
12
11
1
5
3
6
21
22
6
10
17
13
20
5
1
18
4
9
7
3
4
19
2
2
8
14
27
15
26
16
24
25

1. Calibration data

The quantitative analysis of the field data will require a thorough knowledge of the variations of the excitation energy delivered to the sample during the *in situ* measurements. However, the exact incident energy delivered to the *in situ* soil and contamination, for each measurement, is unknown. The available alternative is to measure and record the excitation energy before and after the push and from these measurements to infer the amount of excitation light being delivered to the sample. The calibration process

and the treatment of the data are discussed and described in section 5.B.2.b.1. The excitation data in Figure 32 show that there were significant changes in many of the channels throughout the field test. Channels 258 nm and 266 nm both had fairly constant excitation energy levels, whereas channels 278 nm and 288 nm had low output for the first 16 pushes, after which the energy level increased. The remaining channels showed more variation from push to push throughout the field test. Several channels have large error bars associated with the excitation energy average which can be due to several factors previously described. The error in the excitation energy is propagated in the calculation of the normalized summed fluorescence data. While a channel may have an error that is an order of magnitude or larger, the signal seen on that channel can usually still be interpreted qualitatively to determine the depth of contamination but not the relative amount.

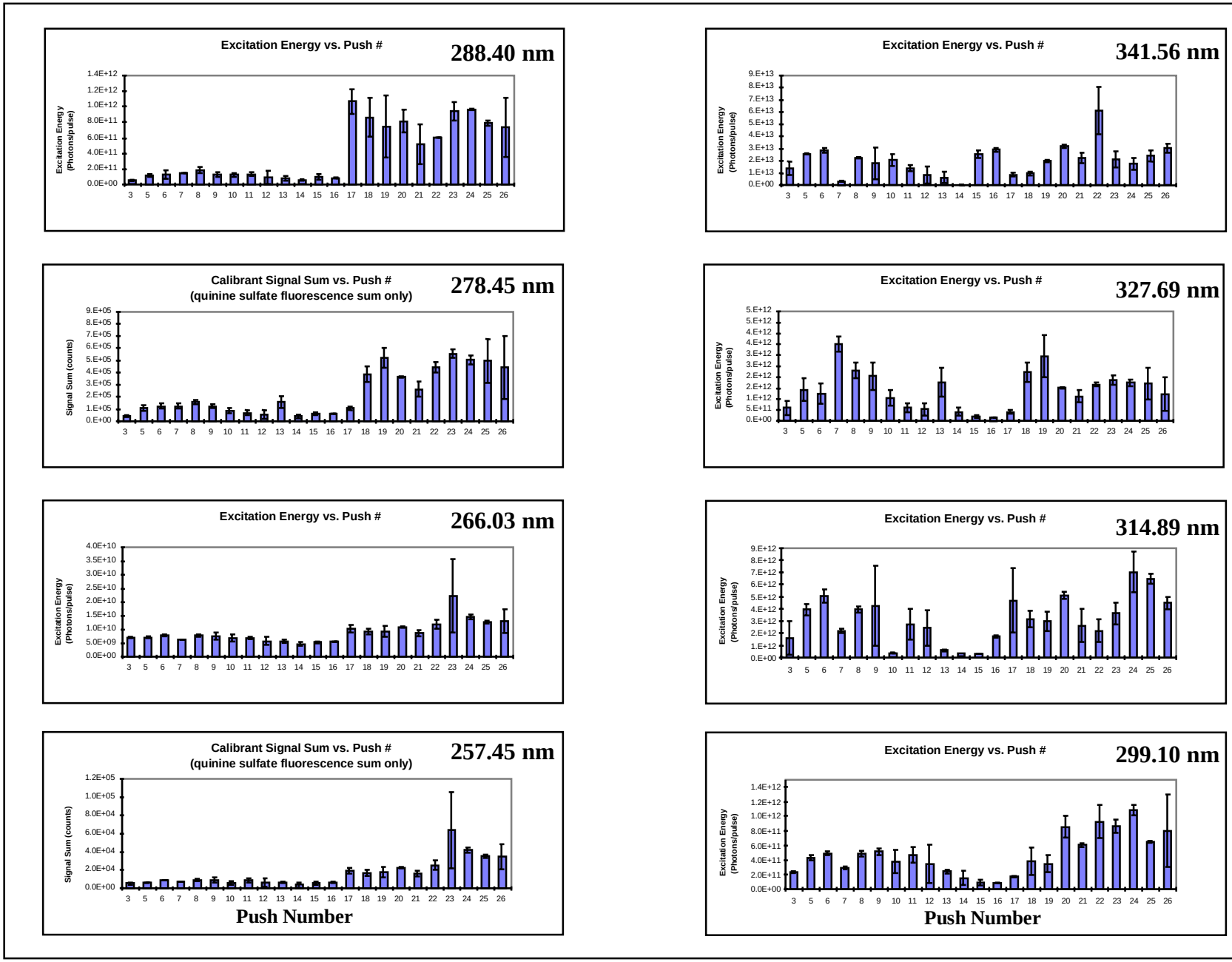

Figure 32. Excitation energy as a function of push number during the field test at the U.S.C.G. Support Center at El;izabeth City, NC. Excitation channels 257.45 nm and 278.45 nm have no calibration data and are therefore expressed as calibrant fluorescence sums only.

2. Depth vs. summed fluorescence

The summed fluorescence data for each push location at the U.S.C.G. Support Station in Elizabeth City, NC are given in Appendix B, Figures 1 - 27. In Figure 1, the data shown were taken "on the fly": 90 eight-channel LIF measurements in 15 minutes to a depth of 37 feet. This push illustrates the capability of the system to acquire data rapidly during real time ASTM (2 cm/s) push rates. Since an automatic data acquisition system was not yet in place, the depth data could not be used to trigger the collection of each file.

Table 6. Summed fluorescence approximate peak depths and contamination depth ranges

Push #	Peak depth average (ft)	σ	Contamination range (ft)
1	na	-	-
2	8.03	0.08	6-12
3	9.00	0.01	4-13
4	8.11	0.10	6-10
5	9.06	0.07	3-11
6	8.08	0.09	5-9
7	9.05	0.07	3-9
8	8.05	0.06	7-13
9	5.05	0.06	5-7
10	4.04	0.16	3-6
11	4.02	0.07	2-5
12	8.05	0.06	6-11
13	nd	-	-
14	7.05	0.06	6-7
15	8.02	0.07	4-9
16	6.02	0.07	4-9
17	8.05	0.06	4-10
18	9.05	0.06	3-11
19	8.05	0.06	5-9
20	8.05	0.27	6-12
21	5.11	0.10	4-6
22	8.11	0.10	5-9
23	nd	-	-
24	6.05	0.06	5-8
25	nd	-	-
26	nd	-	-
27	nd	-	-

na	Not applicable
nd	Non-detect

Instead, the plan was to obtain the time each file was written and correlate it with time-depth measurement recorded by the CPT computer, to obtain depth, but this strategy was unsuccessful. Therefore, the depths were linearly approximated from 0 to 37 ft for the 90 data files. This push, without accurate depth data, is not included in the other analyses.

Measurements were made from window depths of approximately 1.5 ft to 16 - 20 ft, depending upon the contamination plume depth. In Table 6, a summary of the average depth to peak fluorescence intensity for each push location and the contamination zone depth (average of all channels) is given. The contamination had an average peak depth of 7 ft and the contamination depth range was from 3 ft to 13 ft. The plots, in general, are self-consistent in that peaks in the different channels often occur at the same depths. This is expected if the contaminant mixture contains fluorescent species that absorb at all excitation wavelengths, and if the mixture composition does not change significantly with depth. While a jet fuel fluoresces most strongly at central wavelengths, all of our channels respond to high concentrations of fuels such as found in a saturated product zone.

3. Summed fluorescence site map

The normalized summed fluorescence data given in Appendix B have been plotted using the surface x, y, z coordinates of the push locations at the site. The surface elevation, z, was not measured, but was nearly constant for all pushes, and was set equal to the average elevation, 2.4 m $\pm$ 0.3 m, of several other points on the site to generate the 3-D site map in Figure 33.

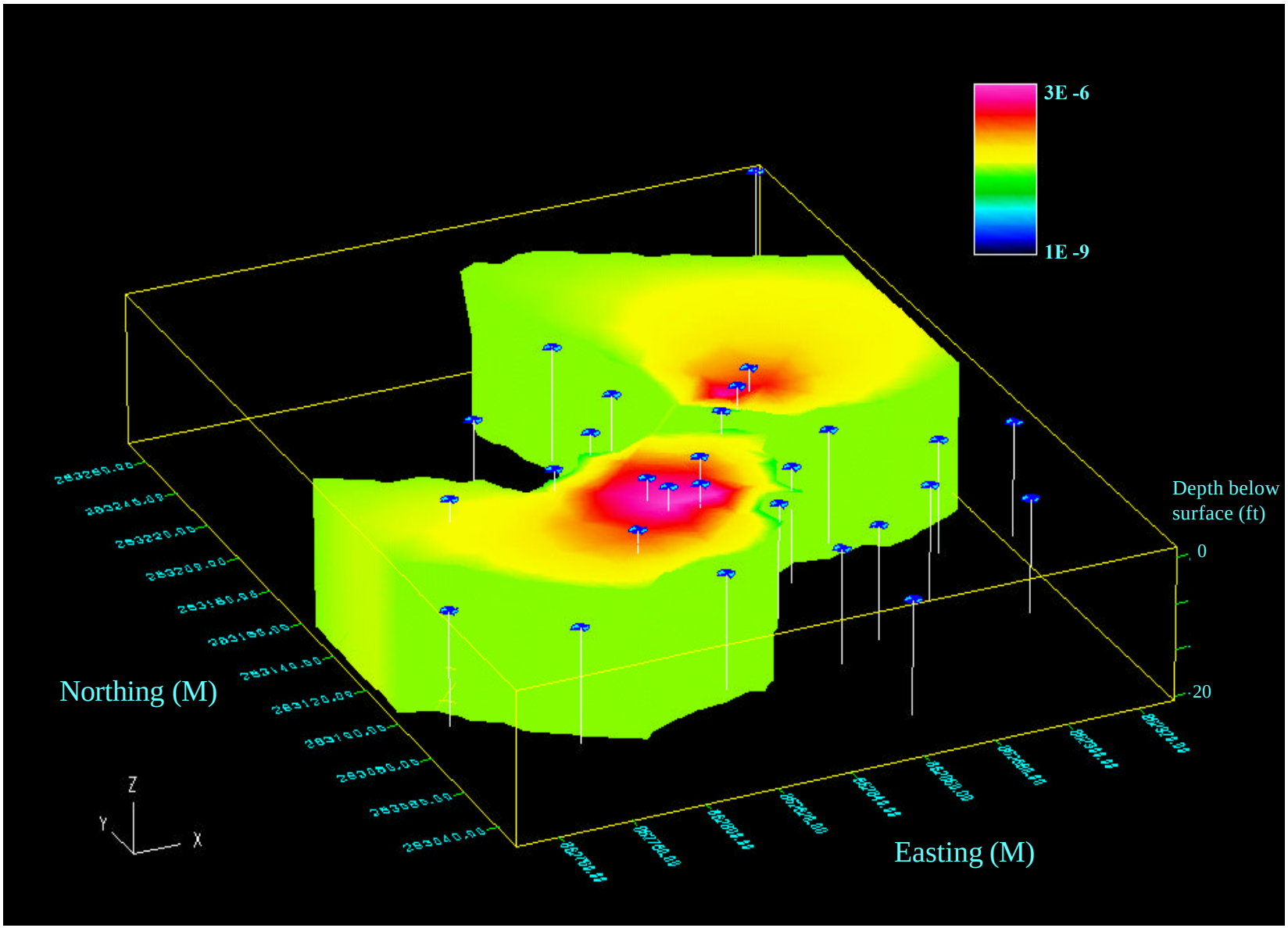

Figure 33. Normalized summed fluorescence data, produced by the 288.4 nm excitation channel, plotted with site coordinates to produce a 3-dimensional map of the fuel farm at U.S.C.G. Support Station at Elizabeth City, North Carolina.

The 3-D site map in Figure 33 was generated using SiteView software. This software uses all of the summed fluorescence data points and creates a 3-D grid within which data points are linearly interpolated to fill the 3-D grid. A weighted sum interpolation algorithm is used to generate the data points that make up the 3D site model. In Figure 33, the parameters of the weighted interpolation had been set to emphasize the horizontal direction and not the vertical plume profile. This allows an aerial-like view of the site, push locations and contamination regions. The summed fluorescence data suggest that there are two main regions of contamination: the stronger in the middle of the sampled region of the site and a slightly weaker plume center just northeast of the first. The data in this summed fluorescence site map were taken from the 288.4 nm excitation channel. This channel was chosen because it produces the maximum fluorescence response in JP-5 jet fuel (refer to section B.2.b). If the jet fuel standard (Figure 14.b) is compared with the in situ EEMs from the U.S.C.G. Support Station in Elizabeth City, NC, all except one peak EEM contain at least some fluorescence pattern that is similar to JP-5. The axes on the contamination intensity scale (color bar, Figure 33, inset) are from 10^{-9} to 3 $x10^{-6}$ fluorescence counts / photons excitation. In terms of JP-5 concentration, these correspond to 0.02 g / L (a non-detect) to 64 g / L of JP-5 in cyclohexane on a medium grade sand.

4. Summed fluorescence comparison with laboratory data

Core samples were taken with a separate drilling rig after our work was completed, at surface locations near where CPT-LIF measurements were made. The crew that collected these samples did not duplicated the coordinates of our push locations as closely as would be necessary for a detailed comparison. In most cases, the core sample locations were within a few meters of the LIF-CPT push location. An x-y plot of the push locations, with site features, is shown in Figure 31. The easting, northing coordinates of the core sample sites and the LIF-CPT sites are given and compared in Table 7. The coordinates for LIF-CPT and core sampling locations for push 2, 4 and 5 are separated to an extent that warrants concern about correlation. For the remaining locations, the data should be similar, but slight shifts in peak locations might occur due to variations in contamination plume depth and profile.

The laboratory analysis on core samples was performed by ManTech Environmental Research Services Corporation in conjunction with the National Risk Management Research Laboratory (NRMRL), Ada, OK. The method used is the EPA Ada Laboratory's in-house standard method RSKERC SOP 72: Quantitative Analysis of Aviation Gasoline and JP-4 Jet Fuel in Coarse and Medium Textured Soils by Gas Chromatography. The analysis for TPH was done using an HP 5880 GC (gas chromatograph) and the data expressed as equivalents of JP-4 jet fuel by using a standard fuel calibration curve. The analysis

of core samples for other specific compounds was performed using an HP 5871A GC/MSD (Mass Spectral Detection) system. The GC/MSD data were quantified using fluorobenzene as an internal standard.

The laboratory data from core samples taken at the Coast Guard Center and comparable LIF data are shown in Appendix C. Figures 1 - 8 provide a comparison of laboratory core sample analysis data for naphthalenes (naphthalene, 1-methylnaphthalene, and 2-methylnaphthalene) and total BTEX with *in situ* LIF data. Figures 9 - 16 are a comparison of TPH (total petroleum hydrocarbons) with the *in situ* LIF data. TPH data expressed as equivalents of JP-4 should be comparable to all channels in the LIF probe, since each channel is sensitive to jet fuel. The comparison of specific compounds is more complex because it requires some interpretation of the EEM data. For our system, it is known that naphthalene is only excited by the 266 nm, 278 nm, 289 nm, and 299 nm excitation channels, with the latter two having the most intense response. The same should be approximately true of the naphthalene derivatives.

Table 7. Summary of LIF-CPT push locations versus core sample locations for lab analysis.

Push name	Easting (m)	Northing (m)	Qualitative Agreement Between Lab and LIF Data
Push 2	862826	283120	Poor
cpt-2	862827	283111	
Difference	0.7	8.7	
Push 3	862829	283113	Fair
cpt-2	862827	283111	
Difference	2.3	1.7	
Push 4	862837	283111	Fair
cpt-2	862827	283111	
Difference	10.3	0.3	
Push 5	862843	283125	Good
cpt-1	862845	283128	
Difference	2.0	3.4	
Push 6	862869	283157	Good
cpt-3	862867	283158	
Difference	1.6	1.2	
Push 7	862800	283168	Fair
cpt-7	862800	283168	
Difference	0.4	0.3	
Push 9	862868	283072	Good
cpt-4	862868	283072	
Difference	0.1	0.3	
Push 10	862909	283069	Poor-Fair
cpt-6	862909	283069	
Difference	0.2	0.2	

are only excited by our lowest two excitation channels: 257 nm and 266 nm. Of these two, 266 nm is the stronger due to a higher energy before launch and less fiber optic attenuation before delivery to the sample. To assist in the correlation of LIF-CPT measured signals with the core sampled lab data, straight lines are drawn in the figures at the depth corresponding to the peaks in the lab data across the *in situ* measured data.

In general, there are summed fluorescence peaks at similar depths to the peaks from the lab core sample analyses. It is difficult to closely correlate these measurements due to their inherent differences. First, our fluorescence data originate from a small sample area (< 1 mm) dictated by the excitation fiber distal cone cross-section on the outside surface of the sapphire window. This is in contrast to lab analyses where a 4 inch core section is homogenized and a sample extracted with methylene chloride. Second, our data are plotted as summed fluorescence at each excitation channel and the lab data is in concentration units for groups of specific compounds (naphthalenes, total benzenes) and for TPH (total petroleum hydrocarbons). For the TPH measurement, the only fluorescent compounds that the analysis detects are BTEX and naphthalenes.

Compound comparison

For LIF-CPT push # 3, the closest core sampling was 32CPT-2, seen in Figure 2, Appendix C. Both the BTEX and naphthalenes contamination ranges correlate with the LIF data. The lab data indicate both contaminants from 5 ft - 9 ft, and the LIF data on the 266 nm channel (sensitive to BTEX) begins at 5 ft and ends at 13 ft. Similarly, the 289 nm and 299 nm channels have signal from 6 ft - 12 ft indicating good overall contamination region overlap. The total BTEX peak at 6.5 ft correlates well with a peak region in the 266 nm summed fluorescence plot. The naphthalenes peak is approximately ¼ foot away from the peak region on the channels most sensitive to naphthalenes, 289 nm and 299 nm. However, the LIF data suggest contamination from 10 ft - 14 ft, whereas the lab data do not show contamination from 10 - 12 ft, the end of their data range. For both pushes #2 and #4, Figures 1 and 3 in Appendix C, the data correlate well for the overall contamination ranges, but the LIF push and core sample locations are farther apart, making the correlation less meaningful.

For LIF-CPT push # 5, the closest core sampling was 32CPT-1, seen in Figure 4, Appendix C. There is good correlation at this location, with a contamination region from 5 ft - 11 ft. Both the lab data and the LIF plots indicate a shallow region of contamination at approximately 2.5 ft - 3 ft. At LIF-CPT push # 6, the core sampling was 32CPT-3, seen in Figure 5, Appendix C. Both the overall contamination region and the two main peaks in the lab data are well correlated with the LIF data. The lab data show a

region of contamination from 5 ft - 8 ft and the LIF data range is from 6 ft - 9 ft. The two main peaks in the naphthalenes plot overlap closely with those in the 289 nm and 299 nm LIF channels.

For LIF-CPT push # 7, seen in Figure 6, Appendix C, the lab data indicate shallow contamination from 2 ft- 5 ft, while the LIF data show contamination from 3 ft - 7 ft. LIF-CPT push # 9, seen in Figure 7, correlates well with the lab data, with contamination beginning at 4 ft and ending at 7 ft. Finally, LIF-CPT push # 10, seen in Figure 8, shows some shallow contamination from 3 ft - 6 ft and 266 nm signal from the surface down to 6 ft. This is comparable to the lab data which indicates surface BTEX contamination down to 3.5 ft, and naphthalene contamination from 2 ft - 3 ft. The fluorescence signal levels during this push were low, consistent with the low concentrations seen at this location.

TPH comparison

For LIF-CPT push # 3, the closest core sampling was 32CPT-2, seen in Figure 10, Appendix C. The TPH contamination range correlates with the LIF data in the range of 5 ft - 11 ft. However, the LIF data indicate contamination from 5 ft to 14 ft, 3 ft beyond that reported by the laboratory. The peak depth in the lab data lies between two peak regions in the LIF data. For LIF-CPT push # 5, seen in Figure 12, Appendix C, there was very good correlation. The lab data shows contamination from 2 ft to 11 ft, while the LIF data indicates contamination from 3 ft to 12 ft. Several peaks in the lab data correlate reasonably well with the LIF data. The remaining data are given in Figures 13 - 16, Appendix C. The results are similar to that seen for the specific compound analysis comparisons.

The correlation of the *in situ* measured LIF data with conventionally sampled and analyzed laboratory data has been generally good, with several LIF pushes in close agreement with the lab data. The fundamental differences in sampling, data interpretation / presentation, and actual push vs. core sample locations prevent a detailed, quantitative comparison.

5. Peak fluorescence EEMs

For each push location, an EEM was generated at the peak summed fluorescence depth. Each probe window is located at a different depth relative to the cone tip during the push, and thus "sees" a different sample. To correct for this, data from several EEMs at different depths were taken and each channel assigned its depth. A new EEM was created by collecting only channels close to the desired depth. These EEMs are effectively depth corrected to within 2 % depth variation. In Table 5, the peak fluorescence

depths are the actual EEM depths with standard deviations. In Figure 34, EEMs are shown from the 21 detects encountered at the U.S.C.G. Support Station in Elizabeth City, NC.

The EEMs in Figure 34 document the changes in the fluorescent contamination profile at the depths of maximum fluorescence depths at the locations sampled. The EEMs contain fluorescence patterns that are indicative of jet fuel type contamination with two notable exceptions: push # 10 and # 11. Many EEMs that contain jet fuel contamination fluorescence signals also contain other patterns of fluorescence indicating other sources of fluorescence. The standard EEMs of both JP-4 and JP-5, Figure 14 a and b, have fluorescence excitation maxima at 299 nm and 288 nm respectively and emission maxima occur at 325 nm – 350 nm. This fluorescence EEM pattern agrees closely with the observed EEMs in Figure 33. A common additional feature of the *in situ* measured EEMs, compared with the reference jet fuel EEMs, is a tail of long wavelength emission. This additional fluorescence emission in the 288 nm or 299 nm excitation channels extends from 350 nm to 450 nm or 500+ nm. The two notable exceptions are push # 10 and # 11, where the emission occurs at long excitation and emission wavelengths. This EEM pattern of emission is indicative of highly conjugated aromatic species such as anthracene (3 - ring structure) and higher. The EEM of anthracene is shown in Figure 15, c, with emission from 375 nm – 425 nm at excitation wavelengths of 314 nm – 342 nm. This provides evidence that the contamination, at the indicated depths and push locations, is likely to contain conjugated aromatic molecules such as anthracene. These EEMs are valuable tools in the characterization of the contamination profile of the site and indicate regions that can be grouped together based upon contamination type.

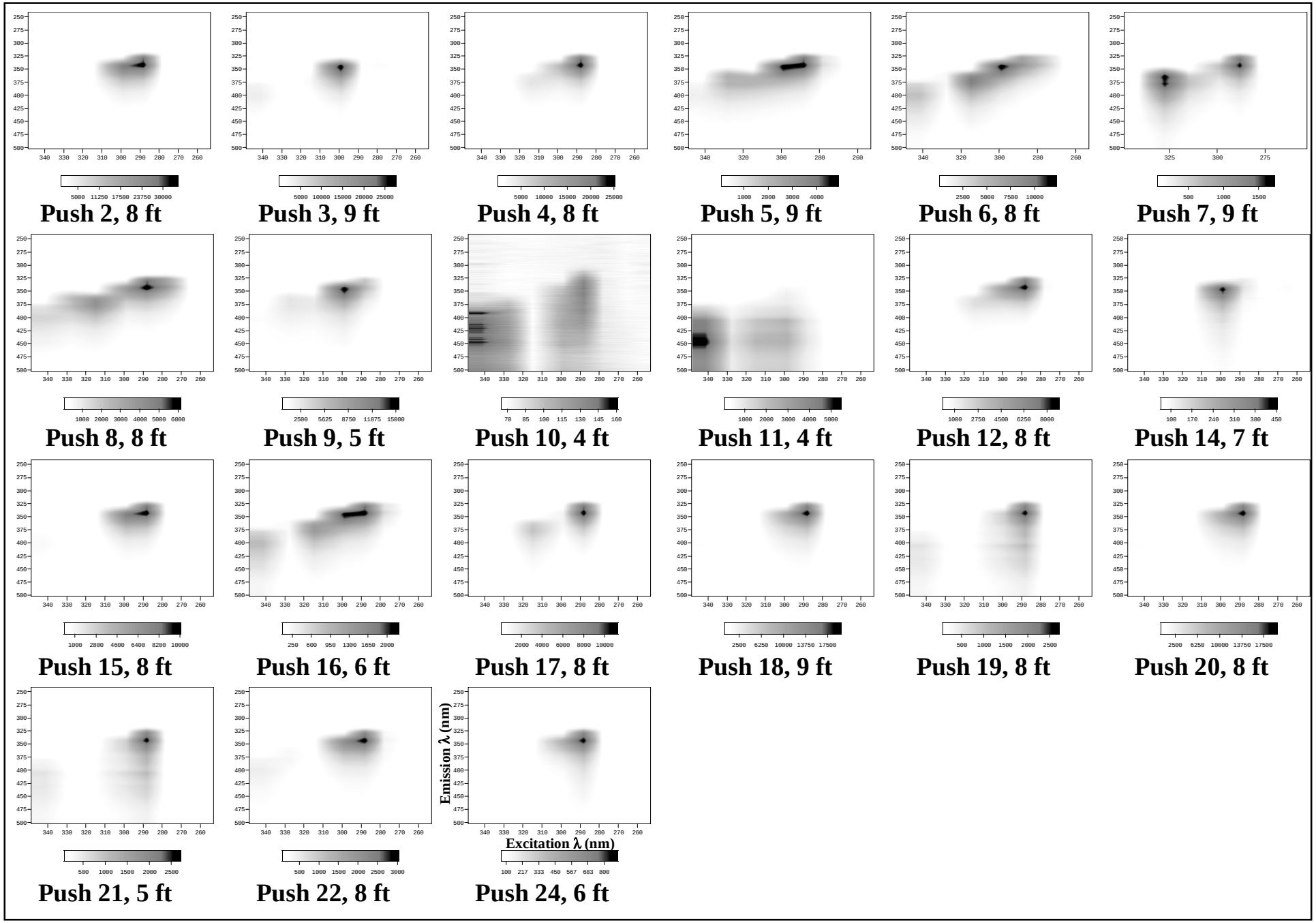

Figure 34. Depth corrected EEMs for each push location at U.S.C.G. Support Center, Elizabeth City, NC. The plot axes are vertical: emission wavelength (nm), horizontal: excitation wavelength (nm), and the labels are push # and depth.

5) Hanscom Air Force Base II

The third field test field test of the summer of 1996 was a second visit to the site described in the Hanscom Air Force Base I section above. A return visit of the instrument and crew was arranged to enable us to further test our instrument and hopefully accomplish a site characterization in the process. The site is shown in Figure 35 with site features and both the first (Hanscom I) and second (Hanscom II) push locations.

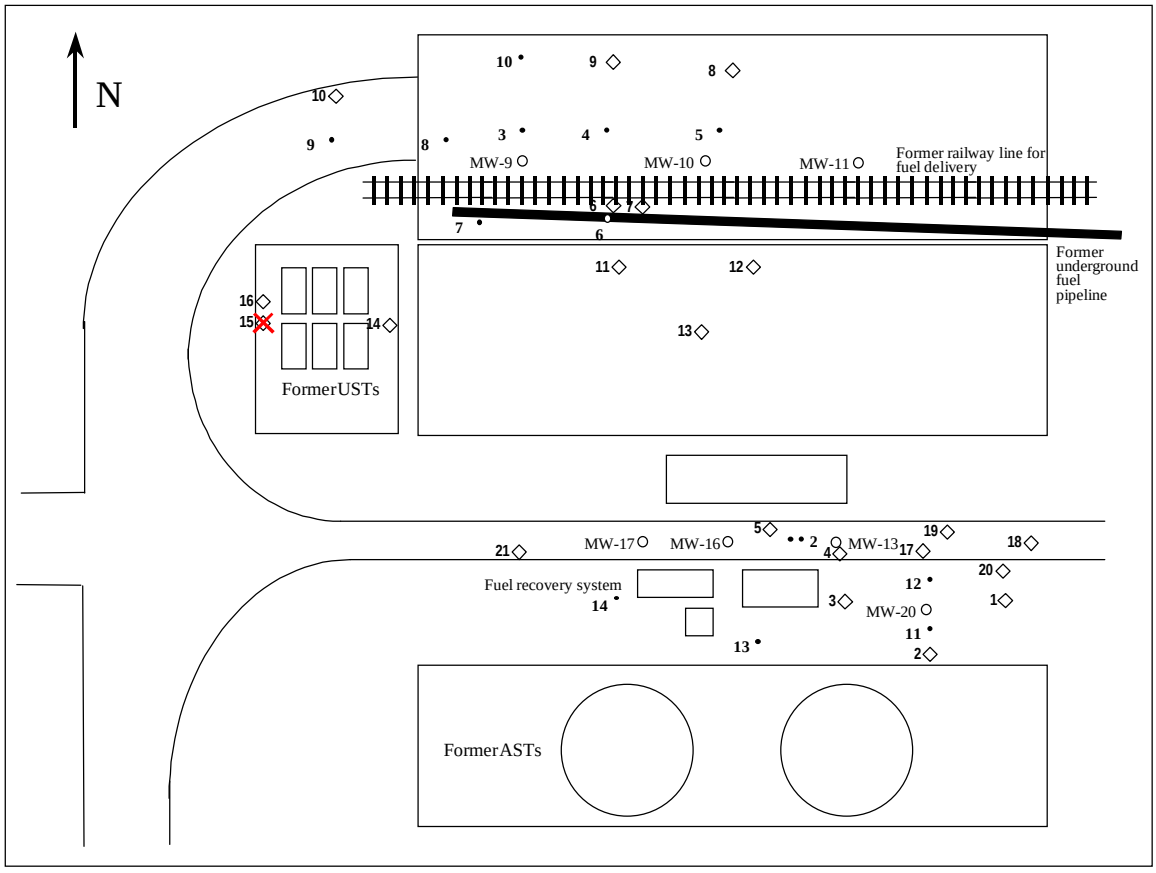

Figure 35. Map of CPT-LIF push locations and site features at Hanscom AFB. The dots are the push locations from the first field test, and the diamonds are the push locations from the second field test. Push location # 15 was crossed out because a shallow concrete slab prohibited further progress.

a) Site Operations

Several organizational changes were made to the layout in the truck once it had returned to Hanscom AFB. There were no major modifications or repairs attempted due to lack of time. In addition, repairs to an essentially operational system would be problematic in that the results taken with the modified system would not be directly comparable with those taken during the previous work. The organizational changes

included the removal of the laser shipping case from the truck, securing the laser directly to the rear cab floor, and repositioning of the computers for easier access.

The CCD camera had to be replaced due to a vacuum leak in the chip chamber and a Peltier cooler malfunction. Luckily, an essentially identical detector was available in our laboratory and this was quickly swapped with the damaged unit after a few modifications. The re-installed system was tested prior to the arrival of the EPA crew and appeared to function normally. However, just prior to the first push, the laser overheated and shut down - the cooling group fans were not functioning. This problem was not trivial and required 1½ days to repair due to the time needed to ship and replace the part (Fan PC board). This action corrected the problem and the field work was begun during the second day.

Having previously done field work at the site, we embarked on this second visit with hopes of accomplishing a complete characterization, with preconceived notions of locations and levels of contamination. We first tried to duplicate our earlier results at several push sites where we had seen large amounts of signal previously. These measurements were initially perplexing because the results were very different from what we had seen before. No one, including the site manager, Tom Best, expected to find such drastic changes. The absence of substantial fluorescence signal was a source of much concern for all involved. Nevertheless, the instrument response from all calibrating solutions (Quinine sulfate, JP5, and fuel from a nearby well mixed with sand) was as expected. The conclusion was that the site contamination had changed since we had sampled there three months earlier. We proceeded with the site characterization. On the fourth day of sampling a highly contaminated subsurface zone was discovered. Its location was consistent with the site manager's expectation: near and in between two pumping recovery wells. In the four days of field sampling, 21 surface locations were probed to depths of 25 feet.

b) Field Results

1. Calibration data

The performance of the LIF instrument can be directly monitored by the fluctuations in the response of the calibrant, quinine sulfate, before and after every push. For the first 6 pushes, 8 channels were in use, until the 266 nm excitation fiber was damaged at the probe end and it was swapped with the 278 nm excitation fiber. From push 7 on, there were only 7 channels: the original eight minus the 278 nm channel. This is seen in Figure 36, with excitation energy as a function of push number during the field test. The data had larger errors during the first half of the field test, until push 11 or 12. This may be attributable to cold weather (outdoors 5 – 10 degrees Celsius) hampering the performance of the laser.

The solution was to allow significantly more warm-up time for the laser (1 hour +), but this was not done until the problem

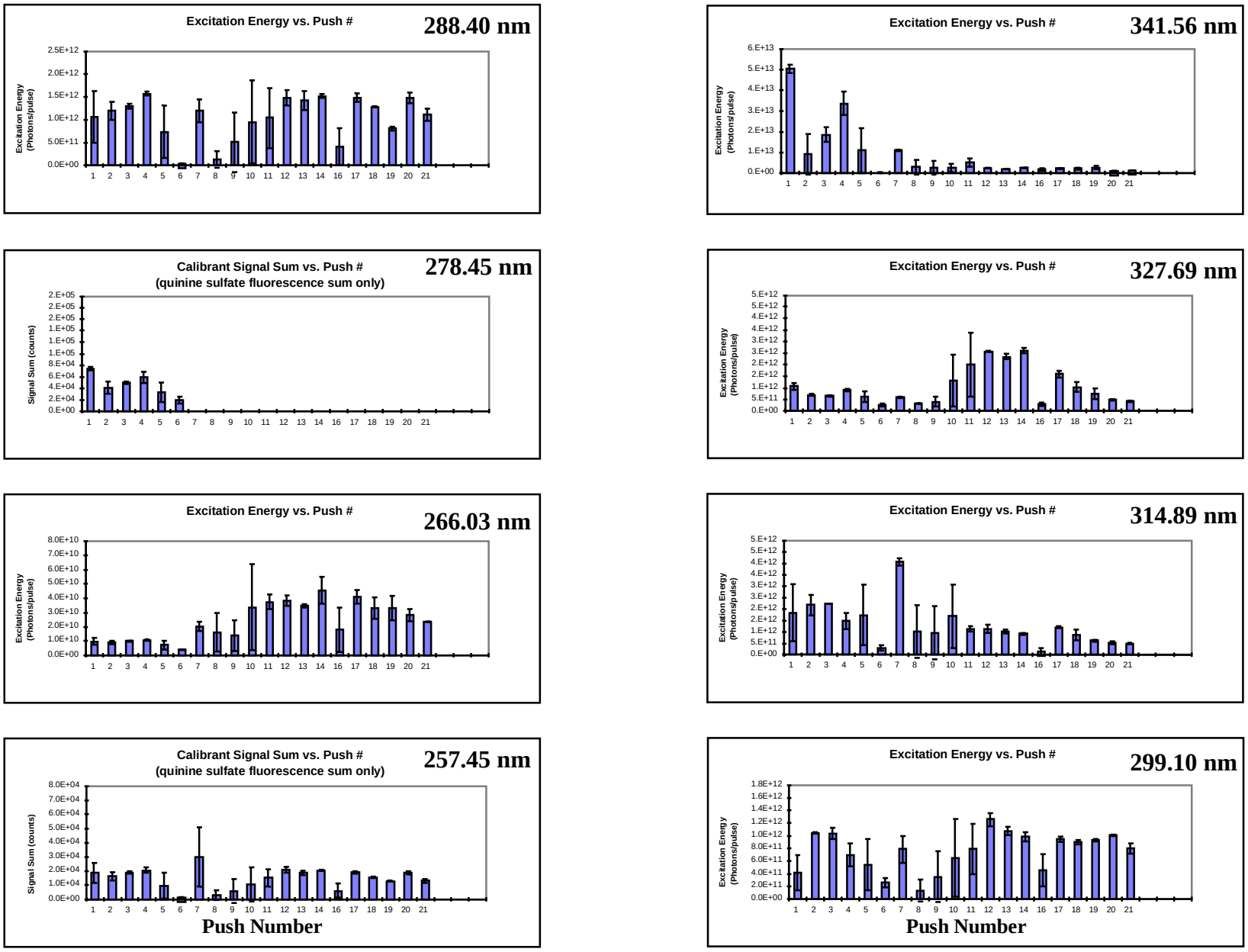

Figure 36. Excitation energy as a function of push number during the field test at Hanscom AFB in Bedford, MA. Excitation channels 257.45 nm and 278.45 nm have no calibration data and are therefore expressed as calibrant fluorescence sums only.

became apparent during push post processing. For excitation wavelengths, 257 nm, 288 nm, and 299 nm, the excitation energy did not show significant long-term degradation over the course of the field test. This is in contrast to excitation wavelengths, 315 nm, and 342 nm, where the excitation energy tapered off significantly. For 266 nm and 327 nm excitation channels, the excitation energy increased as the field test progressed. There are many possible reason for the changes in the excitation energy throughout the field test. These include SRS (stimulated Raman scattering) variations due to Raman shifter gas decomposition or window damage. Damage to excitation beam launch fibers and hardware are other possibilities, such as launch tip damage, and fiber solarization. A very important possibility is damage to either excitation or emission fiber ends in the probe. In either case, the signal returning to the detector will be reduced either through loss of excitation light by the excitation fiber or reduction of fluorescence collection by the emission fiber. The large order of magnitude changes associated with some excitation beams are most likely due to catastrophic damage to the fiber end or changes in the launch hardware. Such large excitation energy variations are accounted for in the error propagation of the summed fluorescence plots. Those excitation beams in each push with unacceptably large error bars can be discarded from any quantitative analysis. However, for qualitative purposes, the *in situ* fluorescence seen by the probe should not be discarded. These data indicates the presence and location of actual contamination, and perhaps even identity, but not quantity.

2. Depth vs. summed fluorescence

The normalized, summed fluorescence data at each excitation wavelength for each push location are shown in Appendix D, Figures 1 – 20. The data are summarized in Table 8, with peak fluorescence depths and ranges of contamination. Surface locations were probed to depths ranging from 13 ft - 15 ft below the ground surface. Several pushes were hampered by a hard sub-surface formation, threatening to damage the probe and optics. In particular, push 15 had barely begun when an underground concrete slab was encountered, ending the push prematurely at 4 ft. The majority of push locations were ended at 18 ft – 20 ft due to a hard glacial till that was impenetrable.

The average depth of contamination, indicated by fluorescence, was 12 ft, with an overall range of 4 ft – 17 ft. There were 11 non-detects (push locations in which there was no significant contaminant fluorescence) out of 21 total push locations. At the locations where signal was encountered, there was partial correlation between the response in the channels, suggesting contamination that has a wide variety of species that absorb and emit on all channels used in the probe. However, there are some depth regions, in certain pushes, where one or more channels do not agree, indicating a contamination region that does not have as broad a range of contaminant species.

Table 8. Summed fluorescence approximate peak depths and contamination depth ranges during Hanscom II.

Push #	Peak depth average	σ	Contamination range (ft)
1	nd	-	-
2	10.0	0.16	5 - 11, 16 - 17
3	nd	-	-
4	nd	-	-
5	5.0	0.07	5 - 8, 14 - 16
6	nd	-	-
7	nd	-	-
8	nd	-	-
9	10.1	0.27	6 - 13
10	nd	-	-
11	12.1	0.27	10 - 14
12	13.1	0.09	10 - 15
13	nd	-	-
14	11.0	0.16	10 - 12
15	nd	-	-
16	16.0	0.08	14 - 16
17	14.8	0.19	5 - 6.5, 14 - 15
18	14.6	0.10	14.5 - 15
19	nd	-	-
20	11.1	0.09	11 - 12
21	nd	-	-
nd	non-detect		

3. Peak fluorescence EEMs

An EEM was generated, for the peak fluorescence region, at each push location where fluorescent species were detected. The EEMs were generated by labeling each detection channel with its actual depth and then collecting individual channels from the same depth from separate acquisition files. The depth corrected EEMs from those push locations with contamination are shown in Figure 37. The depths of the corrected EEMs are given in Table 9 and are generally within 3 % of the given depth. The first two peak EEMs, push # 2 and # 5, had fluorescence EEM maxima at (λ_x,λ_m) of (289 nm, 440 nm) and (342 nm, 445 nm) respectively. These two EEMs have very different peak regions. However, the peak region of

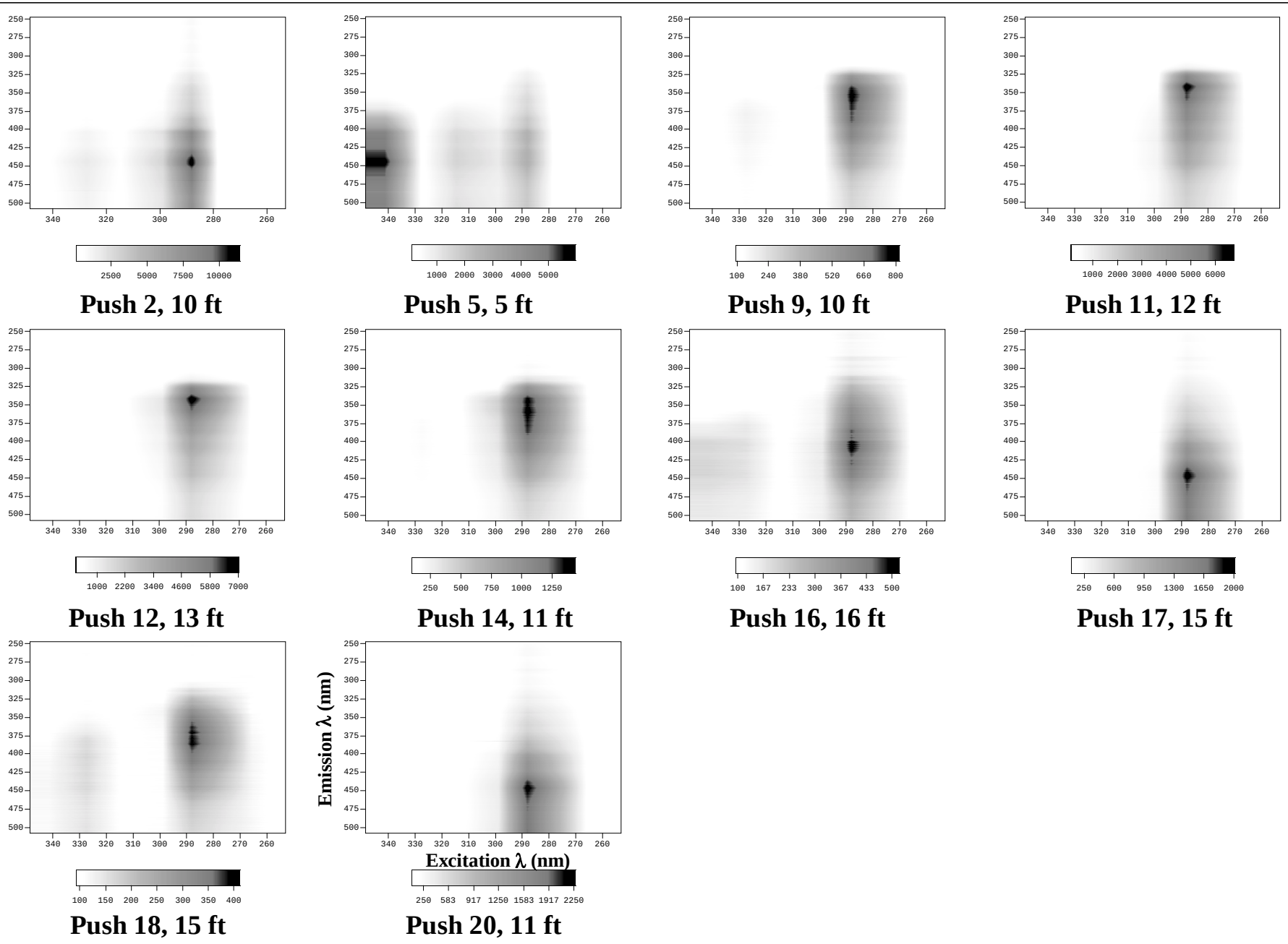

Figure 37. Depth corrected EEMs measured at Hanscom AFB, Bedford, MA. The labels are the push #, EEM depth, and the plot axes are vertical: emission (nm) and horizontal: excitation (nm).

fluorescence in push # 2 was also present in push #5, but to a lesser extent. Both EEMs had fluorescence emission in the 289 nm channel ranging from 325 nm to 500 + nm. For the remaining 8 peak EEMs, the maximum EEM fluorescence was seen on the 289 nm channel. The range of fluorescence emission was from 325 nm to 500 + nm, with a peak ranging from 335 nm to 450 nm. When the peak of the EEM is at (289 nm, 335 nm), such as in push # 11, 12, 14, the EEMs are similar to the reference naphthalene EEM, Figure 15, b. While the peak region is similar, the *in situ* EEMs contain a significant amount of signal due to other species (emission from 350 nm to 500 + nm).

4. Monitoring well sample

A pure fuel product sample was taken from monitoring well 9 (MW-9), seen in Figures 23 and 35. The EEM of that sample mixed with EC USCG sand is shown in Figure 37. This sample is characterized by low to middle wavelength excitation (266 nm - 315 nm), with middle to long wavelength emission (325 nm - 500 nm).

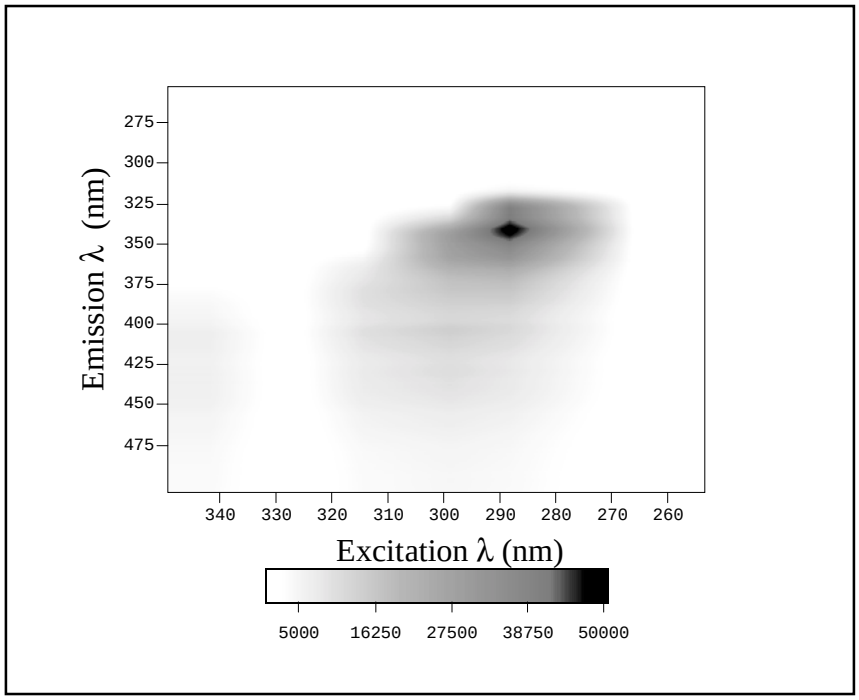

Figure 38. EEM of monitoring well # 9 sample from Hanscom AFB, measured on a medium grade sand.

In addition, there is some long wavelength excitation in the 341.2 nm channel with long wavelength emission (380 nm - 500 nm). A comparison of this EEM with the reference naphthalene EEM, Figure 15, b, and JP-4 and JP-5 EEMs, Figures 14, a and b, indicates some similarities. One would expect the reference samples (naphthalene, JP-4 and JP-5) to compare in a similar fashion due to the presence of naphthalene fluorescence in the jet fuels. The naphthalene EEM has an excitation peak at 288.4 nm and an emission peak at 335 nm compared with an excitation peak at 288.4 nm and an emission peak at 340 nm for the EEM of the well sample. Also, the shape of naphthalene peak is consistent with the peak pattern seen in the well sample EEM. It should be noted that the well sample has significant fluorescence extending from the naphthalene fluorescence region to longer excitation and emission indicating other types of contamination. The JP-4 EEM has significant signal arising from both the 288.4 nm and 299.1 nm excitation channels which also correlates with the well sample EEM. The JP-5 EEM correlates with the well sample in the naphthalene fluorescence region, but does not have the fluorescence in the 341.2 nm excitation channel that JP-4 EEM does. By comparison with the reference EEMs, it is likely that the well sample contains naphthalene and JP-4 type contamination with additional fluorescence due to other species, probably three ring or larger due to the middle wavelength excitation / long wavelength emission.

VI. SUMMARY

A. Overview of Goals Accomplished

The goals that have been achieved include the development and field testing of our fiber optic LIF-EEM CPT probe, software development for data analysis, hardware and software schemes used for data acquisition and data processing. In addition, LIF-CPT measurements have been carried out at a well characterized site, and short term changes (3 months) at a remediated site have been monitored. The detailed calibration of the instrument to include instrument functions and artifacts has been undertaken and accomplished at the summed fluorescence level. The data and calibration schemes are general enough that calibration of the full EEMs can easily be accomplished with software to perform the normalization pixel by pixel. Several reference compounds and mixtures have been measured in a variety of media, allowing comparison with many of the field - measured EEMs. The fiber optic probes have been evaluated quantitatively and tested on various media of different particle sizes to determine response changes.

B. Detailed Summary of Goals Accomplished in This Work

As far as the hardware is concerned, the development of our instrument is nearly complete. The laser, optical table, spectrograph, detector and other equipment have been successfully packaged for and operated in the field in RSKERL's cone penetrometer vehicle, which, with its separate hydraulics and instrumentation compartments is somewhat roomier than the typical SCAPS or commercial CPT vehicle. The instrument fits comfortably in the space allotted, but would have some difficulty squeezing into the latter. Running the instrument off the truck's onboard generator is inconvenient, since this must be turned off between pushes. The problem was solved by the purchase of a commercial gasoline-powered generator, which is mounted on wheels and is dragged alongside the truck during between-push repositioning by CPT and/or LIF personnel. A system should be devised to mount the generator on the front or rear of the truck to obviate the difficulties and dangers of this arrangement.

The laser/Raman shifter has demonstrated potential as a multi-wavelength light source, but it has not achieved a desired level of stability in output power in the various channels. There has been some difficulty in keeping the laser cool enough in warm weather: proper functioning of the truck's air conditioner units would help considerably. We would hope to bring fluctuations in short-term intensity in

each channel down to 10-20% if possible, and develop the capability to provide instantaneous photon normalization (during the push rather than before and after).

The use of the system with optical fiber cables and probe hardware to deliver excitation light in the field has been demonstrated during three separate field tests made during the latter part of 1996. The system performed well and was able to collect data for a significant number of pushes at all sites. There exists some difficulty with both excitation energy stability during some of the pushes and stability from push to push. The stability from push to push is accounted for by the calibration procedure, provided there is signal to calibrate. However, stability during a push remains uncorrected and we rely on measurements before and after the push to indicate if constant excitation power levels were attained. An examination of the error bars of each push average indicate that many of pushes had excitation energies that were within acceptable limits. The histogram of the number of measurement versus CV (%) for individual excitation energy measurements during both the Hanscom II and the North Carolina work is shown in Figure 39. This plot indicates that the majority of the before and after measurements, 71 % (229 / 323), were within $\pm$ 40 % of one another. There are many options for the improvement of system stability and these are discussed in Chapter 6.

The fiber cabling arrangement and probe design proved to be straightforward and functional. The multi-window arrangement, however successful in avoiding cross-talk from channel to channel, makes reconstruction of depth-corrected EEMs difficult. This point is addressed again in the following section.

The first field test at Hill AFB was perhaps slightly premature from the point of view of our readiness, but it accelerated our overall progress and gave us some much-needed field experience. It is difficult to assess the instrument performance during that test because subsequent site characterization by another LIF-CPT crew indicated it was relatively uncontaminated.

In subsequent field work, the hardware performed well as indicated by a number of different measures: transportability; good integration into vehicle and CPT system; reasonably short installation and mobilization times; ability to function and generate both calibration data and soil characterization measurements nearly continuously during scheduled field tests; reasonable productivity in terms of number of pushes per day; success in demonstrating the ability of all channels to generate useful response levels from contaminated soils; qualitative demonstration (clear in visual presentations of the data) of the utility of multidimensional fluorescence measurements in comparing contaminants to each other or to reference chemical compounds and mixtures.

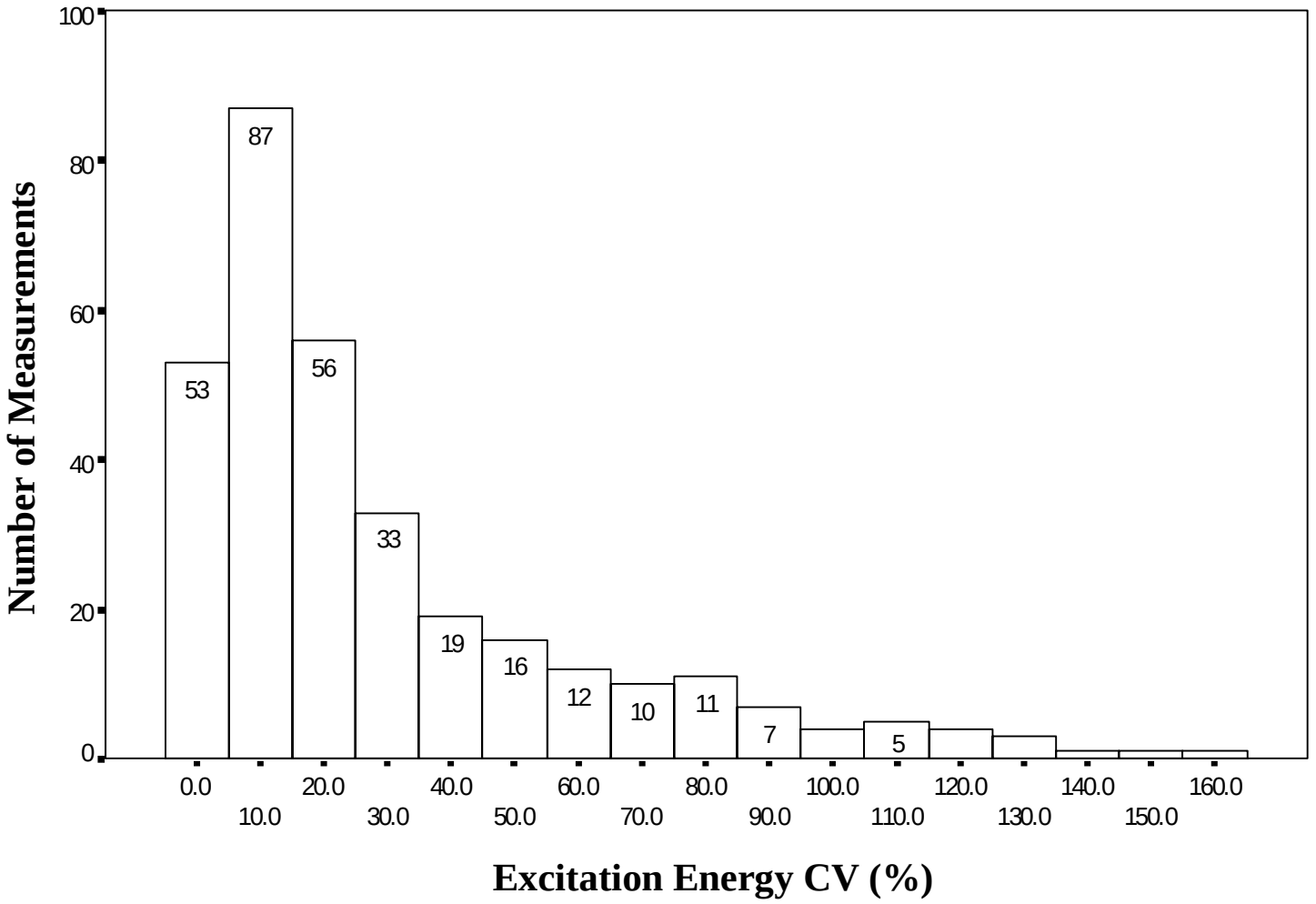

Figure 39. Number of measurements versus the excitation energy CV for individual excitation channels over all pushes for the North Carolina and the Hanscom II field work

The postponement of our subsequent field work until late in the third year of the project, and the intense field work schedule from June to October of that year, resulted in a very limited opportunity for between-test improvements and development of field-data analysis schemes. Our efforts during the six-month no-cost extension were split between implementing the automated data collection routine and trying to develop suitable data reduction schemes for the large amount of field data we had accumulated. It is fair to say that the data analyses accomplished by the end of the project are rudimentary, compared to what we feel the quality and quantity of the field EEMs justify.

To be more specific, the analyses we have described herein fall into two categories: 1) presentation of the fluorescence data in each channel in ways similar to those used in single-channel LIF-CPT instruments; and 2) largely qualitative and visual inspection of the field EEMs, including comparisons to reference EEMs generated on the same instrument. The first category was pursued at the request of our project manager and others who wished to have a simple, real-time display available during data acquisition. Its accomplishment demonstrates our instrument as a multichannel version of previous LIF-CPT instruments. The second category was the shortest, simplest way for us to demonstrate that the multiple excitation channels of our instrument, taken as a whole, represent more than merely the sum of their parts, and open the door to three-dimensional pattern recognition and other EEM data analysis techniques. A quantitative or semiquantitative treatment of the field EEMs that makes full use of the mathematical machinery for analysis of matrix-formatted data is clearly desirable, and constitutes a major focus of our current and proposed future work.
The comparison of in situ LIF data with “true” laboratory data can be problematic in that the truth of laboratory analyses can be compromised.

C. Some Accomplishments of Related Concurrent Work

During this project, we also had a grant from NHSRC for laboratory work in support of the field demonstration, and a demonstration grant from AATDF (DOD-funded through Rice University) for a second-generation field instrument. Finally, another multi-investigator grant from NHSRC helped finance the field work at Hanscom AFB. Some results from these other projects that impact on our assessment of the technology are given in this section.

Because the provision for more than one excitation wavelength adds complexity and cost to various aspects of the instrument, as well as increasing the size of the data sets and the computational time for any data processing, we undertook a limited study to determine what the analytical benefits of additional excitation wavelengths might be. We attempted to analyze two mixtures, one containing four BTEX compounds, benzene, ethylbenzene, toluene and p-xylene, and one containing a benzene, naphthalene,

and anthracene, simple representatives of the one-, two- and three-ring aromatic molecules. For simplicity, the mixtures were prepared in cyclohexane and the spectra were measured on a conventional laboratory fluorimeter. Full EEMs of the mixtures were obtained and rows and columns were eliminated to produce EEMs of various sizes, corresponding to 14, 10, 7 and 5 excitation wavelengths. In brief, the results were that, using least-squares analysis to determine concentrations, we could not accurately discriminate among the BTEX compounds even with the maximum 14 excitation wavelengths; by contrast, even with five excitation wavelengths the different ring sizes could be discriminated reasonably accurately. From this result, we have revised our original suggestion that individual compounds might be identified. While this might still be true for some analyte with a very distinctive spectrum, it is not generally the case. On the other hand, the results also make a strong case for being able to identify classes of similar chemicals. The task before us is to develop some tools for sorting target analytes into classes and doing some studies to determine the quantitative accuracy of analyses based on these classes.

In developing a second version of our LIF-EEM CPT instrument, we attempted a number of improvements. We decreased the footprint of the instrument to effect a comfortable fit into a commercial CPT vehicle, we increased the laser repetition rate from 20 Hz to 50 Hz, with a corresponding decrease in exposure times for each EEM, and we developed a new probe design that puts all ten channels in the same approximately 1 cm diameter window. This last change solves the problem of different beams sampling different depths, although each still looks at a different spot of the soil. The new probe apparently has increased cross-talk among channels, although this problem may be because the imaging spectrograph on the new system is not as aberration-free; a complete analysis is still in progress.

In the area of data analysis, we have developed software that should permit summed fluorescence results to be available in the field. We have reviewed recent developments in rank annihilation analysis and incorporated the more powerful ones into our data analysis schemes. We have also begun addressing the full correction of all instrument artifacts necessary to compare field data to a reference library of standard EEMs. This includes developing a theoretical model for fluorescence intensity appropriate for our probe geometry and applicable beyond the optically dilute limit. We are nearing completion of our own reference library of EEMs of aromatic molecules in various solvents as well as on different soil types.

REFERENCES

Note: A * denotes a publication resulting from this project.

1. "Remote Analysis of Groundwater Contaminants Using Laser Fluorescence", W.A. Chudyk and J.E. Kenny, Proceedings of Fourth National Symposium and Exposition on Aquifer Restoration and Ground-Water Monitoring, 235 (1984).

2. "Remote Detection of Groundwater Contaminants Using Far-UV Laser Induced Fluorescence", W.A. Chudyk, M.M. Carrabba, and J.E. Kenny, *Anal. Chem.*, **57**, 1237 (1985).

3. "Prototype Laser Fluorescence/Fiber Optics Groundwater Contaminant Detector", W.A. Chudyk, M.M. Carrabba, G.B. Jarvis, and J.E. Kenny, Proc. Specialty Conf. on Environ. Eng., EE Div., 1985, p. 98.

4. "Monitoring of Ground-Water Contaminants Using Laser Fluorescence and Fiber Optics", W.A. Chudyk, J.E. Kenny, G.B. Jarvis, and K. Pohlig, *InTech* **34**, (5), 53 (1987).

5. "Remote Laser-Induced Fluorescence Monitoring of Groundwater Contaminants: Prototype Field Instrument", J.E. Kenny, G.B. Jarvis, W. A. Chudyk, and K.O. Pohlig, *Analytical Instrumentation* **16**, 423 (1987).

6. "Instrumentation and Methodology for Multicomponent Analysis Using *In Situ* Laser-Induced Fluorescence", J.E. Kenny, G.B. Jarvis and H. Xu, Proc., First International Symposium on Field Screening Methods for Hazardous Waste Site Investigations, 133 (1988).

7. "Laser Fluorescence EEM Instrument for *In Situ* Groundwater Screening", T.A. Taylor, H. Xu, and J.E. Kenny, Proc., Second International Symposium on Field Screening Methods for Hazardous Waste Site Investigations, US.EPA, Las Vegas, NV (1991).

8. "Laser-Based Fluorescence EEM Instrument for *In-Situ* Groundwater Monitoring", T.A. Taylor, G.B. Jarvis, H. Xu, A.C. Bevilacqua, and J.E. Kenny, *Analytical Instrumentation*, **21**, 141 (1993.)

9. "Rapid, subsurface, *in-situ* field screening of petroleum hydrocarbon contamination using laser-induced fluorescence over optical fibers", S. H. Lieberman, G. A. Theriault, S. S. Cooper, P. G. Malone, R. S. Olsen, P. W. Lurk, *Proc. Second International Symposium on Field Screening Methods for Hazardous Wastes and Toxic Chemicals*, Air & Waste Management Association, Pittsburgh, PA, **1991**, 57-63.

10. "Laser-induced fluorescence in contaminated soils", P. W. Lurk, S. S. Cooper, P. G. Malone, R. S. Olsen, S. H. Lieberman, *SPIE 1434*, 114-118 (1991).

11. "Remote in-situ determination of fuel products in soil: field results and laboratory investigations", S. Apitz, L. M. Borbridge, G. A. Theriault, S. H. Lieberman, *Analusis 20*, 461-474 (1992).

12. "Optimization of the optical characteristics of a fiber-optic guided laser fluorescence technique for the in-situ evaluation of fuels in soils", S. Apitz, G. A. Theriault, S. H. Lieberman, *SPIE 1637*, 241-254 (1992).

13. "The fluorescent response of fuels in soils: insights into fuel-soil interactions", S. Apitz, L. M. Borbridge, K. Bracchi, S. H. Lieberman, *SPIE 1716* (1992).

14. "Subsurface screening of petroleum hydrocarbons in soils via laser induced fluorometry over optical fibers with a cone penetrometer system", S. H. Lieberman, S. E. Apitz, L. M. Borbridge, G. A. Theriault, *SPIE 1716* (1992).

15. "Capabilities and limitations of a cone penetrometer deployed fiber optic laser-induced fluorescence (LIF) petroleum oil and lubricant (POL) sensor", S. H. Lieberman, W. McGinnis, M. Davey, K. C. Wu, *SPIE 2367*, 2-16 (1994).

16. "Transportable tunable dye laser for field analysis of aromatic hydrocarbons in groundwater," R. W. St. Germain, G. D. Gillispie, *Proc. Second International Symposium of Field Screening Methods for Hazardous Waste Site Investigations*, Las Vegas, NV, 789-792 (1991).

17. "In-situ Tunable Laser Fluorescence Analysis of Hydrocarbons", R. W. St. Germain, G. D. Gillispie, *SPIE 1637*, 159-171 (1992).

18. "Variable Wavelength Laser System for field fluorescence measurements," R. W. St. Germain, G. D. Gillispie, and J. L. Klingfus, *Proceedings Field Screening Methods for Hazardous Wastes and Toxic Chemicals*, Air & Waste Management Association, Pittsburgh, PA, 1113-1122 (1993).

19. "Subsurface optical probes: Current status and future prospects", in *Proceedings Field Screening Methods for Hazardous Wastes and Toxic Chemicals*, Air & Waste Management Association, Pittsburgh, PA, 793-805 (1993).

20. "Real-time continuous measurement of subsurface petroleum contamination with the rapid optical screening tool (ROST)", R. W. St. Germain and G. D. Gillispie, in *Proceedings Field Screening Methods for Hazardous Wastes and Toxic Chemicals*, Air & Waste Management Association, Pittsburgh, PA, 467-477 (1995).

21. "Performance Characterization of the rapid optical screening tool (ROST)", G. D. Gillispie and R. W. St. Germain, in *Proceedings Field Screening Methods for Hazardous Wastes and Toxic Chemicals,* Air & Waste Management Association, Pittsburgh, PA, 478-489 (1995).

22. "Evaluation of a Nd:YAG-Pumped Raman Shifter as a Broad-Spectrum Light Source", George B. Jarvis, Sam Mathew, and Jonathan E. Kenny, *Applied Optics 33*, 4938 (1993).

23. * "A Fiber Optic Multichannel Spectrometer System for Remote Fluorescence Detection in Soils", S. J. Hart, Y.-M. Chen, B. K. Lien, and J. E. Kenny, *SPIE 2835*, 73, (1996**)**.

24. "Analysis of Multicomponent Fluorescence Data", I.M. Warner, G.D. Christian, E.R. Davidson, *Analytical Chemistry*, *49*, 564 (1977).

25. * J. Lin, S. J. Hart, T. A. Taylor, J. E. Kenny, "Laser Fluorescence EEM Probe for Cone Penetrometer Pollution Analysis", *SPIE 2367*, 70 (1994).

26. "Cone penetrometer deployed *in situ* video microscope for characterizing sub-surfacesoil prpoerties", S. H. Lieberman, S. S. Knowles, P. M. Stang, J. Kertesz and D. Mendez, *Proceedings Field Analytical Methods for Hazardous Wastes and Toxic Chemicals*, Air & Waste Management Association, Pittsburgh, PA, 579-587 (1997).

27. * "Improved Two Fiber Probe for *in situ* Spectroscopic Analysis", J. Lin, S. J. Hart, and J. E. Kenny, *Anal. Chem., 68*, 3098 (1996).

28. “Toxicological Profile for Jet Fuels JP-4 and JP-7”, Research Triangle Institute, contract # 205-93-0606 and report for U.S. Department of Health and Human Services, Public Health Service, Agency for Toxic Substances and Disease Registry (June, 1995).

29. * "Subsurface Contaminant Monitoring by Laser Fluorescence Excitation-Emission Spectroscopy in a Cone Penetrometer Probe," J. Lin, S. J. Hart, W. Wang, D. Namychkin and J. E. Kenny, *Proc. SPIE 2504, 59* (1995).

30. * "Field Demonstration of a Multichannel Fiber Optic Laser Induced Fluorescence System in a Cone Penetrometer Vehicle," S. J. Hart, Y.- M. Chen, J. E. Kenny, B. K. Lien and T. W. Best, *Field Analytical Chemistry and Technology, 1*, 343 (1997).

31. I. B. Berlman, *Handbook of Fluorescence Spectra of Aromatic Molecules*, 2nd Edition, Academic Press Inc., New York, 1971.

BIBLIOGRAPHY OF OTHER PUBLICATIONS

RESULTING FROM THIS PROJECT OR RELATED PROJECTS:

Research Monograph:

Laser-Induced Fluorescence for Subsurface Contaminant Monitoring, Jonathan E. Kenny, Jane W. Pepper, Andrew O. Wright, Yu-Min Chen, Steven L. Schwartz, and Charles G. Shelton, CRC Press, in press.

Review Article:

"Spectroscopy in the Field: Emerging Techniques for On-Site Environmental Measurements," A. Henderson-Kinney and J. E. Kenny, *Spectroscopy*, Vol. 10, No. 7, p. 32 (1995).

Research Articles:

"Two Fiber Spectroscopic Probe with Improved Scattered Light Rejection, A. O. Wright, J. W. Pepper and J. E. Kenny, *Analytical Chemistry*, in press.

"Laser-Induced Fluorescence and Fast Gas Chromatography/Mass Spectrometry with Subsurface Thermal Extraction of Organics: Field Analytical Technologies for Expediting Site Characterization and Cleanup," A. Robbat Jr., J. E. Kenny, S. Smarason, J. W. Pepper, and A. O. Wright, *Remediation* Winter 1998, 95-111.

"Subsurface Contaminant Monitoring by Laser Excitation-Emission Matrix/Cone Penetrometer," J. Pepper, Y.-M. Chen, A. Wright, R. Premasiri, J.E. Kenny, *SPIE 3534*, pp. 234-242 (1998).

"A Fiber Optic Laser Induced Fluorescence Excitation Emission Detector Applied to Flow Injection Analysis of PAHs, " S. J. Hart, G. J. Hall, and J. E. Kenny, *SPIE 3534*, pp. 601-611 (1998).

GLOSSARY

Absorption – The interaction of light with a chemical species wherein the molecule absorbs a photon and makes a transition to a higher energy state. For visible and ultraviolet light, changes in electronic states are produced. These are followed by relaxation processes to lose the excess energy. These processes can be non-radiative or radiative, examples of the latter being fluorescence and phosphorescence.

Absorption filter – An optical element that is chosen to absorb a certain range of wavelengths for the purpose of blocking unwanted light.

BTEX – Class of aromatic compounds consisting of benzene, toluene, ethyl-benzene, and xylenes (ortho, meta, and para isomers).

CCD (charged coupled device) - A semiconductor device consisting of many pixels that can generate and collect electrons generated by incident light. It is a sensitive photon counting detector with high signal to noise ratios and low background used for imaging and multi channel data acquisition.

Counts – The unit of measurement in a CCD; one count is usually equal to 7-8 photons.

CPT (Cone penetrometer technology) - Technique wherein a steel rod with a tip is pushed hydraulically into the ground to allow *in situ* measurements of many types to be made. These include geophysical measurements such as tip pressure, sleeve friction, and conductivity and also chemical measurements such as LIF, laser induced breakdown spectroscopy, and thermal desorption mass spectrometry.

EEM – Excitation emission matrix, used to describe three dimensional fluorescence data consisting of excitation and emission wavelengths and fluorescence intensity.

Emission – The production of light by a molecule due to a transition to a lower energy state.

Excitation – The absorption of light by a molecule due to a transition to a higher energy state.

Extinction coefficient – See molar absorptivity.

Fiber-optics – A light guide that is comprised of a small glass or plastic solid cylinder, called the fiber core, that is surrounded by a similar material in contact with it called the cladding. The refractive index of the core is greater than the index of the cladding allowing the light to be totally internally reflected within the fiber. This causes light to be propagated from one end of the fiber (launch end) to the opposite end (distal end).

Fiber-optic connector – An assembly into which a fiber optic is placed so that it can be mated to another fiber with as little loss as possible.

Fluorescence – The emission of light due to a transition to a lower energy electronic state of the same spin multiplicity by a molecule.

HPLC (high performance liquid chromatography) – An instrument used to separate molecules in a liquid flow by passing them over a stationary medium chosen for its chemical properties to retain some species preferentially, thus enabling a separation.

LIF – (laser induced fluorescence) – The excitation of aromatic molecules to induce them to fluoresce using a laser as the light source.

LOD (limit of detection) – The lowest, meaningful analytical signal used for quantitative analysis. Commonly defined as 3 times the standard deviation of the baseline signal.

Molar absorptivity – Also called extinction coefficient. Is a measure of a molecule's ability to absorb light of a certain wavelength.

PAH (polycyclic aromatic hydrocarbon) – An aromatic molecule which is comprised of two or more fused aromatic rings. Examples include naphthalene, anthracene, and pyrene.

Photon – A fundamental, quantum unit of light energy that is equal to Planck's constant times the frequency of the light.

Quantum yield (fluorescence) – The number of molecules that emit light as fluorescence divided by the number of molecules excited by the incident light.

Signal-to-noise ratio – The result of the division of a detector's signal by the signal's standard deviation.

SRS (stimulated Raman scattering) – Process by which high intensity laser light is scattered by molecules producing light of different wavelengths, both of shorter and longer wavelength than the pump beam.

INDEX

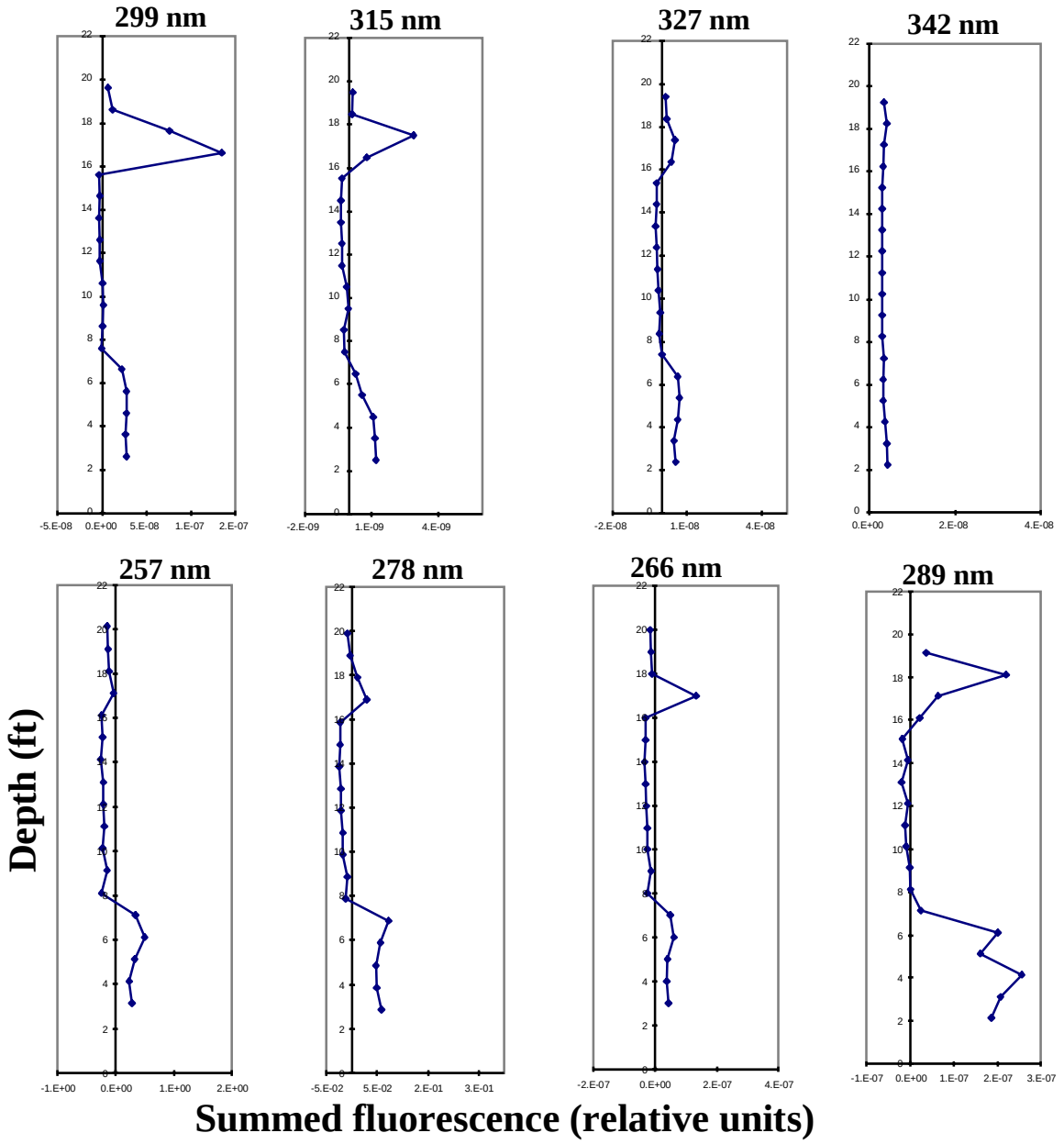

Figure 1. Depth vs. summed fluorescence plots for each excitation wavelength during push 2.

Appendix A

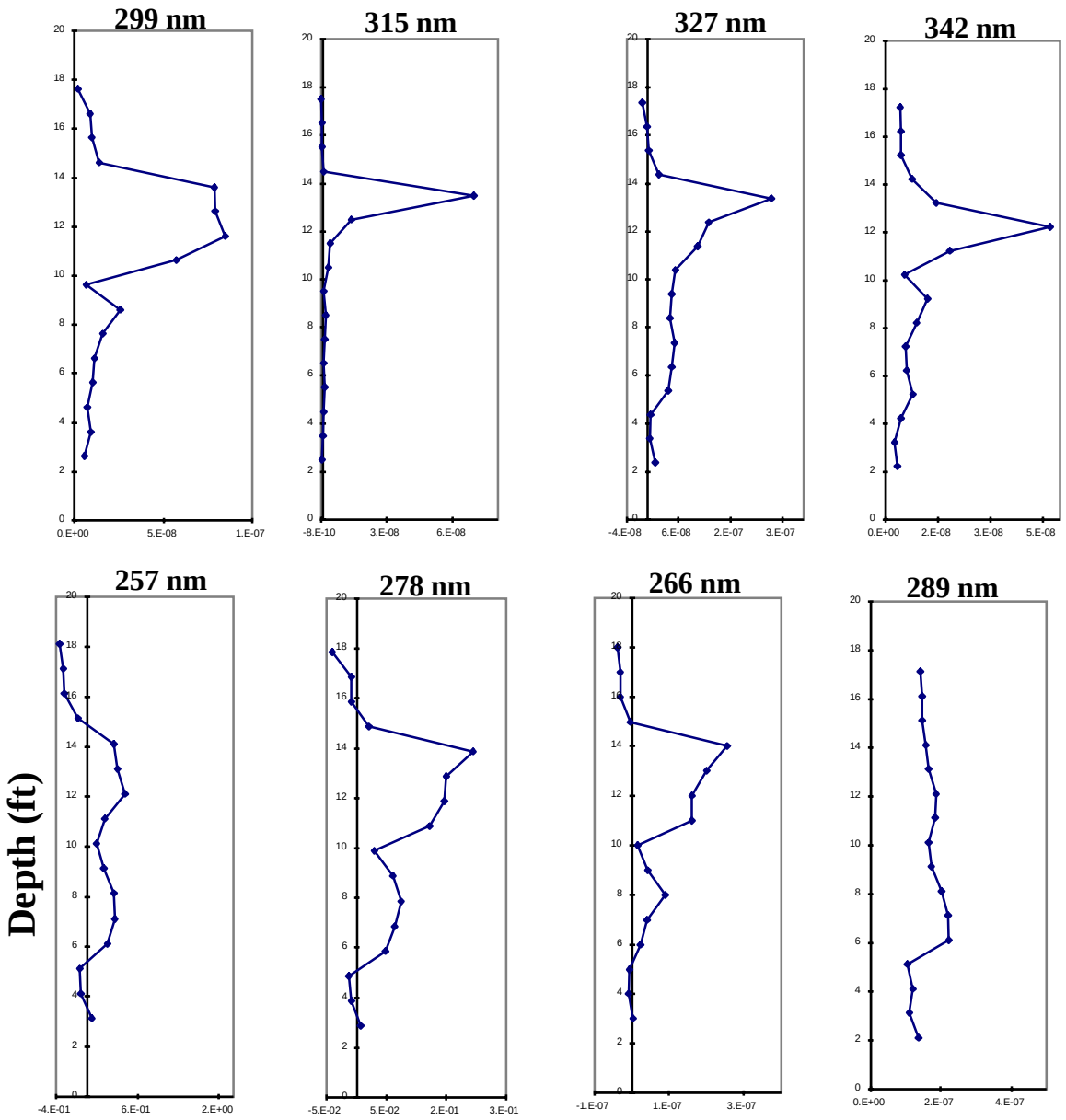

Figure 2. Depth vs. summed fluorescence plots for each excitation wavelength during push 3.

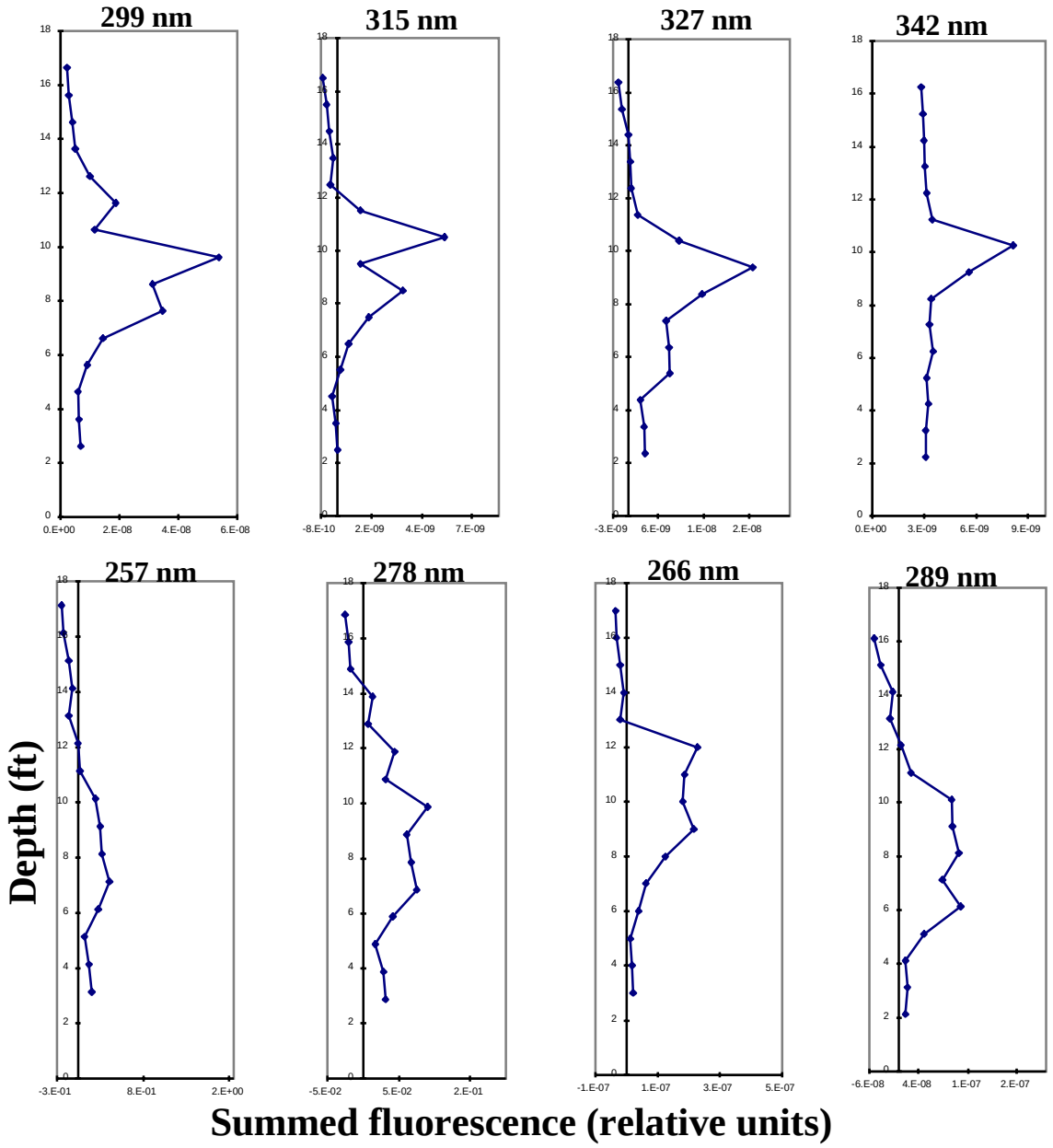

Figure 3. Depth vs. summed fluorescence plots for each excitation wavelength during push 4.

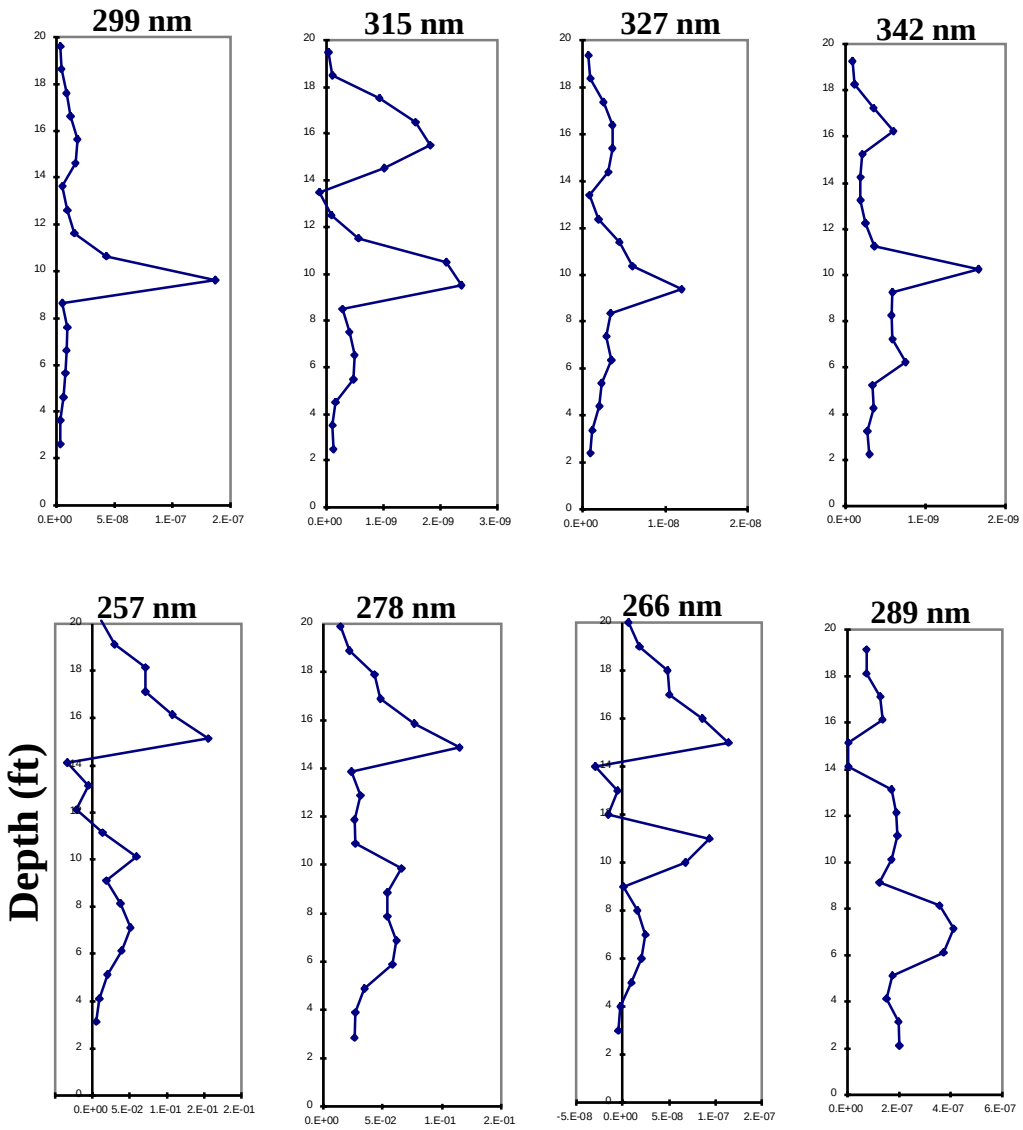

Figure 4. Depth vs. summed fluorescence plots for each excitation wavelength during push 5.

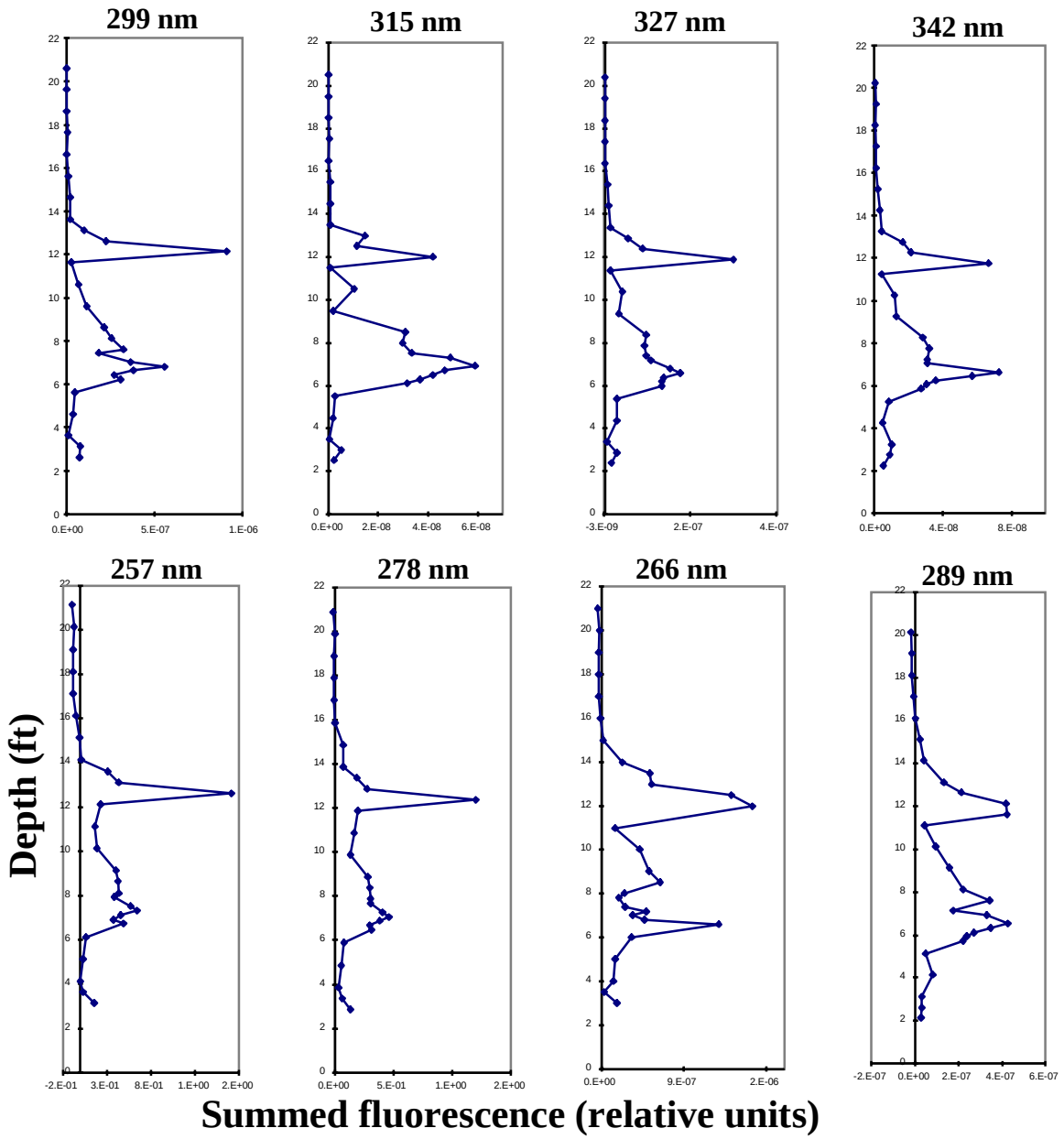

Figure 5. Depth vs. summed fluorescence plots for each excitation wavelength during push 6.

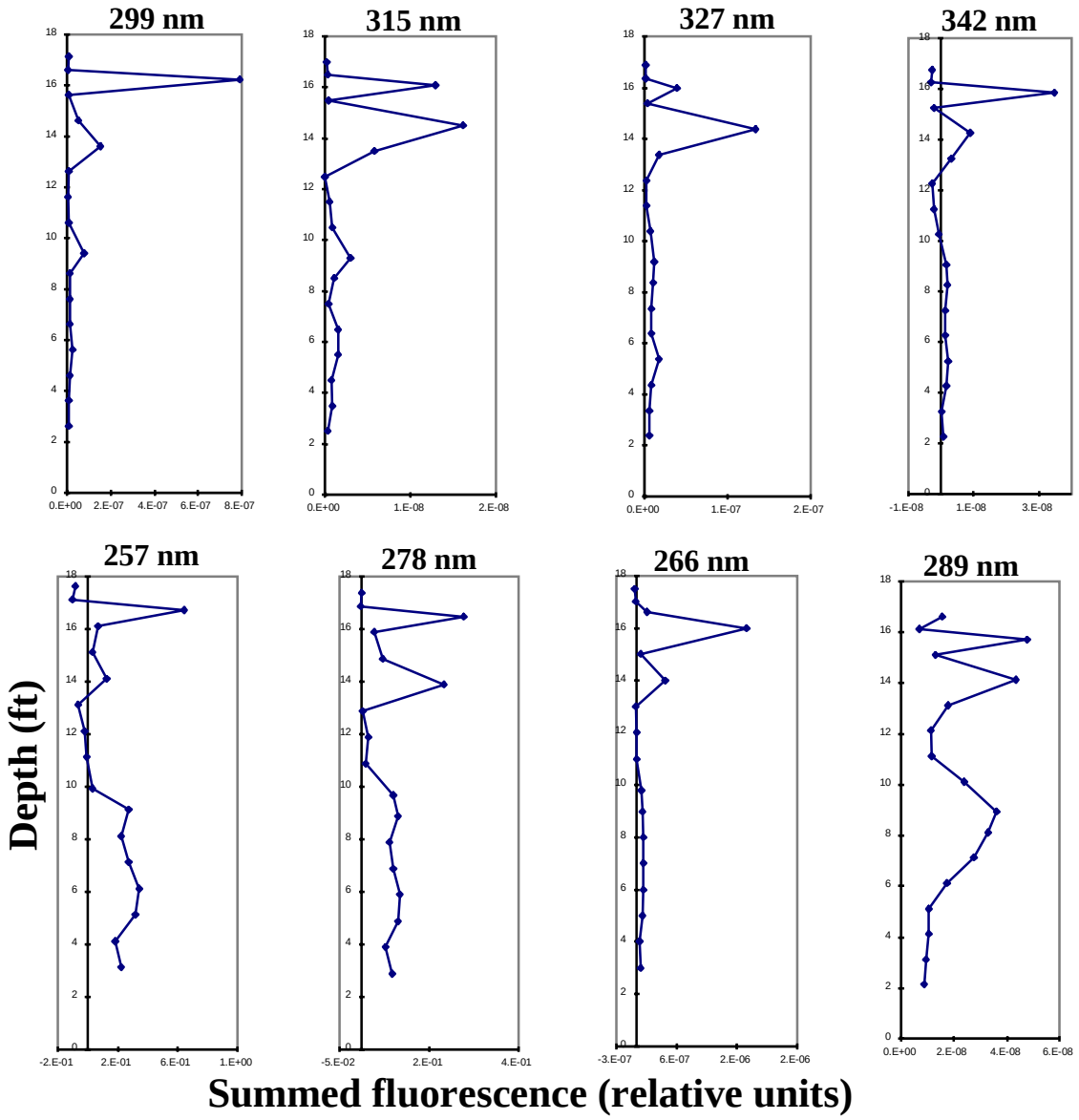

Figure 6. Depth vs. summed fluorescence plots for each excitation wavelength during push 7.

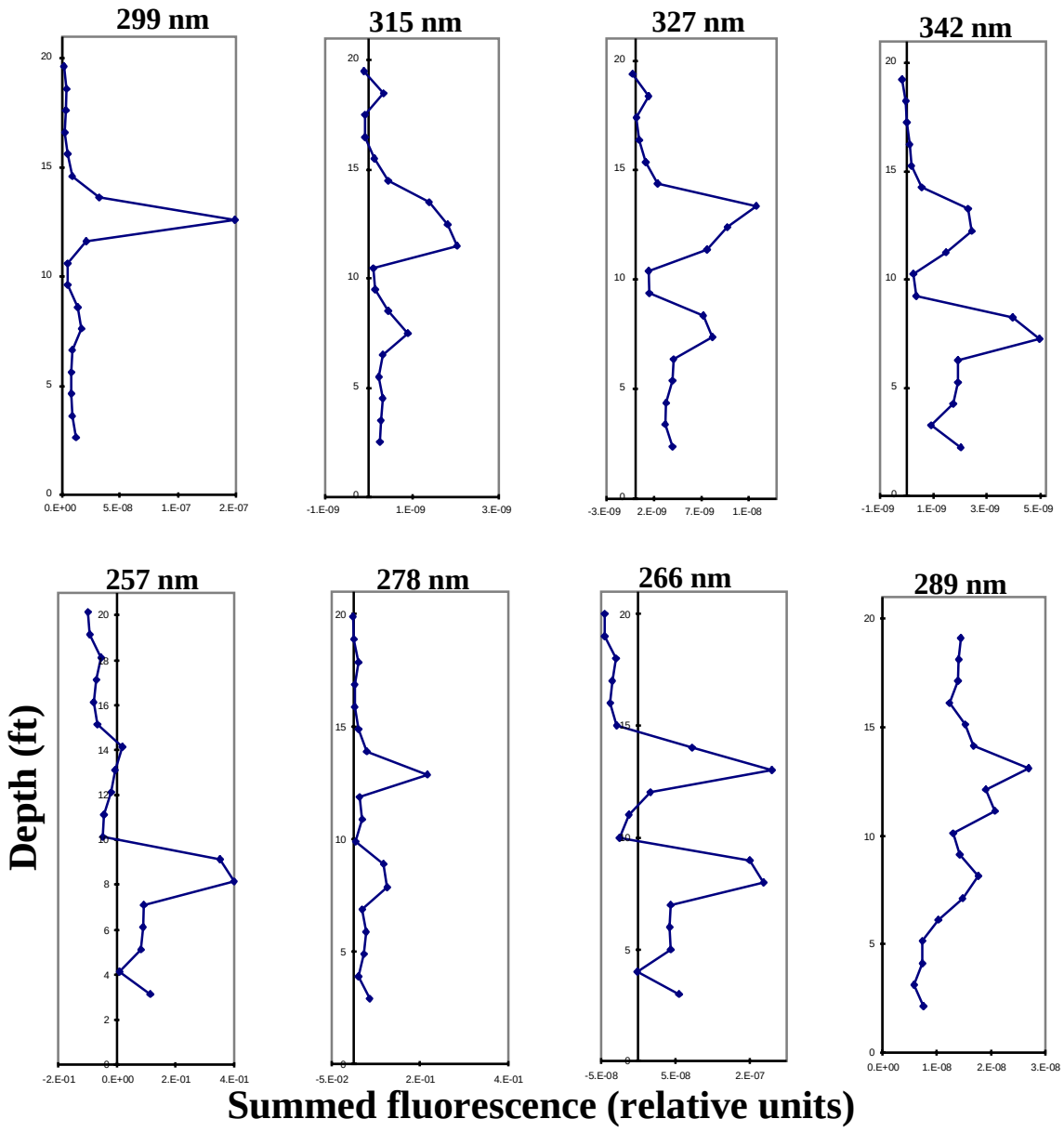

Figure 7. Depth vs. summed fluorescence plots for each excitation wavelength during push 8.

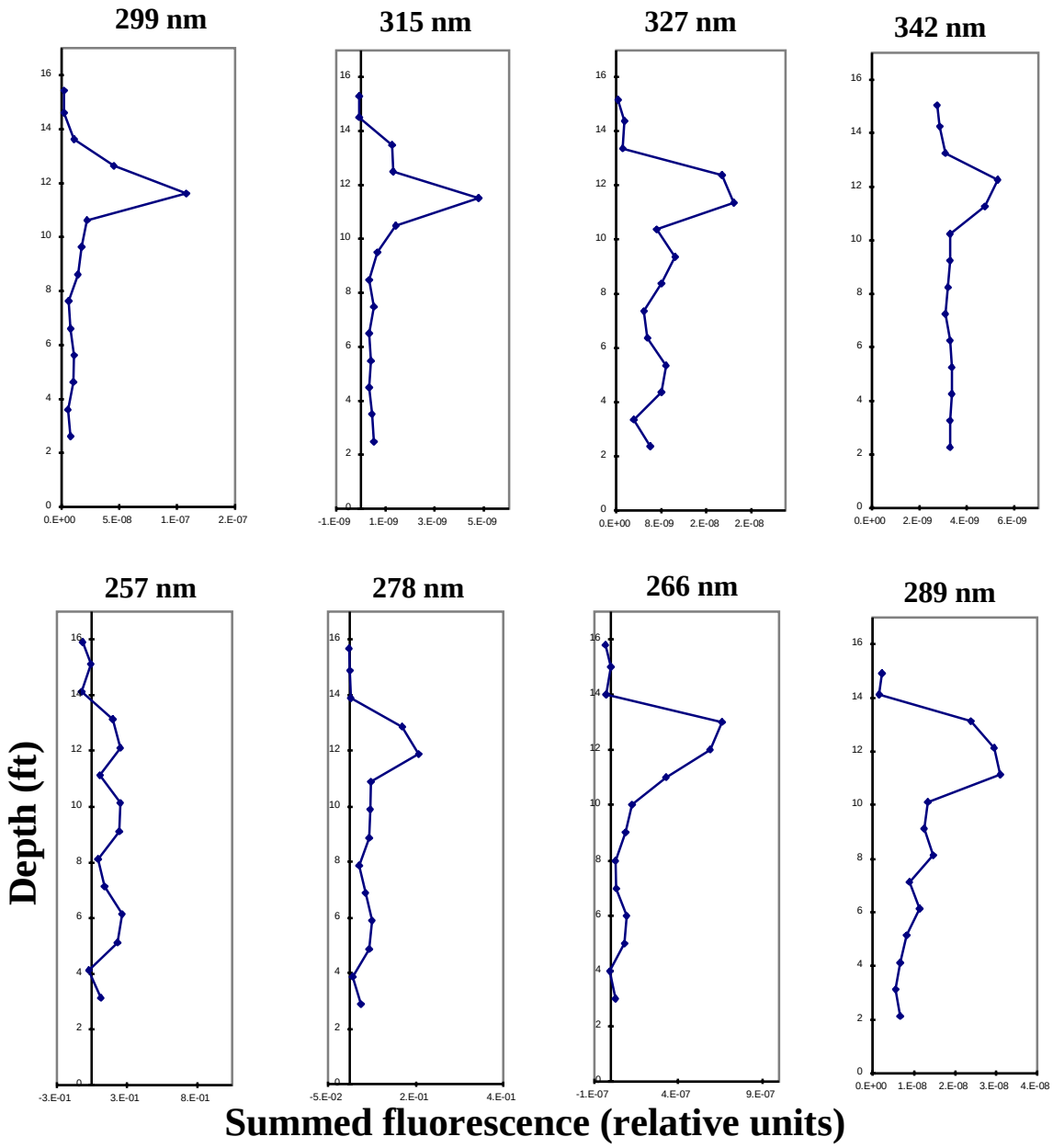

Figure 8. Depth vs. summed fluorescence plots for each excitation wavelength during push 9.

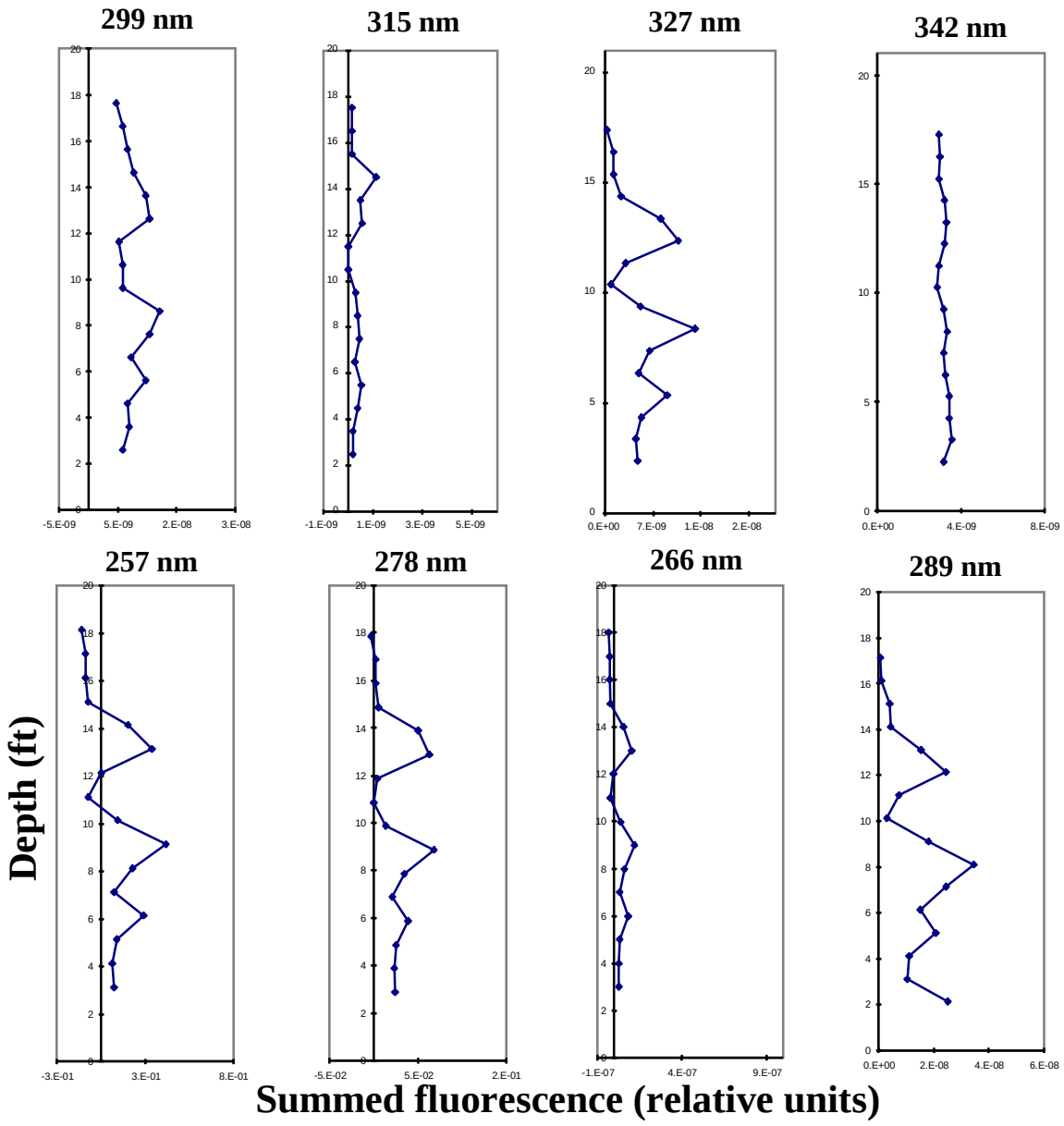

Figure 9. Depth vs. summed fluorescence plots for each excitation wavelength during push 10.

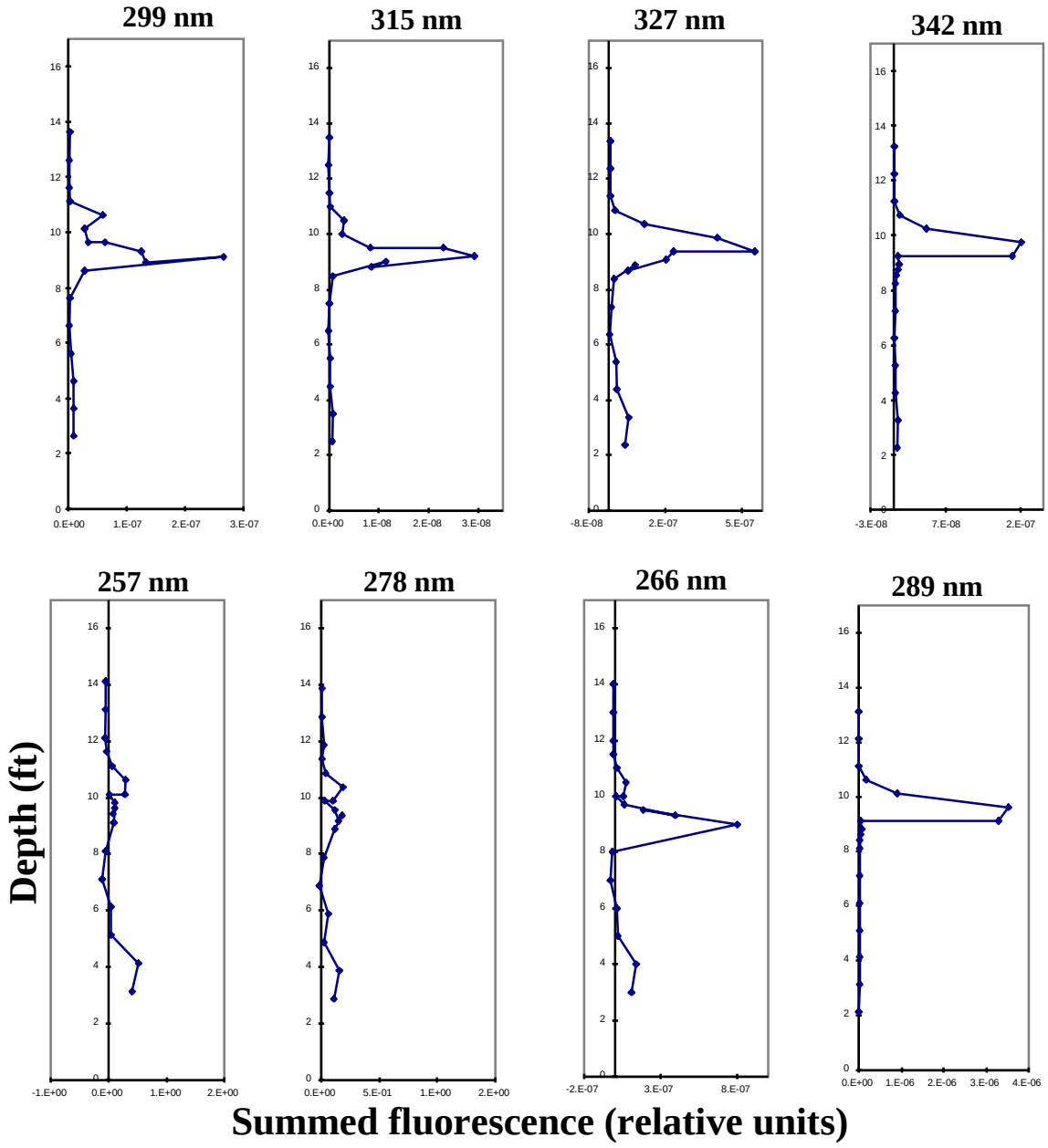

Figure 10. Depth vs. summed fluorescence plots for each excitation wavelength during push 11.

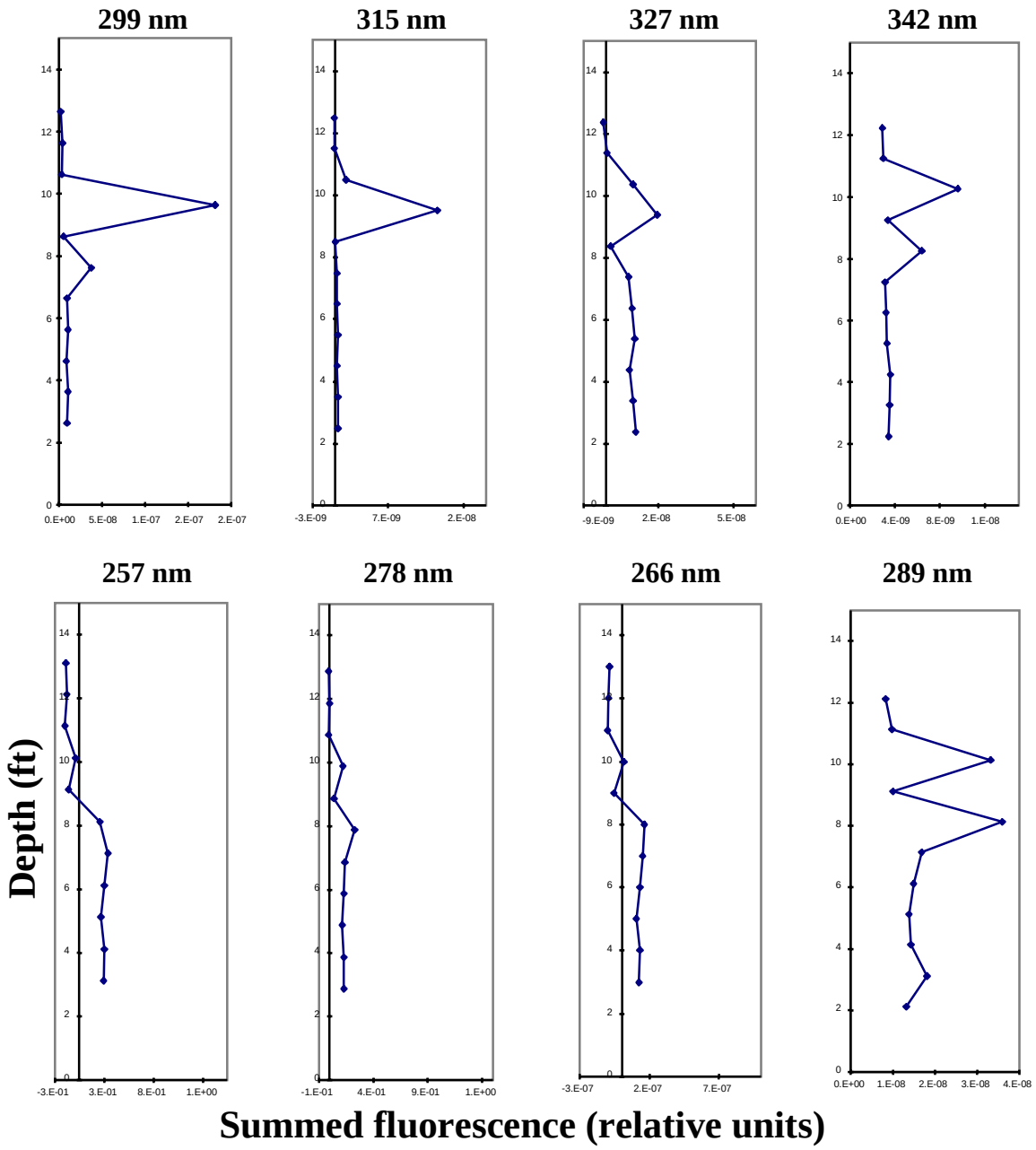

Figure 11. Depth vs. summed fluorescence plots for each excitation wavelength during push 12.

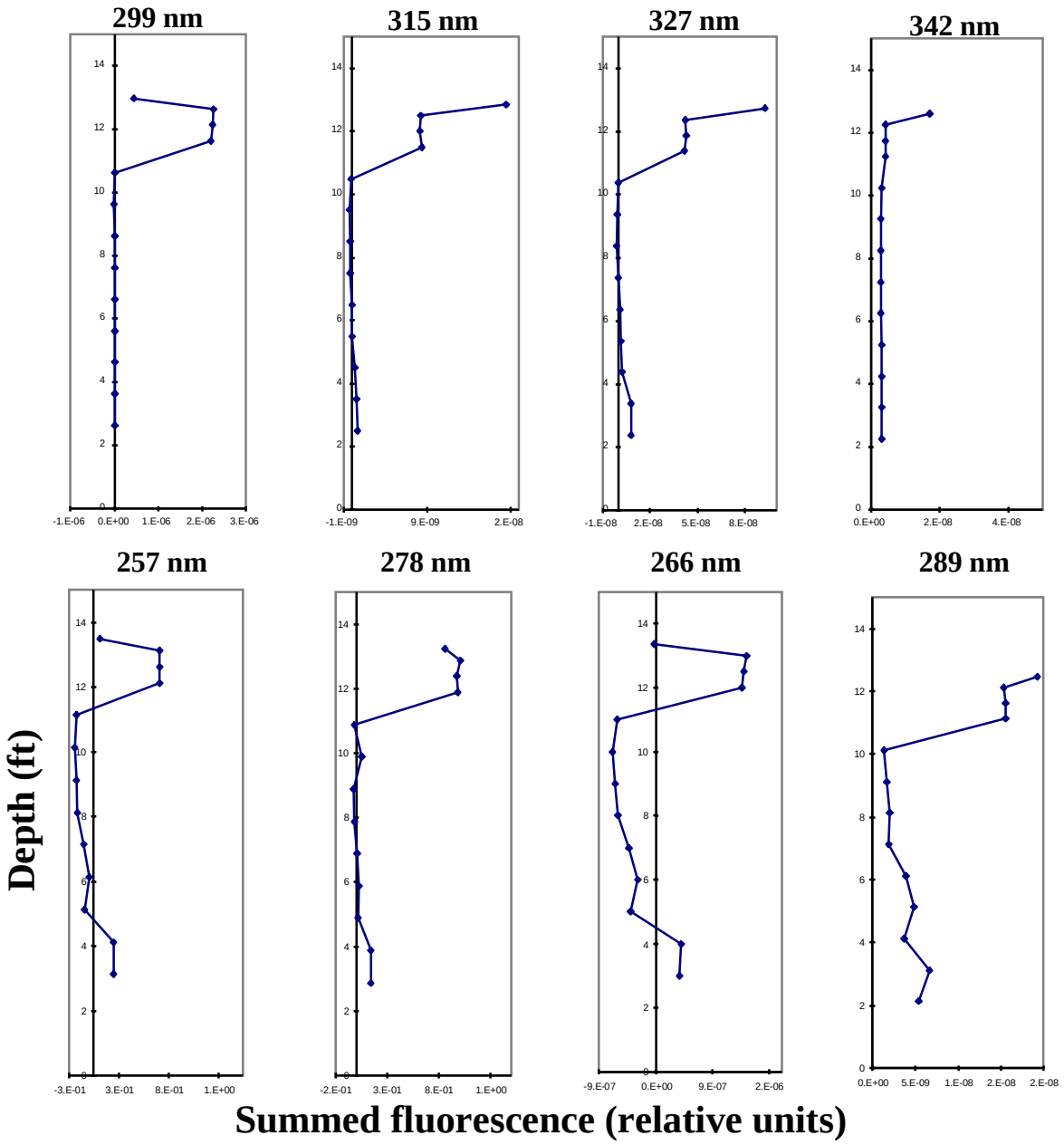

Figure 12. Depth vs. summed fluorescence plots for each excitation wavelength during push 13.

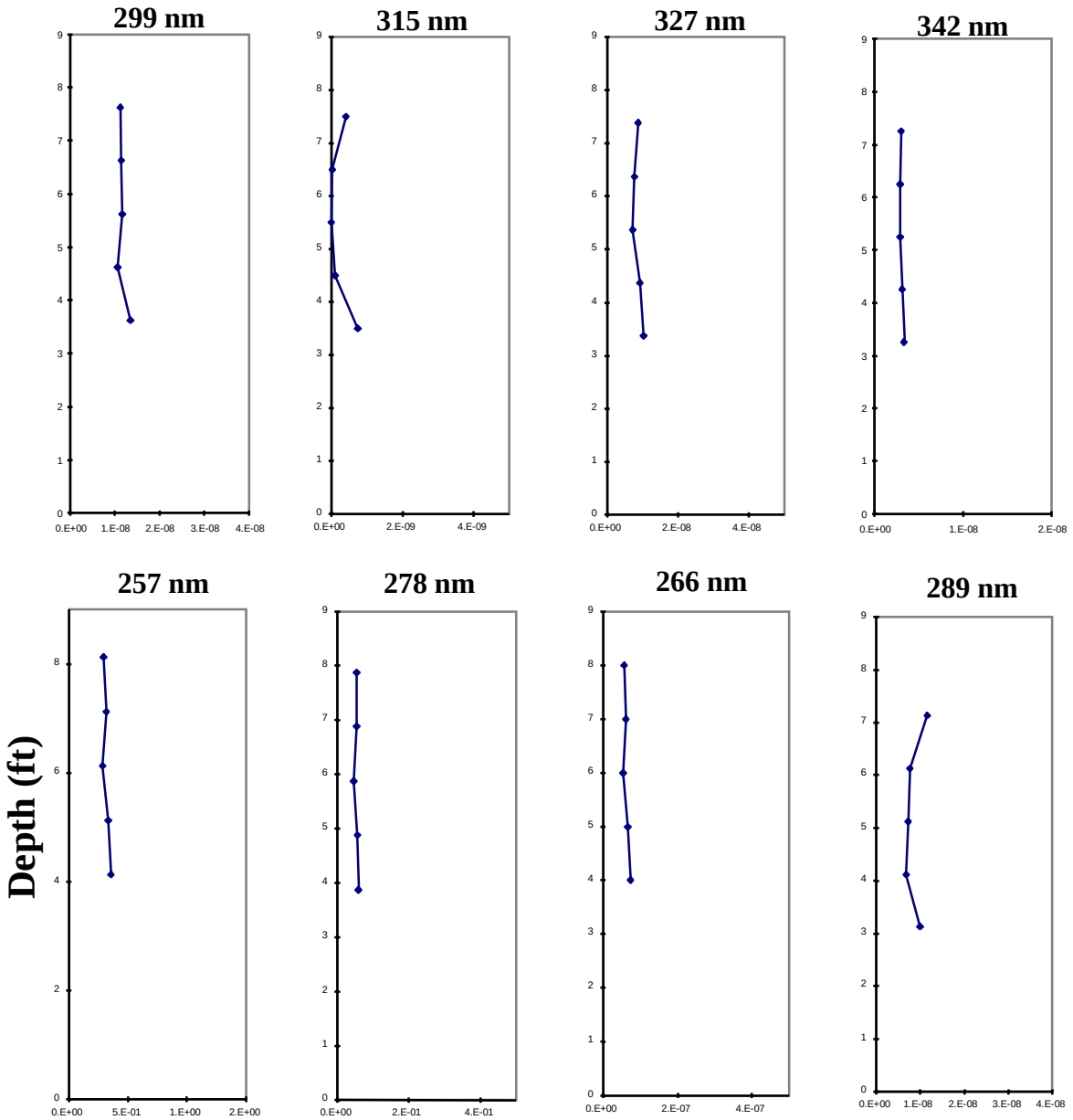

Figure 13. Depth vs. summed fluorescence plots for each excitation wavelength during push 14.

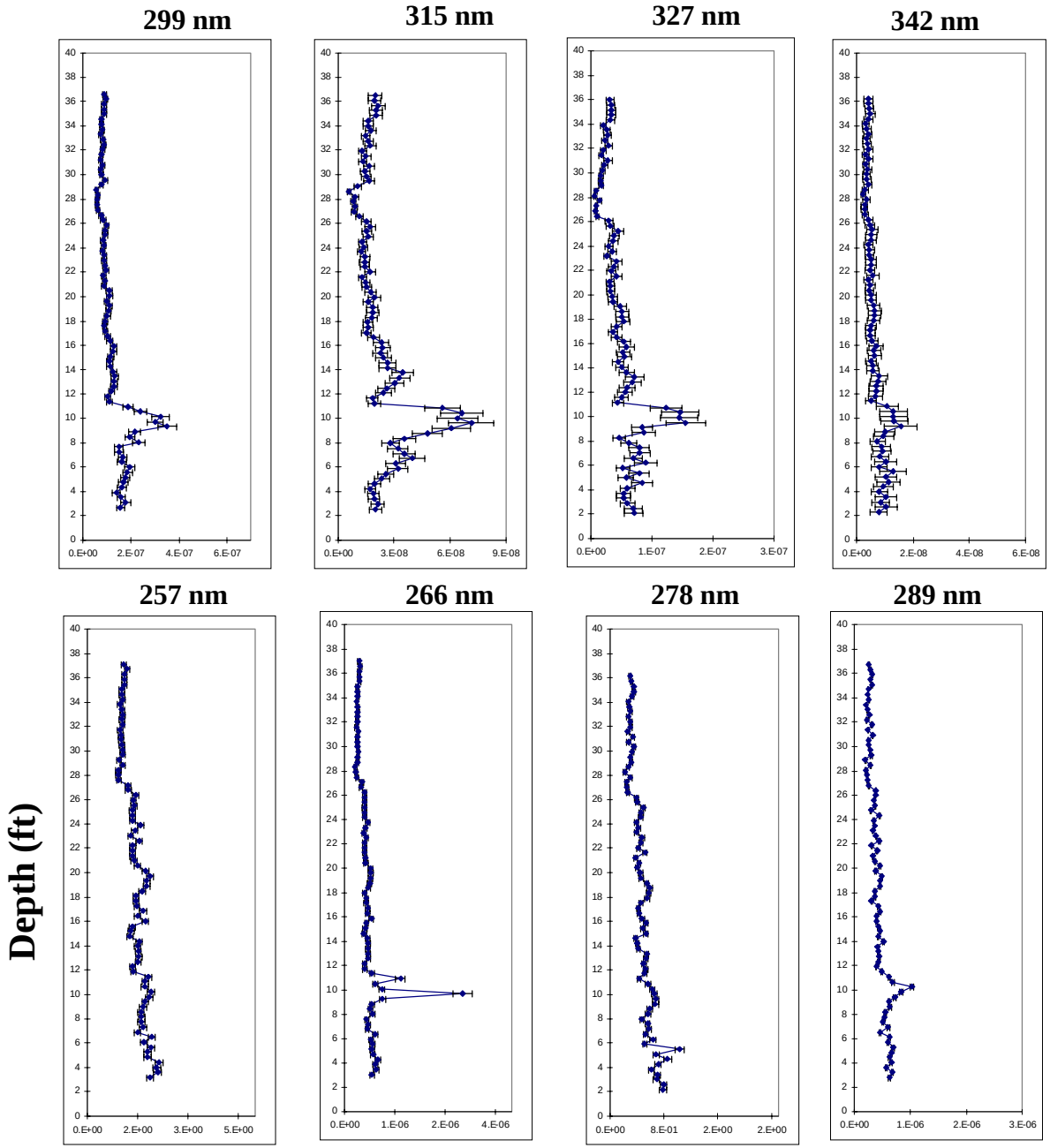

Figure 1. Depth vs. summed fluorescence for each excitation wavelength for push 1.

Appendix B

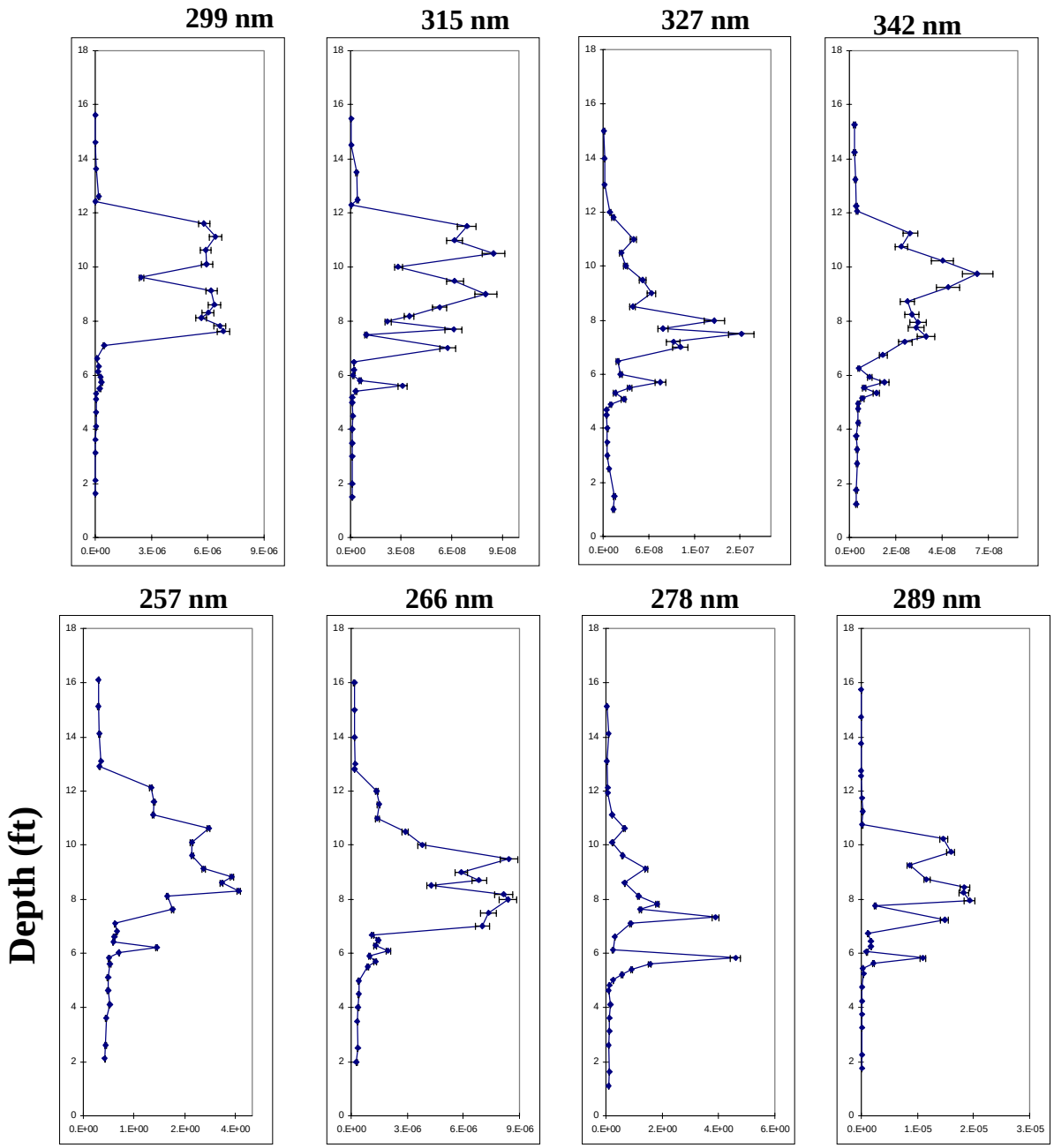

Figure 2. Depth vs. summed fluorescence for each excitation wavelength for push 2.

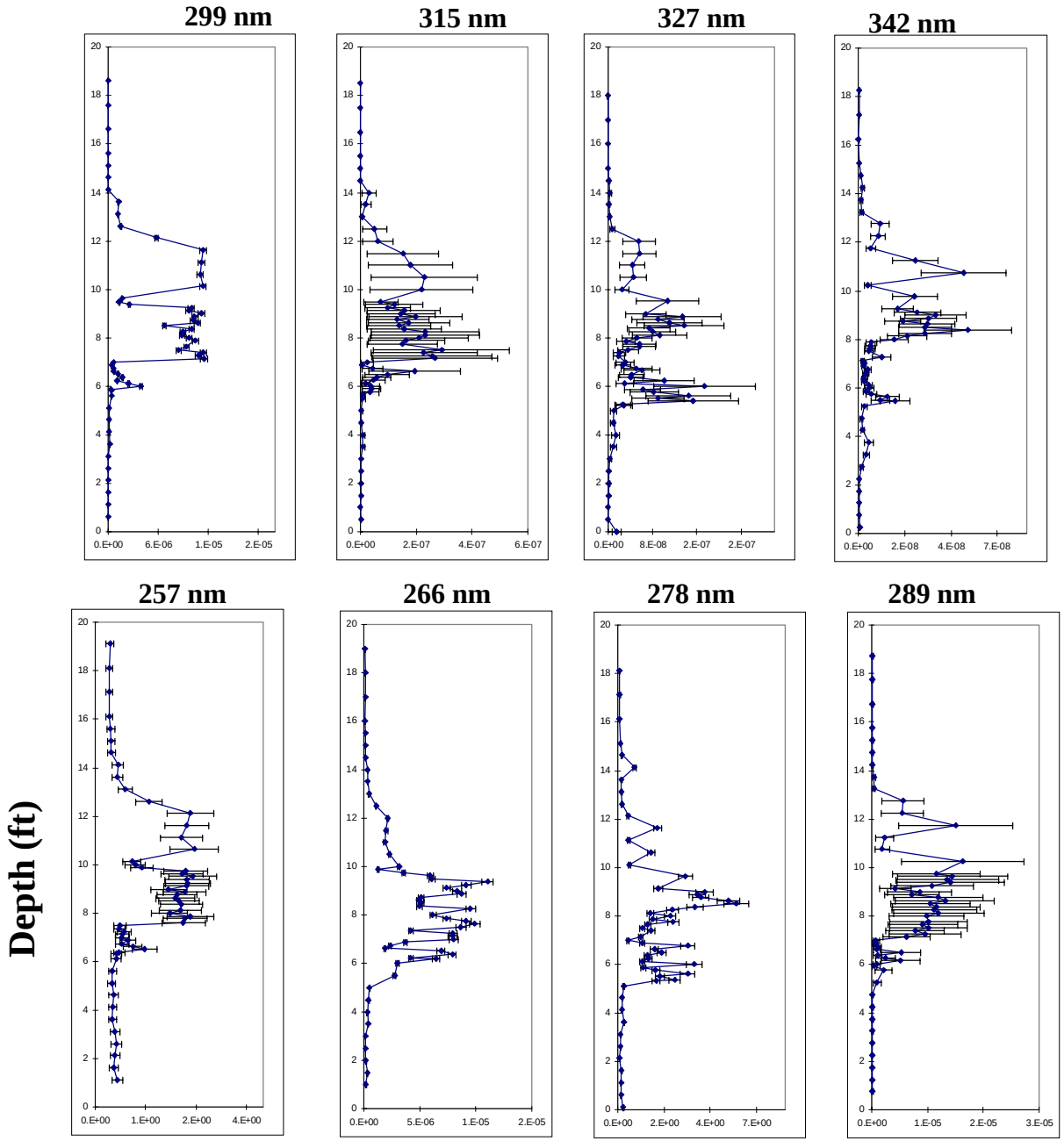

Figure 3. Depth vs. summed fluorescence for each excitation wavelength for push 3.

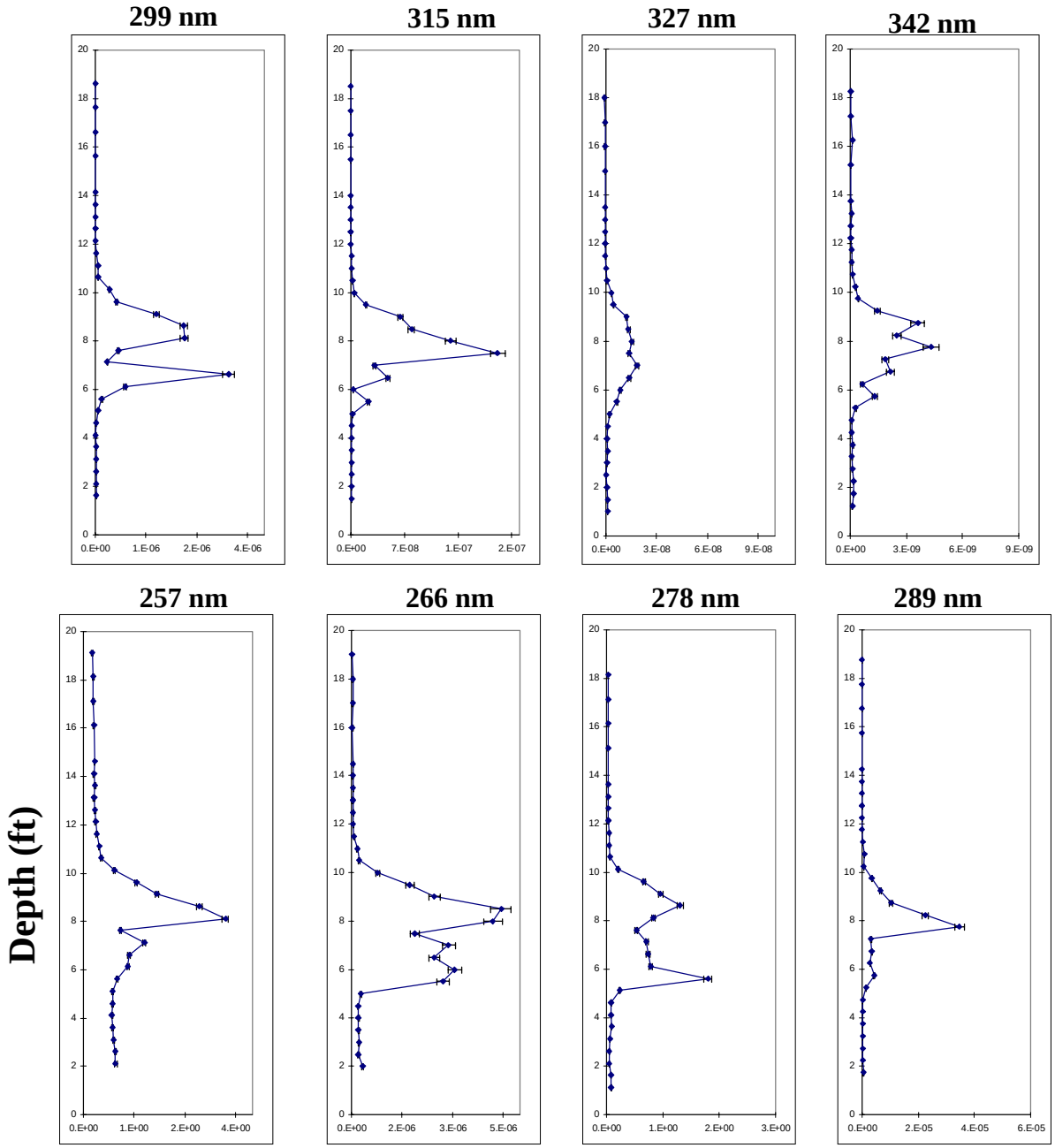

Figure 4. Depth vs. summed fluorescence for each excitation wavelength for push 4.

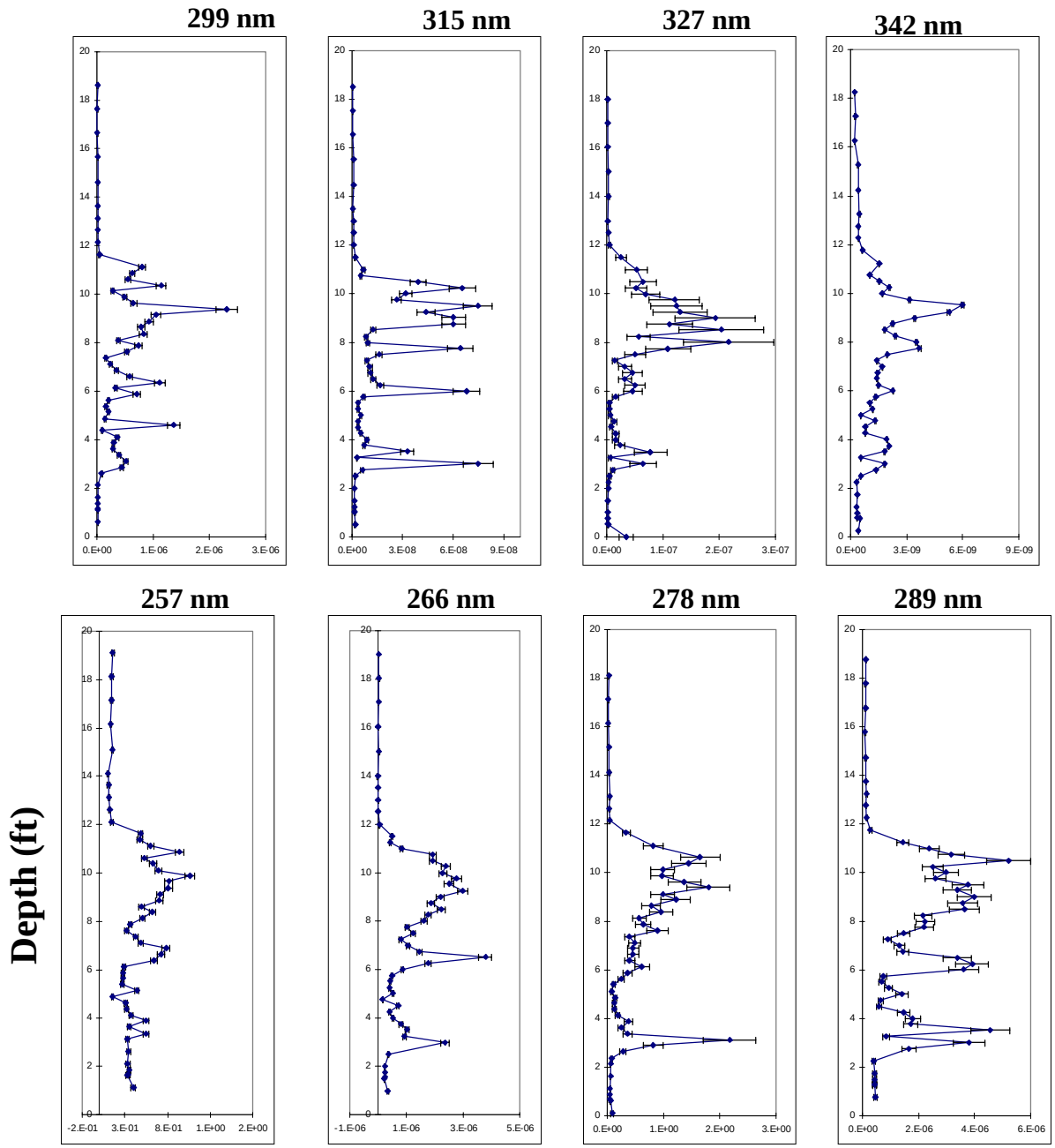

Figure 5. Depth vs. summed fluorescence for each excitation wavelength for push 5.

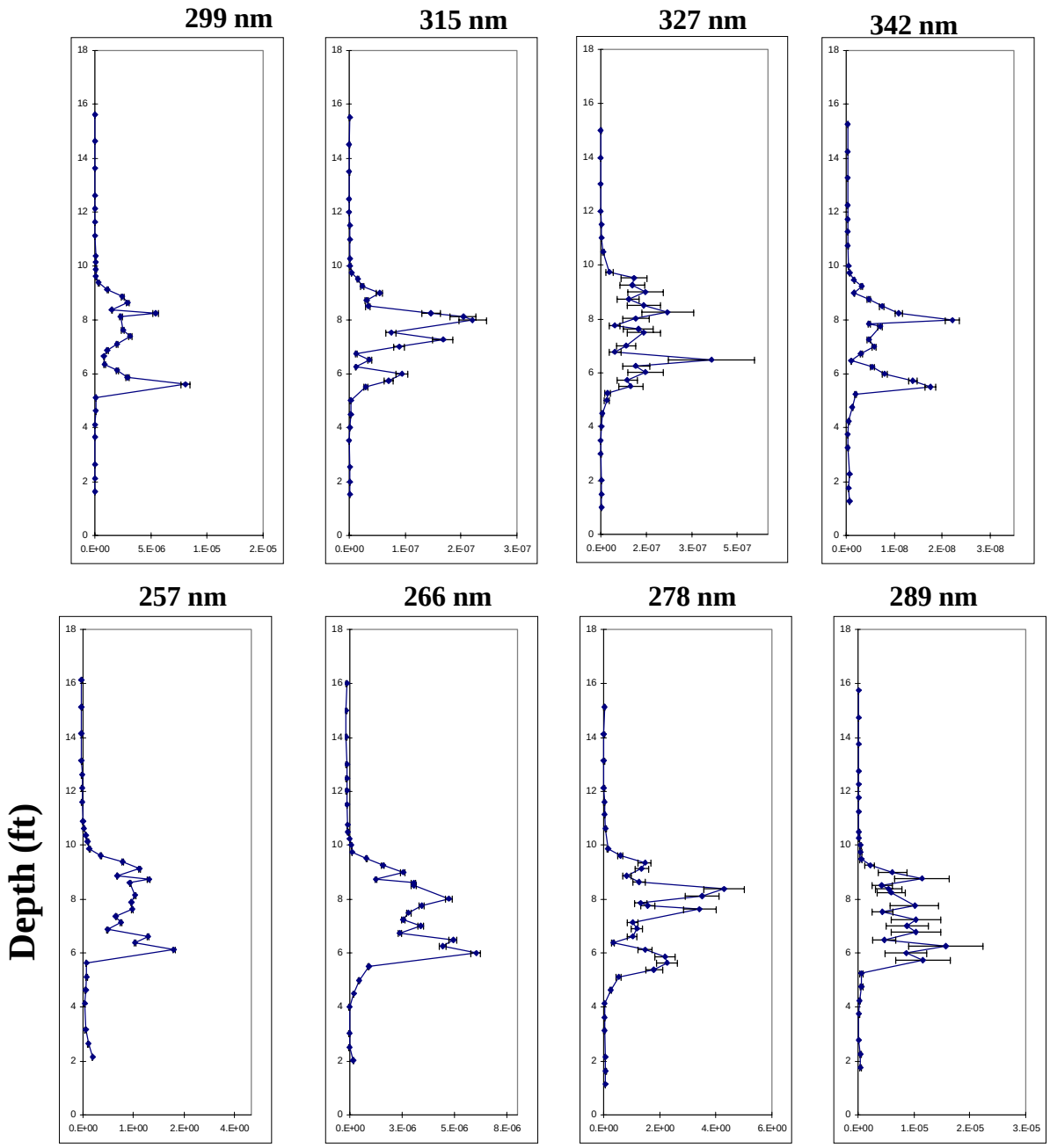

Figure 6. Depth vs. summed fluorescence for each excitation wavelength for push 6.

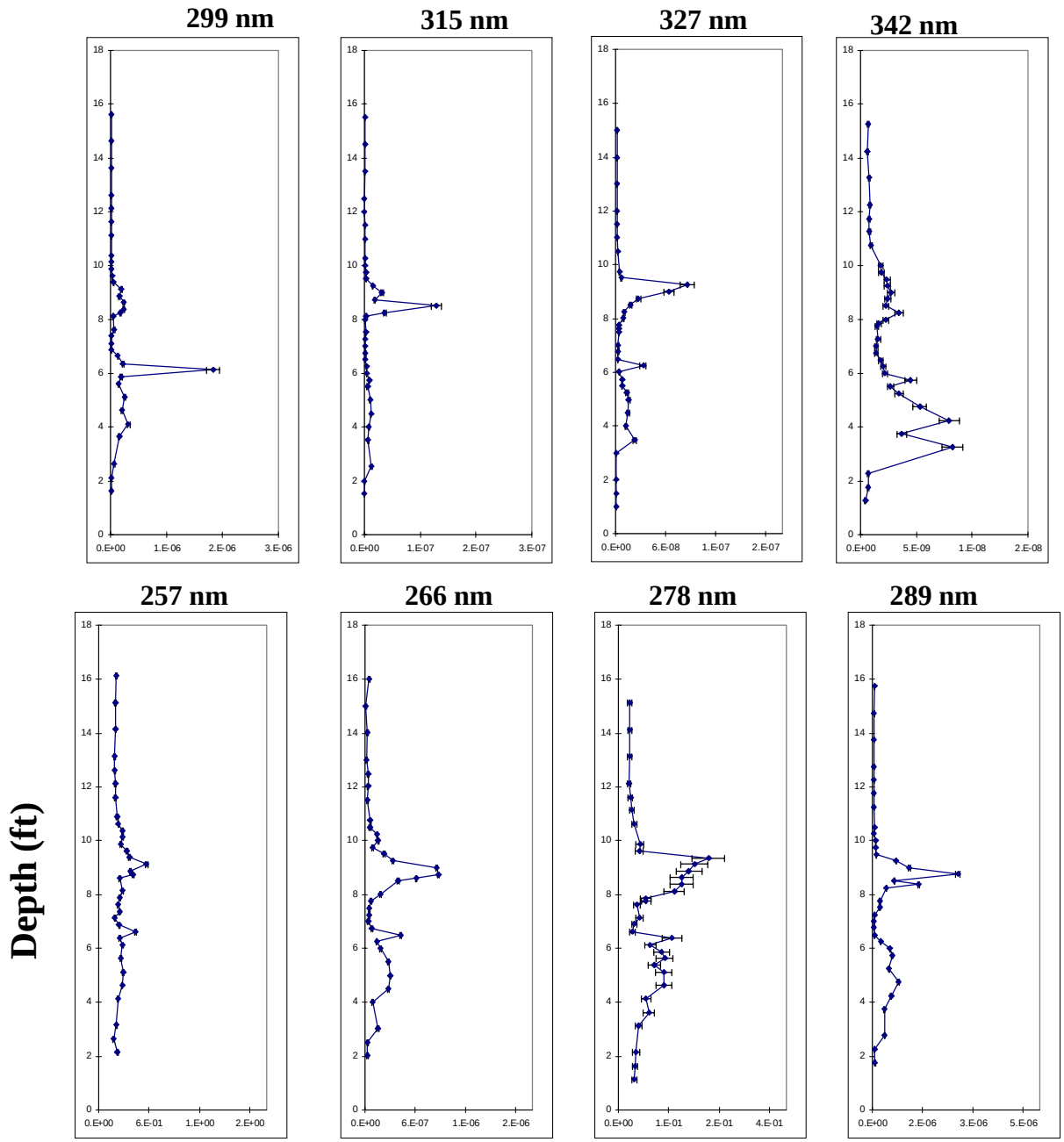

Figure 7. Depth vs. summed fluorescence for each excitation wavelength for push 7.

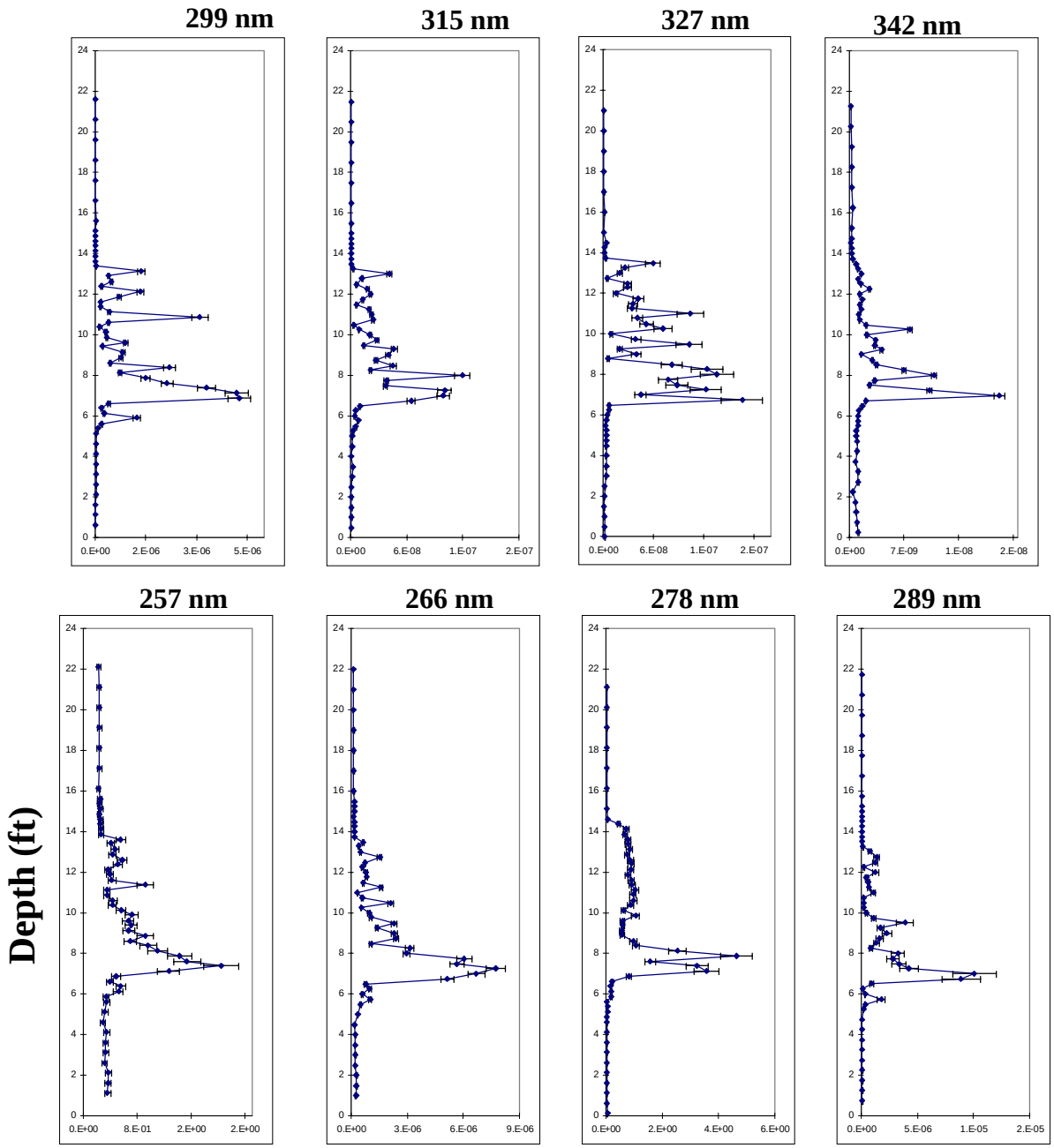

Figure 8. Depth vs. summed fluorescence for each excitation wavelength for push 8.

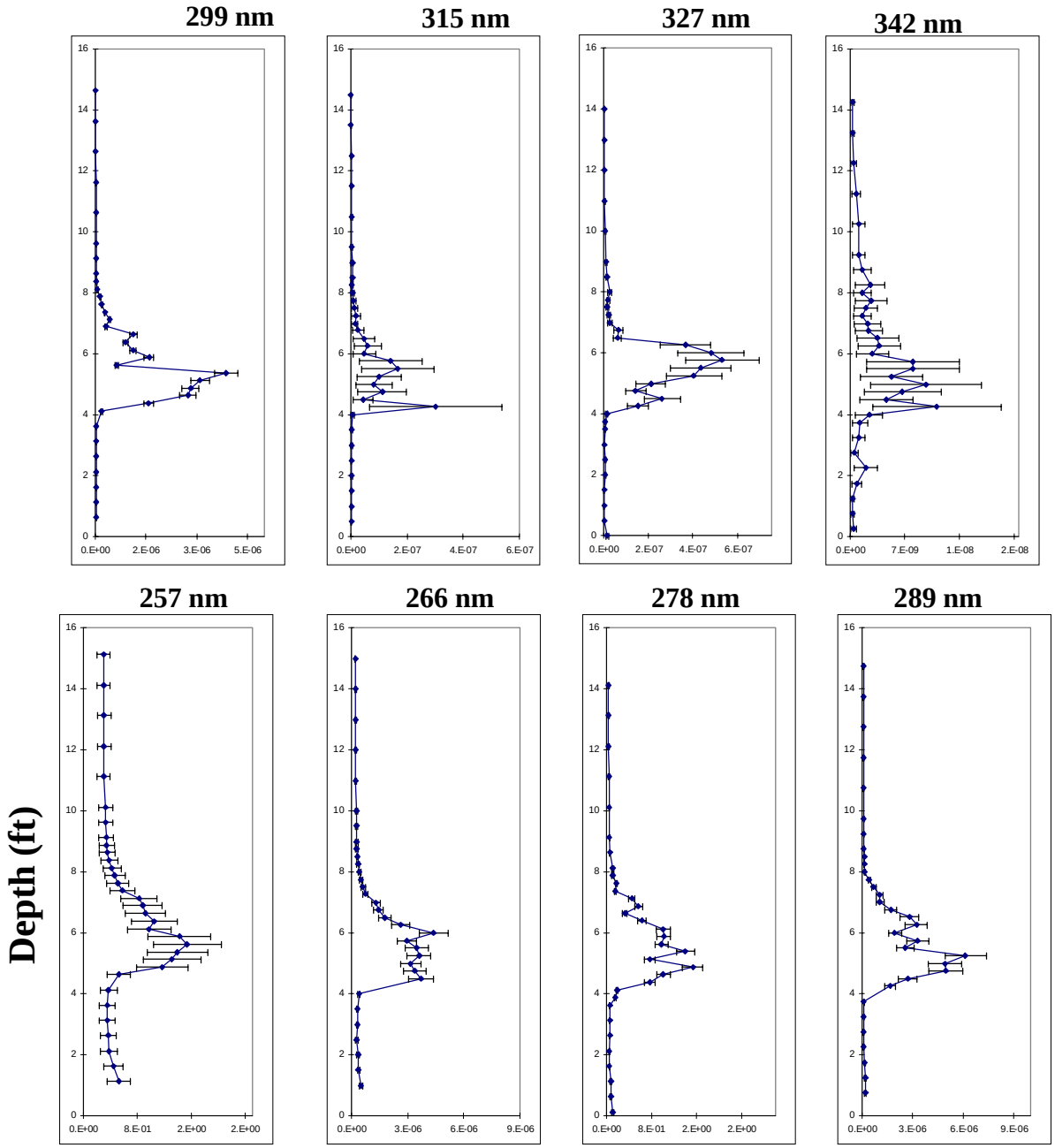

Figure 9. Depth vs. summed fluorescence for each excitation wavelength for push 9.

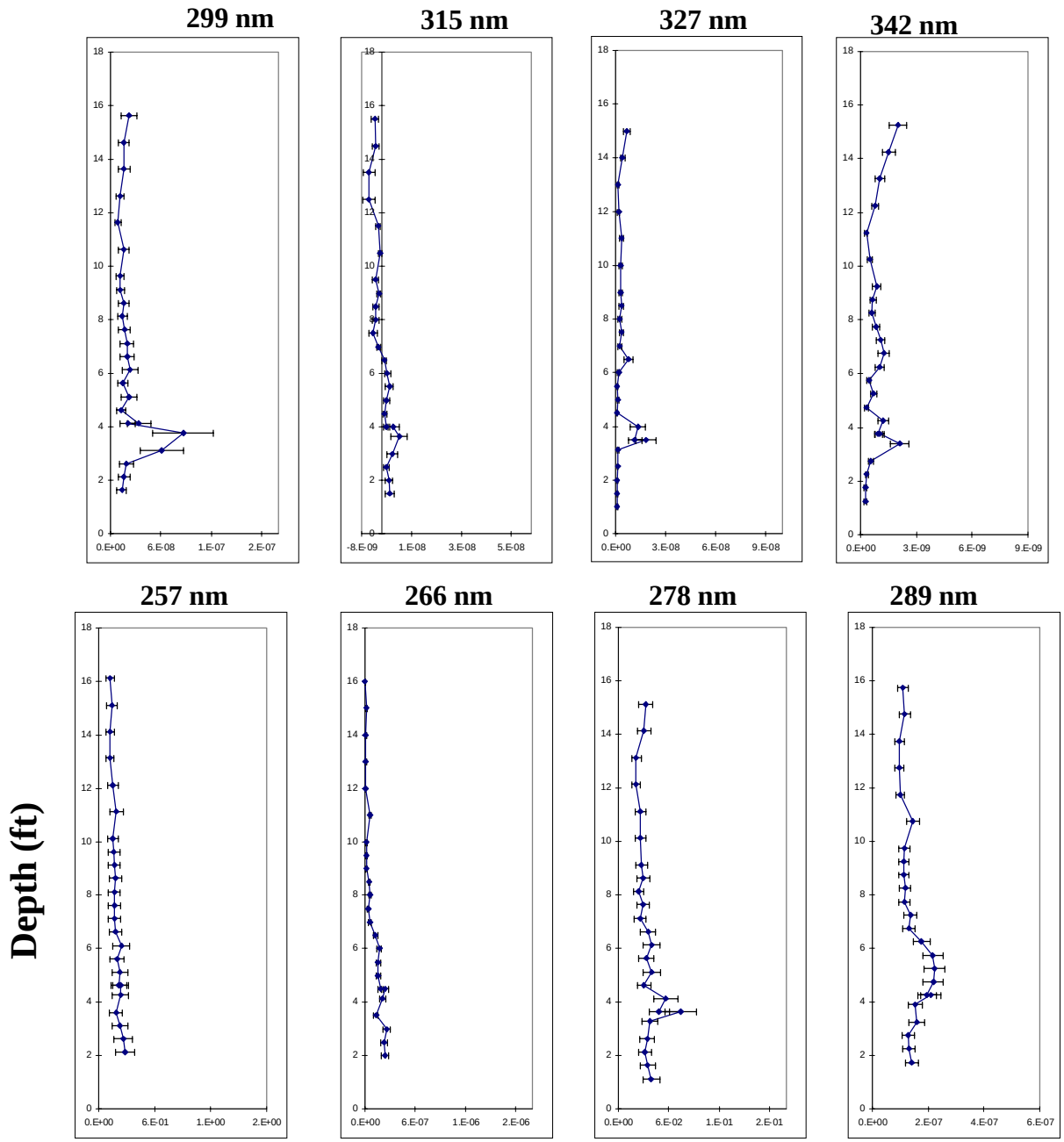

Figure 10. Depth vs. summed fluorescence for each excitation wavelength for push 10.

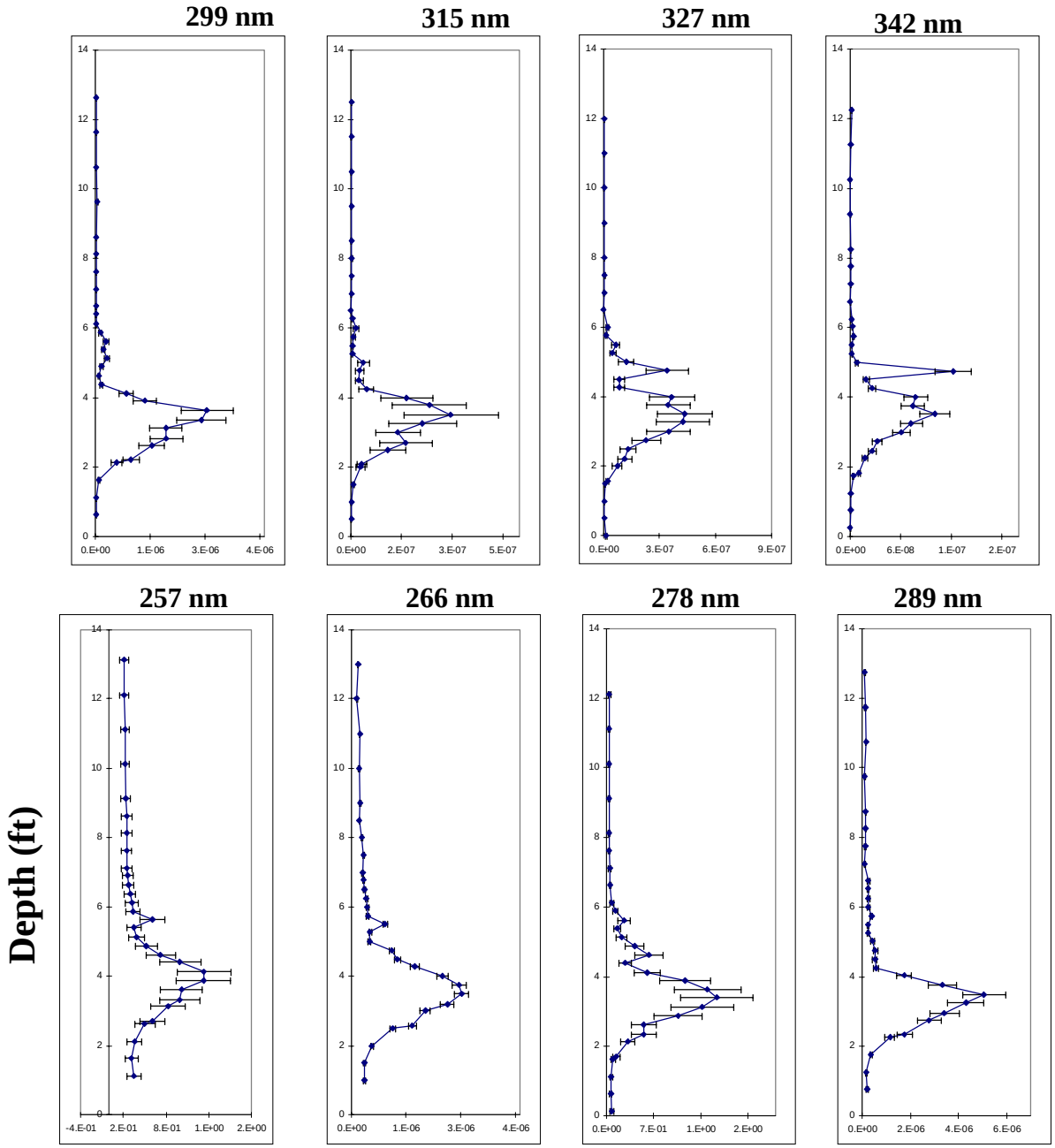

Figure 11. Depth vs. summed fluorescence for each excitation wavelength for push 11.

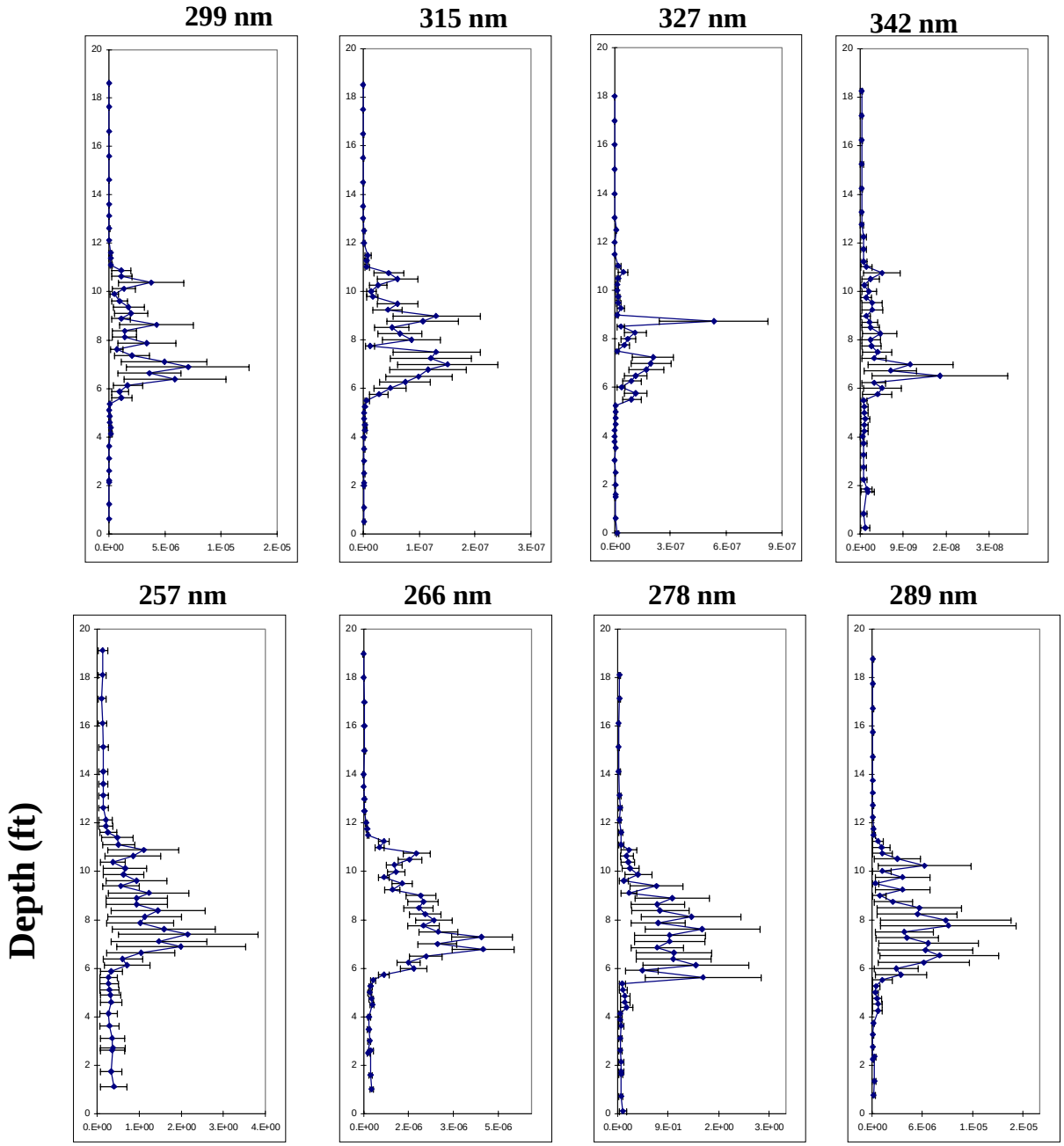

Figure 12. Depth vs. summed fluorescence for each excitation wavelength for push 12.

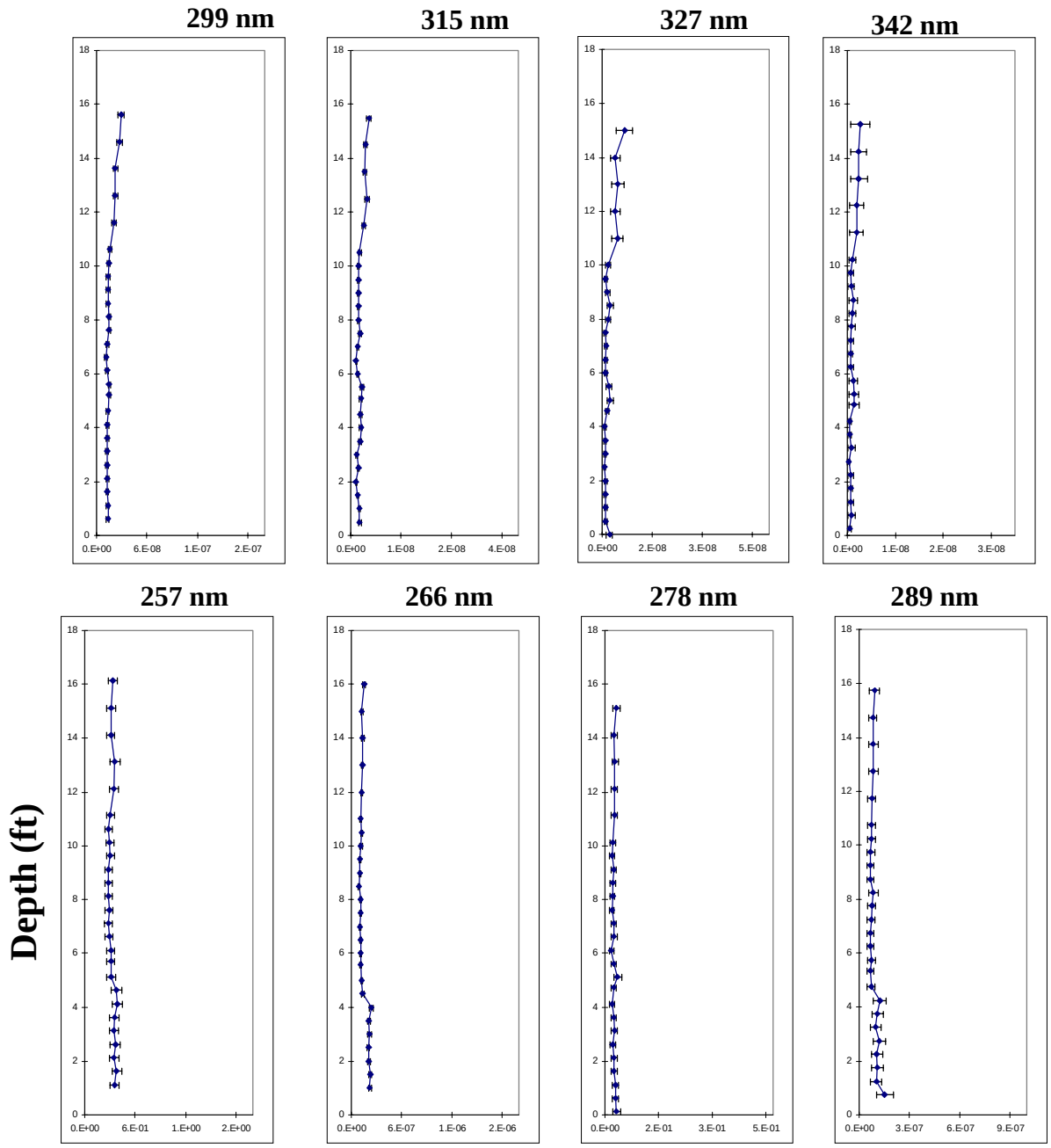

Figure 13. Depth vs. summed fluorescence for each excitation wavelength for push 13.

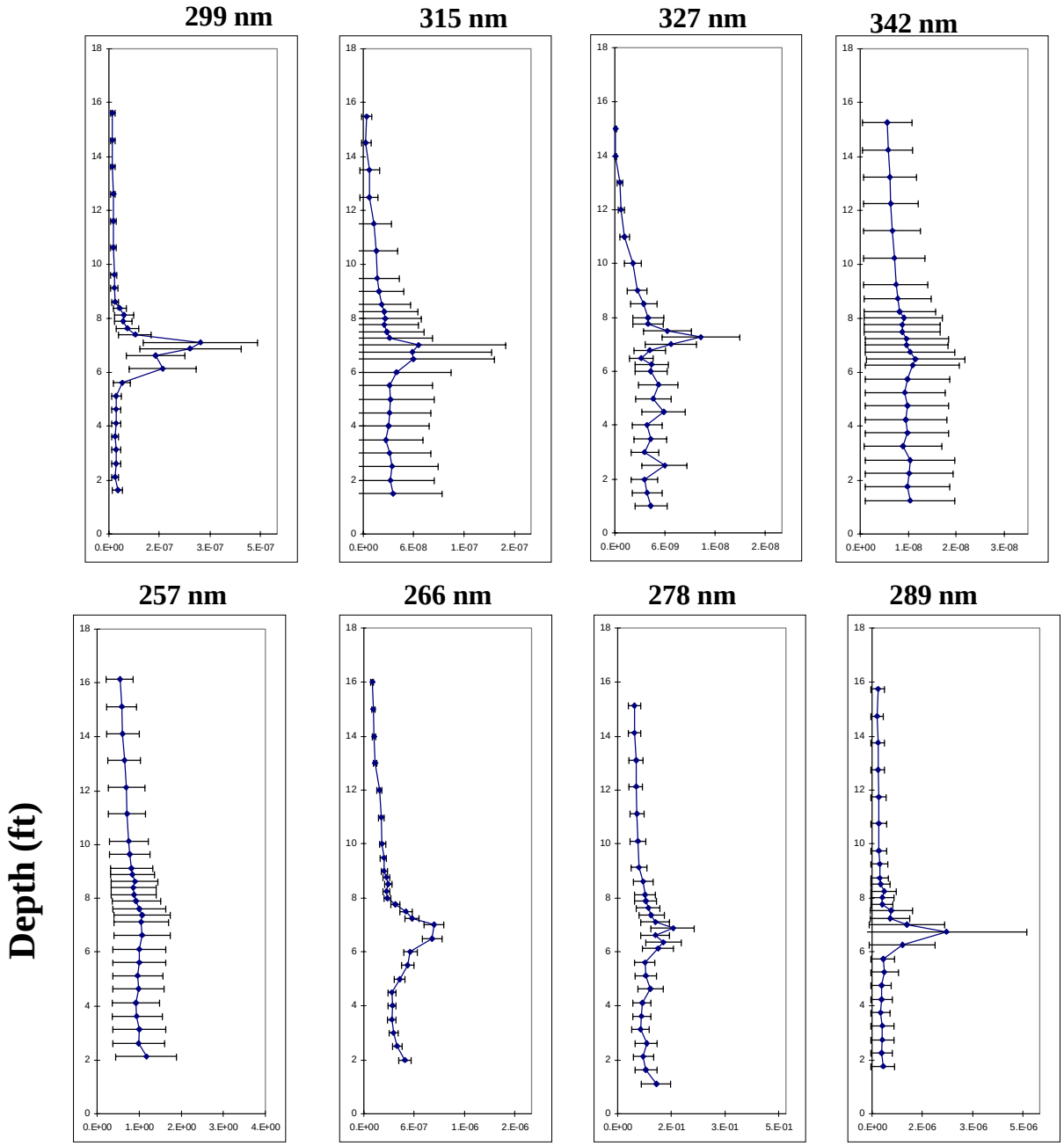

Figure 14. Depth vs. summed fluorescence for each excitation wavelength for push 14.

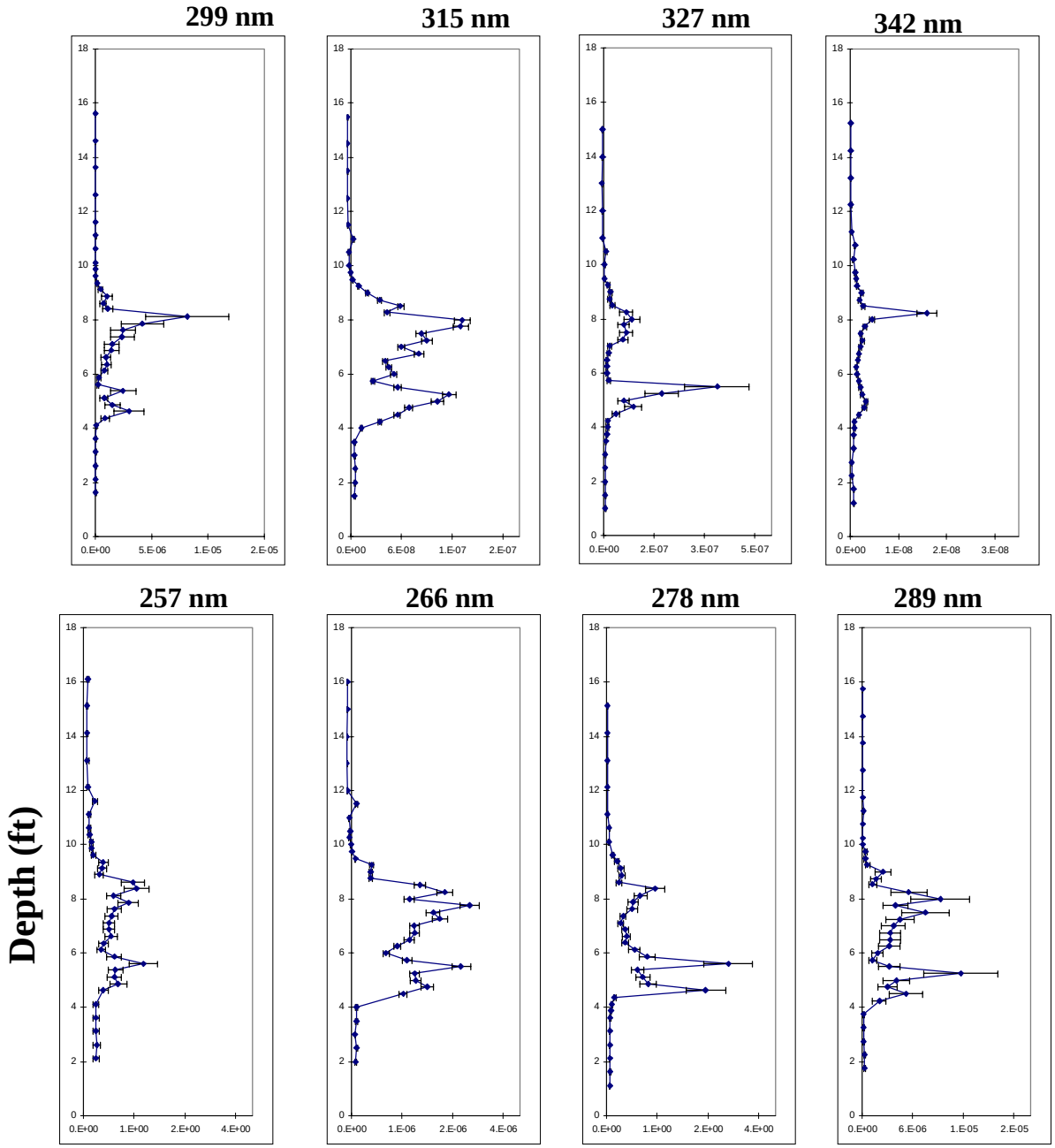

Figure 15. Depth vs. summed fluorescence for each excitation wavelength for push 15.

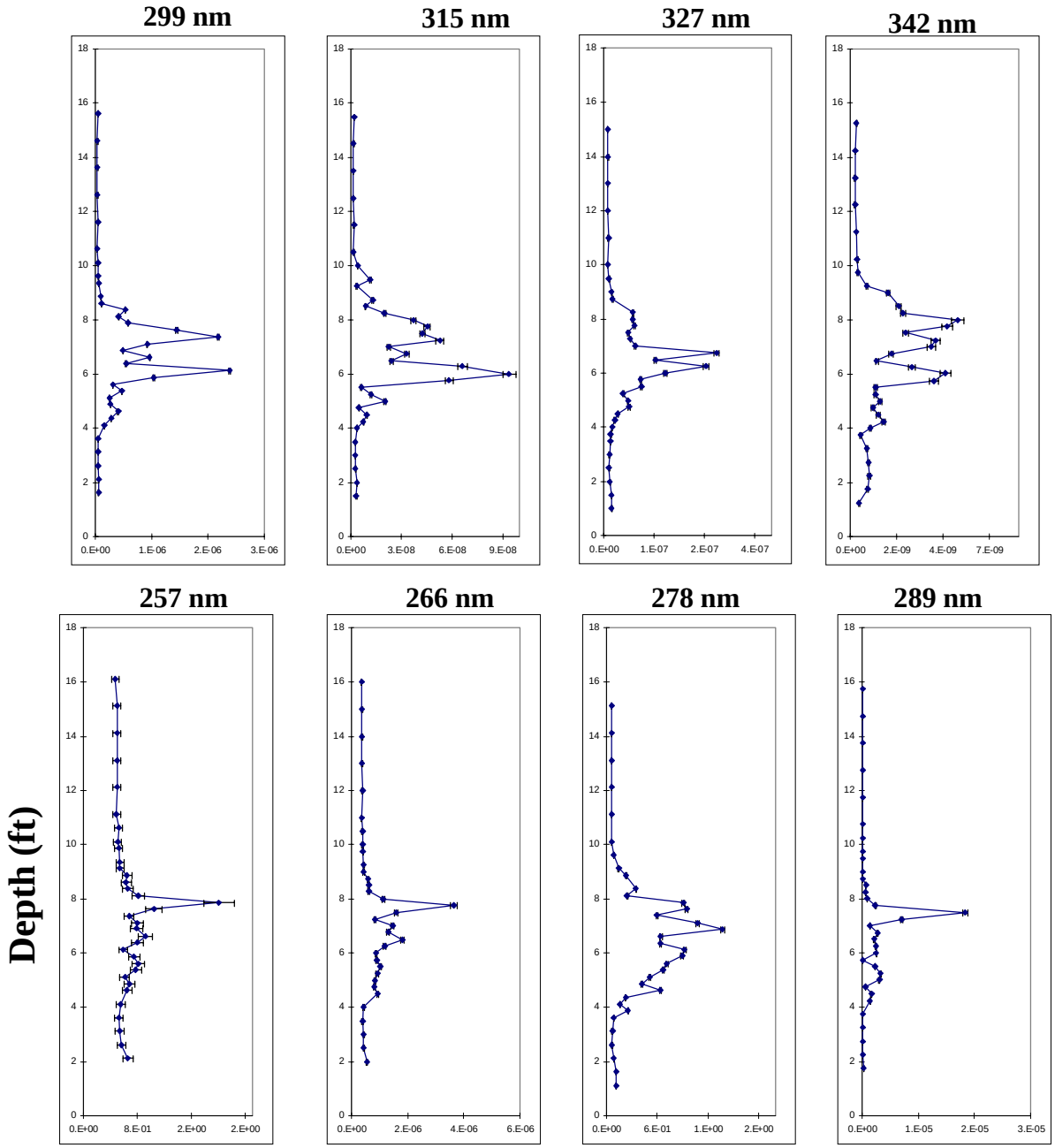

Figure 16. Depth vs. summed fluorescence for each excitation wavelength for push 16.

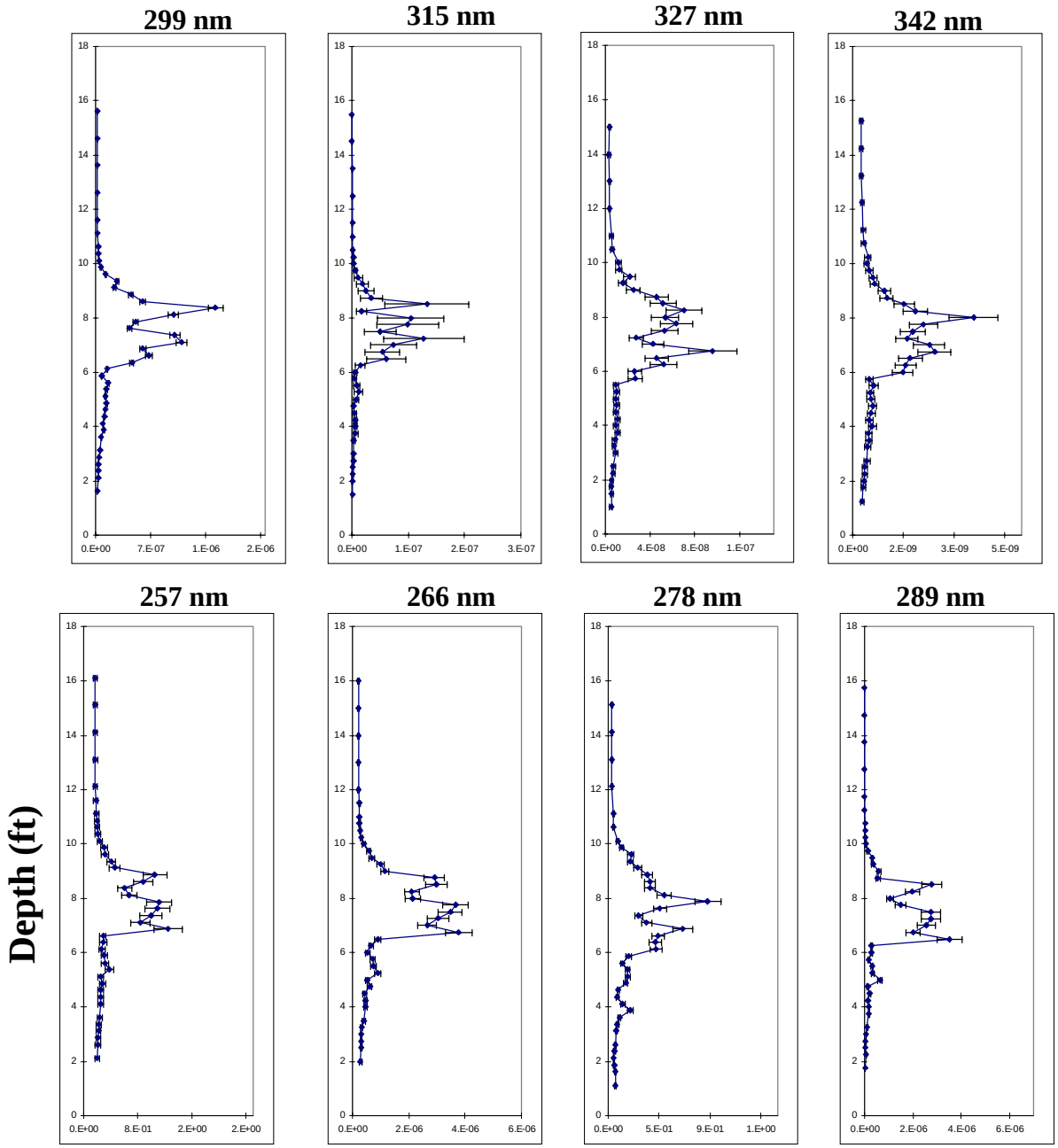

Figure 17. Depth vs. summed fluorescence for each excitation wavelength for push 17.

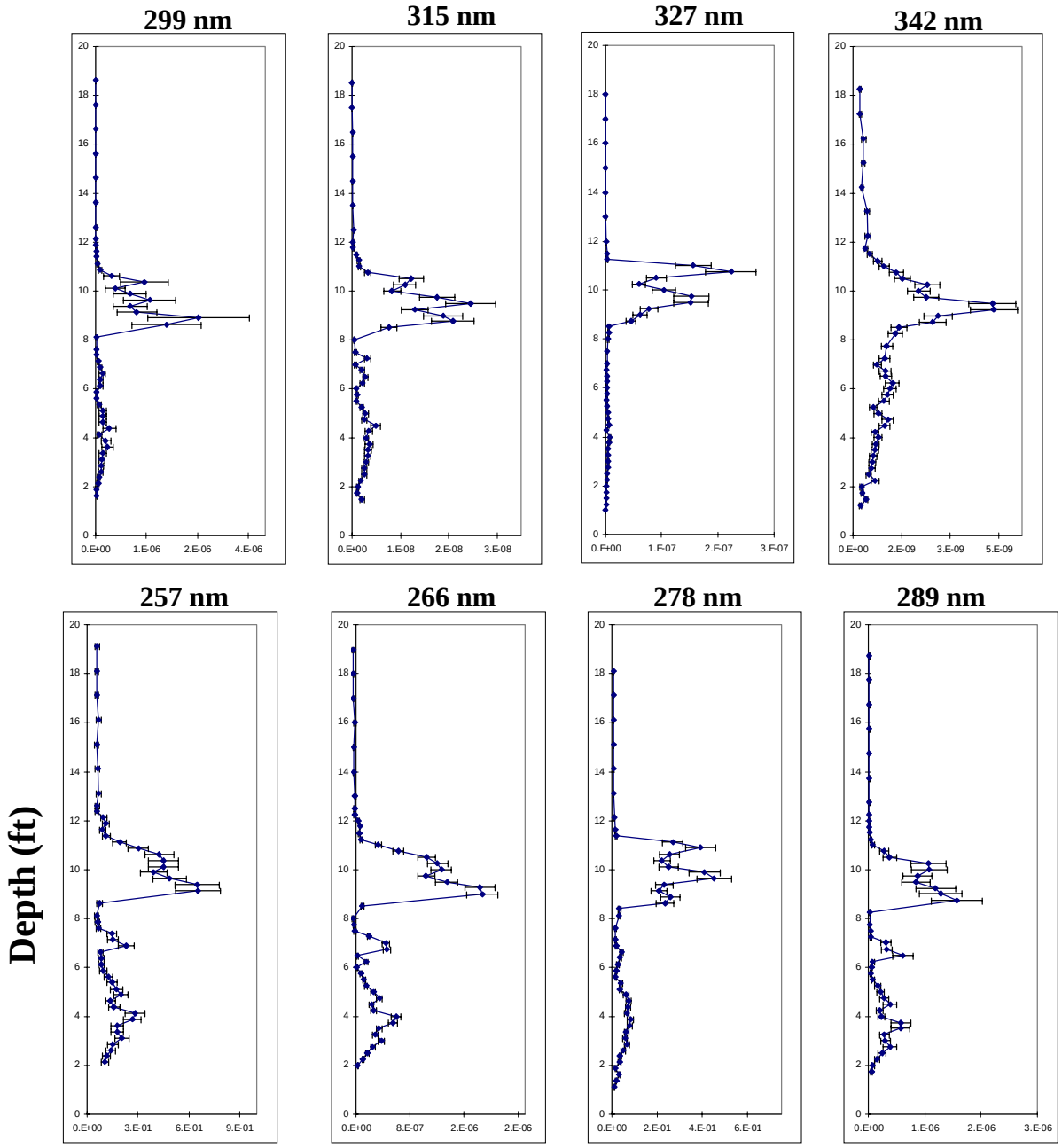

Figure 18. Depth vs. summed fluorescence for each excitation wavelength for push 18.

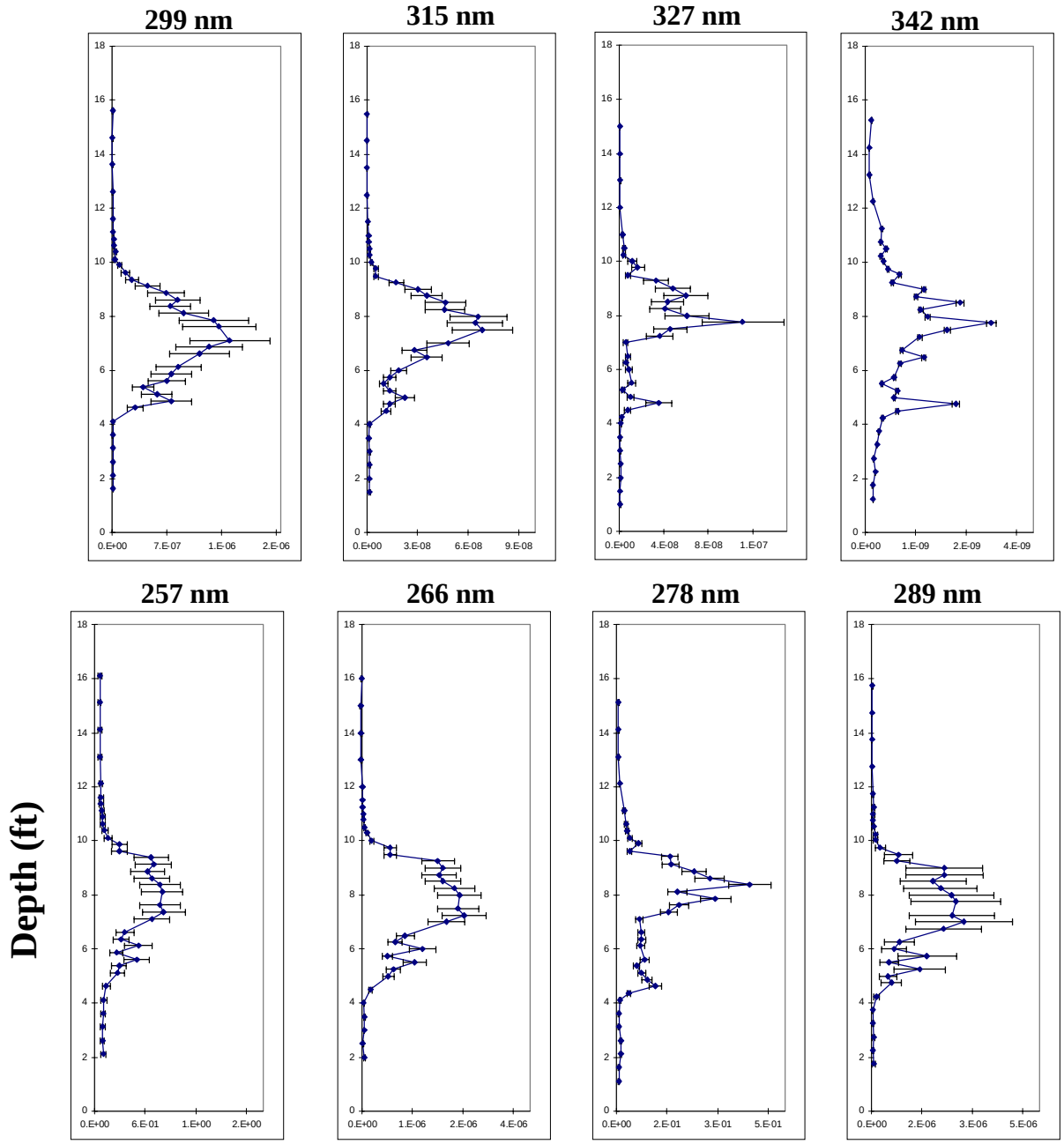

Figure 19. Depth vs. summed fluorescence for each excitation wavelength for push 19.

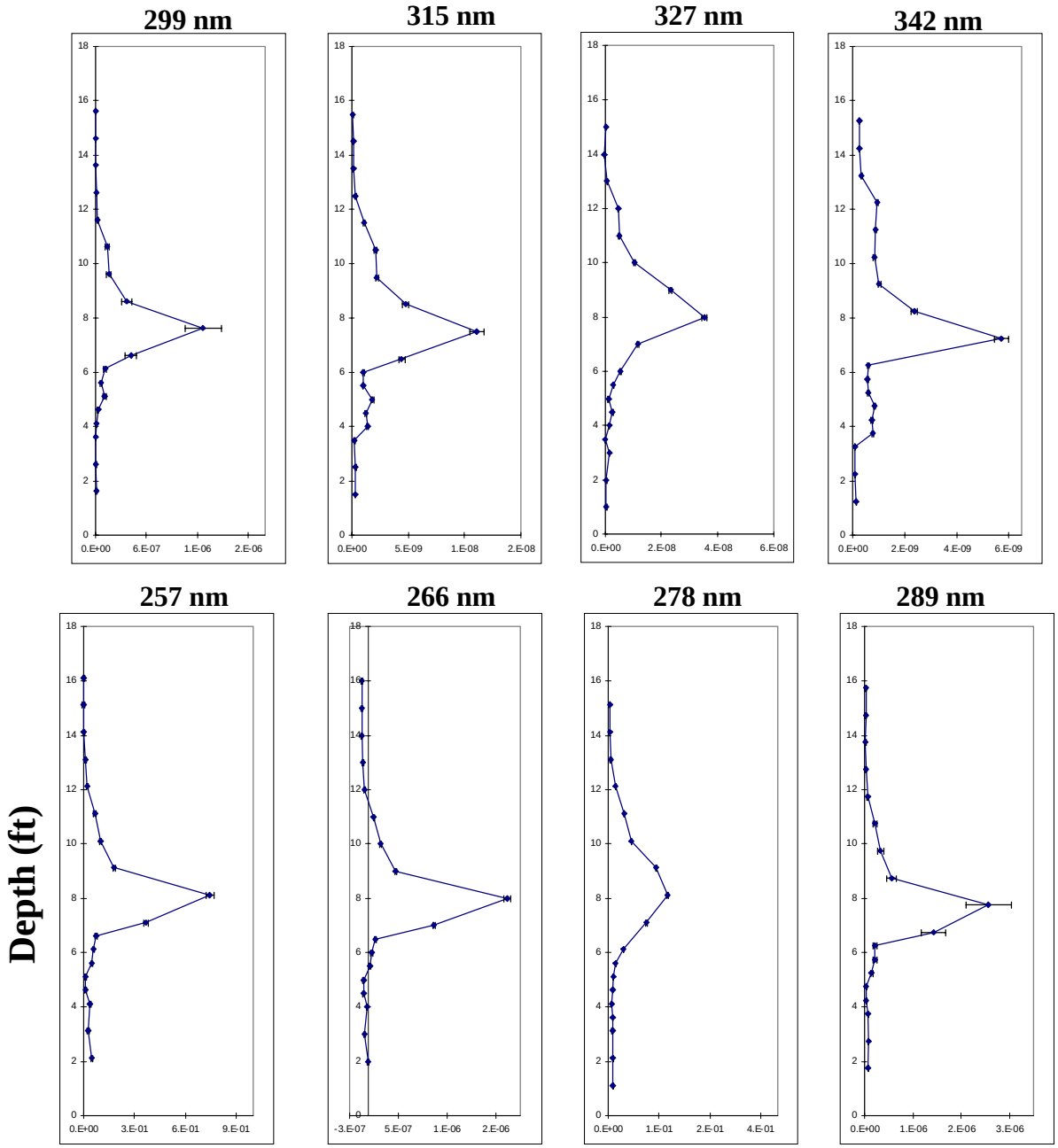

Figure 20. Depth vs. summed fluorescence for each excitation wavelength for push 20.

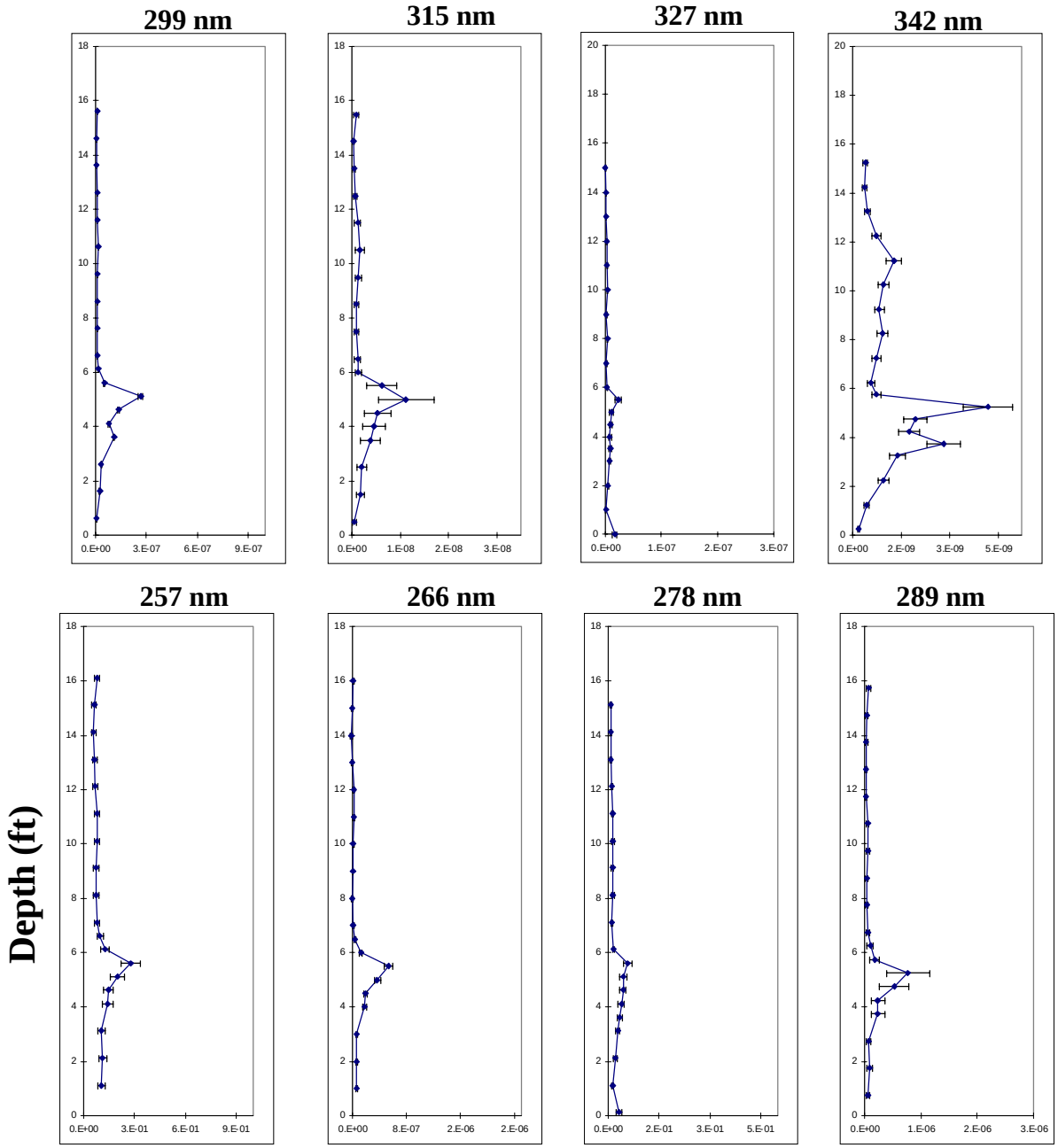

Figure 21. Depth vs. summed fluorescence for each excitation wavelength for push 21.

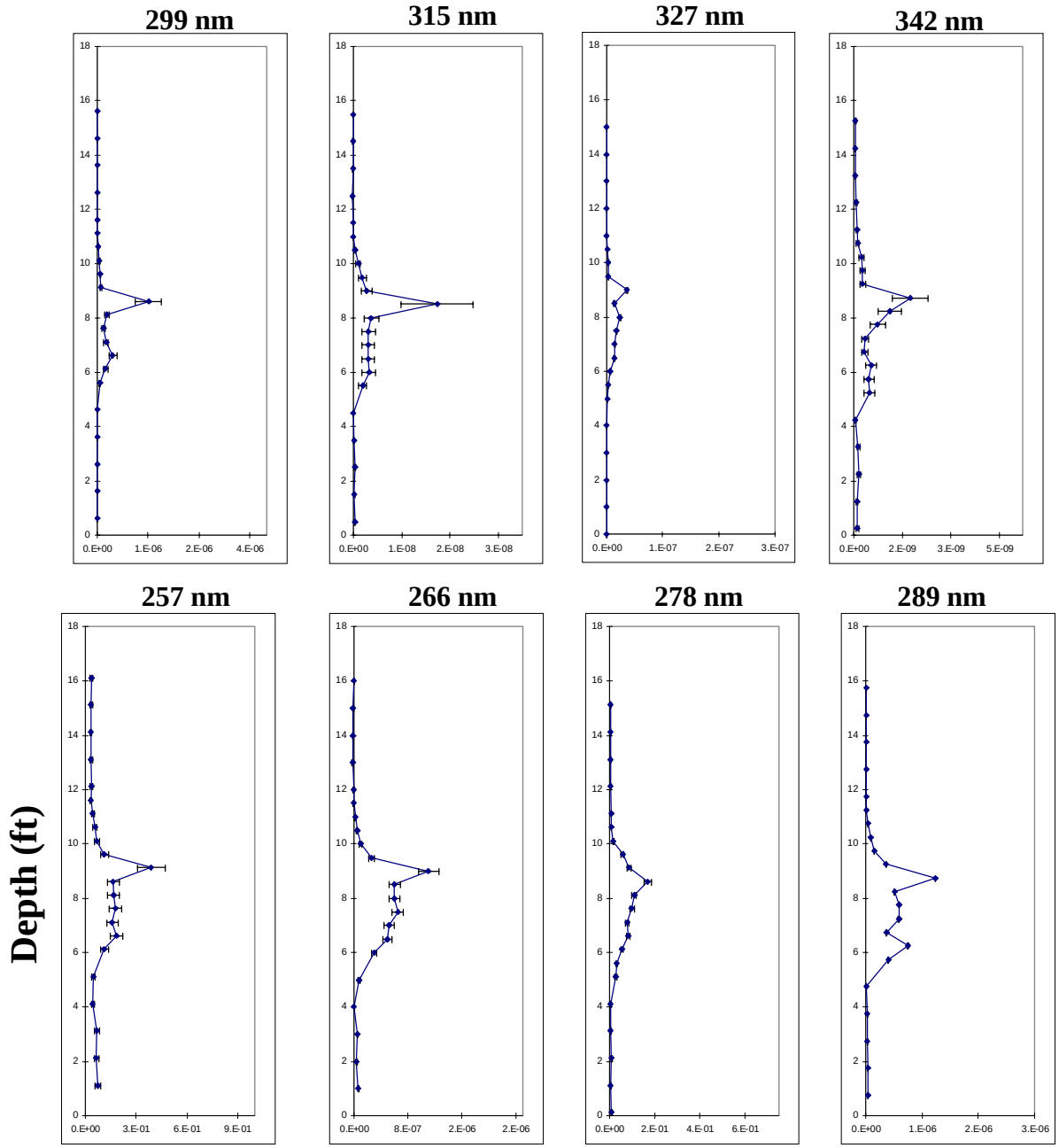

Figure 22. Depth vs. summed fluorescence for each excitation wavelength for push 22.

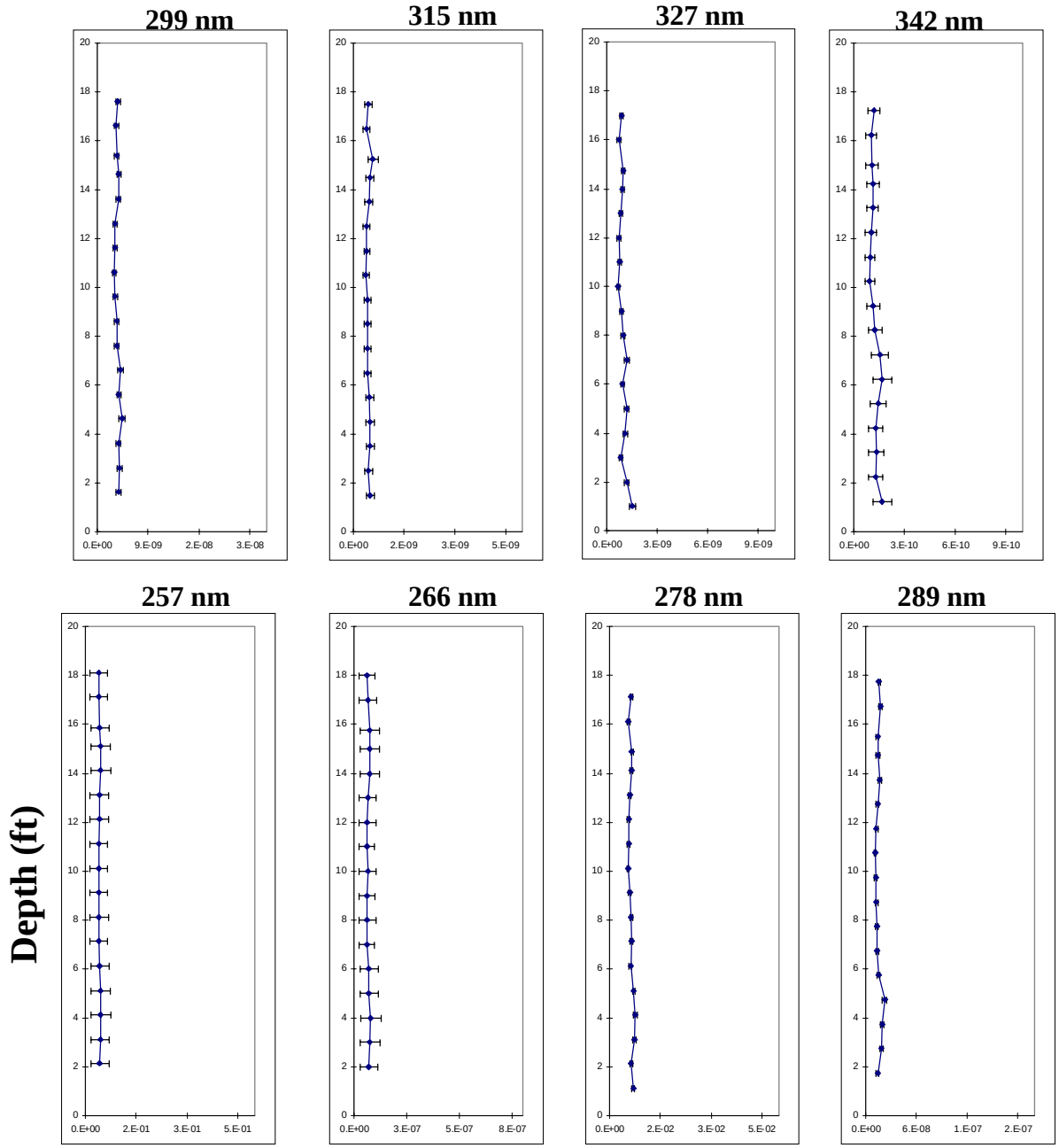

Figure 23. Depth vs. summed fluorescence for each excitation wavelength for push 23.

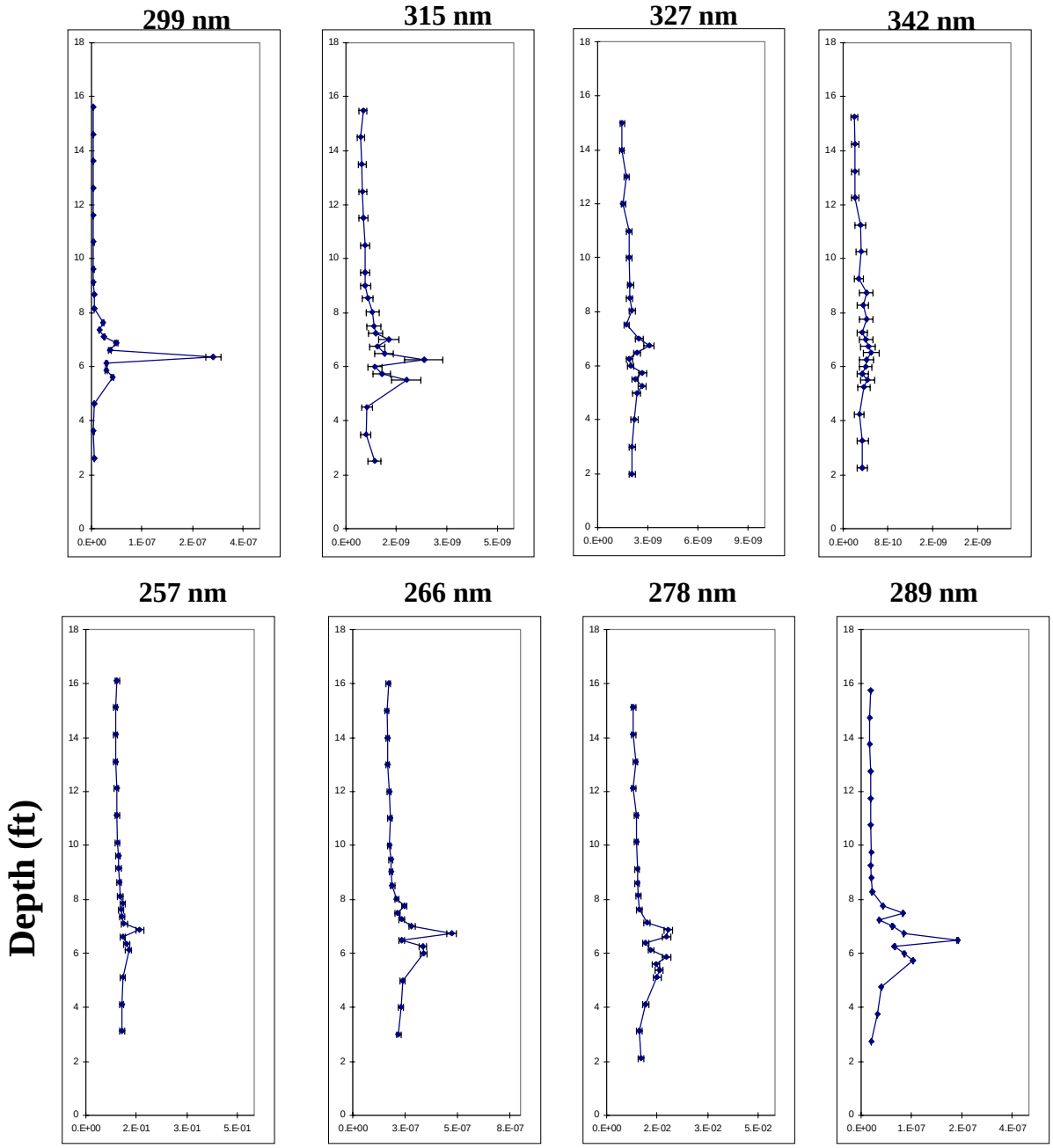

Figure 24. Depth vs. summed fluorescence for each excitation wavelength for push 24.

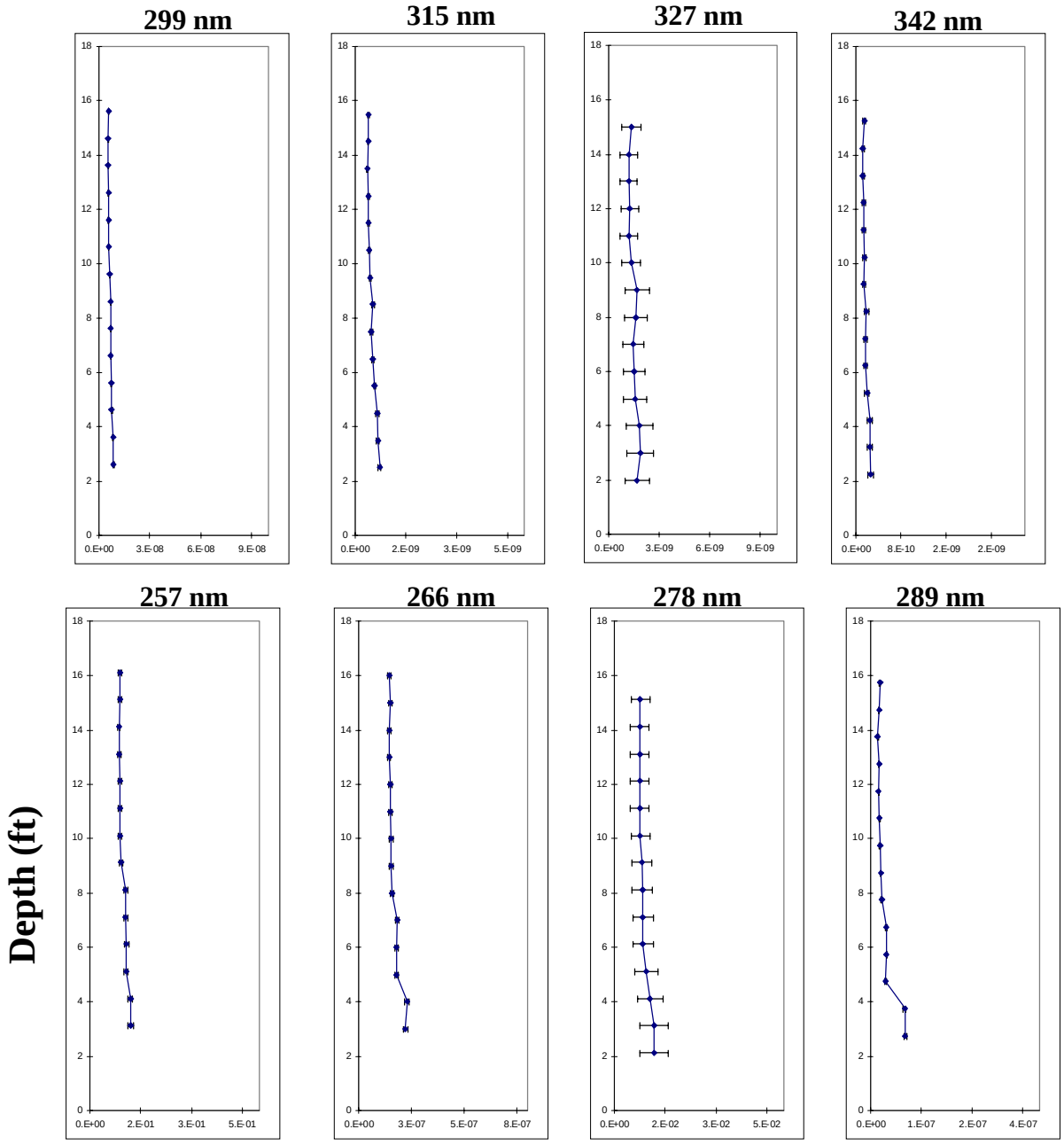

Figure 25. Depth vs. summed fluorescence for each excitation wavelength for push 25.

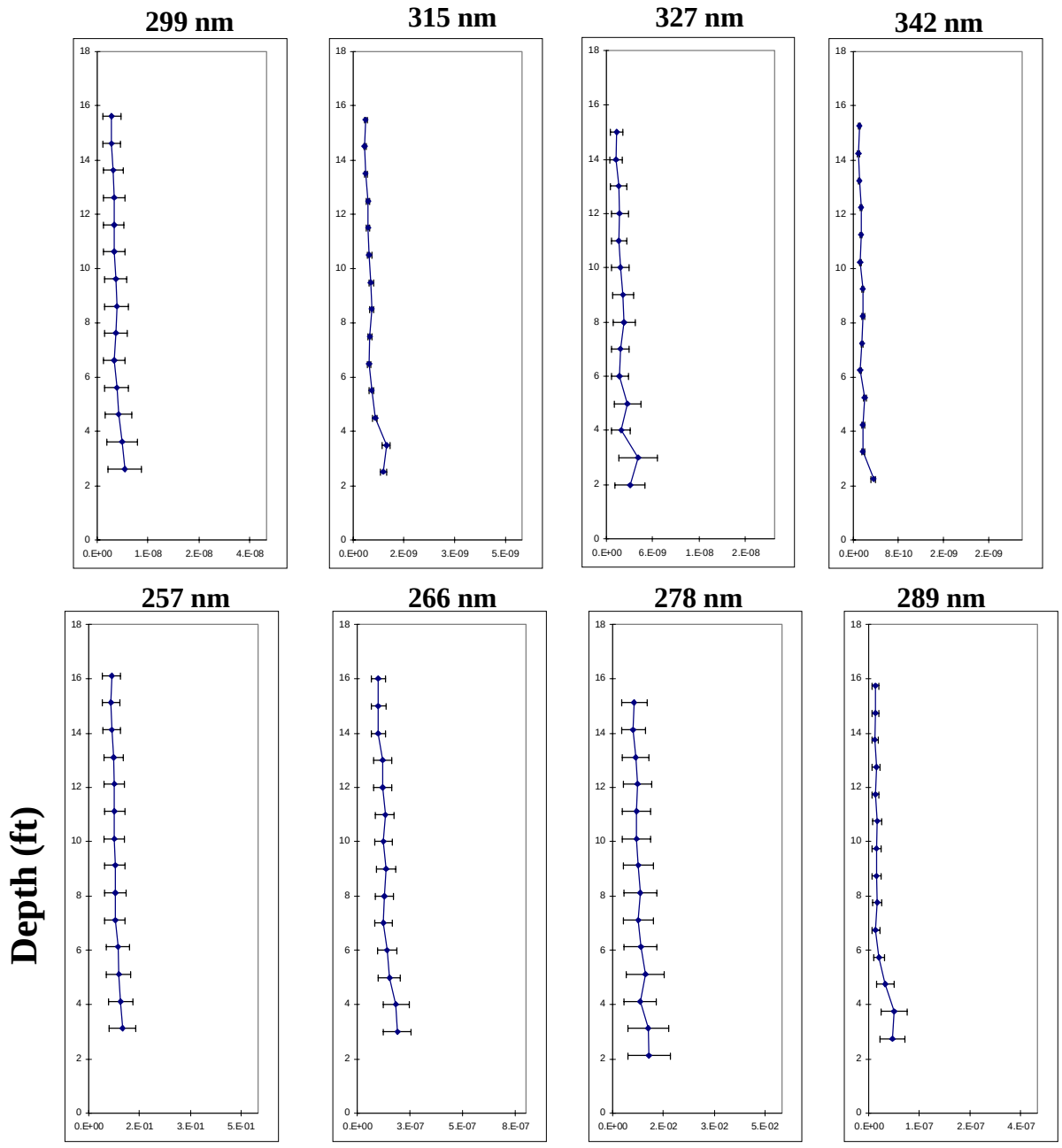

Figure 26. Depth vs. summed fluorescence for each excitation wavelength for push 26.

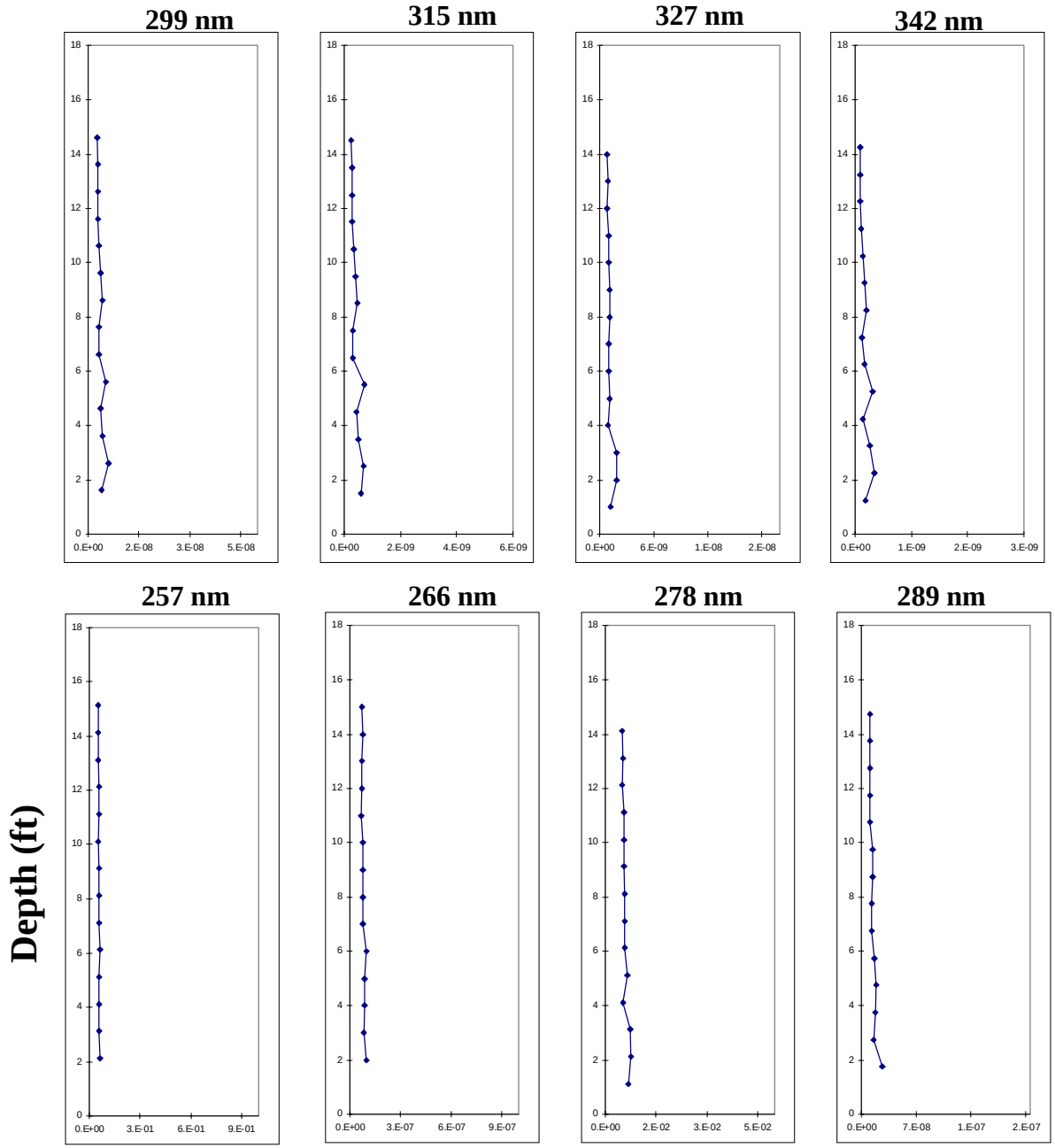

Figure 27. Depth vs. summed fluorescence for each excitation wavelength for push 27.

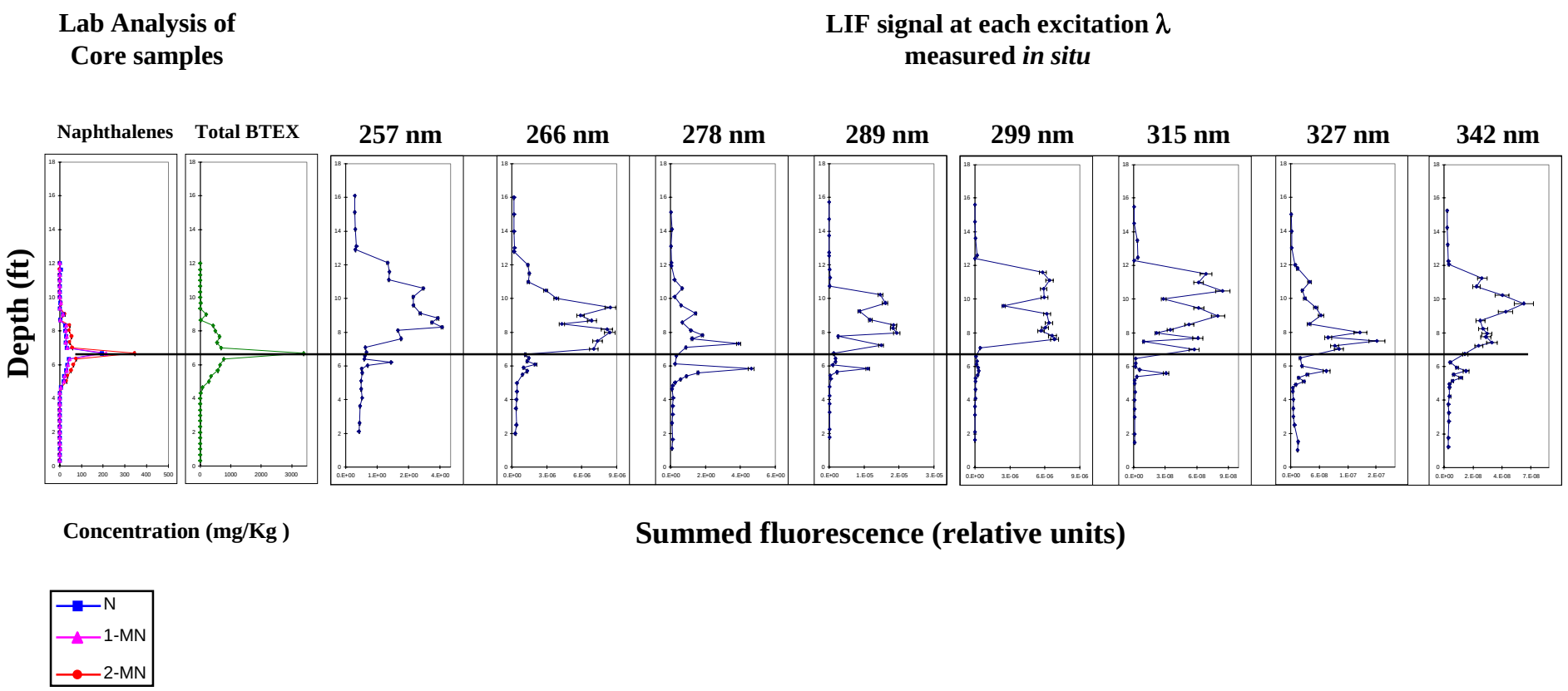

Figure 1. A comparison of laboratory core sample analysis (32CPT-2) with *in situ* CPT-LIF measurements at each excitation wavelength for CPT push #2.

Appendix C.

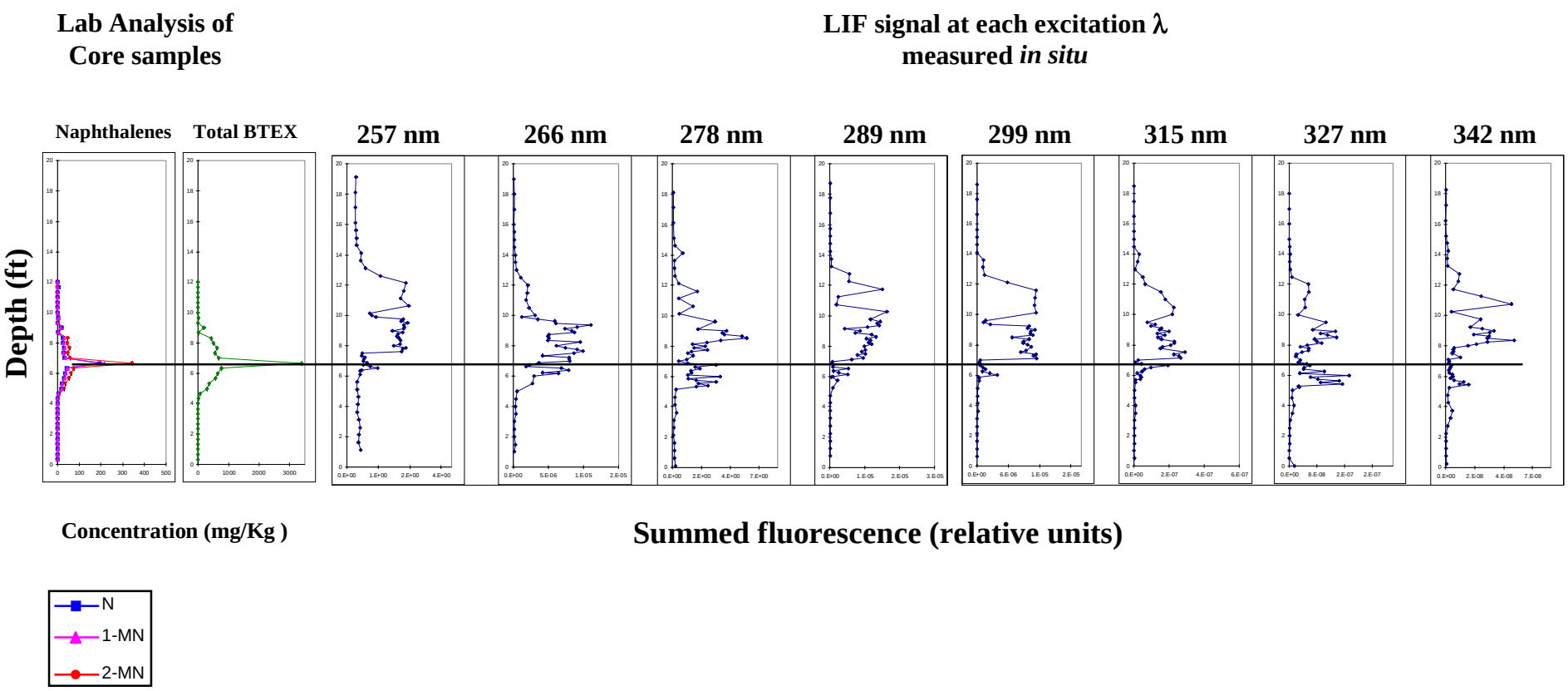

Figure 2. A comparison of laboratory core sample analysis (32CPT-2) with *in situ* CPT-LIF measurements at each excitation wavelength for CPT push #3.

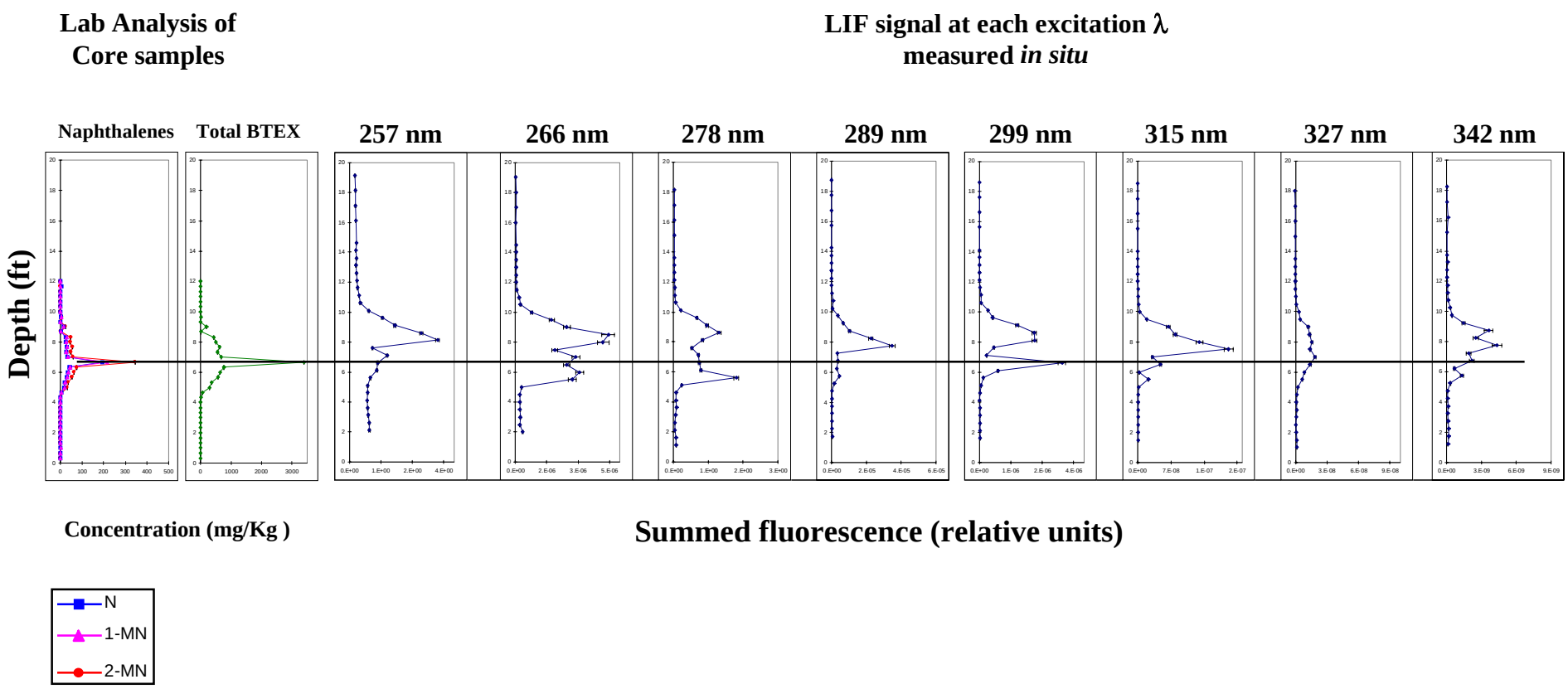

Figure 3. A comparison of laboratory core sample analysis (32CPT-2) with *in situ* CPT-LIF measurements at each excitation wavelength for CPT push #4.

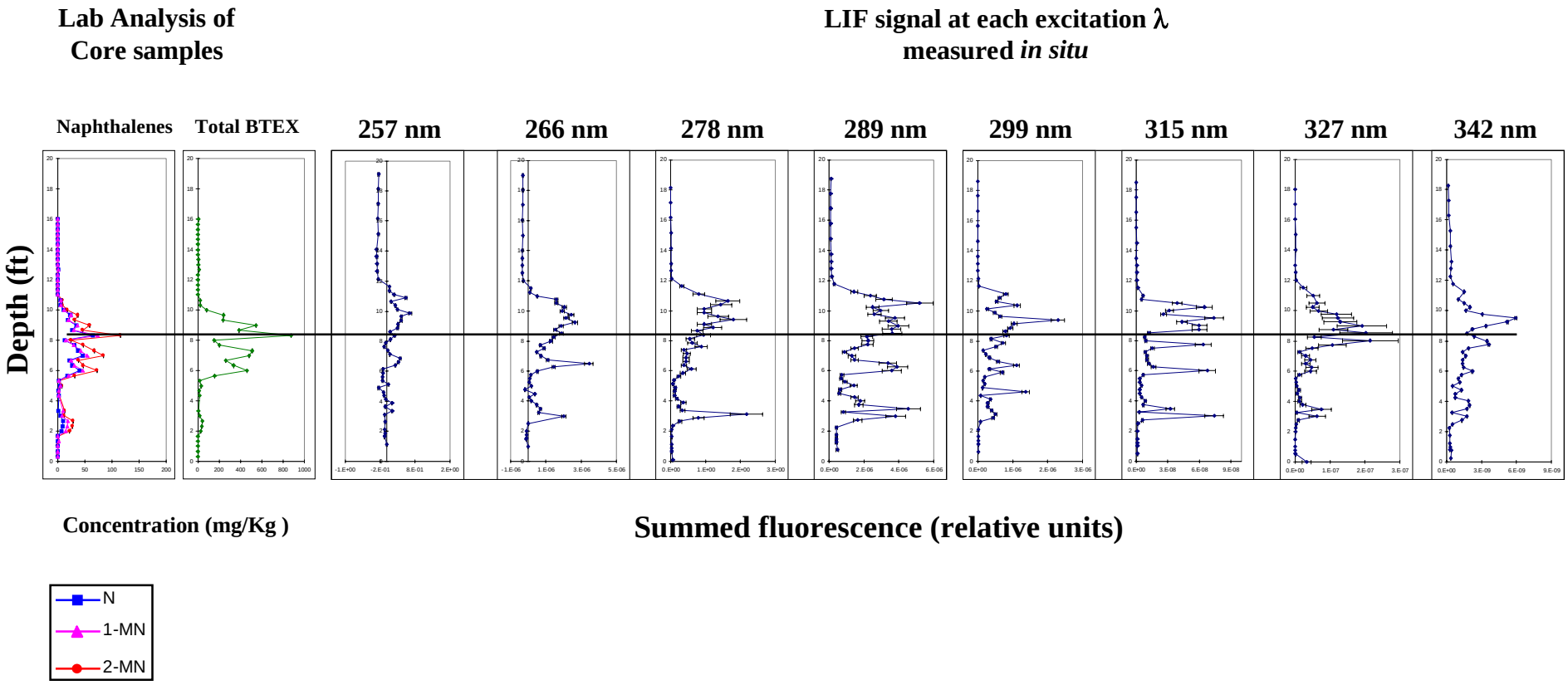

Figure 4. A comparison of laboratory core sample analysis (32CPT-1) with *in situ* CPT-LIF measurements at each excitation wavelength for CPT push #5.

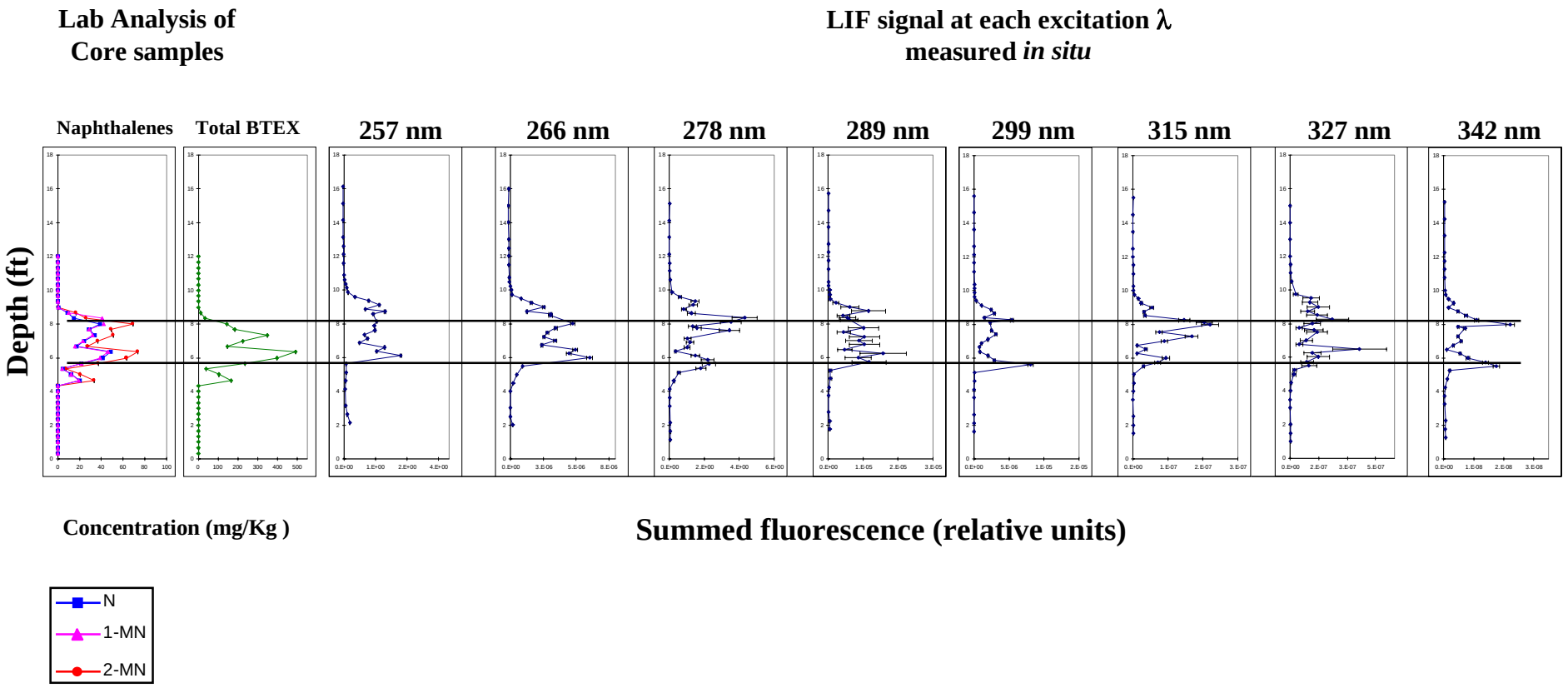

Figure 5. A comparison of laboratory core sample analysis (32CPT-3) with *in situ* CPT-LIF measurements at each excitation wavelength for CPT push #6.

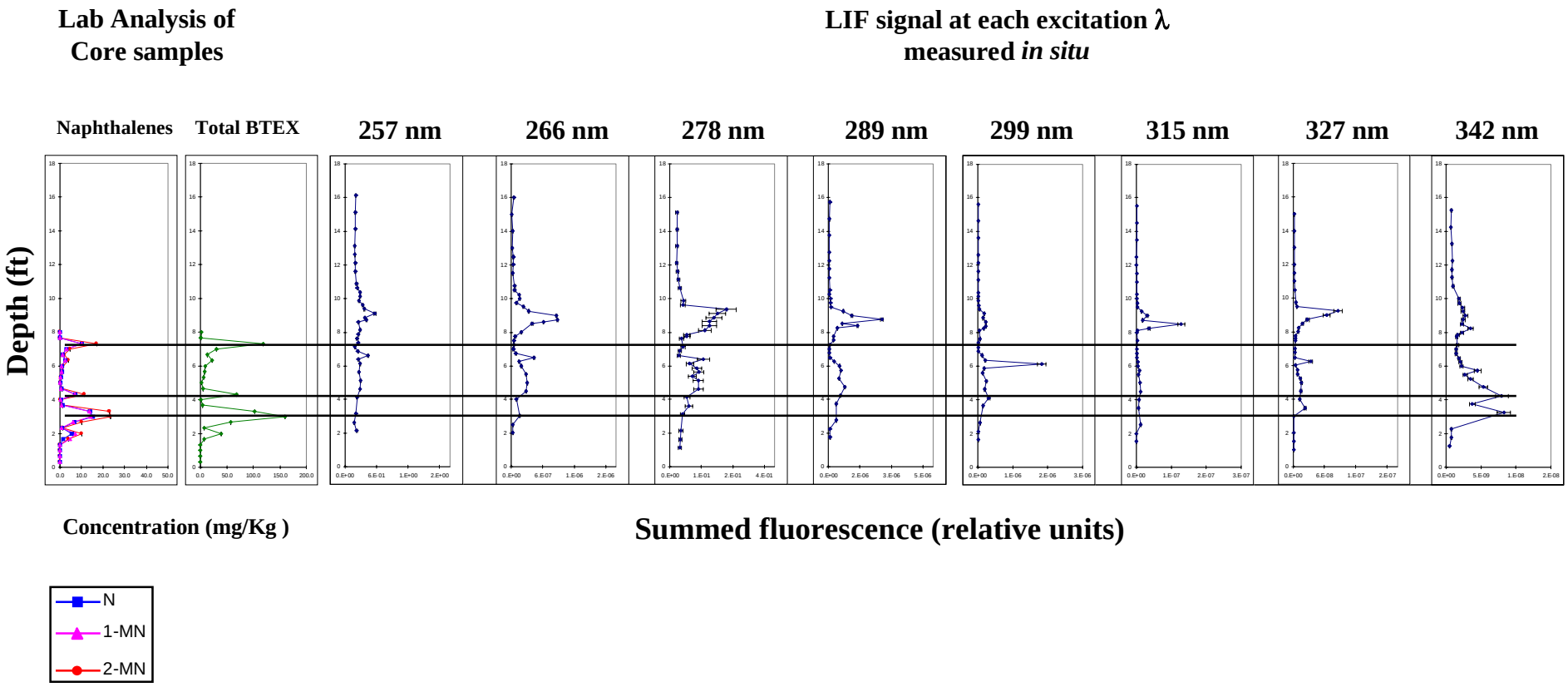

Figure 6. A comparison of laboratory core sample analysis (32CPT-7) with *in situ* CPT-LIF measurements at each excitation wavelength for CPT push #7.

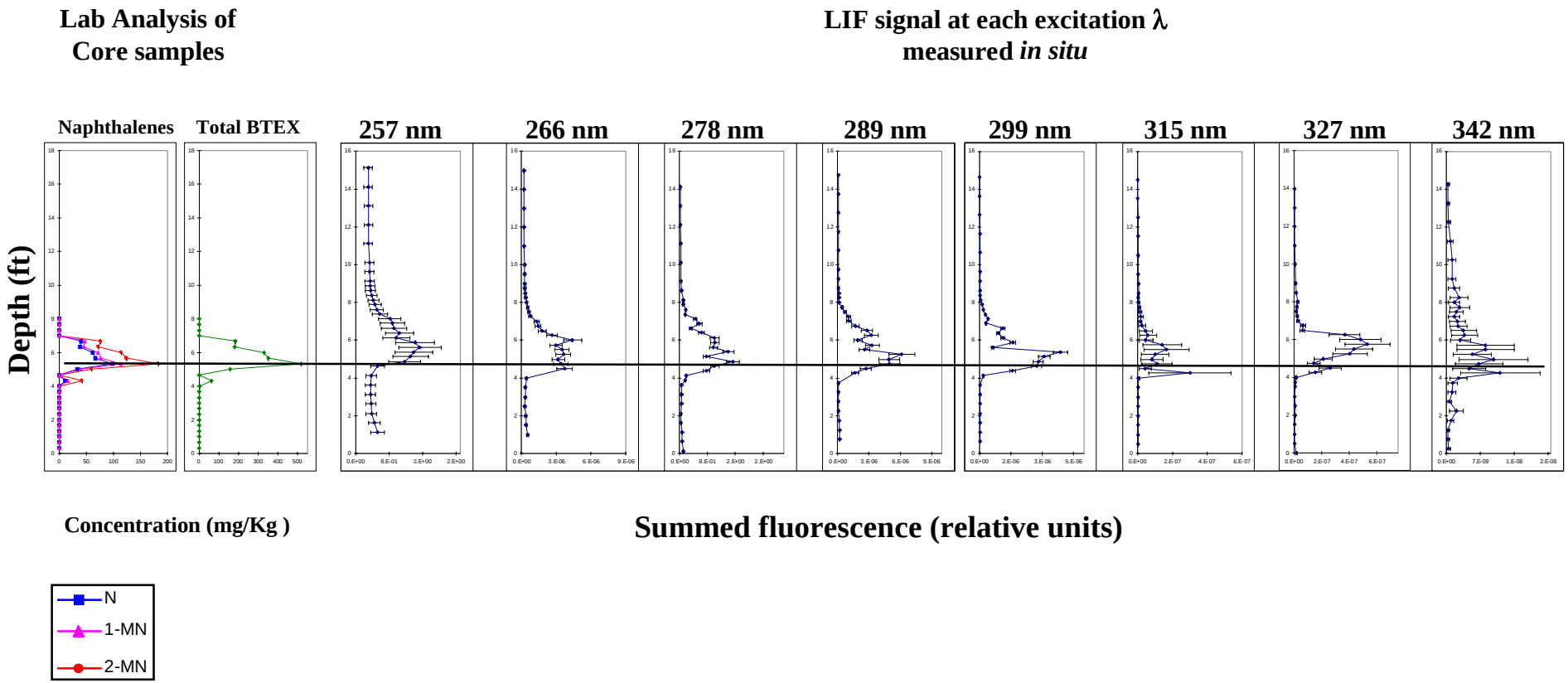

Figure 7. A comparison of laboratory core sample analysis (32CPT-4) with *in situ* CPT-LIF measurements at each excitation wavelength for CPT push #9.

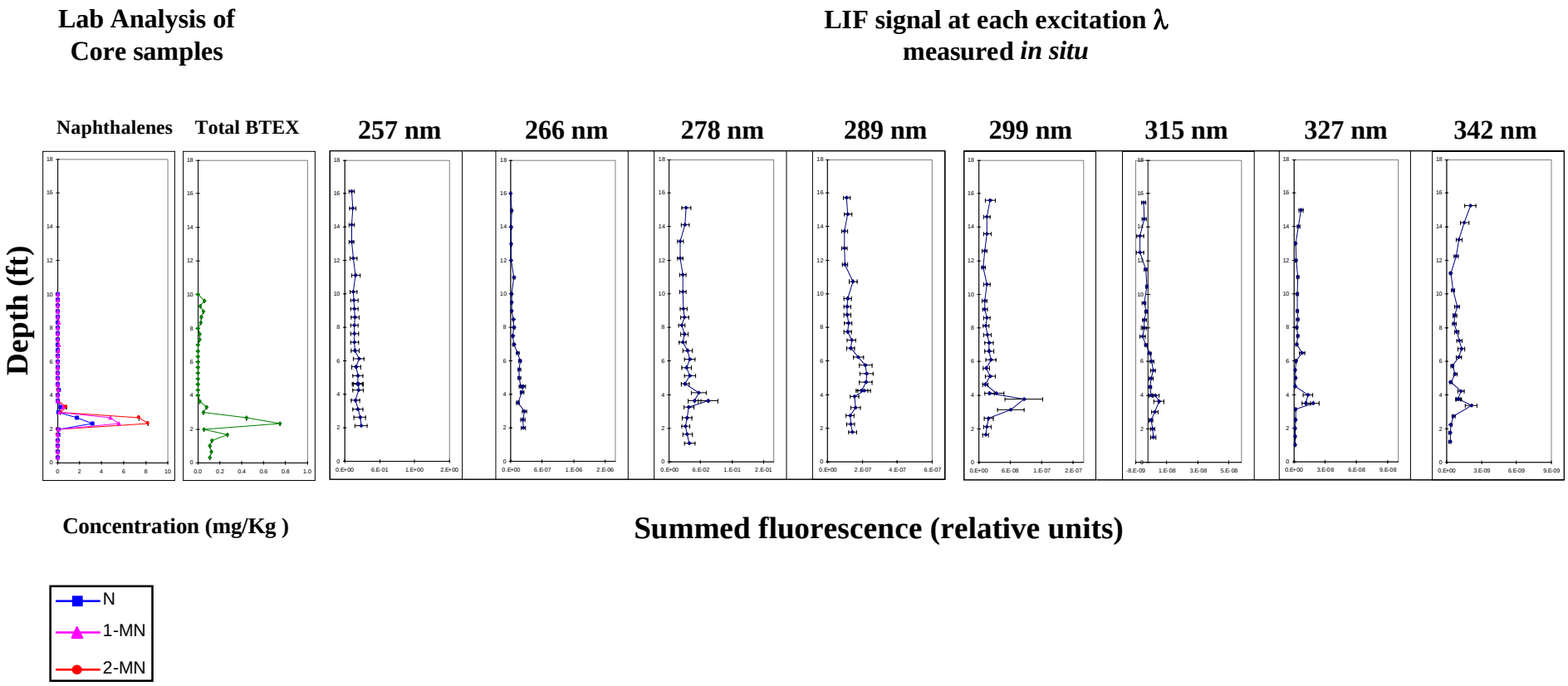

Figure 8. A comparison of laboratory core sample analysis (32CPT-6) with *in situ* CPT-LIF measurements at each excitation wavelength for CPT push #10.

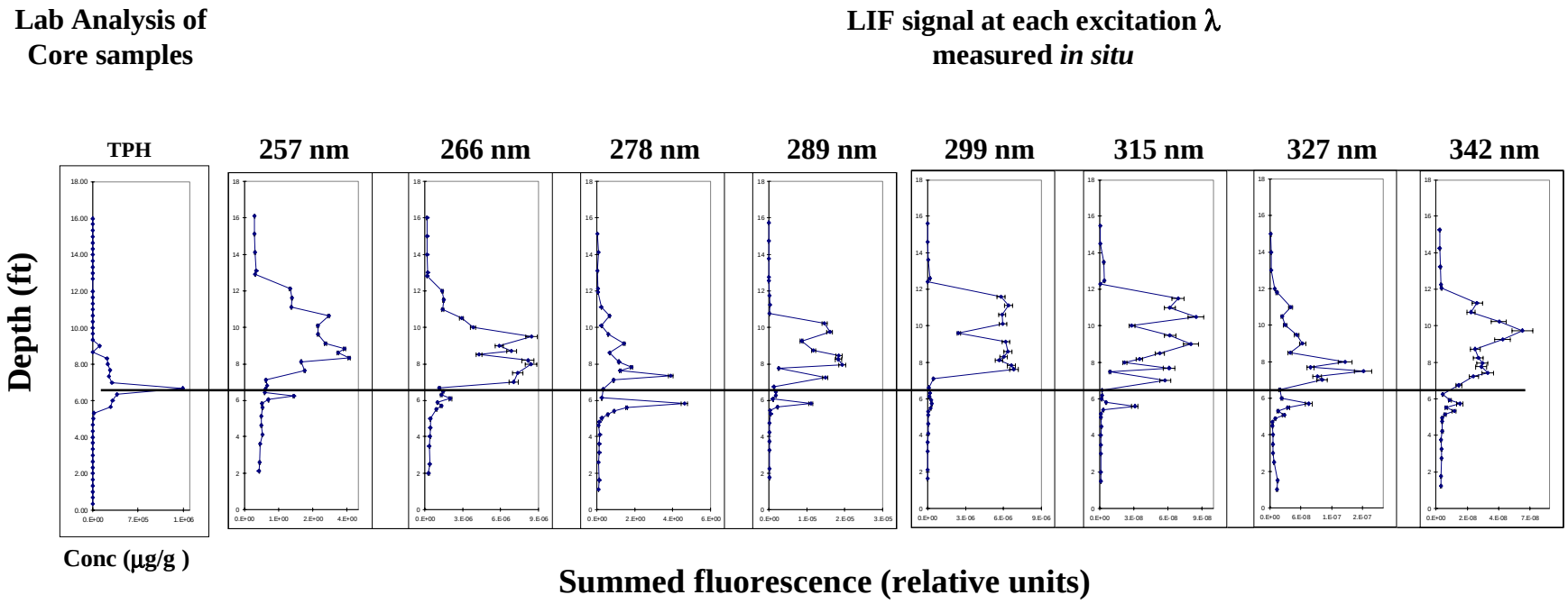

Figure 9. A comparison of laboratory core sample analysis (32CPT-2) with *in situ* CPT-LIF measurements at each excitation wavelength for CPT push #2.

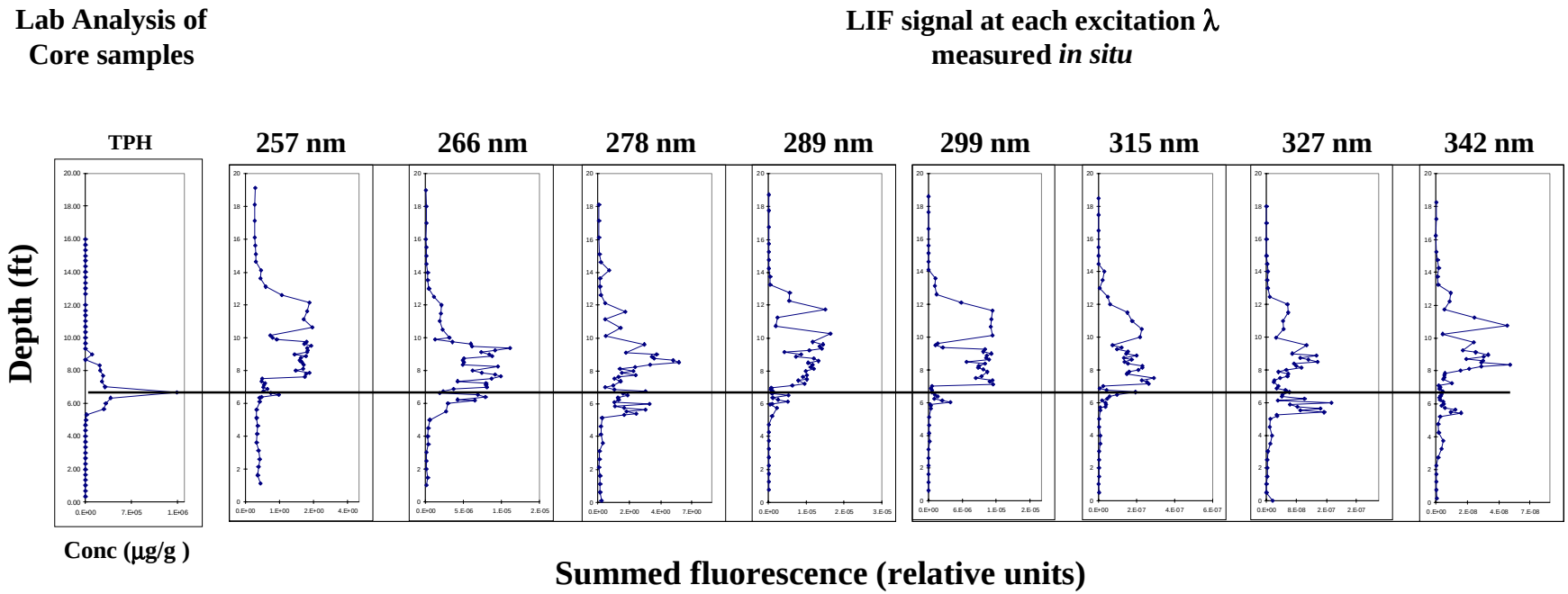

Figure 10. A comparison of laboratory core sample analysis (32CPT-2) with *in situ* CPT-LIF measurements at each excitation wavelength for CPT push #3.

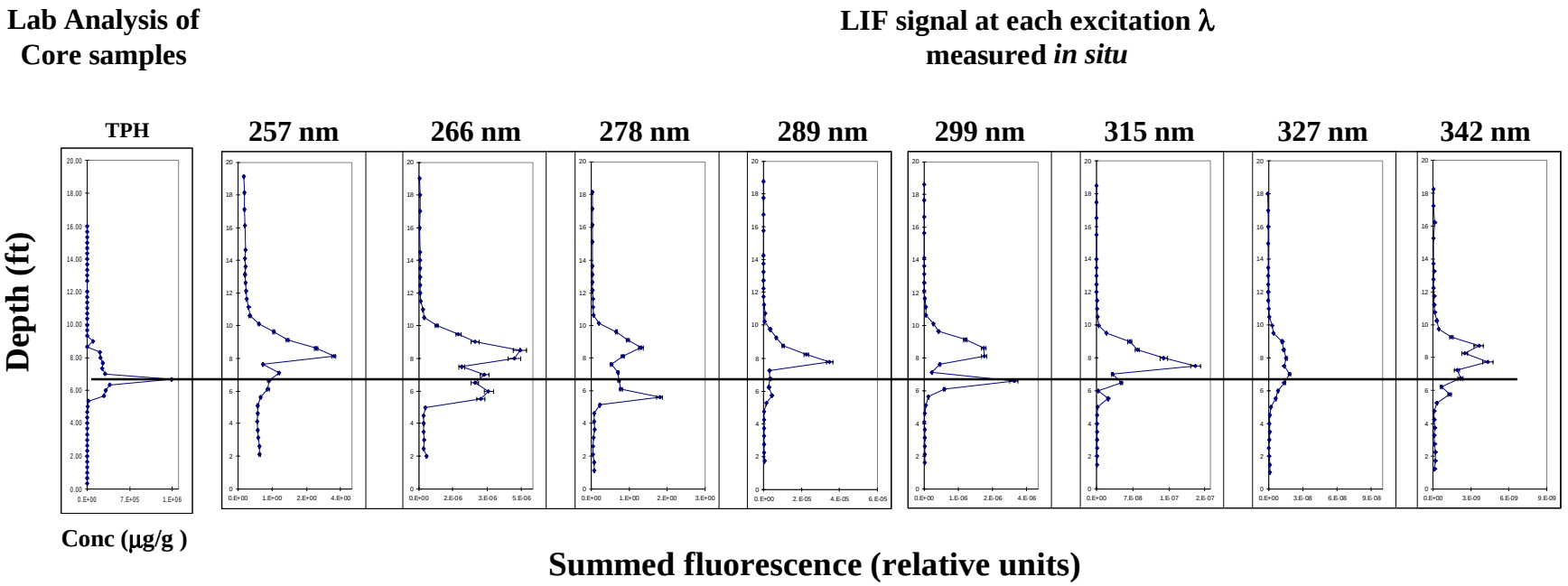

Figure 11. A comparison of laboratory core sample analysis (32CPT-2) with *in situ* CPT-LIF measurements at each excitation wavelength for CPT push #4.

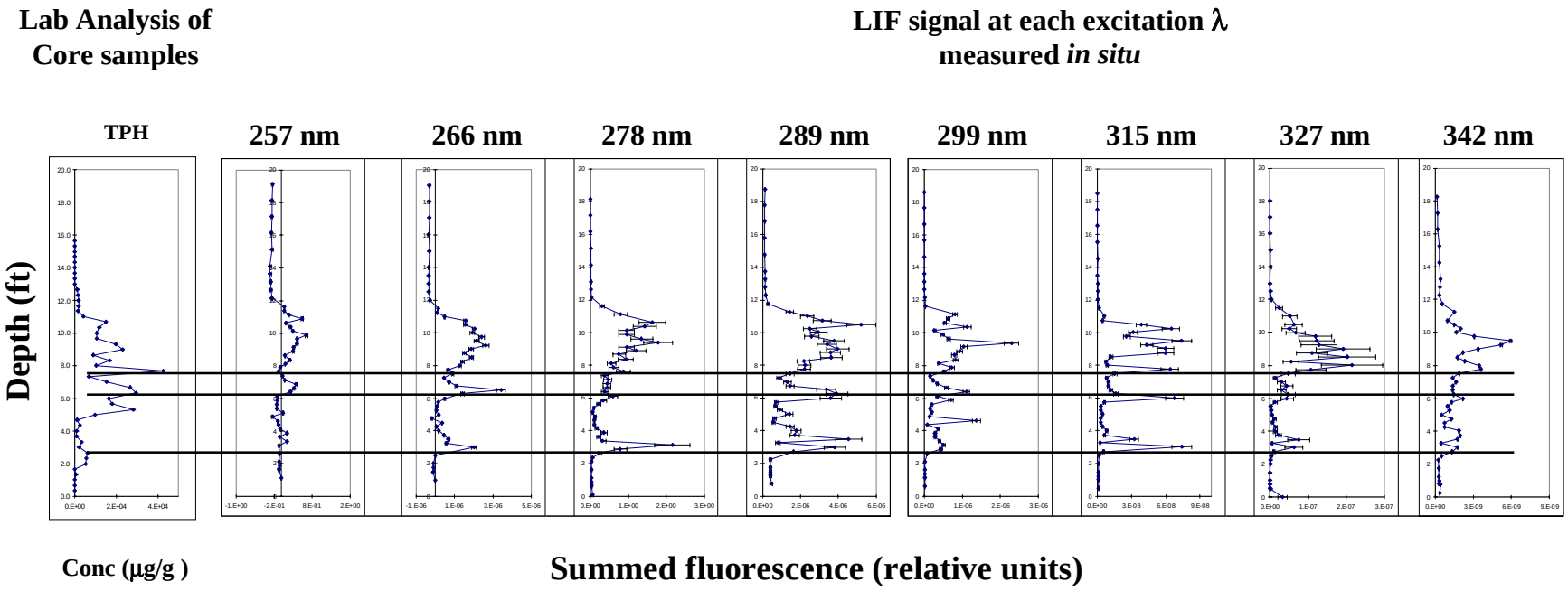

Figure 12. A comparison of laboratory core sample analysis (32CPT-1) with *in situ* CPT-LIF measurements at each excitation wavelength for CPT push #5.

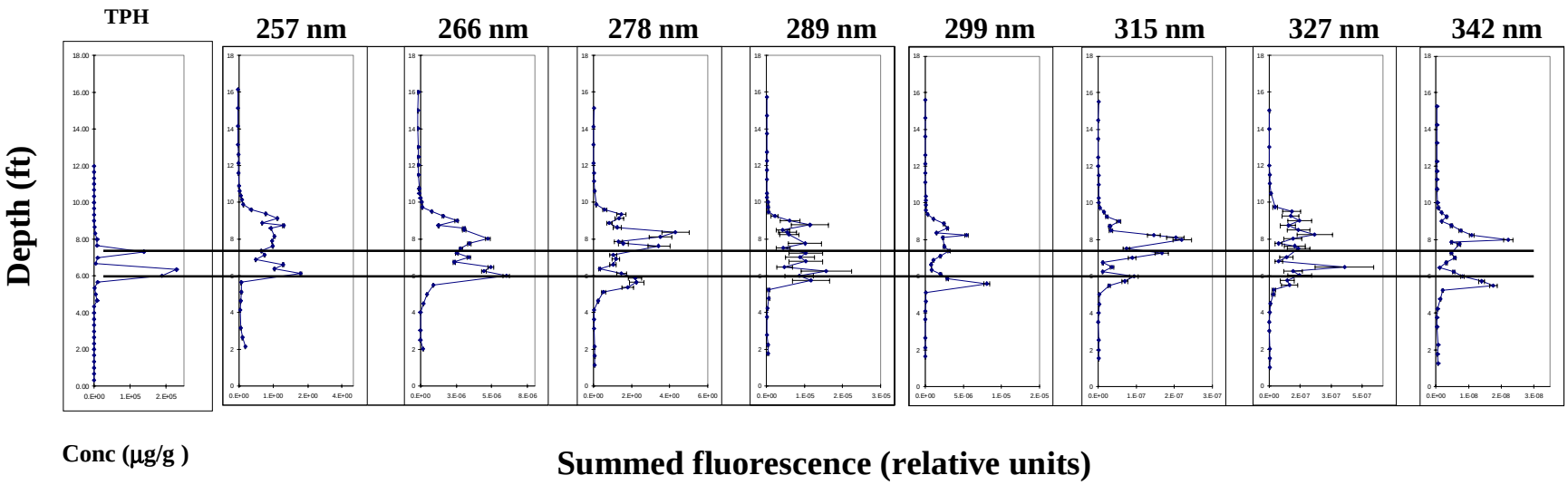

Figure 13. A comparison of laboratory core sample analysis (32CPT-3) with *in situ* CPT-LIF measurements at each excitation wavelength for CPT push #6.

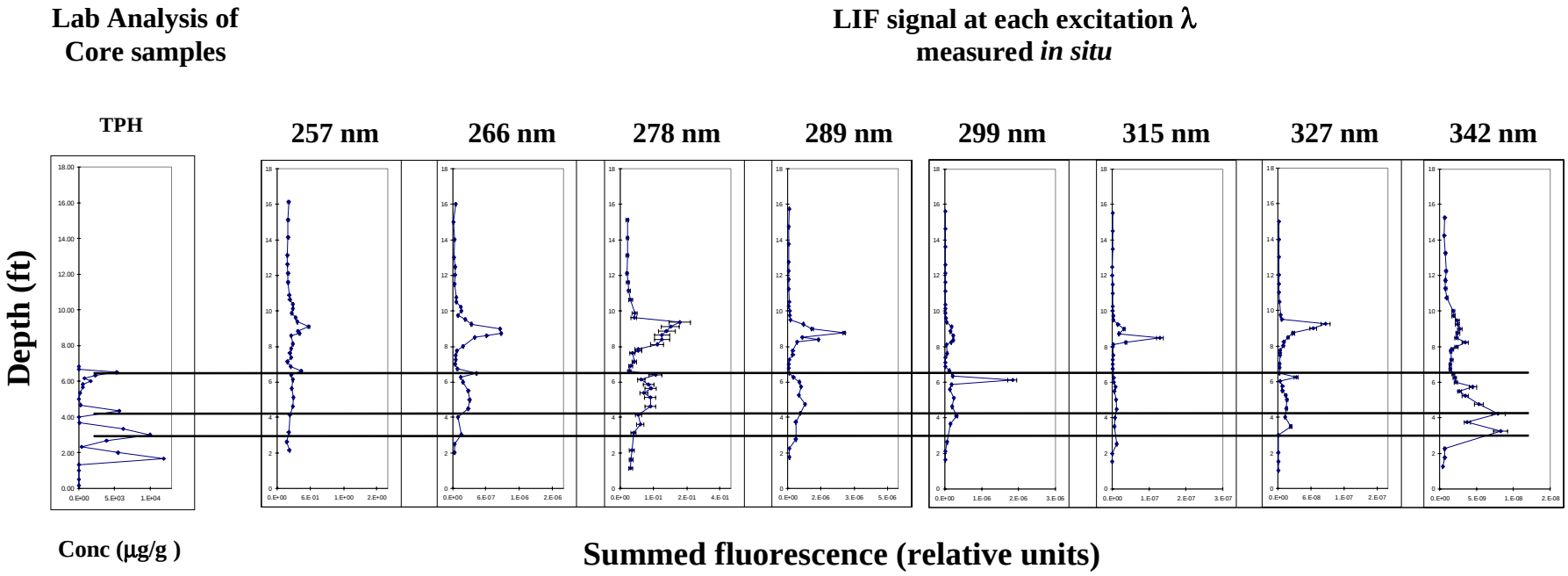

Figure 14. A comparison of laboratory core sample analysis (32CPT-7) with *in situ* CPT-LIF measurements at each excitation wavelength for CPT push #7.

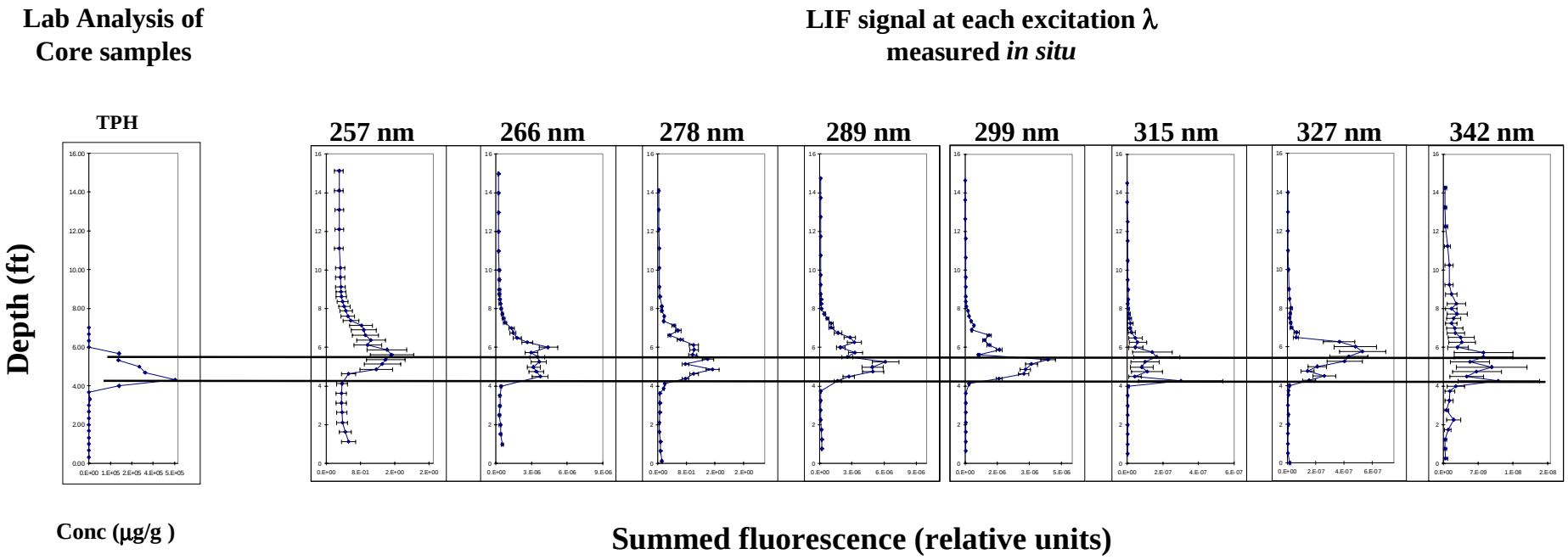

Figure 15. A comparison of laboratory core sample analysis (32CPT-4) with *in situ* CPT-LIF measurements at each excitation wavelength for CPT push #9.

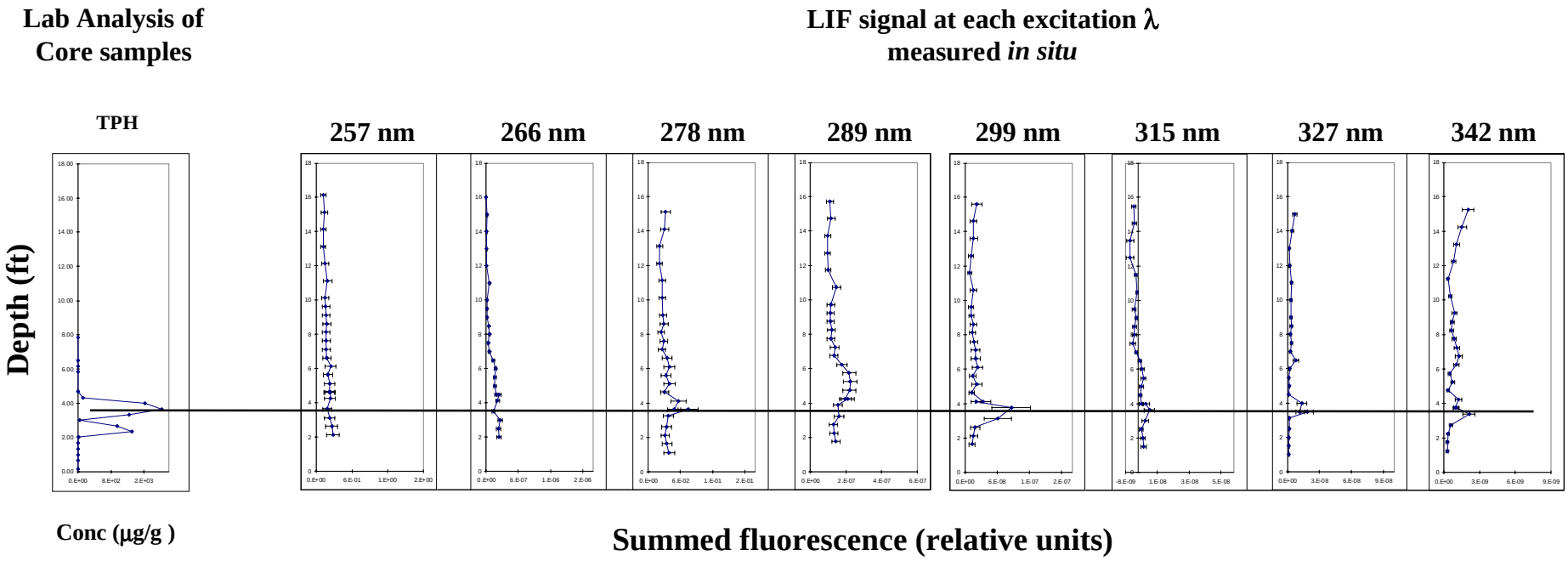

Figure 16. A comparison of laboratory core sample analysis (32CPT-6) with *in situ* CPT-LIF measurements at each excitation wavelength for CPT push #10.

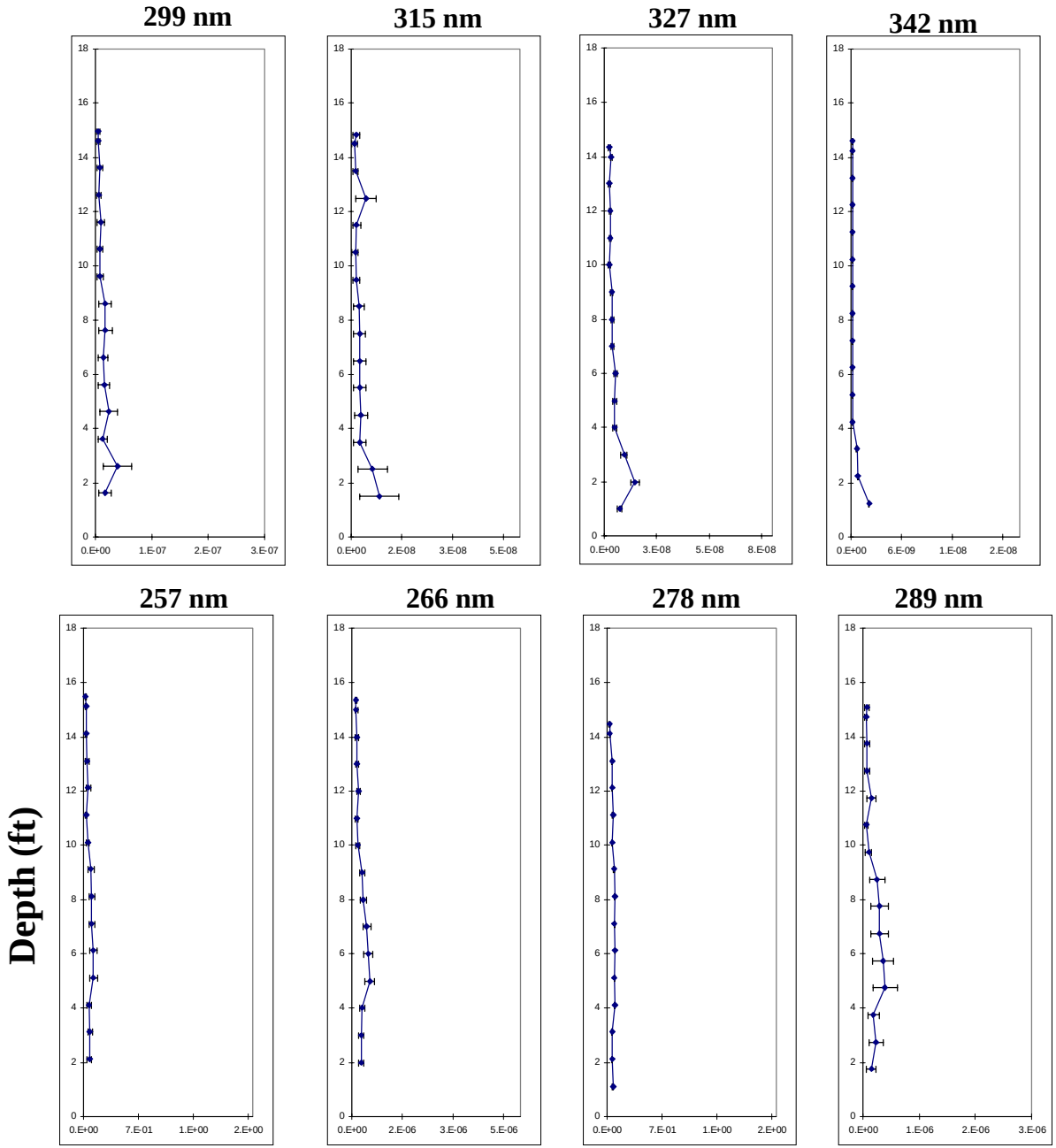

Figure 1. Depth vs. summed fluorescence for each excitation wavelength for push 1.

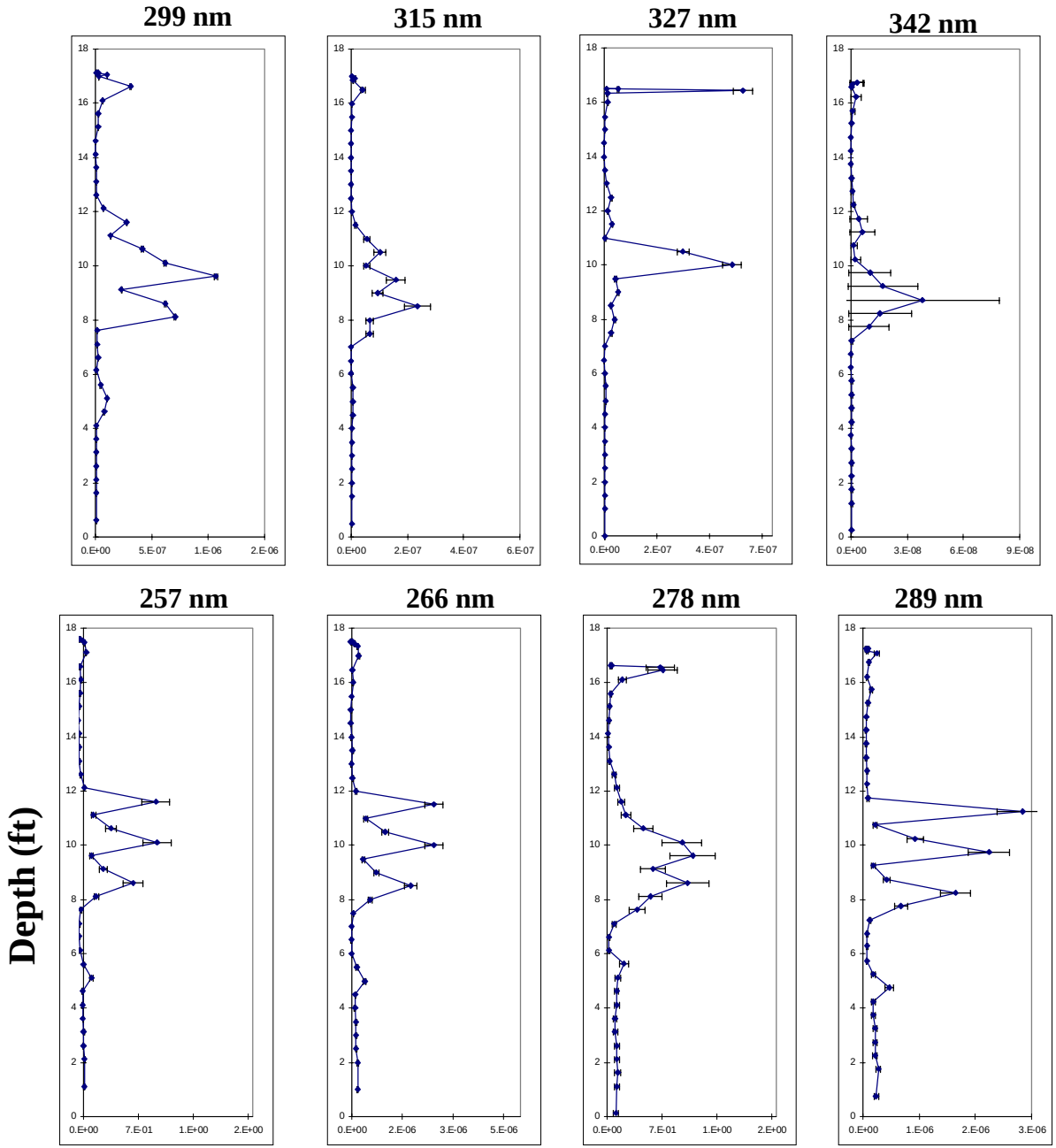

Figure 2. Depth vs. summed fluorescence for each excitation wavelength for push 2.

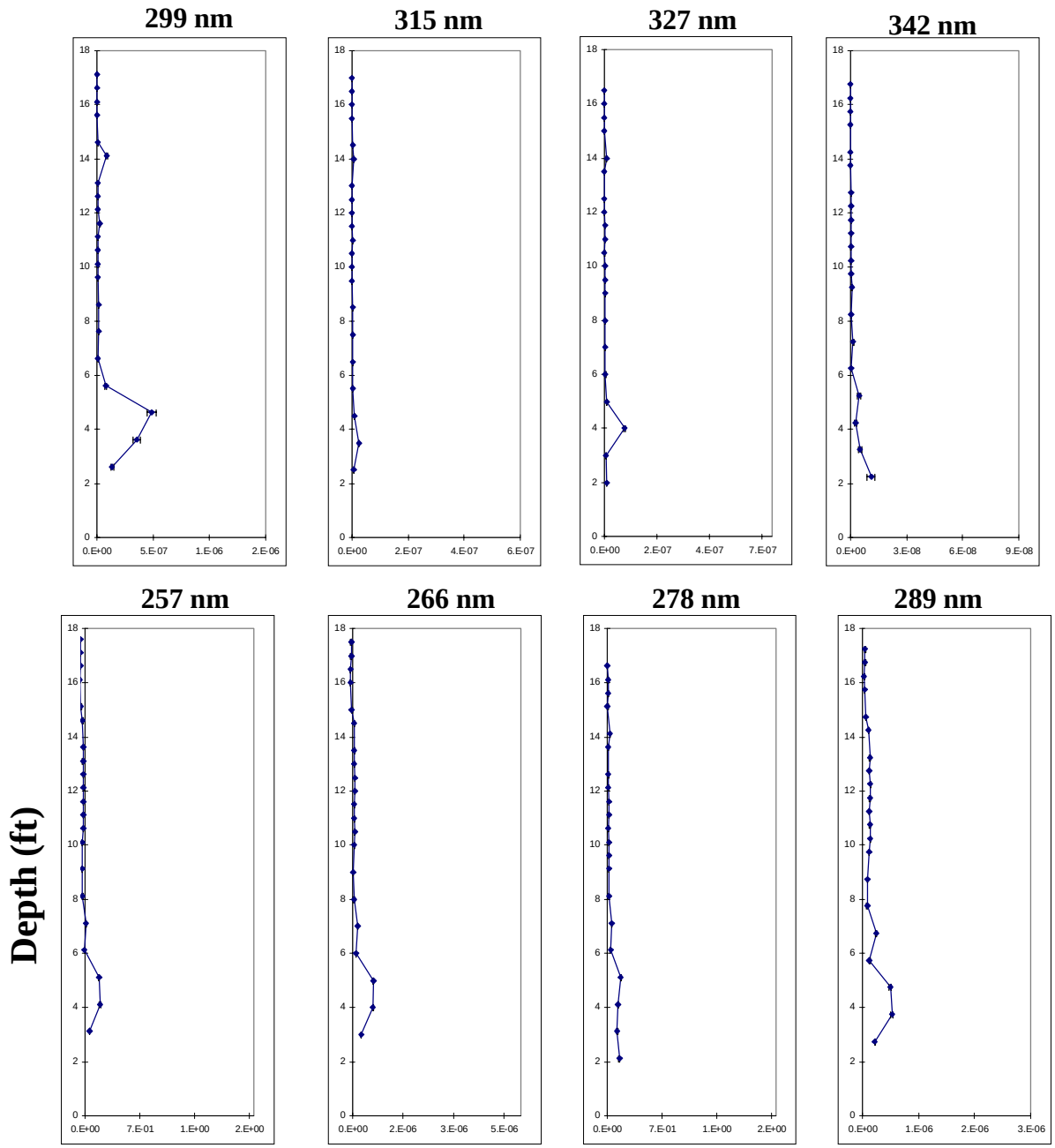

Figure 3. Depth vs. summed fluorescence for each excitation wavelength for push 3.

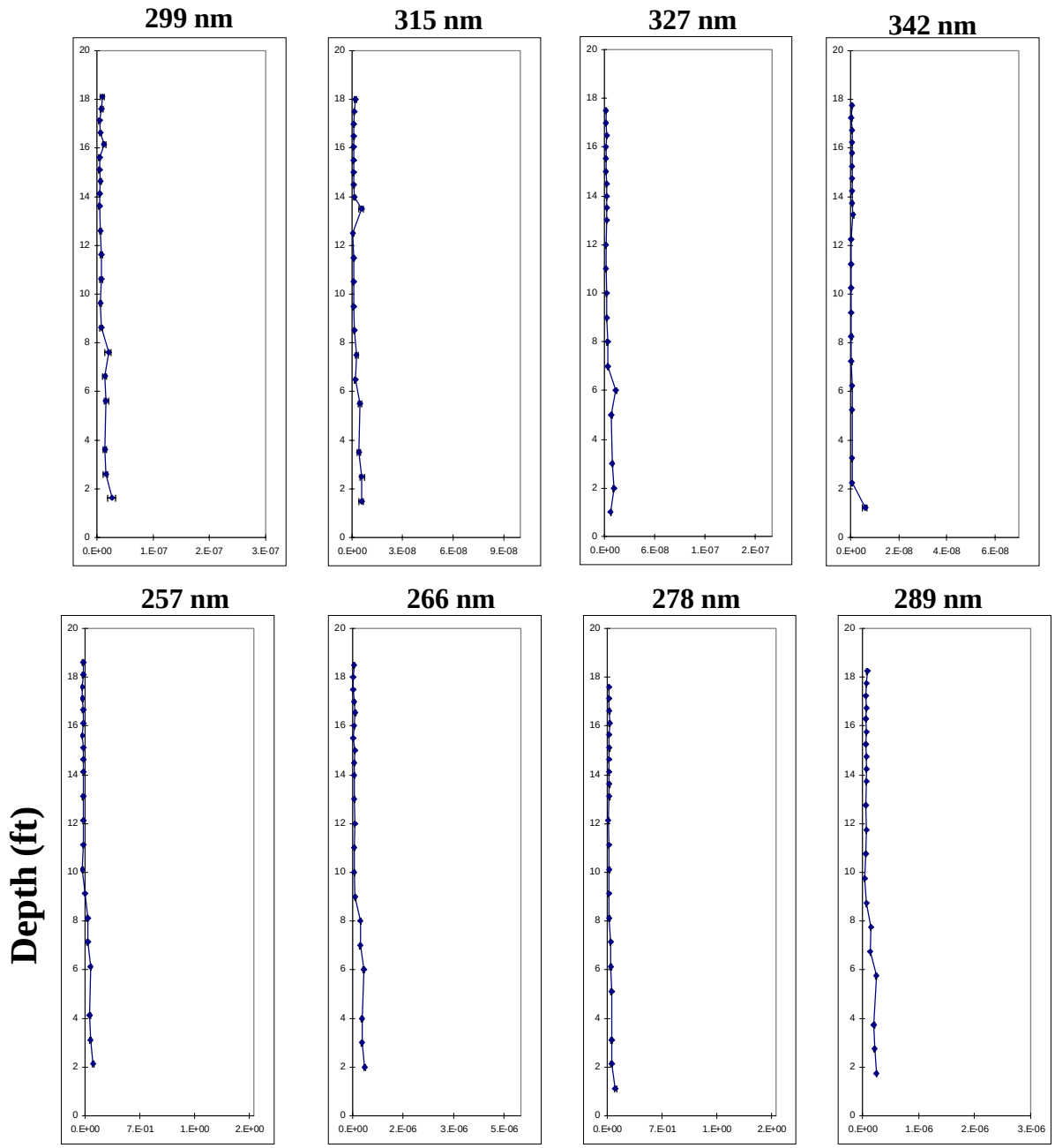

Figure 4. Depth vs. summed fluorescence for each excitation wavelength for push 4.

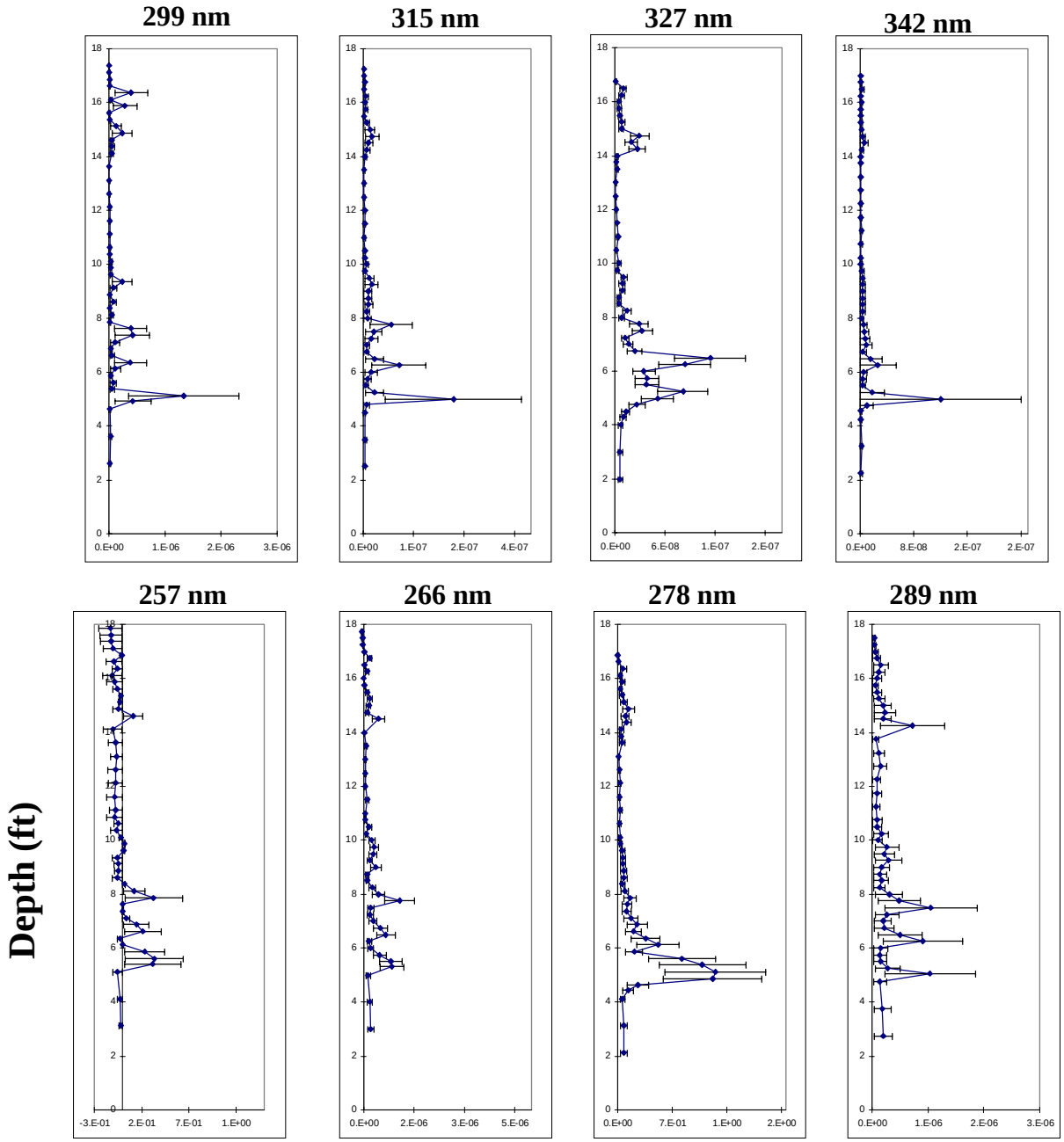

Figure 5. Depth vs. summed fluorescence for each excitation wavelength for push 5.

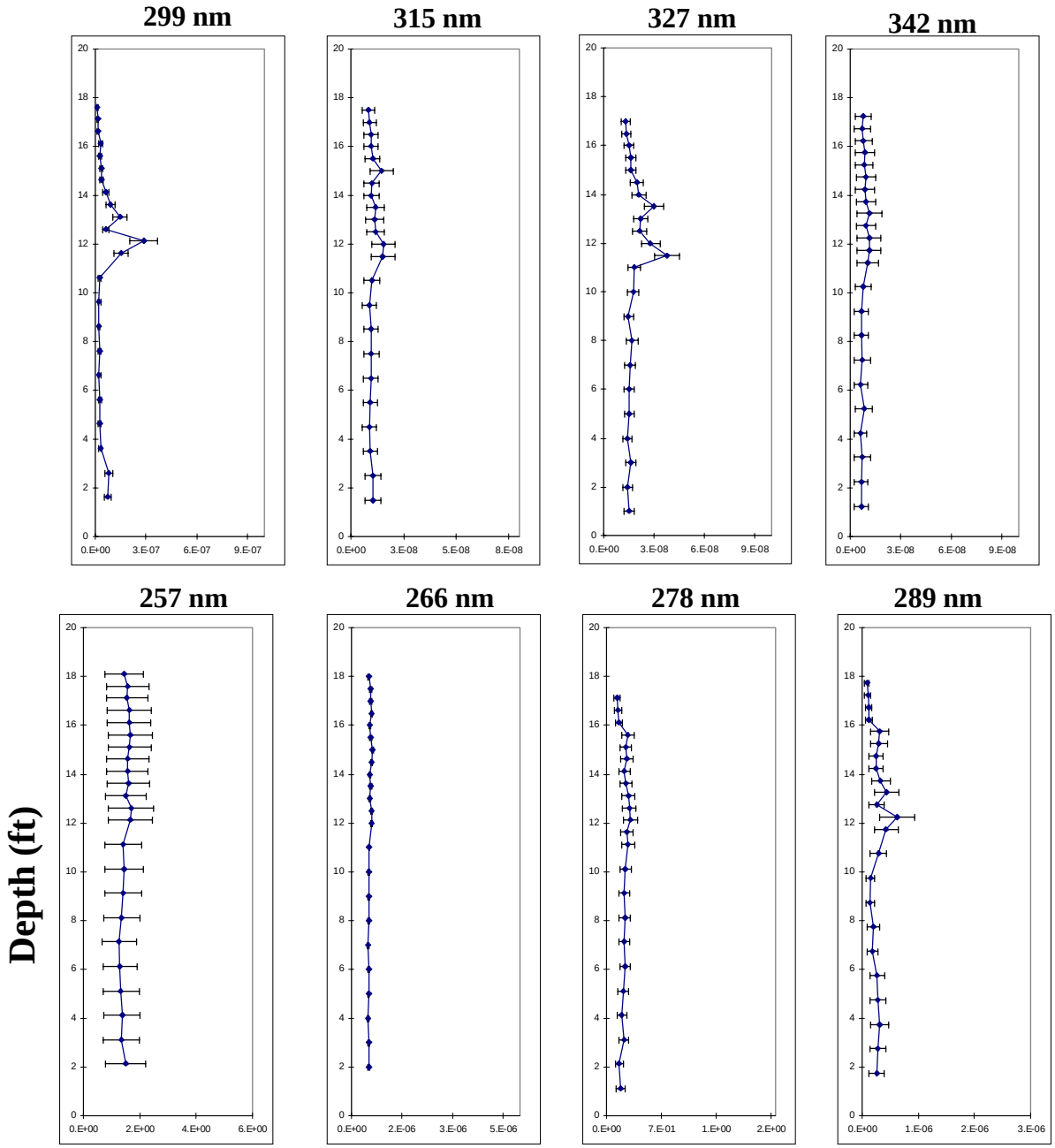

Figure 6. Depth vs. summed fluorescence for each excitation wavelength for push 6.

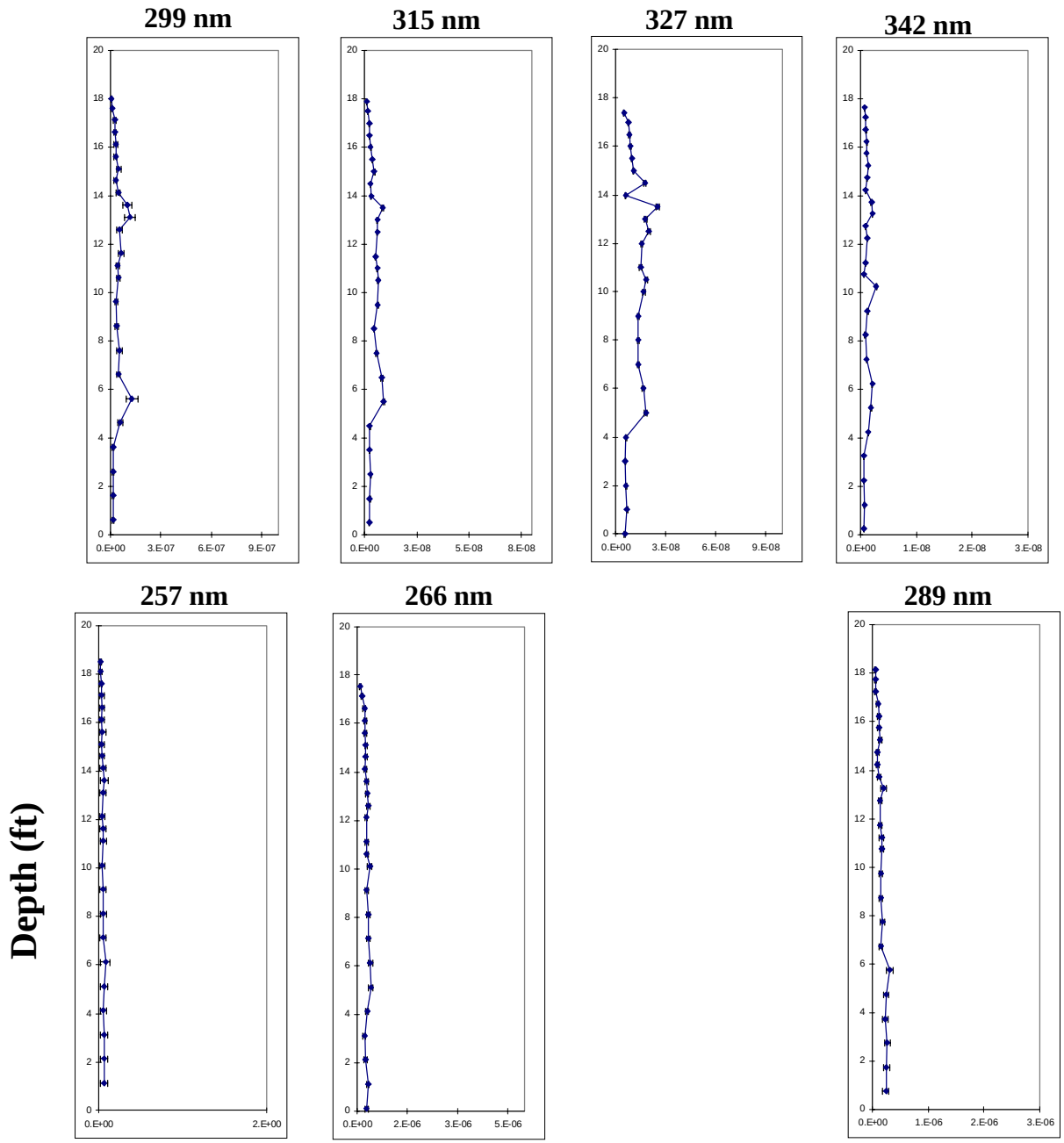

Figure 7. Depth vs. summed fluorescence for each excitation wavelength for push 7.

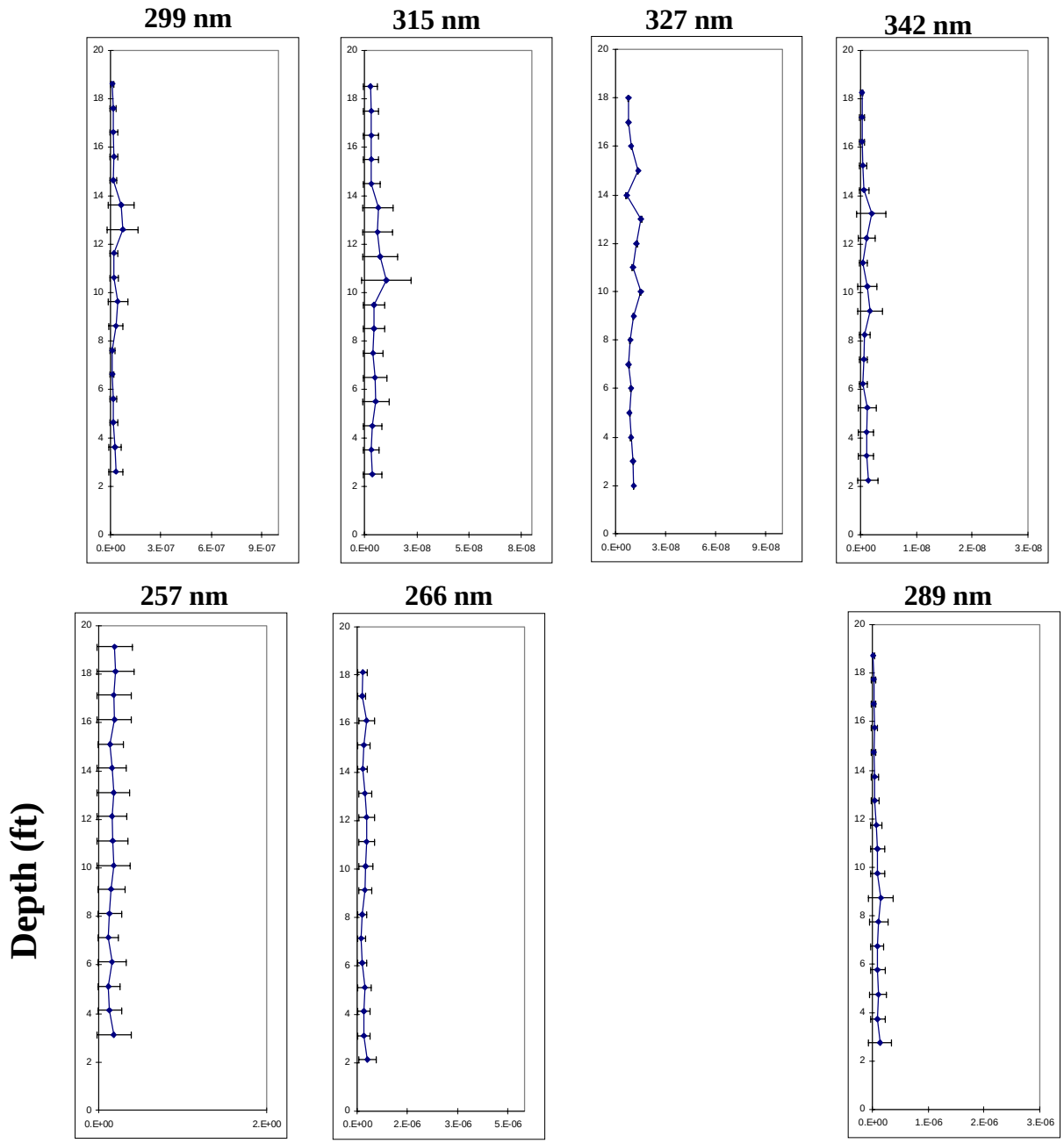

Figure 8. Depth vs. summed fluorescence for each excitation wavelength for push 8.

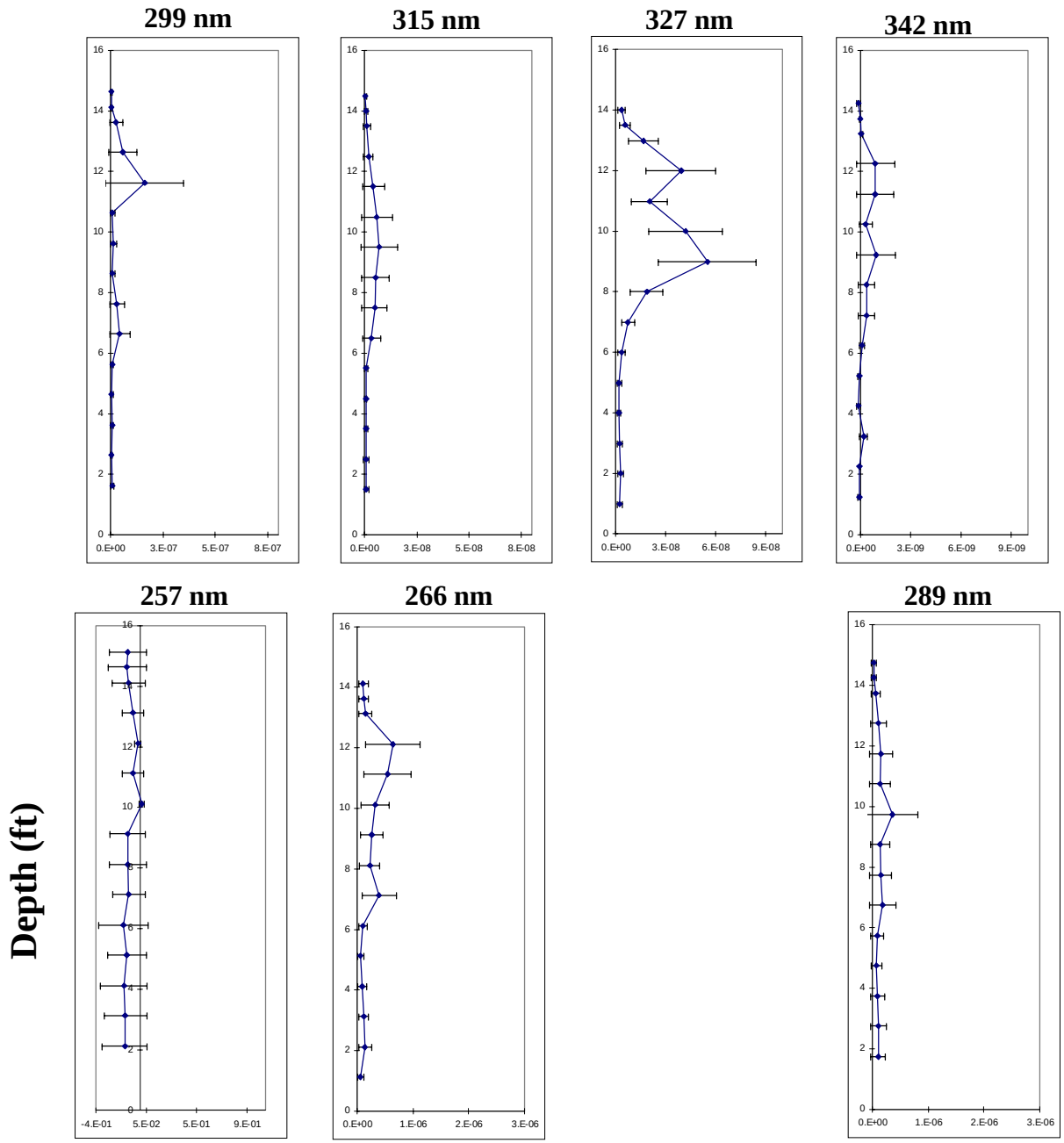

Figure 9. Depth vs. summed fluorescence for each excitation wavelength for push 9.

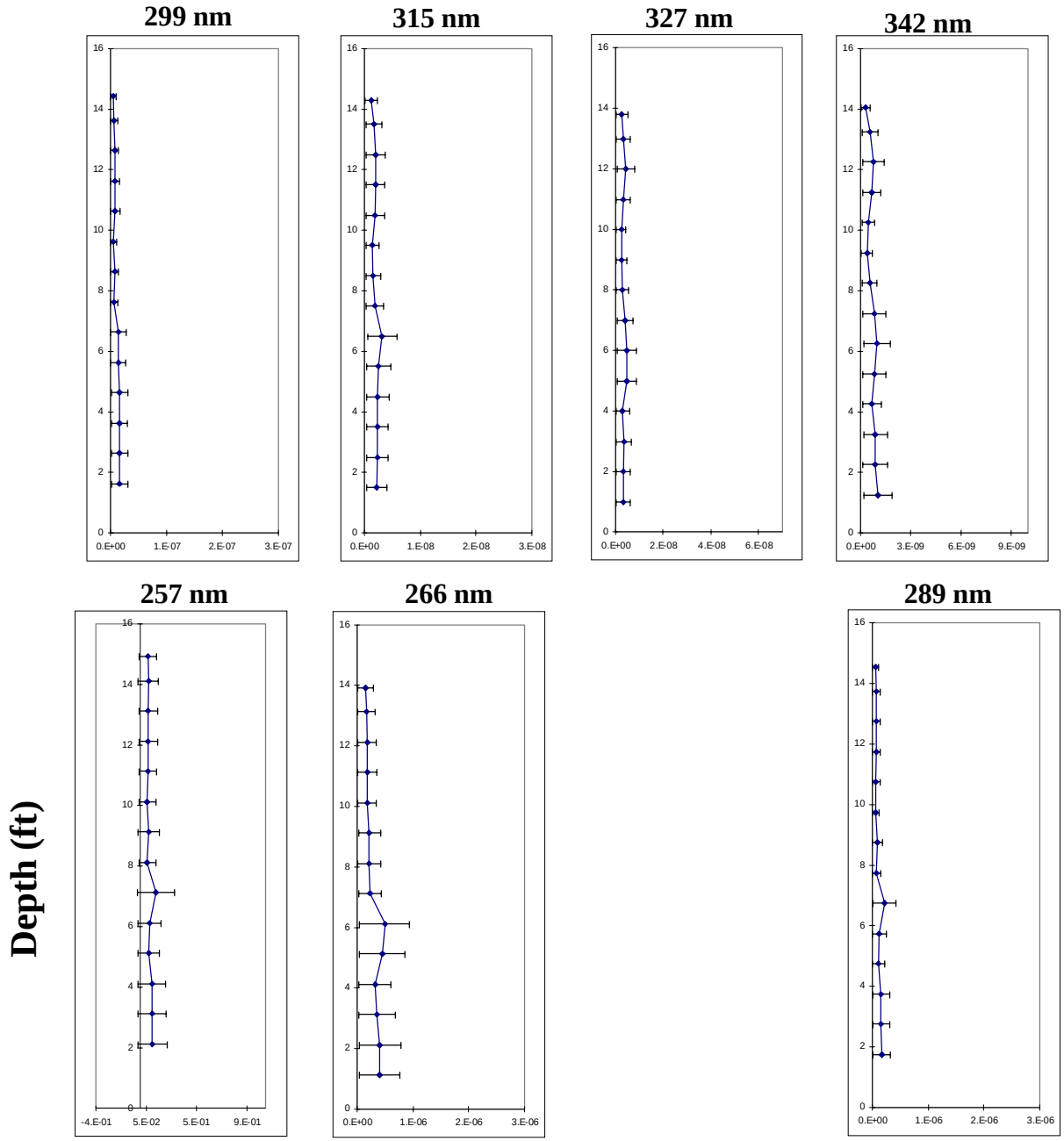

Figure 10. Depth vs. summed fluorescence for each excitation wavelength for push 10.

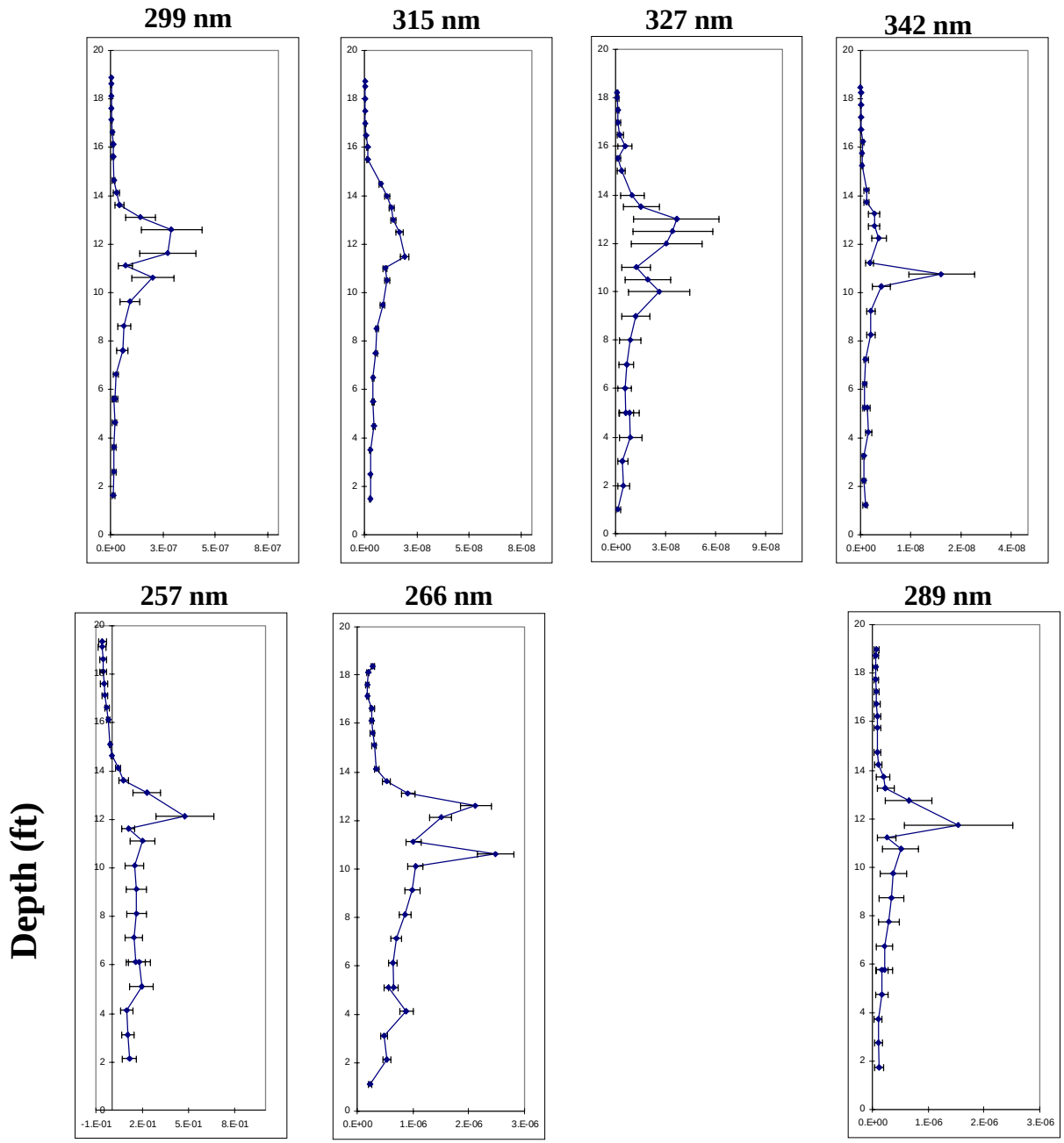

Figure 11. Depth vs. summed fluorescence for each excitation wavelength for push 11.

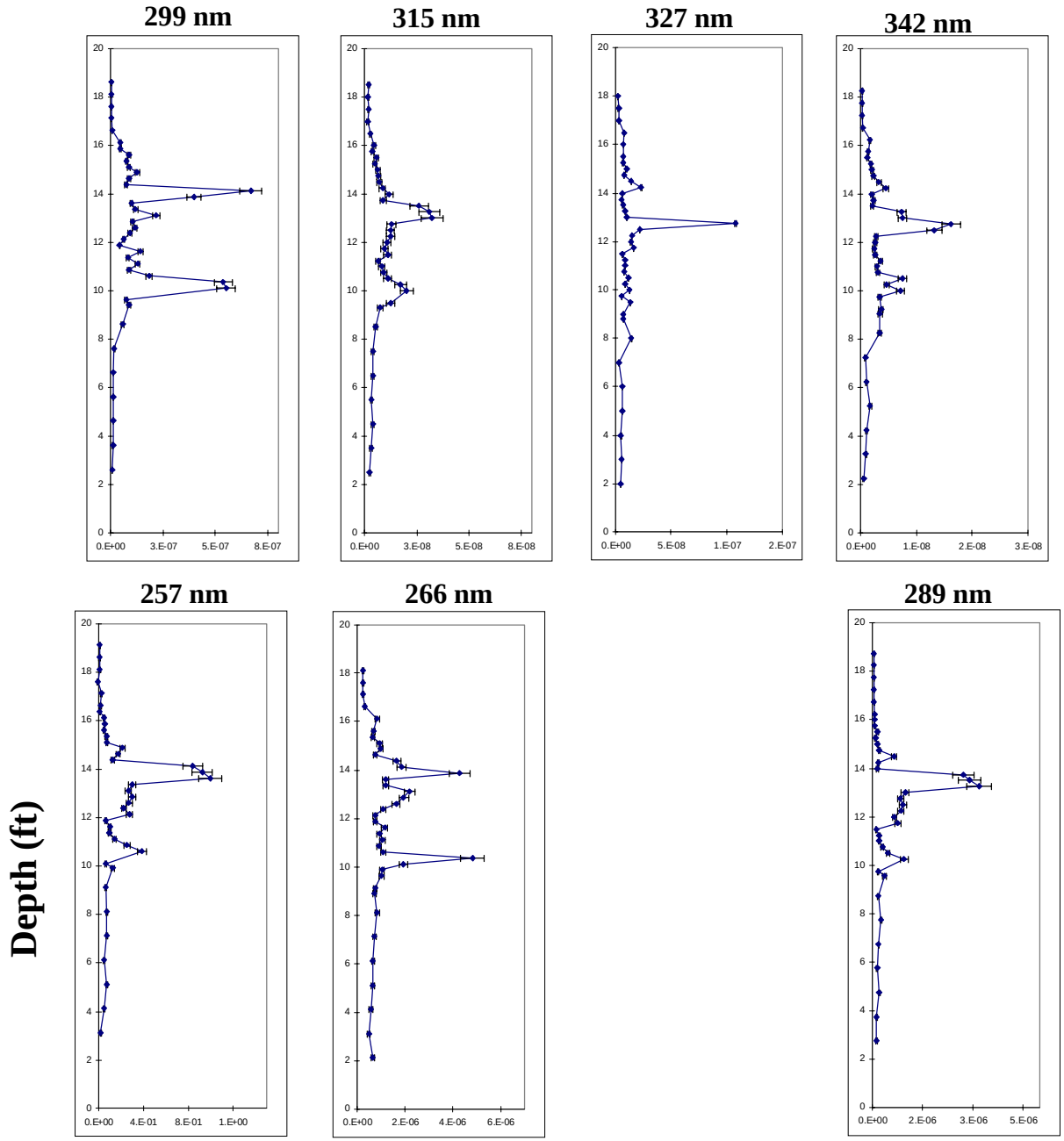

Figure 12. Depth vs. summed fluorescence for each excitation wavelength for push 12.

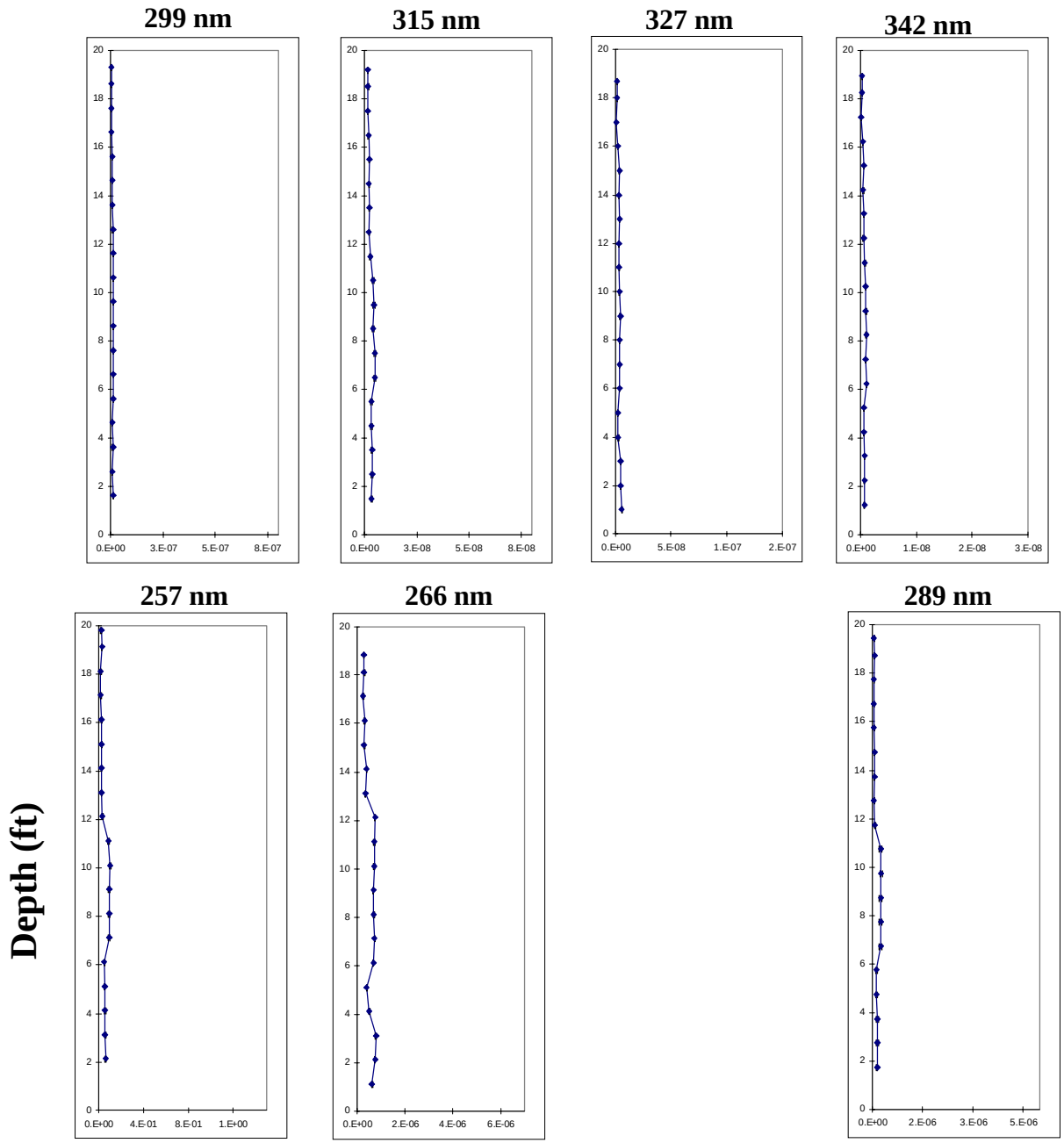

Figure 13. Depth vs. summed fluorescence for each excitation wavelength for push 13.

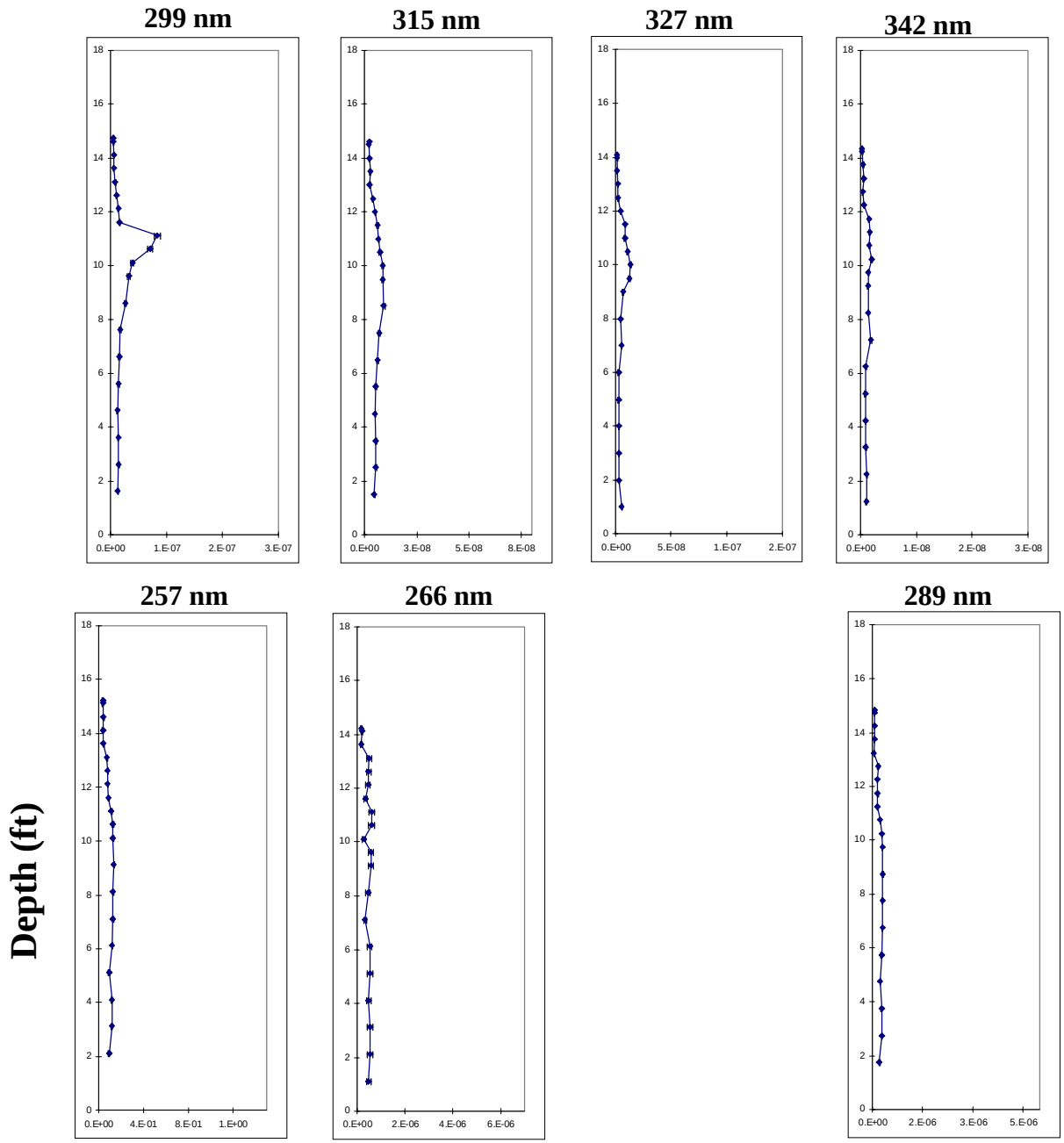

Figure 14. Depth vs. summed fluorescence for each excitation wavelength for push 14.

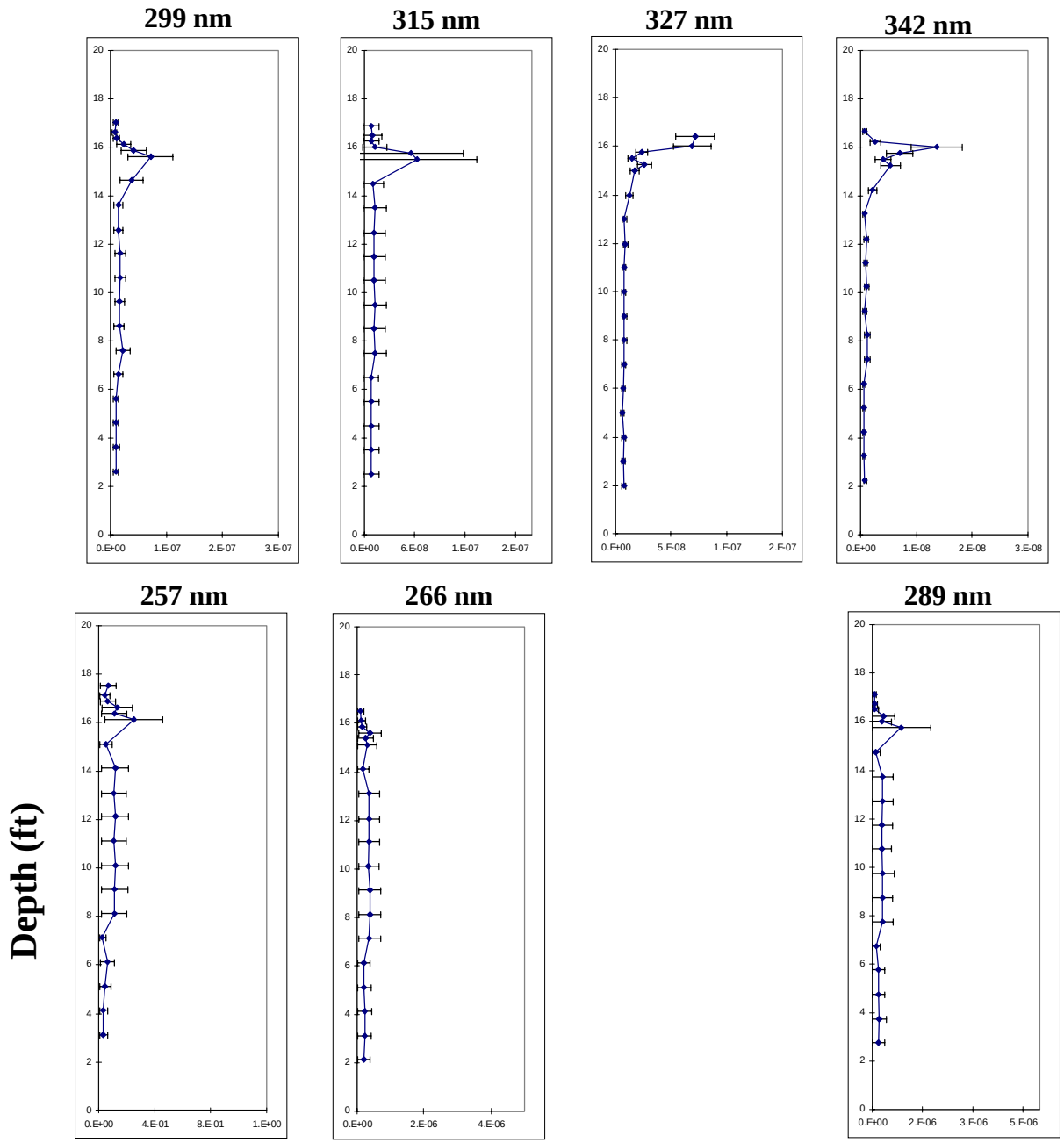

Figure 15. Depth vs. summed fluorescence for each excitation wavelength for push 16.

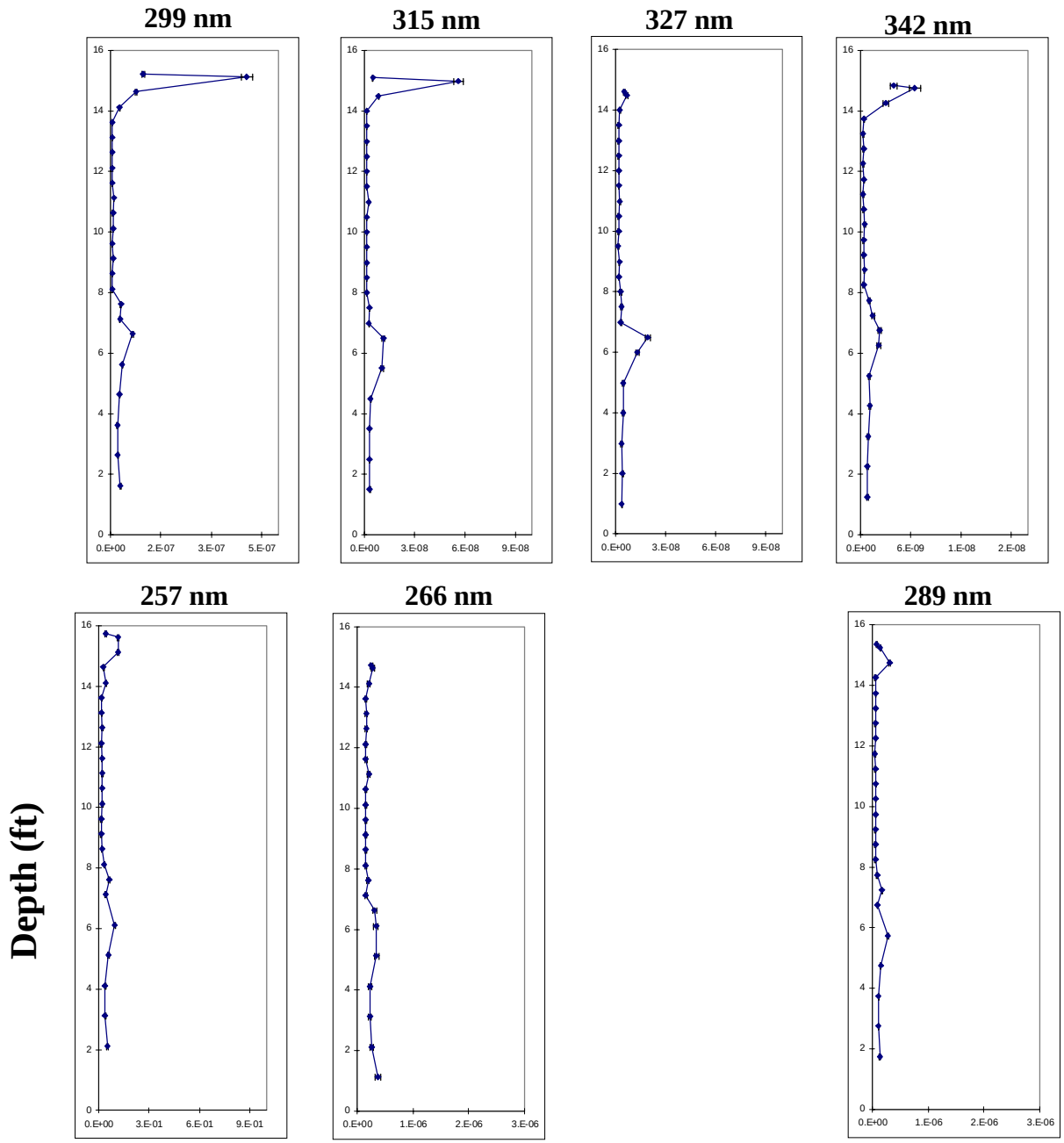

Figure 16. Depth vs. summed fluorescence for each excitation wavelength for push 17.

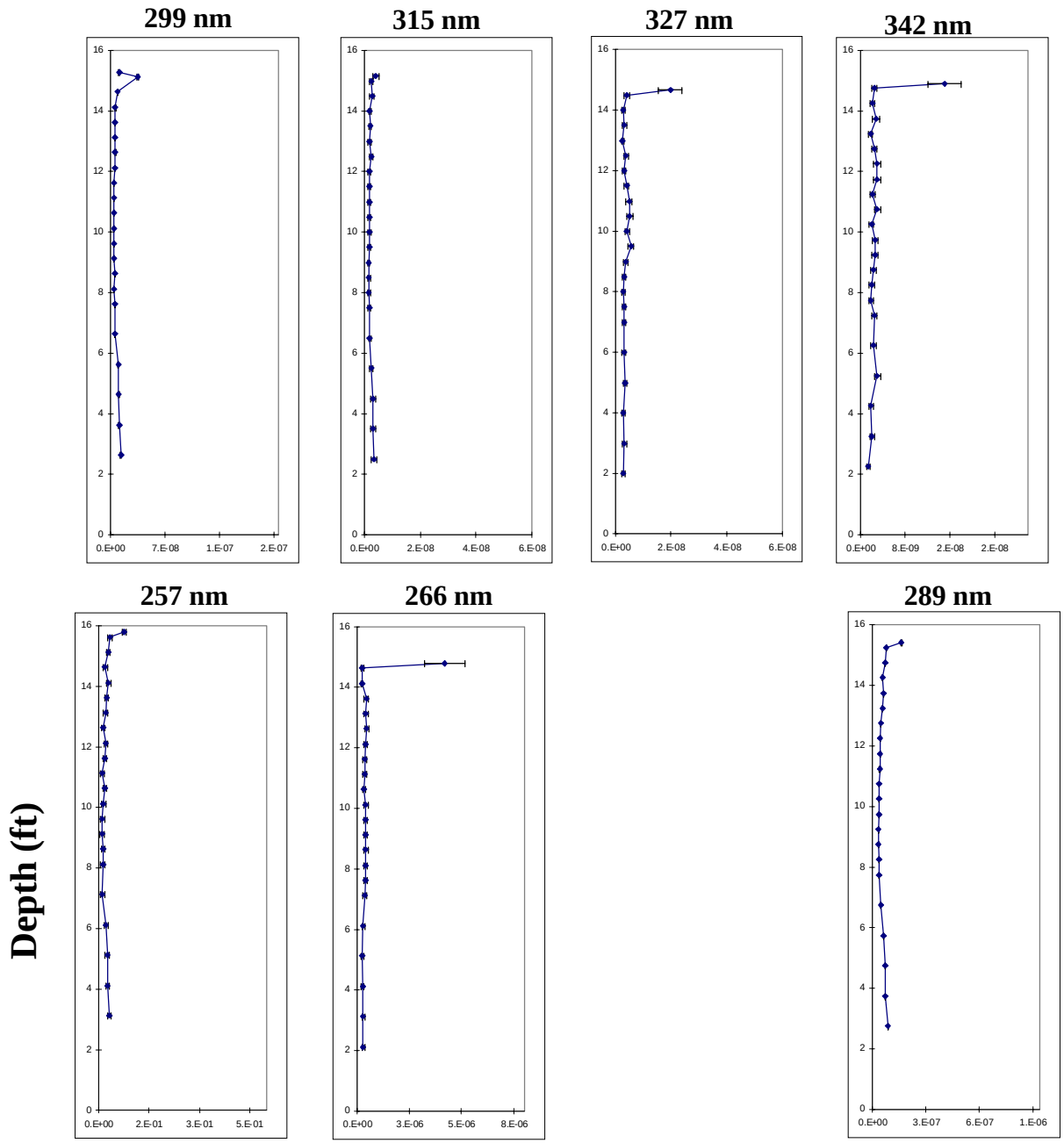

Figure 17. Depth vs. summed fluorescence for each excitation wavelength for push 18.

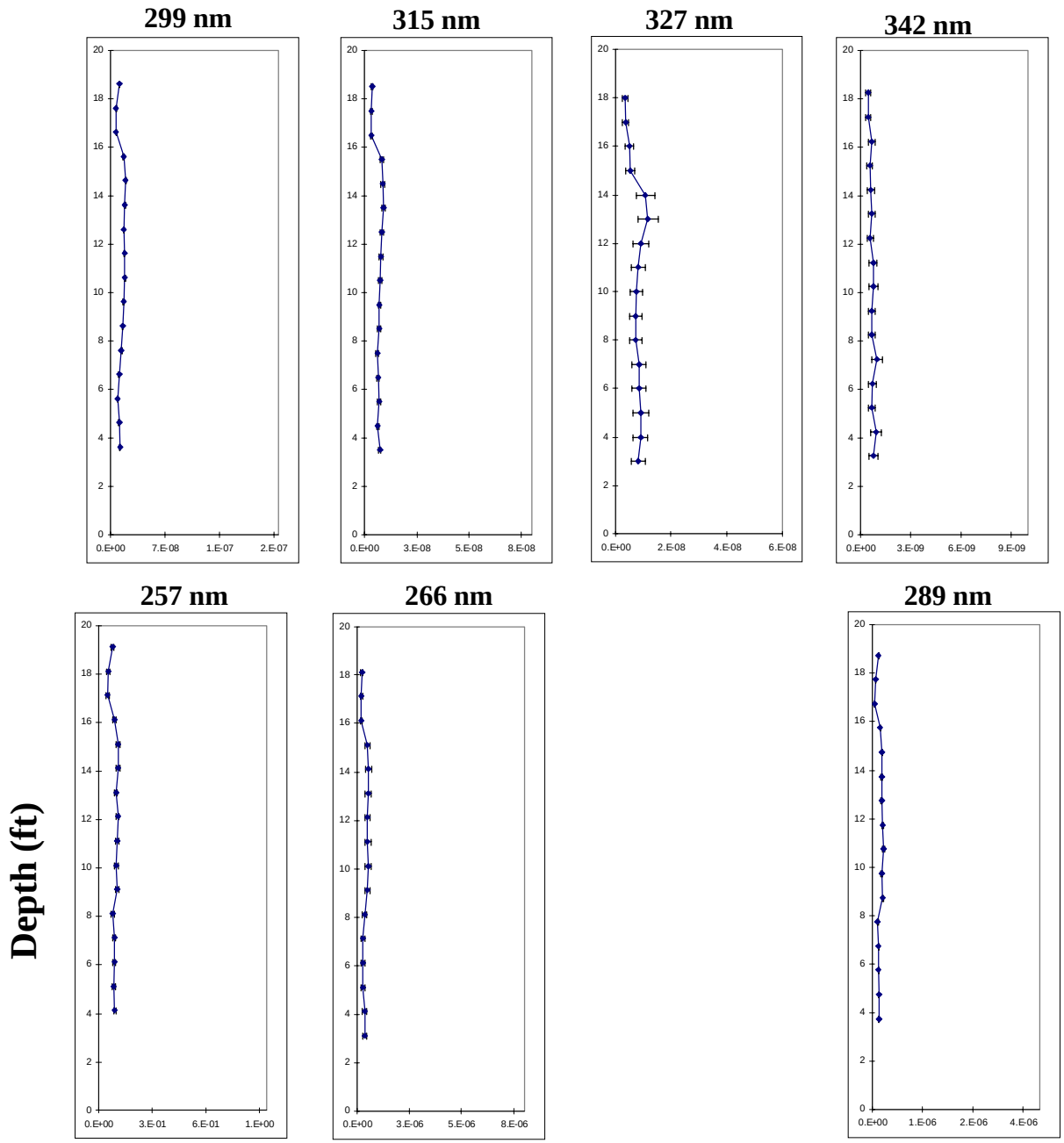

Figure 18. Depth vs. summed fluorescence for each excitation wavelength for push 19.

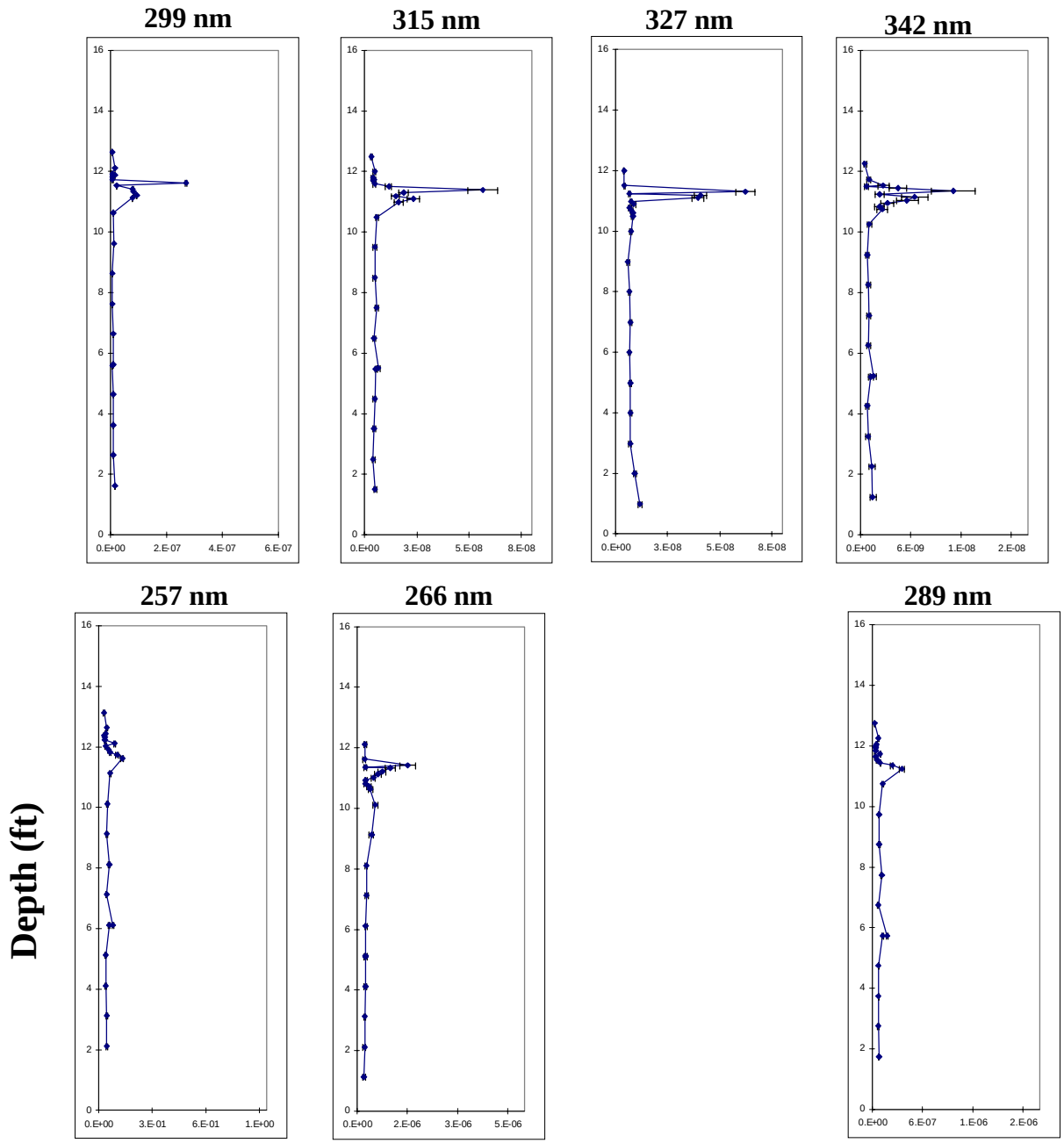

Figure 19. Depth vs. summed fluorescence for each excitation wavelength for push 20.

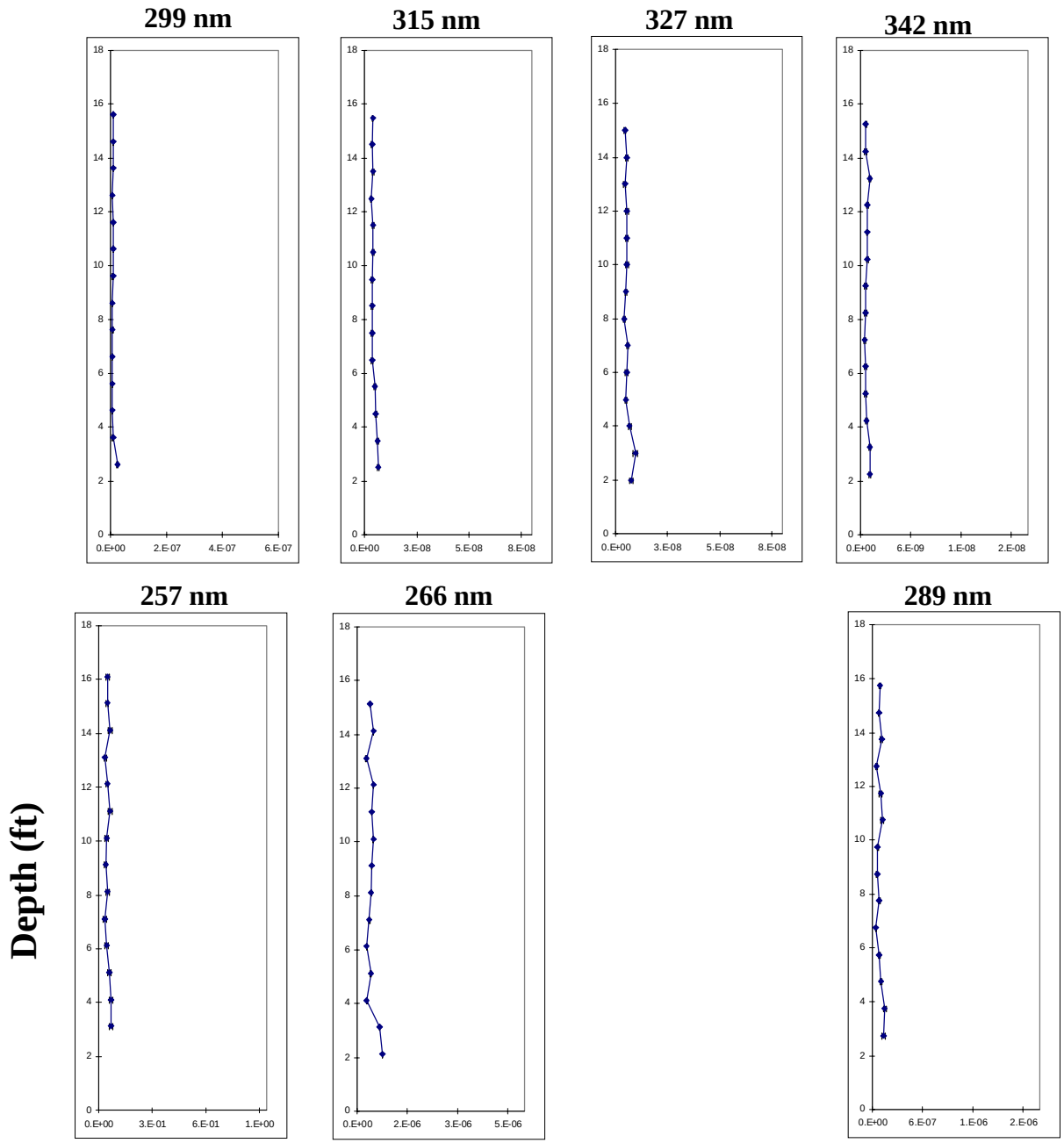

Figure 20. Depth vs. summed fluorescence for each excitation wavelength for push 21.